U.PORTO
FACULDADE DE CIÊNCIAS
UNIVERSIDADE DO PORTO

universidade de aveiro
theoria poiesis praxis

PhD

3rd CYCLE

FCUP
UA
2025

U.PORTO

Mineral Geochemistry for Lithium Exploration in the Barroso-Alvão Pegmatite Field, Portugal: Insights and Applications

Filipa Catarina Lopes Dias

FC

U.PORTO
FACULDADE DE CIÊNCIAS
UNIVERSIDADE DO PORTO

universidade de aveiro
theoria poiesis praxis

Mineral Geochemistry for Lithium Exploration in the Barroso-Alvão Pegmatite Field, Portugal: Insights and Applications

Filipa Catarina Lopes Dias
Doctoral Program in Earth Sciences
Faculty of Sciences of the University of Porto and University of Aveiro
2025

Mineral Geochemistry for Lithium Exploration in the Barroso-Alvão Pegmatite Field, Portugal: Insights and Applications

Filipa Catarina Lopes Dias

Thesis carried out as part of the Doctoral Program in Earth Sciences

Department of Geosciences, Environment and Spatial Plannings

2025

Supervisor

Alexandre Lima, Associate Professor, Faculty of Sciences of the University of Porto

Co-supervisors

Encarnación Roda-Robles, Professor, Universidad del Pais Vasco/EHU

Tânia Martins, Chief Geologist, Precambrian Geosicence Section, Manitoba Geological Survey

POCH PROGRAMA OPERACIONAL CAPITAL HUMANO

NORTE2020 PROGRAMA OPERACIONAL REGIONAL DO NORTE

REPÚBLICA PORTUGUESA
CIÊNCIA, TECNOLOGIA E ENSINO SUPERIOR

UNIÃO EUROPEIA
Fundo Social Europeu

PORTUGAL 2020

fct Fundação para a Ciência e a Tecnologia

ICT
Instituto de Ciências da Terra

Acknowledgements

I would like to express my deepest gratitude to my supervisor, Alexandre Lima, for his patience, guidance, and continuous encouragement throughout all these years, from my undergraduate studies, where I first met him as a teacher, to my master's and PhD, when he kindly accepted the role of my advisor. His ability to offer support without taking away my autonomy was, in my view, one of the key factors that allowed me to grow as a researcher, complete my studies and get to where I am today. I am also sincerely grateful to my co-advisors, Encarnación Roda-Robles and Tânia Martins, for their invaluable support, insightful feedback, and the friendship we built throughout these PhD years.

I would also like to extend my sincere gratitude to Savannah Resources Plc for their generous provision of samples from the NOA, Grandão, and Reservatório aplite-pegmatites, as well as for granting permission to study the NOA aplite-pegmatite outcrops and drill cores, which greatly contributed to the advancement of this research.

A special thanks goes to my colleagues and co-authors, Ricardo Ribeiro and Filipe Gonçalves, who were part of Espaço de Geologia, a place I am proud to have been part of. Together, we enjoyed a collaborative and inspiring environment, where we were motivated to research and work together to bring meaningful results to society, facing and overcoming many challenges along the way.

I am also thankful to all the others who were members of Espaço de Geologia during my time there, even if only for a short period, whose companionship contributed to an experience that was fun, productive, and rewarding.

My gratitude extends to the team at INESC TEC – Instituto de Engenharia de Sistemas e Computadores, Tecnologia e Ciência, particularly Pedro Jorge, Diana Capela, Diana Guimarães, and Miguel Ferreira, for their expertise in LIBS and XRF and for generously allowing us to use their laboratory for producing the pellets used in this study. I would also like to thank Filipe Silva for his consistent kindness, for always welcoming me into the lab, and for providing us with occasional support during this work.

A heartfelt thanks to Maria Irene da Costa (Thin Section Manufacturing Lab) and Cândida Garcia Neto (Scanning Electron Microscope Lab), who were always present in the neighbouring labs at Espaço de Geologia and generously available whenever help was needed.

I would also like to thank Axel Müller and Julien Menuge for their kindness and support during the GREEPEG Summer School in Norway, as well as at the conferences and other academic activities where we had the opportunity to meet during my PhD. Their willingness to listen and provide feedback has been much appreciated every time our paths have crossed.

My sincere gratitude also goes to Dr. Fernanda Guimarães from the Electron Probe Microanalysis (EPMA) at the Laboratório Nacional de Energia e Geologia (LNEG), located in S. Mamede de Infesta, Porto, Portugal, for her patience and kindness towards me.

I would also like to express my gratitude to María Eugenia Sánchez Lorda for conducting the LA-ICP-MS analyses and for her support during the analytical process at the Universidad del País Vasco (UPV/EHU) in Bilbao during my time there.

Finally, I am deeply grateful to my family, my mother, Lina Matias, my father, Carlos Dias, and my little sister, Joana Dias, for their unwavering support throughout this journey, including during my PhD time abroad. A special acknowledgment goes to my father, whose tireless encouragement and genuine interest in my work were a constant source of motivation, particularly towards the end of my thesis.

This research was supported by national funding from Fundação para a Ciência e Tecnologia (FCT), I.P., through the Instituto de Ciências da Terra (ICT) under the projects UIDB/04683/2020 (https://doi.org/10.54499/UIDB/04683/2020) and UIDP/04683/2020 (https://doi.org/10.54499/UIDP/04683/2020). It was also funded by the FCT doctoral grant 2020.05534.BD (https://doi.org/10.54499/2020.05534.BD), with national support from MCTES via FCT, co-financed by the European Social Fund (ESF) through POCH – Programa Operacional Capital Humano, and the NORTE 2020 regional program. Additionally, this work was supported by projects that accompanied my PhD journey: INOVMINERAL 4.0 (POCI-01-0247-FEDER-046083), GREENPEG (869274), and CAVALI – Cadeia de Valor do Lítio (POCI-01-0247-FEDER-047728). This study also received support from the FLAPSYS project – Fiber Laser Plasma spectroscopy system for real-time element analysis (POCI-01-0145-FEDER-031165).

Resumo

A crescente procura por matérias-primas críticas (CRMs), em particular o lítio (Li), impulsionada pela transição global para as energias renováveis e a mobilidade elétrica, tem sublinhado a necessidade de estratégias de prospeção mais eficientes e sustentáveis. Este trabalho doutoral foca-se no Campo Aplito-Pegmatítico do Barroso-Alvão, no norte de Portugal, uma das principais províncias de lítio em rochas cristalinas, com o objetivo de aprimorar a prospeção de lítio por meio da aplicação de ferramentas avançadas mineralógicas e geoquímicas. O estudo integra técnicas de campo e laboratoriais, incluindo a calibração de um sistema portátil de Espectroscopia de Emissão de Plasma Induzido por Laser (LIBS) para a identificação in-situ de espodumena e petalite, o uso de Fluorescência de Raios-X Portátil (pXRF) para avaliar a geoquímica dos feldspatos potássicos como indicadores indiretos da mineralização de lítio, e a aplicação de microscopia de catodoluminescência a frio (CL) para identificação e quantificação de minerais. Além disso, o estudo de campo realizado num afloramento de um dos pegmatitos litiníferos do Barroso-Alvão, juntamente com a análise dos seus tarolos de sondagem, proporcionou um contributo substancial para o aprofundamento do conhecimento sobre a estrutura interna e a distribuição do lítio neste corpo. Este conhecimento certamente abrirá novas perspetivas para compreender a estrutura e distribuição de lítio noutros corpos pegmatíticos da região. As tendências geoquímicas regionais nos feldspatos potássicos, aliadas aos dados petrográficos e LA-ICP-MS de depósitos selecionados, fornecem novas perspetivas sobre a distribuição espacial dos pegmatitos ricos em lítio e seus processos de cristalização. Os resultados demonstram que a integração destas ferramentas analíticas melhora a distinção entre pegmatitos estéreis em lítio, ricos em espodumena e ricos em petalite, contribuindo, assim, para o desenvolvimento de modelos de prospeção mais robustos para os pegmatitos litiníferos. Este trabalho doutoral oferece avanços metodológicos e conhecimentos geocientíficos que poderão contribuir para uma prospeção de lítio mais eficaz, tanto em contextos geológicos semelhantes na Europa como noutros locais ao redor do mundo.

Palavras-chave: prospeção de lítio, Barroso–Alvão, espodumena, petalite, LIBS portátil, FRX portátil, catodoluminescência, geoquímica de feldspatos-K, pegmatitos, matérias-primas críticas

Abstract

The increasing demand for critical raw materials (CRMs), particularly lithium (Li), driven by the global shift towards renewable energy and electric mobility, has underscored the need for more efficient and sustainable exploration strategies. This doctoral research focuses on the Barroso-Alvão Aplite-Pegmatite Field in northern Portugal, one of the leading lithium provinces in hard-rock formations, with the aim of enhancing lithium exploration through the application of advanced mineralogical and geochemical tools. The study combines field-based and laboratory techniques, including the calibration of a portable Laser-Induced Breakdown Spectroscopy (LIBS) system for in-situ identification of spodumene and petalite, the use of portable X-Ray Fluorescence (pXRF) to evaluate K-feldspar chemistry as an indirect indicator of lithium mineralization, and the application of cold cathodoluminescence (CL) microscopy for mineral identification and quantification. Furthermore, a field study conducted on an outcrop of one of the lithium-bearing pegmatites in the Barroso-Alvão region, along with the analysis of its drill cores, made a substantial contribution to advancing the understanding of the internal structure and lithium distribution within these bodies. This knowledge is expected to open new avenues for understanding the structure and lithium distribution in other pegmatitic bodies in the region. Regional geochemical trends in K-feldspar, combined with petrographic and LA-ICP-MS data from selected deposits, offer new insights into the spatial distribution of lithium-rich pegmatites and their crystallization processes. The results demonstrate that the integration of these analytical tools enhances the differentiation between lithium-barren, spodumene-rich, and petalite-rich pegmatites, thereby contributing to the development of more robust exploration models for lithium-bearing pegmatites. This doctoral research provides methodological advancements and geoscientific knowledge that could contribute to more efficient lithium exploration across Europe and in other parts of the world.

Keywords: lithium exploration, Barroso–Alvão, spodumene, petalite, handheld LIBS, pXRF, cathodoluminescence, K-feldspar geochemistry, pegmatites, critical raw materials

Table of Contents

Contribution of the co-authors

Ricardo Ribeiro and Filipe Gonçalves, my colleagues, worked closely with me on the first paper, which focused on the calibration of the portable Laser Induced Breakdown Spectroscopy (LIBS) equipment. They were integral to all sample preparation steps, which included selecting the crystals, milling them, and producing the pellets. Additionally, they collaborated with me in building the calibration lines for LIBS, which involved analyzing the pellets using LIBS and fitting the calibration curves to our samples in the Profile Builder software from Sciaps. They also closely reviewed the manuscript and helped me think through and overcome the various challenges that arose during the calibration process.

For the second paper, Ricardo Ribeiro and Filipe Gonçalves were co-authors due to their involvement in sample preparation, which included all the samples used in both the first and second papers. Following this, they provided valuable input in reviewing the manuscript, and Ricardo Ribeiro kept an eye on the XRF analysis process.

Alexandre Lima, my advisor, facilitated our work by granting access to all the samples used in both papers. He provided financial support to send samples for ICP-MS analysis and was an essential figure throughout the writing process, offering guidance and being consistently available to address any issues that arose.

Tânia Martins and Encarnación Roda-Robles, my co-advisors, significantly contributed to both papers despite being based at different institutions. Their guidance was invaluable in structuring the manuscripts, reviewing the content, and providing expert knowledge that greatly enhanced the quality of the final papers.

Diana Guimarães contributed solely to the second paper, providing valuable insights into the X-Ray Fluorescence (XRF) analysis. Her input helped refine the structure and methodology of the second paper, significantly improving its clarity and focus.

List of Tables

List of Figures

List of Abbreviations

A.L.	Alexandre Lima
Al	Aluminum
Al_2O_3	Alumina
AP	Apatite
As	Arsenic
ASTER	Advanced Spaceborne Thermal Emission and Reflection Radiometer
AI	Artificial Intelligence
B	Boron
Ba	Barium
BA	Barroso-Alvão
BD	Bolsa de Doutoramento
Be	Beryllium
BSE	Backscattered Electron
Ca	Calcium
CAVALI	Cadeia De Valor Do Lítio
CIZ	Central Iberian Zone
Ck	Cookeite
CL	Cathodoluminescence
CL-TNT	Columbite-Tantalite
cm	Centimeter
Co	Colbalt
COMPETE	Programa Operacional Fatores De Competitividade
Cr	Chromium
CRM	Critical Raw Materials
CRMA	Critical Raw Materials Act
Cs	Cesium
Cu	Copper
D1	First Deformation of the Variscan Orogeny
D2	Second Deformation of the Variscan Orogeny
D3	Third Deformation of the Variscan Orogeny
DGPR	Deep Ground Penetrating Radar
DUP	Duplicate
E	East

e.g.	Exempli Gratia (For Example)
E.R.-R.	Encarnación Roda Robles
EDS	Energy Dispersive X-Ray Spectroscopy
EPMA	Electron Micro Probe Analyzer
ESF	European Social Fund
EU	European Union
F	Fluorine
F.D.	Filipa Dias
F.G.	Filipe Gonçalves
FCT	Fundação Para a Ciência e Tecnologia
Fe	Iron
FEDER	Fundo Europeu de Desenvolvimento Regional
Fig	Figure
Ga	Gallium
Ge	Germanium
GIS	Geographic Information System
GTMZ	Galiza Trás-Os-Montes Zone
H_3BO_3	Boric Acid
HCl	Hydrochloric Acid
$HClO_4$	Perchloric Acid
HF	Hydrofluoric Acid
HNO_3	Nitric Acid
Hz	Hertz
ICP-MS	Inductively Coupled Plasma Mass Spectrometry
ICP-OES	Inductively Coupled Plasma Optical Emission Spectroscopy
ICT	Instituto De Ciências Da Terra
ID	Identification
INESC TEC	Instituto de Engenharia de Sistemas e Computadores - Tecnologia e Ciência
IR	Intensity Ratios
K	Potassium
K_2O	Potassium Oxide
KeV	Kilo Electron Volt
Kfs	Potassium Feldspar
km	Kilometer

kV	Kilovolt
LA-ICP-MS	Laser Ablation Inductively Coupled Plasma Mass Spectrometry
Li	Lithium
LIBS	Laser-Induced Breakdown Spectroscopy
LiDAR	Light Detection and Ranging
LNEG	Laboratório Nacional de Energia e Geologia
LOD	Limit of Detection
Ma	Million Years
Mbs	Montebrasite
MCTES	Ministério Da Ciência, Tecnologia e Ensino Superior
MIC	Micas
MC	Mica
mJ	Millijoule
mm	Millimeter
Mn	Manganese
MPa	Megapascal
N	North
Na	Sodium
Nb	Niobium
Nd	Neodymium
Ni	Nickel
NIST	National Institute of Standards and Technology
nm	Nanometer
NS	North-South
NW	Northwest
NYF	Niobium, Yttrium, and Fluorine
ON	Ontario
ORIG	Original
P	Phosphorous
Pb	Lead
PET	Petalite
Ph	Phosphate
PL	Plagioclase
pLIBS	Portable Laser-Induced Breakdown Spectroscopy
P/N	Part Number

POCH	Programa Operacional Capital Humano
POCI	Programa Operacional Competitividade e Internacionalização
PPL	Parallel Polarized Light
ppm	Parts Per Million
psi	Pounds Per Square Inch
pXRF	Portable X-Ray Fluorescence
QA	Quality Assurance
QC	Quality Control
QTZ	Quartz
R.R.	Ricardo Ribeiro
Rb	Rubidium
RC	Reverse Circulation
Rh	Rhodium
s	Seconds
S	Sulfur or south
SAR	Synthetic Aperture Radar
Sc	Scandium
SE	Southeast
SEM	Scanning Electron Microscopy
SFRH	Sistema de Formação de Recursos Humanos
Si	Silicon
SiO_2	Silica
Sn	Tin
SPD	Spodumene
SQ	Spodumene And Quartz
SQI	Spodumene Quartz Intergrowth
Sr	Strontium
SRM	Standard Reference Material
T.M.	Tânia Martins
Ta	Tantalum
Tl	Thallium
U	Uranium
UIDB	Unidades de Investigação e Desenvolvimento Básica
UIDP	Unidades de Investigação e Desenvolvimento Projetada
US	Unitated States

UST	Unidirectional Solidification Textures
V	Vanadium
W	Tungsten or West
XPL	Crossed Polarized Light
XRD	X-Ray Difraction
XRF	X-Ray Fluorescence
YAG	Yttrium Aluminum Garnet
Zn	Zinc
µA	Microampere
µm	Micrometer

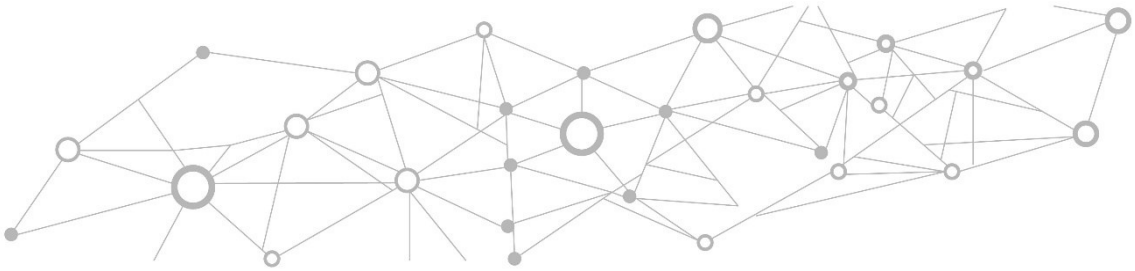

Part I – Introduction

1. Subject
2. Objectives
3. Thesis Structure
4. State of Art
5. Geological Setting

1. Subject

Mineral exploration is essential for maintaining the quality of life we enjoy in Europe today. Every aspect of modern society, including technology, infrastructure, transportation, and energy, relies on the availability of raw materials. These materials are essential for manufacturing, energy production, communication systems, and the electronics that power our daily lives. With the global shift toward a more sustainable energy future, the importance of critical raw materials (CRMs) has grown significantly, especially in sectors such as electric vehicle production, renewable energy, and battery storage technologies. Additionally, the rapid growth of Artificial Intelligence (AI) demands vast amounts of energy, further emphasizing the need for these vital materials (European Commission 2020b, 2023, IEA 2025).

Recognizing the strategic importance of CRMs, the European Union published the Critical Raw Materials Act (CRMA) in 2023 (European Union 2024). The CRMA aims to ensure a stable and sustainable supply of essential materials, reduce reliance on external sources, and reinforce Europe resilience and self-sufficiency. The urgency of this effort is underscored by increasing geopolitical instability, including the exit of the United Kingdom from the EU, unpredictable US trade policies, China dominant control over global CRM markets, and the ongoing war in Ukraine, led by Russia, a nation with significant global influence. These developments highlight more clearly than ever that Europe could face a severe crisis if access to CRMs is disrupted. The EU economic stability, industrial competitiveness, and green transition all depend on reliable CRM supplies.

Although recycling is often seen as a way to reduce dependence on raw material imports and mining, its current limitations make it an insufficient solution. Global lithium (Li) recycling rates, for example, are estimated to be <1% due to technical and economic constraints (Swain 2017), and rare earth elements, essential for technologies such as wind turbines, electric vehicles, and electronics, are also recycled at very low rates (Binnemans *et al.* 2013). While technological advances may enhance recycling capacity in the future, even perfect recycling would fall short of meeting the increasing demand driven by emerging green and digital technologies. This further reinforces the need for investment in domestic prospection and mining across Europe.

However, efforts to expand mining face another significant challenge: widespread public opposition to new mining projects, particularly in residential areas.

This resistance often stems from concerns over environmental degradation and health risks, concerns that, while understandable, are largely based on the legacy of harmful past mining practices. Today, modern mining technologies and strict environmental regulations have significantly reduced these risks. Regulations are far more rigorous than in the past, when industrial development often came at the expense of the environment and human health. Modern operations such as those at Mina de Neves Corvo demonstrate that responsible and sustainable mining is both possible and already happening in Europe (Alves 2022).

Given these global challenges and domestic barriers, it is more critical than ever to thoroughly assess and document the mineral resources of Europe, particularly Li, a key element in the transition to renewable energy and electric transportation. Currently, Li can be obtained from three main types of deposits: brine-based, hard-rock-based, and volcano-sedimentary-based (Putzolu *et al.* 2025). The most significant known Li reserves are located in brine deposits in Argentina, Bolivia, and Chile, as well as in hard-rock deposits in Australia (U.S. Geological Survey 2025). As shown in Figure 1, which presents global Li production, Australia currently leads in hard-rock extraction, primarily from spodumene concentrates. However, between 2021 and 2023, China experienced a production surge from another hard-rock Li source (lepidolite) particularly from Jiangxi Province (IEA 2024).

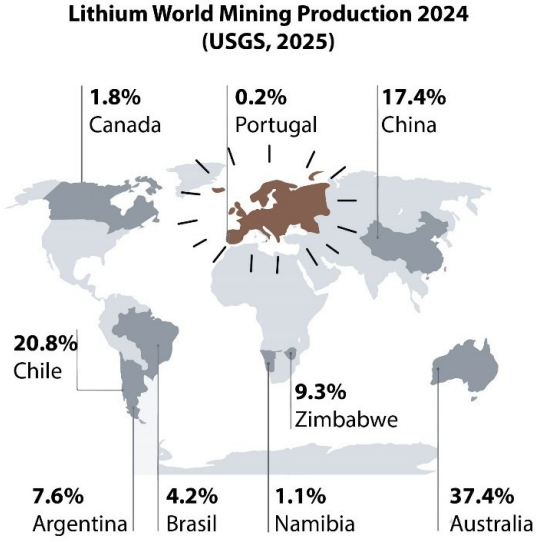

Figure 1. World lithium production (U.S. Geological Survey 2025).

Both spodumene and lepidolite occur in Portugal. At present, lepidolite, along with other Li-bearing minerals such as petalite and amblygonite, is mainly mined for use in the ceramics industry. Although spodumene is also currently used for ceramics, it is considered the preferred hard-rock Li source for producing Li hydroxide, which is

essential for Li-ion battery manufacturing. In northern Portugal, the Barroso-Alvão aplite-pegmatite field contains numerous spodumene-rich pegmatites (Noronha 1987, Savannah Resources 2023).

Beyond Portugal, Li-bearing resources have been identified in several European countries, including Spain, France, the United Kingdom, Germany, Czechia, Austria, Italy, Finland, Ukraine, and Serbia (Gautneb *et al.* 2021) (Figure 2). Germany and Serbia, in particular, host some of the largest Li deposits on the continent (U.S. Geological Survey 2025). However, these resources are not exclusively associated with pegmatites. They may also be associated with rare-metal granites, greisen, and quartz veins, or example, the Beauvoir and Montebras deposits in France and the Argemela deposit in Portugal, as well as with Li-rich clays, such as those in Serbia, and with geothermal brines, like some deposits in Germany (Gourcerol *et al.* 2019, Ribeiro *et al.* 2021, Alms *et al.* 2025).

Hard-rock Li refining has long been dominated by China. However, new alternatives are emerging. In 2022, AMG opened a refining plant in Bitterfeld, Germany, and POSCO is planning a new conversion facility in South Korea, both intended to serve as viable alternatives to the Chinese refinery (IEA 2021).

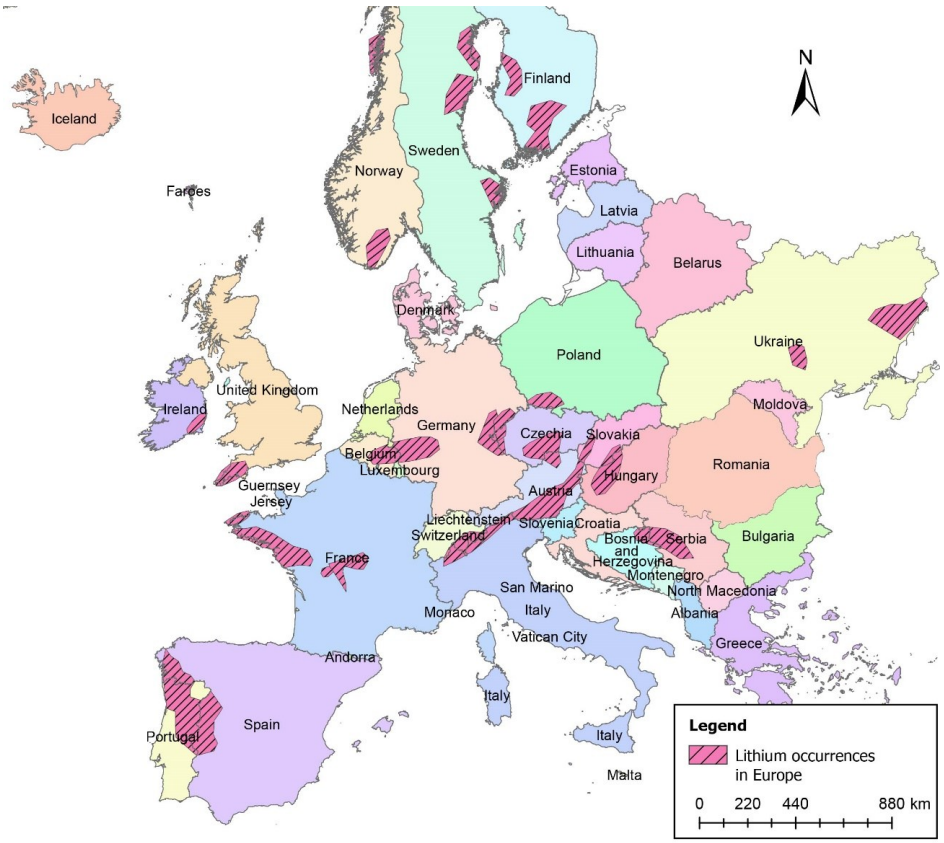

Figure 2. Lithium occurrences in Europe. Adapted from Gautneb *et al.* (2021) and European Commission (2020c).

Objectives

Primary Objective:

To improve lithium (Li) exploration methods in the Barroso–Alvão (BA) Aplite-Pegmatite Field, Northern Portugal, through the development and testing of innovative field and laboratory techniques. This research also aims to establish a robust exploration framework that can be adapted to similar geological settings worldwide, enhancing the efficiency and precision of Li resource identification and characterization.

Specific Goals:

1. Enhance Exploration Techniques: To refine and integrate advanced analytical tools for Li exploration, focusing on both field-based and laboratory methods:
    - Optimizing the use of handheld Laser-Induced Breakdown Spectroscopy (LIBS) for rapid, in-situ detection of spodumene and petalite minerals. This involves calibrating the LIBS instrument using representative samples from the Barroso–Alvão field, with a focus on understanding their individual geochemical signatures and considering their distinct textural characteristics.
    - Applying a portable X-ray fluorescence (pXRF) as an indirect tool to identify Li-rich pegmatites by analyzing the geochemical signature of associated K-feldspar;
    - Evaluating the effectiveness of cathodoluminescence (CL) imaging for detecting high-luminescence impurities in petalite samples, testing the detection of spodumene in reverse circulation (RC) samples, and assessing the applicability of image analysis software to quantify spodumene content from CL-mapped petrographic thin sections.
2. Bring New Insights into Li Distribution Across the BA Field: Use K-feldspar geochemistry to compare aplite-pegmatite types across the BA field, including Li-barren, spodumene-rich, and petalite-rich bodies, at a regional scale.
3. Characterize Lithium Distribution within the BA Pegmatites: Learn the detailed textural and mineralogical characteristics of one of the Li-rich deposits in the Barroso–Alvão field (AL56/NOA), using data from both drill cores and outcrops.

This is especially significant because Li distribution within pegmatites is not homogeneous, with spatial variations observed across the bodies.
In addition, attempt to develop a model explaining the evolution and crystallization processes of the pegmatitic melt. This will involve considering how the melt may have evolved over time, resulting in its present-day structure, Li-distribution, and texture, with a focus on the Li-rich minerals spodumene and petalite.

2. Thesis Structure

This thesis is presented in an article-based format and consists of six parts. The results section is divided into two chapters: one comprising international peer-reviewed papers and the other, conference presentations. The PhD journey began in the United States, at Central Michigan University, where the candidate completed the first academic year (2017–2018). Upon returning to Portugal, the work completed abroad was recognized as equivalent, and the PhD formally resumed in 2020.

Part I - Introduction

This part provides an overview of the research objectives and context, emphasizing the importance of lithium (Li) exploration in response to global supply chain concerns. It outlines the geological characteristics of the Barroso-Alvão Aplite-Pegmatite Field, Northern Portugal, focusing on spodumene-bearing pegmatites and their formation processes. The section highlights the role of portable analytical tools, such as LIBS and XRF, in expediting Li exploration while addressing methodological challenges. The review also discusses trace-element behavior in K-feldspar as an indicator of mineralized pegmatites, supporting efficient resource assessment.

Part II - Methodology

This section outlines the methodologies employed in the study, focusing on sample preparation and analytical techniques, including portable LIBS, portable XRF, ICP-MS, and optical microscopy with cathodoluminescence to evaluate sample purity. It details the sample collection and analysis process used to assess the geochemistry of spodumene, petalite, and K-feldspar, as well as the development of calibration curves for LIBS.

Part III - Results and Discussion

This section compiles the key scientific contributions of the research, organized into two chapters. Chapter I presents two peer-reviewed journal articles. The first article focuses on the calibration of handheld LIBS technology for Li exploration in the Barroso–Alvão aplite-pegmatite field, emphasizing textural effects in the analysis of spodumene and petalite. The second article examines the geochemistry of K-feldspars as a complementary tool for Li exploration in the same geological context. Chapter II includes seven conference papers presented at national and international events between 2021

and 2024. These papers cover a range of topics related to Li-rich pegmatites, including cathodoluminescence-based mineral identification and quantification, mineralogical and textural characterization, evaluation of standard reference materials, and analytical challenges associated with portable XRF techniques. Together, these chapters represent the continued dissemination and advancement of the research within the scientific community. Unlike Chapter I, which contains the unchanged content of the published peer-reviewed journal articles, Chapter II, which includes the Conference Proceedings and Presentations, has been adapted to include additional information from the presentations that cannot be found in the corresponding published abstracts. Other conference works related to LIBS were not included here, as the full LIBS study is already detailed in Chapter I; their inclusion would merely summarize what has already been thoroughly addressed. Additionally, conference contributions in which the author was not the first author have also been excluded from the thesis.

Chapter I: Peer-Reviewed Journal Publications:

Dias, F., Ribeiro, R., Gonçalves, F., Lima, A., Roda-Robles, E., Martins, T. (2023). Calibrating a Handheld LIBS for Li Exploration in the Barroso–Alvão Aplite-Pegmatite Field, Northern Portugal: Textural Precautions and Procedures When Analyzing Spodumene and Petalite. Minerals, 13(4), 470. https://doi.org/10.3390/min13040470

Dias, F., Lima, A., Roda-Robles, E., Martins, T. (2024). "K-Feldspars Geochemistry for Lithium Prospection in the Barroso–Alvão Aplite-Pegmatite Field, Northern Portugal". Submitted to The Canadian Journal of Mineralogy and Petrology.

Chapter II: Conference Proceedings and Presentations:

Dias, F., Lima, A. (2021). "Cathodoluminescence characteristics of spodumene and petalite from the Iberian massif pegmatites". Presented at Jornadas do ICT, 2021.

Dias, F., Lima, A. (2021). "Quantification of spodumene in thin-sections by crossing cathodoluminescence microscopy with a software of image analysis". Presented at XI Congresso Jovens Investigadores em Geociências, LEG 2021, Estremoz, Portugal, 2021.

Dias, F., Lima, A., Roda-Robles, E., Martins, T. (2023). "Li-exploration and processing: The case study of spodumene from the Barroso-Alvão field, Northern Portugal".

Presented at GAC-MAC-SGA, Sudbury, Canada, 2023. https://doi.org/10.12789/geocanj.2023.50.200.

Dias, F., Lima, A., Roda-Robles, E., Martins, T. (2023). "Textural and mineralogical characterization of one lithium deposit, from the Barroso-Alvão aplite-pegmatite field: preliminary study". Presented at SEG 2023 - Society of Economic Geologists: Resourcing the Green Transition, London, UK, 2023.

Dias, F., Ribeiro, R., Gonçalves, F., Lima, A., Roda-Robles, E., Martins, T. (2023). "Evaluating the purity of the NIST Standard Reference Material 182 (petalite) when compared with the petalite from the Barroso-Alvão field, Portugal". Presented at Mineral Deposits Studies Group 2023, Leicester, UK.

Dias, F., Ribeiro, R., Gonçalves, F., Lima, A., Roda-Robles, E., Martins, T. (2024). “Lithium Aluminosilicate Textures and Lithium Distribution from the Aplite-Pegmatites of Northern Portugal: Outcrop and Drill Core Comparisons”. Presented at PEG2024, Brandon, Manitoba. Publishes in The Canadian Journal of Mineralogy and Petrology. Vol. 00. pp 7-8. https://doi.org/10.3749/AB00032

Dias, F., Ribeiro, R., Gonçalves, F., Lima, A., Roda-Robles, E., Martins, T. (2024). "Impact of using a 3.5 μm film to analyze the chemical composition of crystal samples with a handheld X-Ray Fluorescence equipment". Presented at EGU General Assembly 2024, Vienna, Austria. https://doi.org/10.5194/egusphere-egu24-21098.

Part IV – Final Conclusions

The conclusion summarizes the key findings of this research, emphasizing its contribution to Li exploration. It presents the final conclusions on the effectiveness of LIBS for Li-exploration and the use of K-feldspar as an indicator for distinguishing Li-mineralized pegmatites from barren ones. Additionally, it discusses how K-feldspar geochemistry can help differentiate petalite-rich pegmatites from spodumene-bearing ones and how analyzing the distribution of pegmatites based on their K-feldspar composition provided new insights into Li distribution within the field.

Part V – Future Work and Publication Plan

This section outlines the proposed follow-up studies building on this thesis. It details two planned scientific papers: one investigating advanced mapping techniques for lithium-bearing minerals using cathodoluminescence and LIBS, and another focused on constructing a 3D geological model of the AL56/NOA pegmatite. This section highlights how these studies aim to enhance exploration methods and improve geological understanding of lithium-rich pegmatites.

Part VI – References

This part includes all the bibliographic references cited throughout the thesis. It compiles the scientific literature, data sources, and supporting materials that underpin the research, providing full citations for all works referenced in previous parts.

Part VII – Appendices

This section includes supplementary materials such as tables presenting the LA-ICP-MS and EPMA analyses, as well as additional figures showing the analysis locations on the thin sections, including images under parallel polarized light, crossed polarized light, reflected light, and backscattered electron (BSE) imaging.

3. State of Art

Spodumene was first identified in the Barroso-Alvão Aplite-Pegmatite Field in Noronha (1987). However, its first discovery in Portugal dates back to 1954, at Gelfa Beach, Esposende (Torre de Assunção 1954). The discovery in Barroso-Alvão prompted further research (e.g. Charoy *et al.* 1992, Pires 1995) and a exploration campaign by the Portuguese Geological Survey (Instituto Geológico e Mineiro - IGM) in the late 1990s and early 2000s to evaluate the potential of Li-bearing pegmatites in the region (Farinha Ramos 1998, Farinha Ramos & Lima 2000). These efforts led to additional studies (Lima *et al.* 1999a, Lima *et al.* 1999b, Charoy *et al.* 2001) and a doctoral thesis that examines the geological characteristics of the Alijó, Veral, and Adagói pegmatites located in the study area (Lima 2000).

Later, petalite, another lithium (Li) mineral, was identified in the Barroso-Alvão field (Lima *et al.* 2003), further reinforcing the economic interest in these pegmatites, especially for the ceramics industry. Continued research, including a comprehensive study by Martins (2009), contributed to a broader understanding of the field.

These findings led to the establishment of several mining operations for ceramics in the Barroso-Alvão region, including the Alijó (C-111), Lousas (C-110), and Gondiães (C-108), were established to exploit these resources.

Subsequently, Silva (2014), in a master thesis, applied spatial statistical analysis to study the Barroso–Alvao pegmatite field. The work involved the use of satellite imagery, particularly ASTER (Advanced Spaceborne Thermal Emission and Reflection Radiometer), to identify and interpret spatial relationships between the pegmatites and surrounding geological structures such as shear zones, faults, and granite bodies. The study proposed that the pegmatites were emplaced along dextral shear zones with NW–SE to NNW–SSE orientations.

Later, two additional master theses, Dias (2016b) and Dias (2016a), used stream sediment data from the Barroso–Alvao field collected during the Pires (1995) field campaign. These studies focused on delineating catchment basins enriched in Li and Sn for the purpose of Li exploration, using Geographic Information Systems (GIS). Additionally, they provided an overview of various Li-rich aplite-pegmatites identified in the region.

Interest in Li extraction for battery-grade material gained momentum in 2016, when Dakota Minerals initiated an exploration campaign in petalite-rich pegmatites in the Montalegre region. This marked the beginning of the modern push for Li extraction in Portugal, with Dakota Minerals rebranding as Novo Litio in 2017. The project was later transferred to Lusorecursos Portugal Lithium in 2018 (AgriPro Ambiente Consultores 2021). Around the same time, Savannah Resources PLC launched a project in the Barroso region, targeting spodumene-rich pegmatites near Boticas region (Savannah Resources 2023).

Despite this recent momentum, Li mining in Portugal dates back to the 1920s, when amblygonite was briefly exploited (Lima *et al.* 2011). In the 1970s, mining resumed with the extraction of lepidolite pegmatites for the ceramics sector, a practice that has continued ever since (Sousa *et al.* 2018).

Therefore, Portugal has a long history of mining Li-rich pegmatites, though exclusively for the ceramics industry. The ceramics industry has been seeking sources where feldspar and Li can be mined together, as adding Li minerals to feldspar products lowers the melting point of ceramic materials, resulting in significant energy savings during the manufacturing process (Lima, 2020).

As shown in Figure 3, several Li occurrences have been identified in Portugal. In addition to Gelfa (#1) and Barroso-Alvão (#3), these include: #2-Serra de Arga (Leal Gomes 1994, Pereira & Leal Gomes 2014), #4-Seixoso-Vieiros (Rodrigues 2008, Lima *et al.* 2009), #5-Almendra-Barca d'Alva (Vieira 2010), #6-Queiriga (Puga *et al.* 2003), #7-Gonçalo-Seixo Amarelo (Farinha Ramos 2000, Neiva & Farinha Ramos 2010), #8-Pega-Sabugal (Bravo Silva *et al.* 2007, Neiva *et al.* 2011), #9-Argemela (Charoy & Noronha 1996, Ribeiro *et al.* 2021), and #10 Segura (Antunes *et al.* 2010).

The dominant Li-bearing phase varies among these occurrences: at Gelfa (#1), it is spodumene, found as individual centimetric crystals (up to 10 cm long and 1–2 cm wide), hosted in small pegmatites typically less than 1 meter wide, emplaced within medium- to fine-grained granitic gneiss. In Serra de Arga (#2), petalite and lepidolite are the dominant Li-bearing phases, hosted within aplite-pegmatites emplaced in metasedimentary rocks. In Seixoso–Vieiros (#4), the primary phase is petalite; in Almendra–Barca d'Alva (#5), the dominant Li-bearing phases are spodumene, petalite, and Li-rich muscovite. In Queiriga (#6), the dominant phase is petalite. In Gonçalo–Seixo Amarelo (#7), lepidolite and amblygonite are the main Li-bearing phases; in Pega–Sabugal (#8), the dominant Li-bearing phase is Li-mica; in Argemela (#9), it is

montebrasite; and in Segura (#10), it is lepidolite.(Lima *et al.* 2010, Roda-Robles *et al.* 2018).

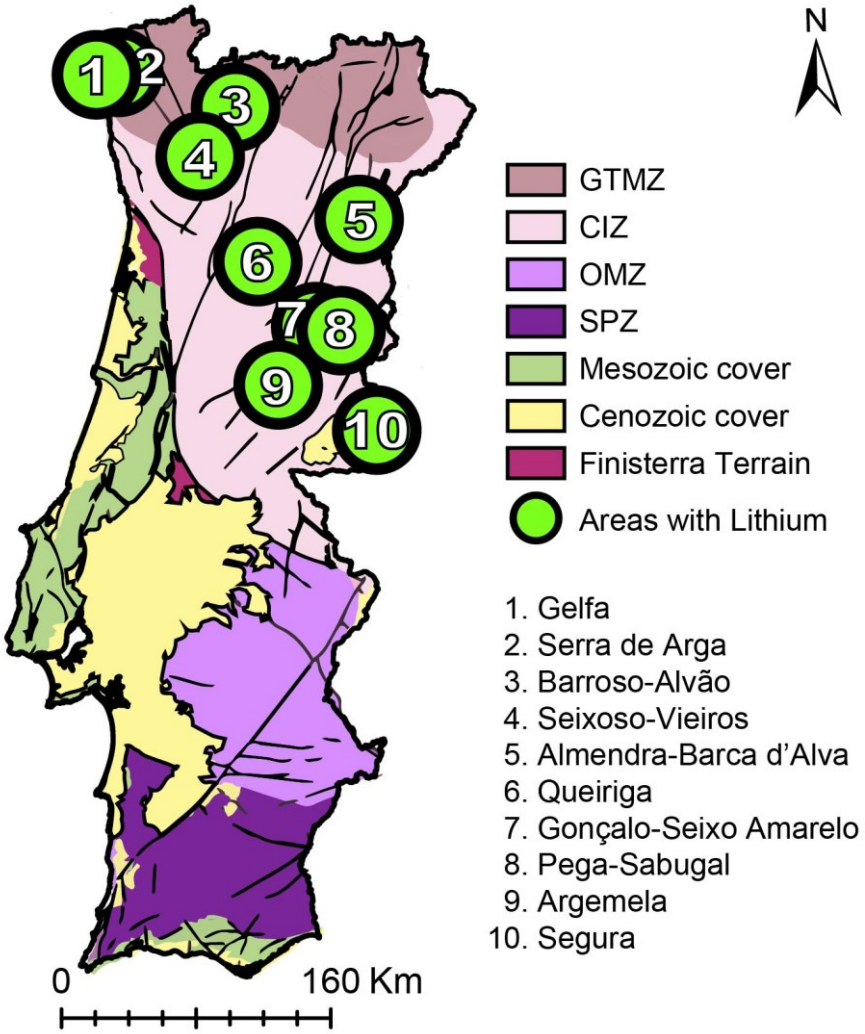

Figure 3. Known Lithium occurrences in Portugal (adapted from Roda-Robles *et al.* (2018), Lima *et al.* (2010) and Rodríguez Fernández *et al.* (2015). GTMZ: Galicia–Trás-os-Montes Zone; CIZ: Central Iberian Zone; OMZ: Ossa-Morena Zone; SPZ: South Portuguese Zone.

4. Variscan Orogeny and its Role in the Mineralization of the Iberian Peninsula

The lithium (Li) mineralization in the Iberian Peninsula is intrinsically linked to the geodynamic, tectonic, and magmatic evolution of the Variscan Orogeny, a major mountain-building event that profoundly shaped Western Europe during the Late Paleozoic. This orogeny resulted from the collision between Laurussia (Laurentia-Baltica) and Gondwana, culminating in the assembly of the supercontinent Pangaea (Ribeiro *et al.* 2007, Martínez Catalán *et al.* 2008, Noronha *et al.* 2013, Noronha 2017).

The Variscan Belt is defined by a series of distinct geotectonic zones that trend roughly E-W, each exhibiting unique paleogeographic, structural, metamorphic, and magmatic characteristics (Noronha 2017). These zones form a discontinuous orogenic belt that stretches across central and western Europe, cropping out in isolated massifs separated by Mesozoic and Cenozoic covers (Ribeiro *et al.* 2007). In the Iberian Peninsula, the Variscan orogen forms the basement of the Iberian Massif, which consists of rocks ranging in age from the Upper Proterozoic to the Carboniferous, and displays a continuous and well-preserved record of orogenic processes (Martínez Catalán *et al.* 2008).

As Martínez Catalán *et al.* (2008) highlights, the Iberian Massif is globally significant due to the exceptional quality and continuity of its outcrops, allowing for detailed analysis of continental crust evolution, lithospheric dynamics, and tectono-metamorphic processes from the latest Precambrian through the Paleozoic. This massif forms part of the extensive Variscan orogenic belt, which streches northward and eastward through central Europe into Poland and continues into Asia. To the south, it extends into northern and northwestern Africa, running parallel to the present-day Atlantic margin. However, at the time of the Variscan orogeny, the Atlantic Ocean had not yet opened. Instead, the landmass now known as North America (then part of Laurentia) lay adjacent to the western edge of the Variscan belt, forming a vast, continuous orogenic system that linked the Variscan belt of Europe with the Appalachian Mountains of eastern North America (Figure 4).

The Variscan Orogeny lasted for approximately 80 million years, from the Late Devonian to the Permian (~370 to 290 Ma), and involved a series of geological processes including crustal shortening, intense deformation, partial melting, oceanic crust and

mantle accretion, and the formation of granitoids (Dias & Ribeiro 1995, Martínez Catalán *et al.* 2008).

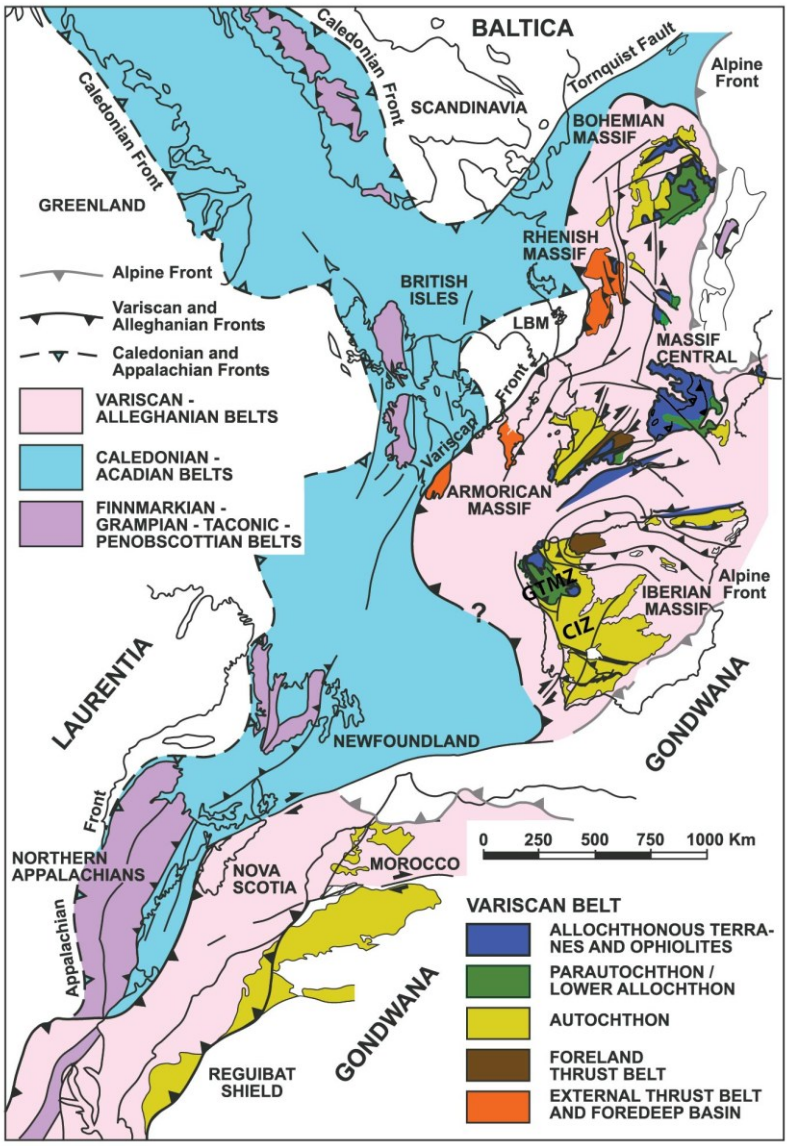

Figure 4. Paleogeographic sketch illustrating the position of Iberia at the end of Variscan convergence, highlighting its connection to the Appalachian, Caledonian, and Variscan orogenic belts within the pre-Atlantic configuration (adapted from Martínez Catalán *et al.* (2007)).

In the NW Iberian Peninsula, particularly in the Central Iberian Zone (CIZ) and the Galiza-Trás-os-Montes Zone (GTMZ), this tectonic activity is reflected in a complex structural and metamorphic record. The CIZ is mainly composed of an extensive sequence of metasedimentary rocks deposited from the Precambrian/Cambrian to the Carboniferous, overlying a pre-Variscan basement. It represents an autochthonous

domain strongly affected by the Variscan deformation and plutonism (Ribeiro *et al.* 2007, Noronha 2017).

The GTMZ, although originally part of the northern Gondwanan margin like the CIZ, followed a distinct tectonic evolution during the Variscan orogeny. It includes both allochthonous and parautochthonous tectonic units that were transported onto the CIZ during continental collision. The parautochthonous units, mobilized at the front of the thrust sheets, consist of metasedimentary sequences ranging from Upper Ordovician to Devonian in age and lie structurally below the main allochthonous complexes (Ribeiro *et al.* 2007, Moreira *et al.* 2011, Sant'Ovaia *et al.* 2011).

Three main deformation phases, D1, D2, and D3, shaped the NW Iberian Variscan belt. As described by Noronha (2017) and Roda-Robles *et al.* (2023), D1 (360–350 Ma) is characterized by WNW–ESE folds and thrusts. Structures from this phase are well-preserved at higher levels but overprinted by later phases. D1 marks the initial stages of crustal thickening and the development of low-grade foliation. D2 (330–320 Ma) represents the peak of orogenic metamorphism, with conditions of ~650–700°C at pressures <5 kbar. This phase generated the main regional schistosity (S2) and caused significant crustal thickening. D3 (320–305 Ma) developed during retrograde metamorphism and gave rise to first-order ductile transcurrent sub-vertical shear-zones with associated S3 foliation, marking the last stage of deformation of the basement.

A significant consequence of the Variscan orogeny was the emplacement of extensive plutonic magmatism, particularly in CIZ and ZGTM. According to Noronha (2017), the granites can be divided into two main types: (1) Two-mica granites, mainly syn-D3 (315–310 Ma), considered S-type granites formed from wet, peraluminous melts at mesocrustal levels. These granites are associated with the cores of thermal domes and the peak of metamorphism (T ~500–550°C; P ~300–350 MPa). They are typically found in the areas with intense Variscan deformation and are characterized by their high peraluminous nature, derived from a metasedimentary source. (2) Biotite granites, which range from syn-D3, to late- and post-D3 (320–305 Ma), or post-D3 (290–280 Ma), originating from deeper crustal levels and related to drier, less evolved melts. Their emplacement coincided with a phase of thermal metamorphism at lower pressures (150–200 MPa).

These granites are closely associated with rare-element pegmatite fields and hydrothermal systems. The mineralizing events linked to these two granite types differ in terms of their metallogenic associations. The two-mica granites are related to the

formation of Li-Sn pegmatites and cassiterite-bearing quartz veins. In contrast, the biotite granites, especially the post-tectonic ones, are associated with W-(Sn) and W-(Mo-Cu-Sn) mineralizations hosted in quartz veins that include oxide and sulfide assemblages (Noronha 1988, Almeida *et al.* 2002, Noronha *et al.* 2006, Noronha 2017).

While this framework integrates both tectonic and petrogenetic criteria, a more detailed geochemical classification, proposed by Villaseca *et al.* (2011) and developed further by Roda-Robles *et al.* (2018, 2022, 2023)), divides the granites into four S-type subgroups and one I-type, emphasizing variations in peraluminosity, phosphorus content, and protolith maturity. This system has been used to interpret the origin of Li-rich aplite–pegmatites, particularly those in the Fregeneda–Almendra region, as derived from highly evolved, P-rich, peraluminous melts.

Applying this scheme to some of the Li occurrences discussed here leads to a reinterpretation of their host granites. According to Noronha (2017), the pegmatites at #7 Gonçalo–Seixo Amarelo, #8 Pega–Sabugal, and #9 Argemela are all hosted in late-tectonic biotite granites, derived from dry magmas emplaced at deeper crustal levels. In contrast, using the Vilaseca/Roda-Robles classification, #7 and #9 would fall into the S4-type group (moderately to weakly peraluminous), while #8 would be hosted by an S2-type granite (highly peraluminous and phosphorus-rich).

Importantly, there is agreement between both classifications regarding most of the syn-tectonic two-mica granites, which correspond to S1-type granites (two-mica leucogranites) in the alternative scheme, reflecting their highly evolved, peraluminous character and similar petrogenetic origin (Figure 5).

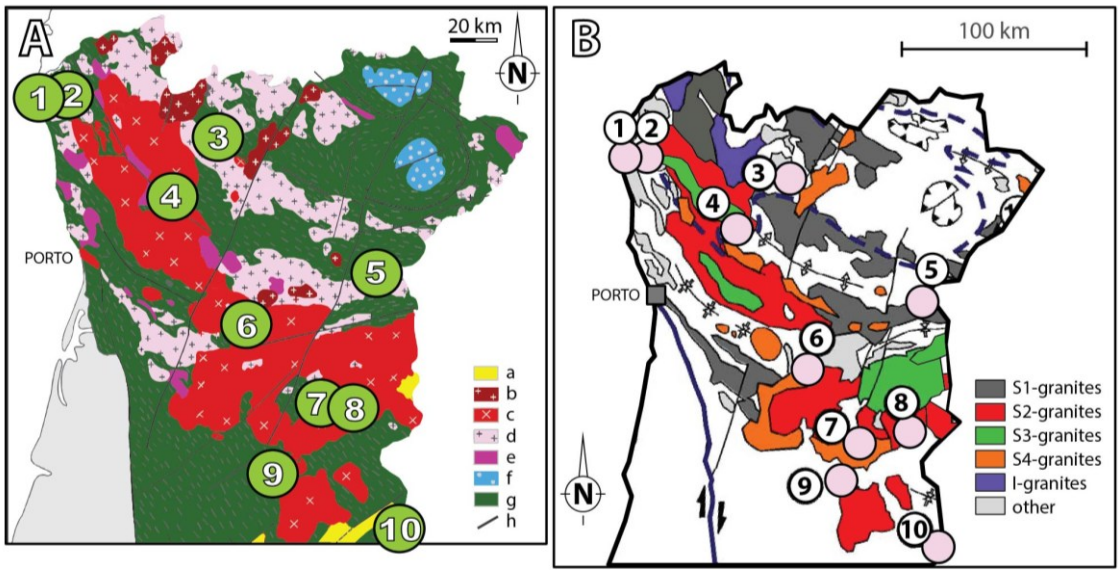

Figure 5. Spatial distribution of Li occurrences and granitic units in northern Portugal, illustrating the spatial association between the Li ocurrences and various granite types. (A) Adapted from Noronha *et al.* (2013) and Lima *et al.* (2010), showing: a. post-Paleozoic rocks; b. post-tectonic biotitic granites; c. late-tectonic biotitic granites; d. Syn-tectonic two-mica granites; e. Syn-tectonic biotitic granites; f. Basic and ultrabasic rocks; g. Metasedimentary rocks; h. Faults and shear zones. (B) Adapted from Roda-Robles *et al.* (2018) showing: S1-granites (two-mica leucogranites), S2-granites (P-rich highly peraluminous), S3-granites (P-poor moderately peraluminous), S4-granites (moderately to low peraluminous), I-granites (low peraluminous), other (other Variscan granites). The locations of the Li occurrences are numbered as follows: 1) Gelfa; 2) Serra de Arga; 3) Barroso-Alvão; 4) Seixoso Vieiros; 5) Alemendra-Barca d'Alva; 6) Queriga; 7) Gonçalo-Seixo Amarelo; 8) Pega-Sabugal; 9) Argemela; 10) Segura.

According to Roda-Robles *et al.* (2016), the Li mineralization in the Iberian Peninsula is mainly associated with pegmatites, but is also found in leucogranitic cupolas and quartz-rich hydrothermal veins. These mineralized pegmatites and veins are widely distributed across Portugal and Spain, particularly in Galicia, northern Portugal, Salamanca, Cáceres, and Badajoz, and are considered part of a common metallogenic province related to Variscan granitic magmatism (Roda-Robles *et al.* 2011, Roda-Robles *et al.* 2016, Roda-Robles *et al.* 2018).

The location and formation of these pegmatites are strongly controlled by the Variscan structural framework. Many pegmatite bodies are spatially and temporally associated with syn- to late-D3 granites and are often emplaced along major tectonic discontinuities. These structures acted as fluid conduits during the late stages of orogeny, facilitating the circulation of aqueous fluids and promoting the formation of rare-element mineralization at shallow crustal levels (Noronha 2017).

In conclusion, the Li-bearing pegmatites and related mineralizations in the Iberian Peninsula are direct geological products of the Variscan orogeny, shaped by a combination of crustal collision, metamorphism, magmatism, and deformation, within a framework of well-preserved orogenic zones that offer a globally important natural laboratory for understanding Paleozoic lithospheric processes.

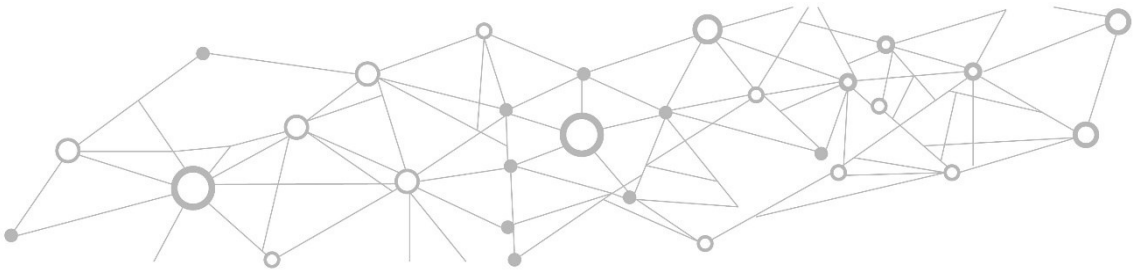

Part II: Materials and Methods

Methodologies

Most of the samples analyzed in this study for the peer-reviewed journal publications were sourced from archival collections (Lima 2000), with the exception of several samples used in petrographic analyses, which originated from the NOA aplite-pegmatite and were kindly provided by Savannah Resources Plc. For the conference presentation chapter, additional samples from the NOA and Reservatório aplite-pegmatites were also supplied by Savannah Resources. Further samples were obtained from various Portuguese pegmatites and form part of the Faculty of Sciences pegmatite collection, curated by Professor Alexandre Lima. The development of the proposed melt-related pegmatite formation model for one of the lithium (Li) deposits in the Barroso–Alvão (BA) field was also made possible through Savannah's permission to study their pegmatite outcrops and drill cores.

For the peer-reviewed journal publications, individual samples of spodumene, petalite, spodumene–quartz mixtures, and K-feldspar crystals were extracted. Each crystal was divided into three or four parts, when its size permitted the removal of a portion for thin-section preparation. Of the three parts, two were milled, while the third was retained in its original form for direct analysis using portable equipment (LIBS/XRF). One portion of the milled material was sent to a certified laboratory for ICP-MS analysis, and the other was used to produce pellets. Figure 6presents a flowchart summarizing the methodology followed in this study.

For the spodumene and petalite samples, the ICP-MS results were uploaded into the LIBS equipment. Each corresponding pellet was then analyzed with LIBS to obtain intensity ratios (IR) for the elements of interest. These IR values were matched with the ICP-MS concentrations, allowing for the construction of calibration curves by plotting IR against concentration for each element. The calibration lines were generated by fitting the best curve to these data points.

After establishing the calibration curves for spodumene and petalite, LIBS analysis was performed on the pellets of spodumene-quartz mixtures to assess how the presence of quartz affected the LIBS results.

For the K-feldspar samples, the ICP-MS results not only served as a comparison for the XRF data but also enabled the study of trace-elements in K-feldspars from different aplite-pegmatites across the Barroso-Alvão field (both mineralized and

non-mineralized). This analysis helped identify their distinct geochemical signatures and understand how their geochemistry varies throughout the field.

The petrographic study was conducted to assess the purity of the samples. For this purpose, regular optical microscopy (using both parallel and crossed polarized light), cold cathodoluminescence, and scanning electron microscopy (SEM) with Backscattered Electron Imaging (BSE) and Energy Dispersive X-Ray Spectroscopy (EDS) were employed to identify and analyze any mineral impurities.

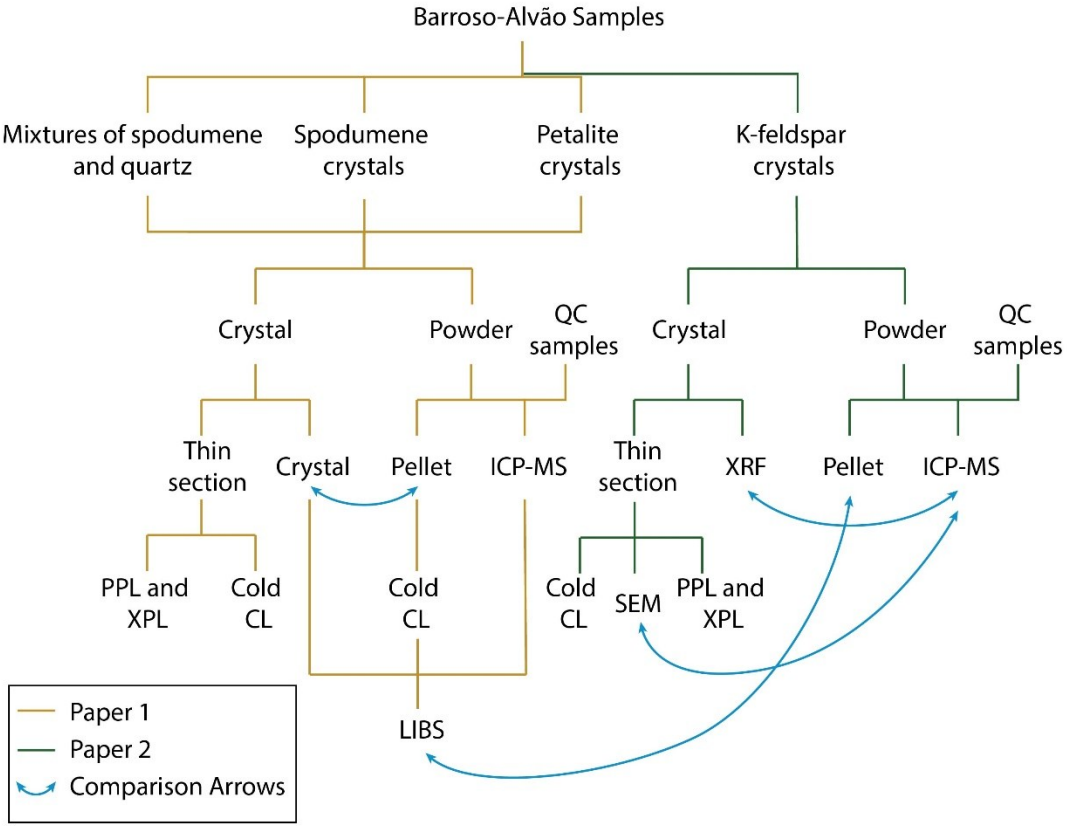

Figure 6. Flowchart outlining the methodology followed in this study for the Peer-Reviewed Journal Publications. Abbreviations: PPL – plane-polarized light; XPL – cross-polarized light; CL – cathodoluminescence; ICP-MS – inductively coupled plasma mass spectrometry; QC – quality control; SEM – scanning electron microscopy.

However, the following description of the analytical techniques represents the full set of methods used in both the peer-reviewed journal publications and the conference presentations:

- Inductively Coupled Plasma Mass Spectrometry (ICP-MS) and Optical Emission Spectroscopy (ICP-OES)

The samples of spodumene, petalite, and K-feldspar from the BA field were sent to Activation Laboratories Ltd. (Actlabs) for ICP-MS/ICP-OES analysis. The process began with sample digestion to break down the minerals and release the elements into solution. After digestion, the resulting solution was split into portions for sequential analysis. One portion was introduced into an ICP-OES instrument, where it was carried by argon gas into a plasma. In the plasma, atoms were excited to higher energy levels and emitted light at characteristic wavelengths as they returned to their ground state. The intensity of this light was measured to quantify elements. ICP-OES is more robust to matrix effects and better suited for major elements, avoiding signal saturation that can occur in ICP-MS. Another portion of the solution was analyzed using ICP-MS, where the argon plasma ionized the atoms, producing positively charged ions. These ions were separated in a mass spectrometer based on their mass-to-charge ratio, enabling the detection of trace elements at very low concentrations. ICP-MS not only provides extremely low detection limits in the sub-parts per trillion (ppt) range but also enables quantitation at the high parts per million (ppm) level. In contrast, ICP-OES is traditionally used for the detection of higher concentrations (Thomas 2004, Winter 2014, Beauchemin 2020).

The primary objective of this analysis was to obtain reference values for the geochemical composition of spodumene and petalite, and to assess the geochemical variations among K-feldspars from aplite-pegmatites based on their Li enrichment, such as spodumene-rich, petalite-rich, and barren varieties.

- Laser Ablation Inductively Coupled Plasma Mass Spectrometry (LA-ICP-MS)

LA-ICP-MS was employed for in-situ analysis of spodumene and cookeite crystals from thin sections of drill cores and outcrops of the pegmatite AL56/NOA. The analyses were carried out at the Universidad del País Vasco (UPV/EHU), Bilbao. This method involved focusing a laser beam onto a small area of the sample, which caused the material to vaporize and form a plasma. The ablated material was then carried into the ICP by an argon gas stream. Once in the plasma, the ions are separated in a mass spectrometer based on their mass-to-charge ratio, similar to traditional ICP-MS. The LA-ICP-MS technique offers high spatial resolution, enabling the analysis of individual mineral grains and providing precise elemental concentrations. This methodology was particularly useful for determining accurate Li concentrations in spodumene from the BA field. These measured values were then integrated with image analysis of

cathodoluminescence (CL) images to calculate bulk Li content based on the modal abundance of spodumene, avoiding reliance on theoretical lithium concentrations, which are rarely observed in natural samples due to common chemical substitutions within the crystal structure (Winter 2014).

- Portable Laser-Induced Breakdown Spectroscopy (pLIBS)

A portable Laser-Induced Breakdown Spectroscopy (LIBS) device (SciAps Z 300) (Figure 7) was used in this study to rapidly identify Li-rich minerals, specifically spodumene and petalite, in the Barroso–Alvão (BA) field. A portion of each sample was analyzed directly in crystal form using the LIBS device, while the remainder was ground and divided: one part was compacted into pellets, and the other was sent to Activation Laboratories (Actlabs) for ICP-MS analysis. The resulting ICP-MS data were matched with the LIBS-analyzed pellets to generate calibration curves using the Profile Builder software from SciAps. This same portable LIBS model has also been applied in other Li exploration studies, such as those by Fabre *et al.* (2021) and Wise *et al.* (2022) highlighting its growing relevance for rapid field-based geochemical analysis.

LIBS is an analytical technique that involves focusing a high-energy laser pulse onto the surface of a sample, causing a minute amount of material to vaporize and form a plasma. This plasma is composed of free electrons, ions, and atoms from the material being analyzed. As the plasma cools and recombines, it emits light at specific wavelengths corresponding to the characteristic emission lines of the elements present. The emitted light is captured by a spectrometer and dispersed into a spectrum. By analyzing this spectrum, the elements can be identified and their concentrations estimated (Cremers & Radziemski 2006).

Figure 7. Portable LIBS equipment (Sciaps Z300) used for this study.

- Portable X-Ray Fluorescence (pXRF)

In this study, K-feldspar samples were analyzed using a portable X-ray Fluorescence (pXRF) device (Bruker S1 Titan 600) to assess its effectiveness in geochemical characterization and its utility for rapidly identifying Li-rich pegmatites in the field (Figure 8).

The pXRF technique irradiates solid samples with high-energy X-rays, exciting inner-shell electrons. As the electrons return to their ground state, they emit element-specific fluorescent X-rays, which are diffracted and detected to generate a spectrum used to calculate the sample composition (Winter 2014).

XRF has long been a standard method in geochemistry for bulk analysis of rocks and minerals, offering good accuracy and detection limits down to 1 ppm for major elements. Although initially limited to laboratory instruments, the development and widespread use of portable handheld pXRF devices have enabled fast, non-destructive in-situ analysis (e.g. Brand & Brand 2014, Newlander *et al.* 2015, Young *et al.* 2016, Declercq *et al.* 2019, Ribeiro *et al.* 2021, Zhou *et al.* 2022). These systems automate

data acquisition and processing, allowing real-time geochemical characterization and reducing the need for laboratory-based analysis (Reed 2005; Winter 2014).

To validate pXRF performance in the field, results were compared with ICP-MS analyses performed at Activation Laboratories (Actlabs).

Figure 8. Portable X-Ray Fluorescence (pXRF) device (Bruker S1 Titan 600) used in this study for geochemical analysis of K-feldspar samples, demonstrating its effectiveness for rapidly identifying Li-rich pegmatites in the field.

- Scanning Electron Microscopy (SEM)

A Scanning Electron Microscope (SEM) was used to analyze the composition of mineral samples with high spatial resolution. The SEM operates by directing a focused electron beam onto the sample. Beam electrons interact elastically and inelastically with the specimen, producing a range of emissions, such as backscattered electrons (BSE), secondary electrons, characteristic X-rays, and cathodoluminescence (CL) radiation, which can be captured by dedicated detectors to provide different types of information (Goldstein *et al.* 2003). In BSE imaging, signal intensity varies with the atomic number of the elements: elements with lower atomic numbers reflect fewer electrons and appear darker, while those with higher atomic numbers reflect more and appear brighter in the image.

Energy-dispersive X-ray spectroscopy (EDS) was used for qualitative and semi-quantitative elemental analysis. In EDS, the incident electron beam ejects inner-shell electrons from atoms in the sample, creating vacancies that are filled by electrons from

higher energy levels. The resulting energy difference is emitted as characteristic X-rays, which are unique to each element. The detector measures the energy of each X-ray photon, creating a spectrum where each peak corresponds to a specific element. The software then analyzes the spectrum to estimate the elemental composition, either qualitatively or semi-quantitatively (Goldstein *et al.* 2003, Reed 2005).

SEM-CL (cathodoluminescence performed in a SEM) was also used to compare with optical microscopy cold-CL. SEM can be equipped with a dedicated CL detector allowing precise imaging of cathodoluminescence at micrometer or sub-micrometer scale. SEM-CL uses a focused, high-energy, scanned electron beam, producing high-resolution images. Similarly to hot-CL, the electrons in SEM-CL are generated from a heated filament and thus has higher sensitivity than cold-CL, enabling better imaging of low-intensity luminescence (Pagel *et al.* 2000, Götze & Kempe 2008, Edwards & Lee 2014).

SEM analyses were performed using a Hitachi FlexSEM 1000 equipped with the Bruker QUANTAX 80 EDS system and XFlash 630H silicon drift detector at the University of Porto, Faculty of Sciences, Department of Geosciences, Environment, and Spatial Planning, Portugal (Figure 9).

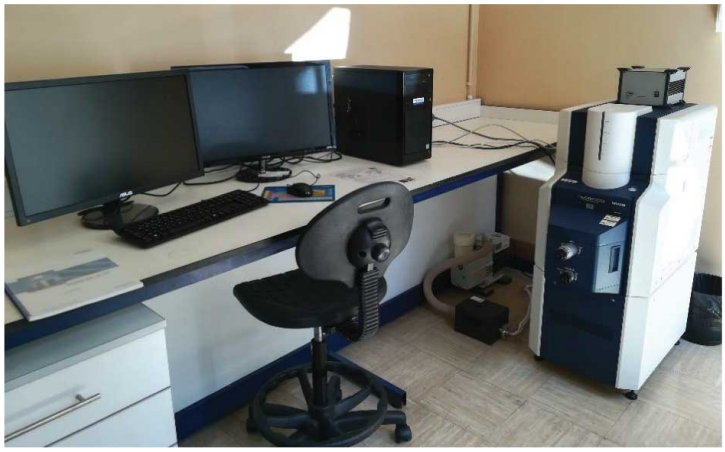

Figure 9. Hitachi FlexSEM 1000 Scanning Electron Microscope (SEM) equipped with a Bruker QUANTAX 80 EDS system and XFlash 630H silicon drift detector, used in this study at the University of Porto, Faculty of Sciences, Department of Geosciences, Environment, and Spatial Planning (Portugal).

- Optical Microscopy Cold-Cathodoluminescence

Returning to cathodoluminescence (CL) after its mention in the context of Scanning Electron Microscopy (SEM), a more detailed explanation follows.

Luminescence can be broadly classified by its excitation mechanism, including photoluminescence, thermoluminescence, X-ray luminescence, triboluminescence, chemoluminescence, and cathodoluminescence (CL). Specifically, CL is the emission of low-energy (IR, visible, or UV) photons from a solid material when stimulated by electron irradiation (Götze & Kempe 2008, Edwards & Lee 2014).

This light emission is a result of electron–matter interactions: the impacting electrons excite electrons within thecrystal lattice of the material to a higher energy state. When these excited electrons subsequently return to a lower (or ground) energy state, the excess energy is released in the form of a photon (light). The precise characteristics of this emitted light, its wavelength, intensity, and stability, are fundamentally determined by the crystal structure of the material, trace-element composition, and the presence of luminescence activators like Manganese (Mn) and/or quenchers like Iron (Fe) (Pagel *et al.* 2000).

CL can be generated using several electron-beam instruments, including SEMs, Electron Microprobes (EPMAs), and optical microscopes equipped with an electron gun. Crucially, although the fundamental excitation mechanism is the same across all instruments, the resulting images and data differ significantly based on the equipment used; hence, optical-microscope CL systems are distinct from SEM-CL. As detailed by Götze & Kempe (2008), these instrumental differences lead to variations in CL colours, intensities, contrast behaviour, and phosphorescence effects, meaning that SEM-CL, cold-CL, and hot-CL offer complementary, yet non-equivalent, information.

Cold-CL and hot-CL imaging use optical microscopes and, unlike SEM-CL, produce true-color images, although with lower spatial resolution. Between the two optical methods, hot-CL employs elevated temperatures, resulting in significantly higher CL intensity than cold-cathode instruments, which makes it particularly useful for investigating weakly luminescent materials (Götze & Kempe 2008).

In this study, cold-CL optical miscrosopy was performed using a CITL CCL 8200 MK4 system, coupled to a Nikon OPTIPHOT-POL microscope, to validate the purity of the petalite samples in the LIBS calibration paper. CL was used to assess the response of milled petalite-rich pegmatites, compare the CL characteristics of spodumene and petalite crystals from the Barroso-Alvão field, and evaluate the response of milled RC from areas with varying Li content. Additionally, CL was tested for its efficiency in combination with image analysis software to quantify spodumene in thin-sections. The equipment is located in the microscope lab of the Department of Geosciences,

Environment, and Spatial Planning (Departamento de Geociências, Ambiente e Ordenamento do Território) at the Faculty of Sciences, University of Porto (Faculdade de Ciências da Universidade do Porto), Portugal (Figure 10).

Figure 10. Cathodoluminescence (CL) system: CITL CCL 8200 MK4 with Nikon OPTIPHOT-POL microscope (University of Porto, Faculty of Sciences). Used to verify petalite purity, compare CL features of spodumene and petalite, and explore CL-based image analysis for spodumene quantification.

- Electron Microprobe Analysis (EPMA)

Electron Probe Microanalysis (EPMA) which was used to precisely determine the concentration of silicon (Si) in spodumene and cookeite samples from the Barroso–Alvão (BA) field, was a necessary step for subsequent LA-ICP-MS analysis. EPMA is a technique that chemically analyzed small, localized areas by focusing an electron beam to excite X-rays. The emitted X-ray spectrum contains lines characteristic of each element, allowing for quantitative determination of elemental concentrations through comparison with known standards. The method provides high analytical accuracy, typically within 1% relative error, and detection limits in the tens of ppm. Spatial resolution is generally limited to about 1 μm due to beam interaction volume within the sample (Goldstein *et al.* 2003, Reed 2005).

The EPMA measurements were performed using a JEOL JXA 8500-F at the National Laboratory of Energy and Geology (LNEG) in S. Mamede de Infesta, Porto, Portugal (Figure 11). Elemental quantification was achieved using a set of well-characterized standards, selected according to the elements present in each specific analysis. The standards used included: albite (Na), apatite (Ca), orthoclase (Si, Al, K), YPO_4 (Y), Fe_2O_3 (Fe), synthetic glass (Rb, Cs), PbS (Pb), ZnS (Zn), $BaSO_4$ (Ba), $MnTiO_3$ (Mn, Ti), CaF_2 (F), vanadinite (Cl), Cr_2O_3 (Cr), celestite (Sr), and SnO_2 (Sn). These

standards ensured reliable calibration and accuracy across the suite of elements analyzed.

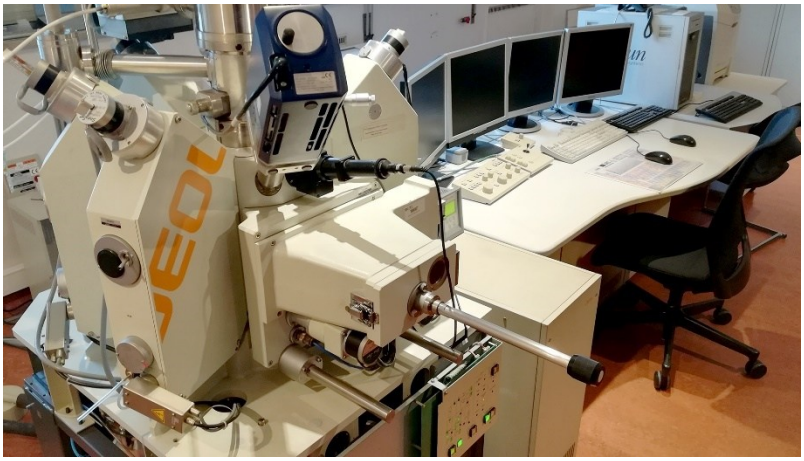

Figure 11. JEOL JXA 8500-F electron microprobe used for EPMA analyses at the National Laboratory of Energy and Geology (LNEG) in S. Mamede de Infesta, Porto, Portugal. This instrument was employed to determine the concentration of silicon (Si) in spodumene and cookeite samples from the Barroso–Alvão field in preparation for LA-ICP-MS analysis.

- X-Ray Diffraction (XRD)

To investigate the mineralogical composition of SRM 182 (petalite), a small quantity of the reference material, as it was received from the supplier, was sent to the National Laboratory of Energy and Geology (LNEG), located in S. Mamede de Infesta, Portugal. X-ray powder diffraction (XRD) was performed using a Panalytical XPERT-PRO diffractometer (Figure 12)The aim was to confirm the presence of additional mineral phases, such as spodumene or quartz, in the SRM 182 material, since cathodoluminescence performed on a pellet from this material had shown minerals with strong luminescence that could not be petalite.

The XRD technique is particularly valuable for identifying and characterizing crystalline minerals based on their diffraction patterns. When X-rays are directed at a powdered sample, the crystal lattice of the minerals causes the X-rays to diffract at specific angles, which are characteristic of the atomic arrangement of the minerals. These diffraction patterns produce a series of peaks, each corresponding to a unique set of planes within the crystal. The positions, intensities, and shapes of these peaks can be compared with standard mineral databases to identify specific minerals and phases present in the sample. This allows for precise mineralogical identification, even if the minerals are present in low concentrations (Cullity & Stock 2014).

Figure 12. X-ray powder diffraction (XRD) setup used for the mineralogical characterization of SRM 182 at the National Laboratory of Energy and Geology (LNEG), S. Mamede de Infesta, Portugal. The instrument shown is a Panalytical Diffractometer XPERT-PRO, equipped with a PW3050/60 goniometer, with a Theta-2Theta geometry and X-ray tube with a copper (Cu) anticathode.

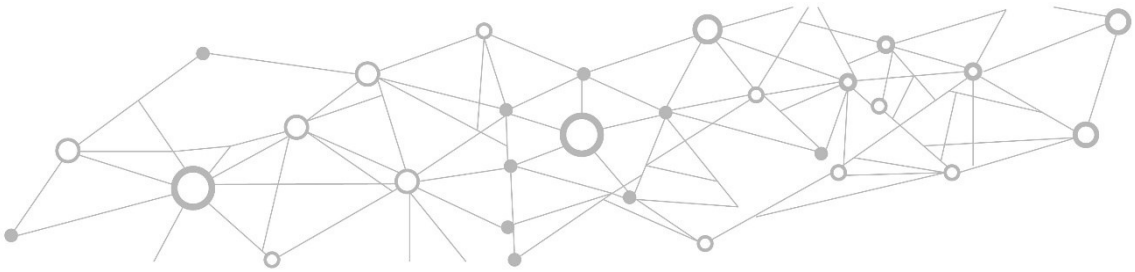

Part III - Results and discussion

Chapter I: Peer-Reviewed Journal Publications

Chapter II: Conference Proceedings and Presentations

Chapter I: Peer-Reviewed Journal Publications

---

1. Calibrating a Handheld LIBS for Li Exploration in the Barroso–Alvão Aplite-Pegmatite Field, Northern Portugal: Textural Precautions and Procedures When Analyzing Spodumene and Petalite

Adapted from: Filipa Dias, Ricardo Ribeiro, Filipe Gonçalves, Alexandre Lima, Encarnación Roda-Robles and Tânia Martins

Minerals (2023) 13, 470. https://doi.org/10.3390/min13040470

Published: 26 March 2023

Abstract

In pegmatites containing abundant petalite and spodumene, such as those from the Barroso–Alvão (BA) aplite-pegmatite field, calibrating a portable laser-induced breakdown spectroscopy (pLIBS) equipment to identify and analyze these minerals may be challenging. Forty-nine samples of spodumene, petalite and spodumene + quartz were collected from 22 aplite-pegmatites from the BA field and sent for inductively coupled plasma-mass spectroscopy analysis. One calibration for both spodumene and petalite has been proven to be impossible since almost all the LIBS intensity ratios, including for Li, overlapped on both minerals. Thus, three calibrations were developed: one qualitative to distinguish both minerals and two more quantitative, specifically made for each mineral. The first LIBS calibration only has Fe since it is the sole element with intensity ratios different enough to distinguish both minerals. Eleven calibration lines were created: Li, Al, Si, Be, Na, P, K, Mn, Fe, Rb and Cs; however, only the Li, Al, and Si have consistent errors below 20%. Thin sections were produced and observed with optical microscopy and cathodoluminescence (CL) to control the purity and mineral

paragenesis of the samples. The petalite pellets were also controlled with cold CL since petalite crystals often present fine spodumene and quartz inclusions.

1.1. Introduction

The rising market of the lithium (Li) batteries used in a wide variety of products, from electric cars to smartphones and laptops, is feeding a crescent Li demand, increasing the risk of Li supply failure and skyrocketing the Li prices (IEA 2021). The mining and exploration companies keep investing in Li exploration to find new deposits and try to meet this demand. Exploration tools such as handheld laser-induced breakdown spectroscopy (LIBS) are practical field tools that quantify Li and identify Li mineralization in a short-time analysis, requiring less than 5–10 s. However, for LIBS to work properly and provide reliable results, it requires calibrations with high accuracy and precision specifically made for each type of mineral that will be analyzed. Theoretically, each pegmatite field has its own geochemical signature, meaning that the same mineral can have slight differences in the crystal matrix shared by all the aplite-pegmatites of the same field. This study considers the necessity of a specialized calibration using the example of one of the Li deposits with the most potential in Western Europe, the Barroso–Alvão (BA) aplite-pegmatite field, in Northern Portugal, which contains a large quantity of two Li minerals: spodumene ($LiAlSi_2O_6$) and petalite ($LiAlSi_4O_{10}$).

Our study found that using one calibration for both spodumene and petalite does not provide accurate results for either mineral. However, thanks to Fe, one of the trace elements of spodumene, it was possible to develop three different calibrations and successfully analyze both minerals: calibration 1 (Fe_Barroso) to distinguish spodumene from petalite, and calibrations 2 (Pet_Barroso) or 3 (Spd_Barroso) to measure the lithium content and the other constituent elements of petalite (pet) and spodumene (spd).

1.2. Geological Setting

The Barroso–Alvão aplite-pegmatite field is located in the Northwest of the Iberian Peninsula, where hundreds of aplite-pegmatites, some spodumene-rich, other petalite-rich and Li-barren can be found mixed and without an apparent regional zonation (Figure 13).

The aplite-pegmatites are emplaced in Silurian metasediments from the parautochtonous units of the Galiza Trás-os-Montes Zone (GTMZ). The GTMZ tectonic setting is due to the Variscan Orogeny (370 to 290 Ma), defined by a succession of three main deformation phases D1, D2 and D3, where the maximum metamorphic conditions correspond to the andalusite zone (Charoy & Noronha 1999b). The emplacement of some aplite-pegmatites is controlled by the D2 and can be locally deformed by D3 (N130° and NS to N10°), whereas others have their emplacement controlled by D3. Therefore, the emplacement of the pegmatitic melt seems to have been ante- to sin-D3, with regional metamorphic conditions of 300 to 350 MPa, and temperatures reaching 500–550 °C (Ribeiro 1998). Some aplite-pegmatites appear to have filled sub-horizontal and sub-vertical weakness zones, such as shear zones, and can be found parallel to each other in echelon-like structures.

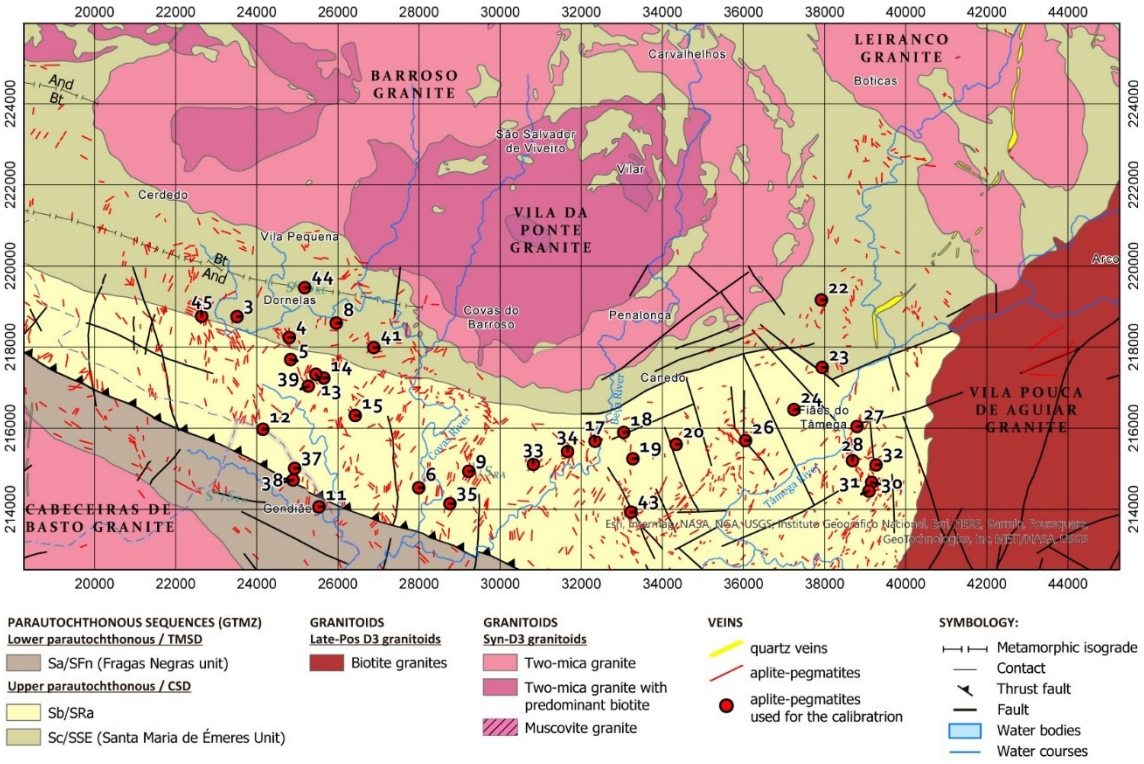

Figure 13. Geologic map of the Barroso–Alvão aplite-pegmatite field with the location of the pegmatites used for the LIBS calibrations (red dots). Coordinates system: ETRS 1989 Portugal TM06. Adapted from Rodríguez Fernández *et al.* (2015), Agência Portuguesa do Ambiente and (Agência Portuguesa do Ambiente), Sant'Ovaia *et al.* (2011) and Ribeiro *et al.* (2000). © Agência Portuguesa do Ambiente (APA). Available online: https://sniamb.apambiente.pt/content/geo-visualizador (accessed on 19 July 2022).

1.3. Spodumene and Petalite Petrography

The shear zones, besides being able to control the aplite-pegmatites emplacement, can also affect their Li mineralogy, Li distribution and mineralogical texture. Therefore, the shear zones may form alignments of fine mixtures of spodumene + quartz, corresponding to Li-rich zones where Li has been concentrated both in spodumene-rich and petalite-rich aplite-pegmatites. These fine-grained mixtures can be difficult to identify as two different minerals since they look homogenous to the naked eye (Charoy *et al.* 1992, Lima 2000, Martins 2009, Noronha *et al.* 2013, Dias 2016b, Lima & Dias 2019). The breakdown of petalite into spodumene + quartz (SQI—Spodumene Quartz Intergrowth) is also a common phenomenon in the petalite-rich aplite-pegmatites of the BA aplite-pegmatite field.

Currently, it is assumed that not all the aplite-pegmatites from the BA field are coetaneous (Martins *et al.* 2005). At least two different pulses of crystallization have been recognized. Lithium- aluminosilicates (spodumene and petalite) have been found in aplite-pegmatites belonging to the two pulses, with different textural relationships among them. Three generations of spodumene and two of petalite have been found (Figure 14). The first generation of spodumene is primary (Figure 14, example 1) and occurs in the aplite-pegmatites crystallized during the first pulse. The associated pegmatitic melt was Sn-poorer and Fe-richer than the next pulse of melt that formed aplite-pegmatites containing primary petalite (Figure 14, example 2). These later aplite-pegmatites present a significant amount of cassiterite, which was mined for Sn during World War II. Now they are commonly found as old mining works that left narrow holes in the landscape in the place where the aplite-pegmatites outcropped. A second generation of petalite can also be found surrounding other minerals from the matrix of aplite-pegmatites, including primary spodumene (Charoy *et al.* 2001, Dias 2016b) (Figure 14, example 1B). The second generation of spodumene is the spodumene and quartz intergrowths formed through the breakdown of the primary petalite (Figure 14, example 2A–C). Later, a third generation of spodumene (subsolidus) was formed favored by regional deformation and can be found in aplite-pegmatites belonging to the two pulses as alignments of fine aggregates of spodumene and quartz or acicular crystals of spodumene (<100 μm) growing around crystal contacts or crosscutting other crystals (Figure 14, example 1A and Figure 14, example 1D).

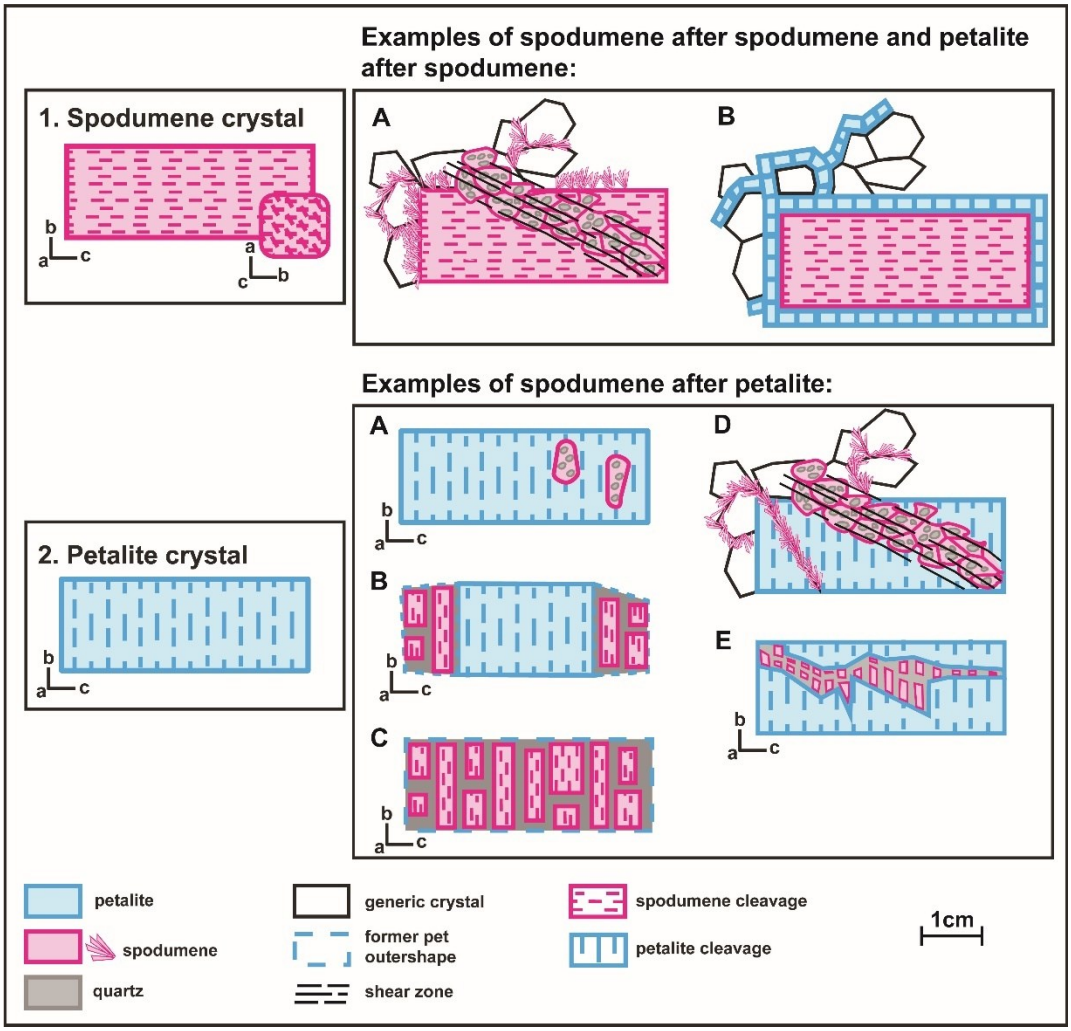

Figure 14. Examples of the distinct spodumene and petalite textures found in the aplite-pegmatites of the Barroso–Alvão pegmatite field

1.4. Materials and Methods

Forty-nine samples were used for the LIBS calibration with crystals collected from the BA aplite-pegmatite field: B—petalite; C—spodumene; and D—mixtures of spodumene and quartz.

The samples were retrieved from 22 aplite-pegmatites from Li-barren and Li-rich aplite-pegmatites containing spodumene and/or petalite. There was a total of 15 petalite crystals from 9 aplite-pegmatites, 19 spodumene crystals from 11 aplite-pegmatites, and 14 mixtures of spodumene and quartz from 9 aplite-pegmatites. Some of these aplite- pegmatites contributed to all three types of crystal samples: B, C and D.

All the crystal samples were photographed and divided into three parts: 1/3 was kept in crystal form (

Figure 15) and the other 2/3 were milled with a mortar grinder Retsch Mortar Grinder RM 200 (Retsch GmbH, Haan, Germany) and sifted with a Retsch Test Sieve (Retsch GmbH, Haan, Germany) to <125 µm of grain size. From the sifted sample, 1⁄2 was pressed with the hydraulic press Specac Atlas Manual (Specac Ltd., Orpington, England) at 10 tons during 45 s into 13 mm diameter pellets (0.6 to 0.7 g) (Figure 16). The other 1⁄2 was sent to the certificated laboratory ActLabs, in Ancaster, ON, Canada, to be analyzed using inductively coupled plasma mass spectrometry (ICP-MS). To control the quality of the Actlabs results, we also sent (with other names) two duplicates (one of a spodumene crystal and another of a mixture of the spodumene and quartz), two blanks (hydrothermal quartz from the Panasqueira mine) and a Standard Reference Materials (SRM): NIST SRM 182—Petalite.

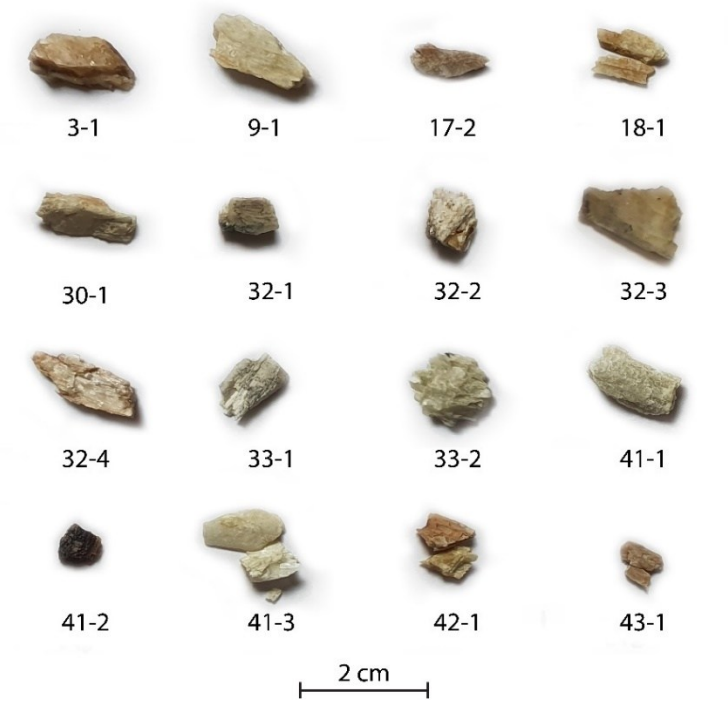

Figure 15. Spodumene crystals (after dividing them into three parts) from the aplite-pegmatites: 3, 9, 17, 18, 30, 32, 33, 41, 42 and 43 (the numbers after the dash correspond to the identification number of the crystal collected from each aplite-pegmatite, since sometimes more than one crystal was collected from the same aplite-pegmatite).

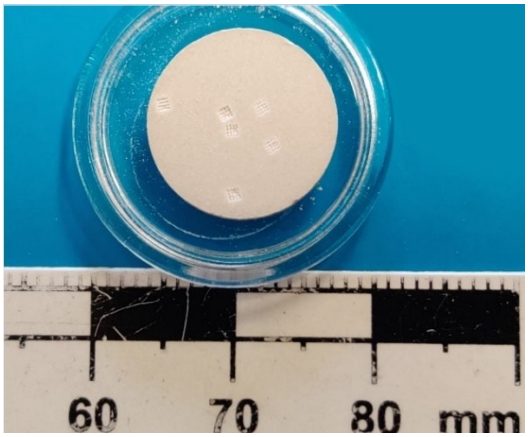

Figure 16. Spodumene pressed pellet used for the LIBS calibration.

The Al, Li, K and Si results from ICP-MS used for the pLIBS calibration were from sodium peroxide fusion (Actlabs package: Ore-Assays—8-Peroxide ICP-OES + ICP-MS), where the ActLabs procedure consisted in fusing the samples in a zirconium crucible, dissolving them in purified water, acidifying them with concentrated nitric and hydrochloric acids, and analyzing them with an ICP-MS and ICP-OES (inductively coupled plasma optical emission spectrometry). As QA and QC, ActLabs also prepared and analyzed a duplicate at each 10th sample, and a blank at every 30th sample.

The As, Be, Cs, Ca, Fe, Ga, Mn, Na, Nb, Ni, P, Pb, Rb, Sn, Sr, Ta, Tl, U and Zn results from ICP-MS were obtained by digesting the samples with four acids (HF, HClO4, HNO_3 and HCl), (package: 4-Acid “Near Total” Digestion—UT-6M). According to ActLabs, the digestion of the samples started with hydrofluoric, followed by a mixture of nitric and perchloric acids, and after heating the samples to incipient dryness, they were brought back into solution using aqua regia. Only then were the samples analyzed with ICP-MS.

When the selected crystals from the BA aplite-pegmatite field were sufficiently large (>2 × 1 cm), a fourth piece was saved to produce thin sections and check the sample purity.

Thus, six thin sections were made: four petalites (from the aplite-pegmatites 5, 38, 41 and 44) and two mixtures of spodumene and quartz (from the aplite-pegmatites 4 and 8). No pure spodumene crystal was made into a thin section due to their smaller size.

The thin sections and all the petalite pellets were observed under cold-cathodoluminescence (CL) microscopy with a cold cathode electron gun Citl Mk 4 coupled to a Nikon OPTIPHOT- POL polarizing microscope. The goal was to verify the purity of the petalite pellets since petalite and spodumene are often found together in the BA field. CL can easily show spodumene next to petalite since their luminescence intensity is very different, even if the material is milled into fine powders. As much as 5 kV in CL is sufficient to see the bright luminescence of spodumene; however, see the dark blue luminescence of petalite, the voltage must be increased to 9–10 kV.

The observations from CL led to an X-ray diffraction (XRD) analysis on the NIST SRM 182 (petalite) performed at the National Laboratory of Energy and Geology (LNEG, São Mamede de Infesta, Portugal), with a Panalytical Diffractometer XPERT-PRO, equipped with a PW3050/60 goniometer, with a Theta-2Theta geometry and X-ray tube with a copper (Cu) anticathode.

The ICP-MS chemical results from ActLabs were uploaded to our handheld SciAps Z-300 LIBS in a .csv file using the software Profile Builder to build the calibration curves to analyze the samples.

The LIBS equipment SciAps Z-300 analyzes the samples by focusing a pulsed laser (5 mJ per pulse, 1064 nm Nd:YAG laser) on its surface and forming a plasma that vaporizes small spots of the sample in an atmosphere of Argon (10–11 psi). A portion of the plasma light (emitted by excited atomic and ionic species in the plasma) is then directed into the inbuilt spectrometer system (with a resolution of 190–950 nm) that disperses the light and records the emission signals producing a spectrum. Most elements have at least a few strong emission lines and the wavelengths of those emission lines are the identification parameters. The location of the emission lines at specific wavelengths, the intensity of the lines and the relative intensities of the lines is what is used to analyze the spectrum to determine the composition of the sample after creating the calibration curves [17,18].

The acquisition settings for the calibration were the following: 12 locations (4 locations by 4 locations, total size of the area analyzed = 0.5 × 0.5 mm), spot size of 50 µm, 1 clean shot per location, 4 data shots per location, test rate of 10 Hz.

1.4.1. Construction of Calibration Lines for the Handheld LIBS

The following tables contain the data from the ICP-MS analysis uploaded in the handheld LIBS to produce the calibration lines used in the Spd_Barroso calibration (Table 1) to analyze spodumene, Pet_Barroso calibration (Table 2) to analyze petalite and Fe_Barroso calibration (Table 1 and Table 2) to use in case of not knowing whether the mineral is spodumene or petalite.

For each calibration, three shots were performed in the same spot for each pellet to avoid surface contamination. The 3rd shot of each sample was used to create the calibration lines for the chemical elements detected both in ICP-MS and LIBS in spodumene and petalite: Li, Al, Si, Be, Na, P, K, Mn, Fe, Ga, As, Rb, Sr, Nb and Sn.

The calibration lines were produced by plotting each sample in an XY-chart with the ICP-MS concentration against the Intensity Ratio (IR) of that element in the spectra.

In the LIBS spectra, each chemical element displays certain peaks at specific wave- lengths with different intensities. The IR was calculated by dividing the total area of the peaks by the total area of all the peaks in the spectra. For example, Li in the spectra of spodumene and petalite has three main peaks (610 nm, 670 nm and 810 nm). The sum of the area of the three peaks divided by all the peaks in the spectra is equal to the IR of Li in the sample.

Theoretically, less concentration should result in a lower IR and a higher concentration in a higher IR.

.

Table 1. Geochemical results of spodumene (spd) from the ICP-MS used on the “Spd_Barroso” and “Fe_Barroso” calibrations of the portable LIBS

	3 spd 1*	3 spd 2	9 spd 1	17 spd 1	17 spd 2	18 spd 1	30 spd 1	32 spd 1	32 spd 2*	32 spd 3	32 spd 4*	33 spd 1	33 spd 2	34 spd 1	41 spd 1	41 spd 3	41 spd 4	42 spd 1
Si %	22.00	26.30	30.00	28.10	29.30	27.90	29.40	26.60	29.30	31.70	29.90	27.70	26.70	29.70	28.30	28.70	32.50	30.30
Al %	12.70	12.70	13.80	14.30	12.40	12.40	14.00	13.60	13.20	14.60	13.50	15.10	12.30	13.70	12.40	12.30	15.00	12.70
Li %	3.06	3.08	3.32	3.08	2.73	2.73	3.14	3.26	2.32	3.52	2.67	2.38	2.81	3.23	2.77	2.79	3.35	2.93
K %	0.30	0.30	0.30	0.70	0.50	0.30	0.50	0.30	1.10	0.40	1.10	0.70	0.40	0.40	0.50	0.60	0.70	0.30
Fe %	0.17	0.19	0.33	0.09	0.25	0.38	0.27	0.22	0.26	0.19	0.27	0.25	0.18	0.20	0.14	0.15	0.25	0.33
Na %	0.10	0.11	0.08	0.10	0.12	0.17	0.09	0.04	0.51	0.12	0.45	0.08	0.14	0.08	0.20	0.11	0.27	0.07
Mn ppm	237	225	238	484	602	323	259	165	172	229	184	297	339	216	166	182	269	214
Sn ppm	209	194	57	8	19	21	7	4	12	5	40	147	43	13	11	7	13	6
P ppm	110	840	490	410	490	680	480	100	350	200	380	80	610	30	360	90	170	340
Be ppm	105	108	8	7	25	21	8	7	8	5	4	13	8	8	11	11	14	12
Ga ppm	11	12	14	14	15	12	11	9	15	12	16	20	17	15	17	17	19	14
Nb ppm	9	9	18	2	3	6	1	1	6	2	7	3	14	12	6	5	6	5
Ta ppm	9	8	1	1	1	1	0	0	5	0	3	7	6	7	1	1	2	1
Zn ppm	5	5	20	20	10	40	30	20	90	5	30	60	70	20	40	50	60	20
Rb ppm	4	5	7	71	60	13	36	2	131	19	181	54	50	21	67	92	88	7
Sr ppm	3	3	24	12	34	37	1	0	6	0	1	2	106	1	3	2	8	2
Cs ppm	3	3	1	3	8	2	2	0	7	1	6	15	4	2	7	12	23	1
As ppm	1	0	4	1	2	6	3	1	2	2	1	5	1	0	1	0	1	5
Ni ppm	0	0	1	4	3	6	2	3	1	1	2	13	2	3	2	1	3	12
U ppm	0	1	1	0	1	1	5	1	3	1	3	3	2	5	2	2	4	0

Some of these aplite-pegmatite names are already known from previous works with other names: 32-Adagói, 33-Aldeia, 34-Alijó and 41-NOA (Lima 2000, Charoy *et al.* 2001, Dias 2016a, Dias 2016b, Tucker Vasques 2021)

Samples with possible mineral contaminations or error during sample analysis indicated by the following anomalies:

*3-1: duplicate sample of the 3-2. 3-1 has a negative anomaly in the Si-content and an enormous difference in P.

*32-2: positive anomaly in the Na-content

*32-4: positive anomaly in the Na-content

Table 2. Petalite (pet) chemical results from the ICP-MS (inductively coupled plasma mass spectrumetry) used on the "Pet_Barroso" and "Fe_Barroso" calibrations of the portable LIBS (laser-induced breakdown spectroscopy).

	5 pet 1	5 pet 2	14 pet 1	37 pet 1	37 pet 2	38 pet 1	39 pet 1	39 pet 2	39 pet 3	41 pet 1	41 pet 2	44 pet 2
Si %	34.30	28.50	34.40	35.40	24.10	34.90	32.90	29.50	24.30	27.80	23.20	35.40
Al %	8.65	8.80	9.68	8.84	9.14	8.97	8.70	8.73	8.70	8.57	8.73	8.77
Li %	2.24	1.98	2.15	2.23	2.03	2.15	2.07	2.01	2.18	2.10	2.13	2.13
K %	0.10	0.20	0.30	0.10	0.20	0.30	0.20	0.30	0.20	0.20	0.20	0.20
Fe %	0.01	0.02	0.01	0.02	0.02	0.04	0.06	0.04	0.01	0.02	0.01	0.06
Na %	0.02	0.16	0.16	0.06	0.01	0.01	0.05	0.31	0.02	0.02	0.04	0.04
Mn ppm	9	72	23	76	314	25	68	65	32	12	151	17
Sn ppm	0	3	1	1	1	12	3	13	0	0	1	0
P ppm	100	1020	470	180	50	100	190	420	50	90	320	110
Be ppm	11	25	6	10	4	4	7	30	7	5	5	10
Ga ppm	11	12	14	10	19	25	10	16	9	7	7	8
Nb ppm	1	9	0	0	0	1	2	4	0	0	0	0
Ta ppm	0	5	0	0	0	1	1	2	0	0	0	0
Zn ppm	20	10	30	30	70	80	20	5	5	5	5	5
Rb ppm	3	25	18	13	14	101	28	60	2	3	5	3
Sr ppm	4	6	3	0	6	2	18	5	2	4	7	0
Cs ppm	1	3	1	2	3	9	5	67	1	1	4	0
As ppm	2	1	1	1	1	1	2	1	2	1	1	2
Ni ppm	1	1	1	1	1	1	1	0	2	4	1	1
U ppm	3	1	4	7	7	2	0	1	8	0	1	1

Some of these aplite-pegmatite names are already known from previous works through other names: 37-Gondiães, 38-Gondiães 91, 39-Lousas, 41-NOA, 44-Antigo and 45-Vila Grande (Lima 2000, Charoy *et al.* 2001, Dias 2016a, Dias 2016b, Tucker Vasques 2021). Samples with possible mineral contaminations indicated by the following anomalies (calculated as outliers by subtracting the first quartile from the third quartile and multiplying it by 1.5): * 14-pet 1: positive anomaly in Al, K and Na. * 38-pet 1: positive anomaly in K, Rb, Zn, Ga and Sn. * 05-pet 2: positive anomaly Na, P, Be, Nb and Ta. * 37-pet 2: positive anomaly in Al, Mn, and Zn. * 39-pet 2: positive anomaly in Na, K, Cs, Rb, Be, Sn and Ta

1.5. Results

1.5.1. Petrography of the Thin sections

1.5.1.1. Petalite Crystal 1 of the Aplite-Pegmatite 38 (Also Known as Gondiães 91)

The sample 38-B1 (Figure 17) was almost pure petalite except for a part with spodumene and quartz crosscutting the petalite crystal, just as in example E of spodumene after petalite, from Figure 14. The petalite from the thin section did not show signs of deformation, hydrothermal alteration or weathering.

Since spodumene has a very strong luminescence in cathodoluminescence (CL) (bright orange to purple) (Figure 17b), it is easy to find it next to petalite that has a dark blue luminescence (Figure 17a). Petalite will look black and overshadowed by the strong luminescence of spodumene. To see the blue luminescence of petalite, it needs to be distant from spodumene. In CL, quartz also looks almost black next to spodumene

since it has a very dark luminescence and is commonly found intergrowing with spodumene. Thus, the petalite sample 38-B1, used for ICP-MS and LIBS, could contain traces of spodumene and quartz mixed within the petalite, as it was later demonstrated by the CL microscopy on the petalite pellets.

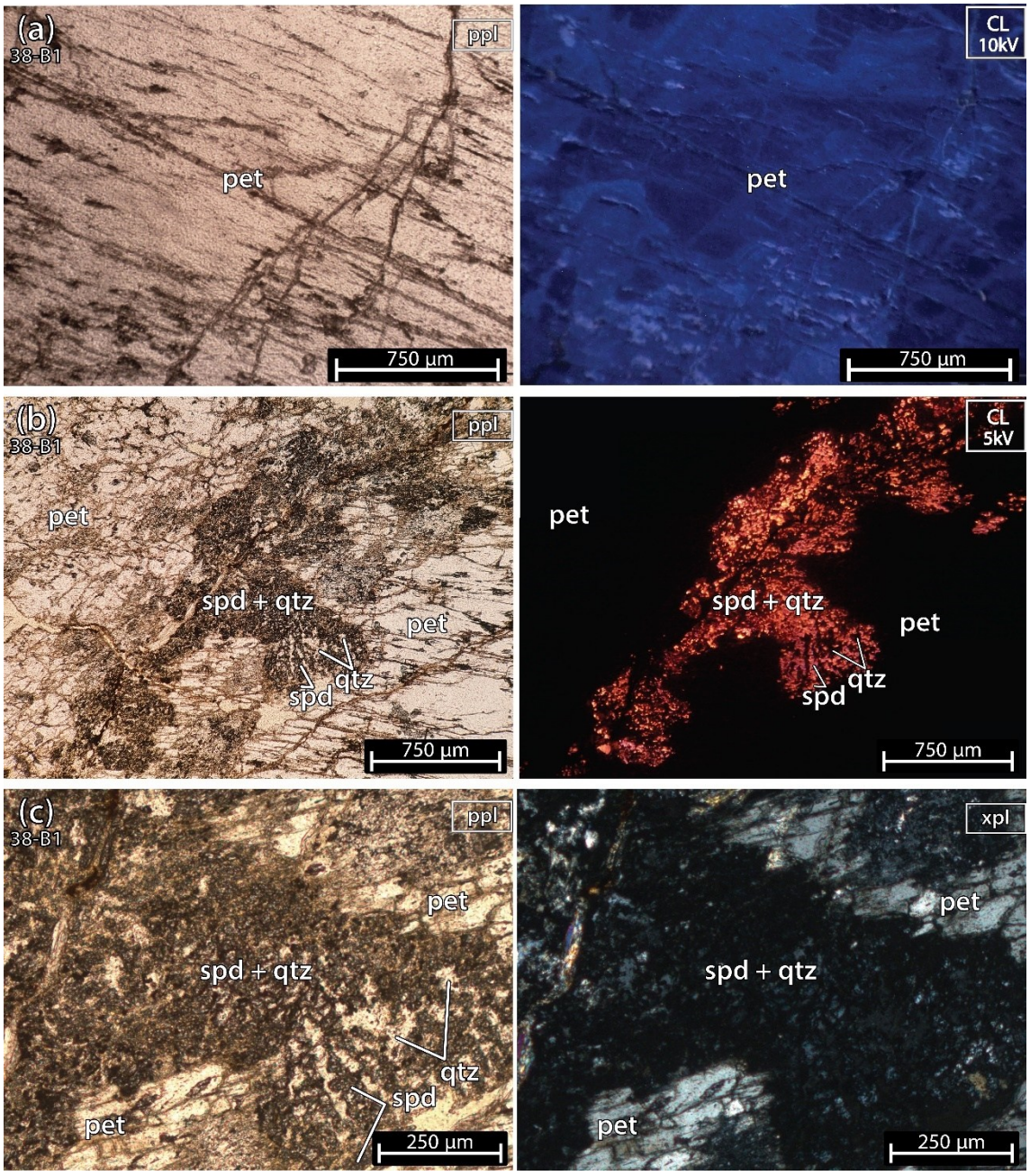

Figure 17. Microphotographs in parallel polarized light (ppl), crossed polarized light (xpl) and cold cathodoluminescence (CL) microscopy from a petalite (pet) fragment of the crystal sample 1 of the aplite-pegmatite 38 (38-B1). Although most of the sample is petalite, there is an alignment of spodumene (spd) and quartz (qtz) crosscutting the petalite crystal from one side of the thin section to the other. (a) petalite; (b,c) spodumene and quartz mixture crosscutting the petalite crystal.

1.5.1.2. Petalite Crystal 2 of the Aplite-Pegmatite 5 (Also Known as 59-AL-023)

The sample 5-B2 (Figure 18) was almost pure petalite except for a microscopic fine spodumene and quartz inside one of the petalite fractures (similar to example A, of spodumene after petalite, from Figure 14). Locally petalite was altered into micas and clay.

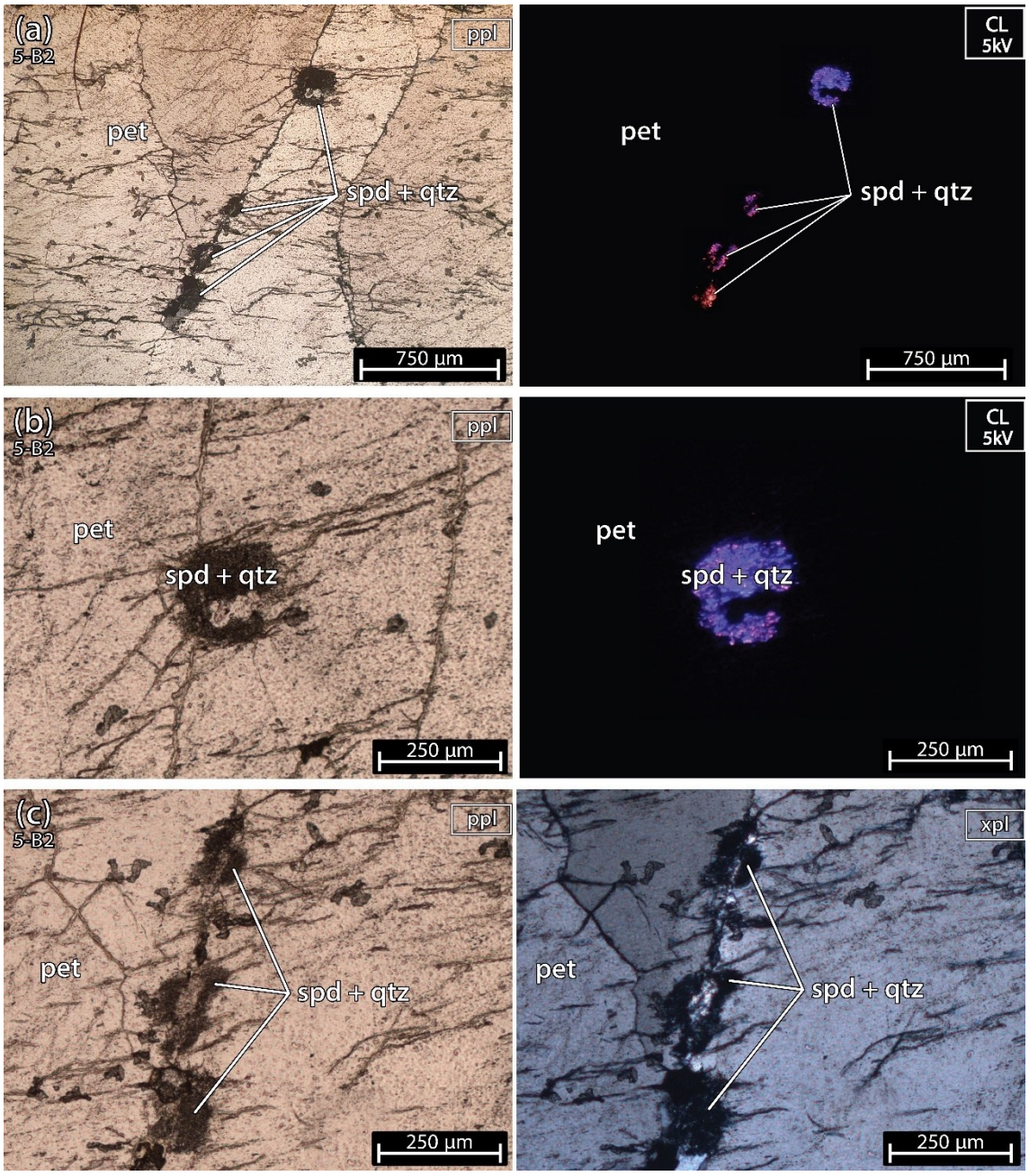

Figure 18. Microphotographs in parallel polarized light (ppl), crossed polarized light (xpl) and cold cathodoluminescence (CL) microscopy (CL) from a petalite (pet) fragment of the crystal sample 1 of the aplite-pegmatite 38 (38-B1). (a–c) spodumene + quartz in a fracture of petalite. In CL, the color of spodumene varies from bright purple to orange, while petalite and quartz look almost black next to spodumene observed at 5–6 kV.

The petalite in this sample was deformed, showing undulose extinction, and in CL the spodumene had a purple-to-orange luminescence (Figure 18a,b in CL). The purple luminescence of spodumene could be related to the deformation and formation of this type of fine spodumene + quartz association. Cathodoluminescence in silicates is known to be used to recognize brittle or ductile deformation phases, pressure dissolutions, relict structures, and recrystallizations (Pagel *et al.* 2000).

The pellet 5-B2 also shows some spodumene in the CL microscopy, as was observed in the thin section (Figure 23).

1.5.1.3. Petalite Crystal 2 of the Aplite-Pegmatite 41 (Also Known as NOA)

Sample 41-B2 (Figure 19) was pure petalite and did not have undulose extinction recrystallization and/or alteration. Despite the sample not having spodumene, previous studies have identified its presence in this aplite-pegmatite (e.g., Dias (2016b), identified as AL-56).

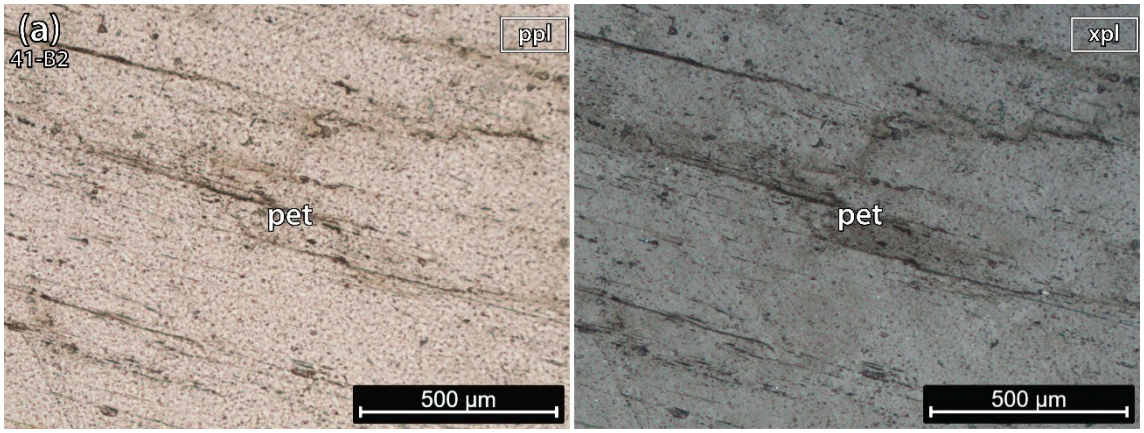

Figure 19. Microphotographs in parallel polarized light (ppl) and crossed polarized light (xpl) from a petalite (pet) fragment of the crystal sample 2 of the aplite-pegmatite 41 (41-B2). This is a pure petalite crystal without any traces of other minerals.

The petalite pellet 41-B2 observed in CL microscopy did not have any spodumene (Figure 23).

1.5.1.4. Petalite Crystal 2 of the Aplite-Pegmatite 44 (Also Known as Antigo)

Sample 44-B2 (Figure 20), besides containing several crystals of petalite, also contained a part of the aplite-pegmatite rock where quartz, plagioclase, white micas, Fe-

Mn phosphates and apatites could be seen. In CL, next to petalite (dark blue color) at 10 kV, the quartz looked black, the micas and the Fe-Mn phosphates non-luminescent, the plagioclases dark green and the apatite had a bright greenish yellow luminescence (Figure 20a).

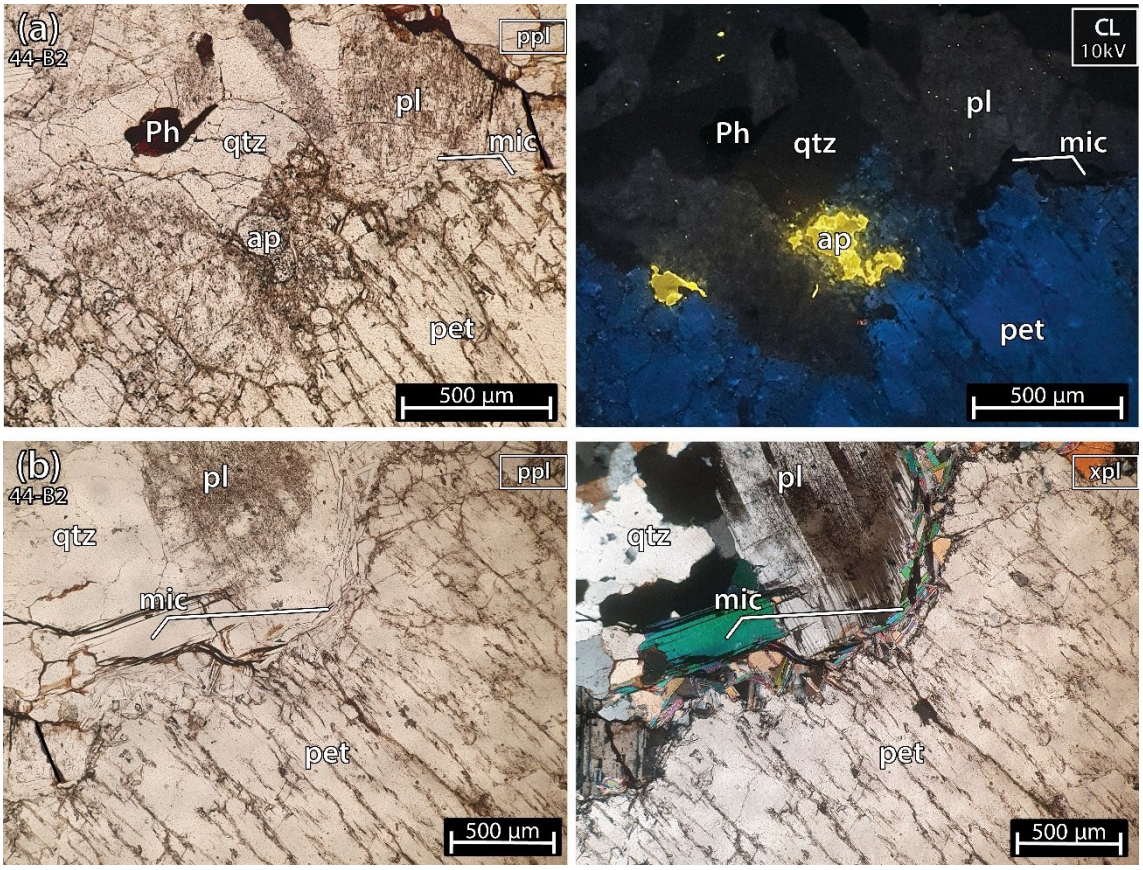

Figure 20. Microphotographs in parallel polarized light (ppl), crossed polarized light (xpl) and cold cathodoluminescence (CL) microscopy from a petalite (pet) fragment of the crystal sample 2 of the aplite-pegmatite 44 (44-B2), also known as Antigo. This sample contains a great amount of other minerals such as: (a) plagioclases (pl), quartz (qtz), Fe-Mn phosphates (Ph) and apatites (ap); (b), white micas (mic), plagioclases (pl), quartz (qtz).

The crystals of petalite did not host any spodumene or quartz, and had some micas along the contacts (Figure 20b). Thus, if the rest of the 44-B2 sample used for ICP-MS and LIBS also only had petalite, the petalite could be relatively pure, as was demonstrated by the CL performed in the 44-B2 pellet.

In CL at 10 kV, the petalite has a dark blue luminescence, the plagioclases are dark green, the quartz is almost non-luminescent, the white micas and the Fe-Mn phosphates seem non-luminescent and the apatites are bright greenish yellow.

1.5.1.5. Mixture of Spodumene and Quartz 2 of the Aplite-Pegmatite 8 (Also Known as 59-AL-52)

Sample 8-D2 (Figure 21) was almost only spodumene and quartz except for a small altered part with clay and micas.

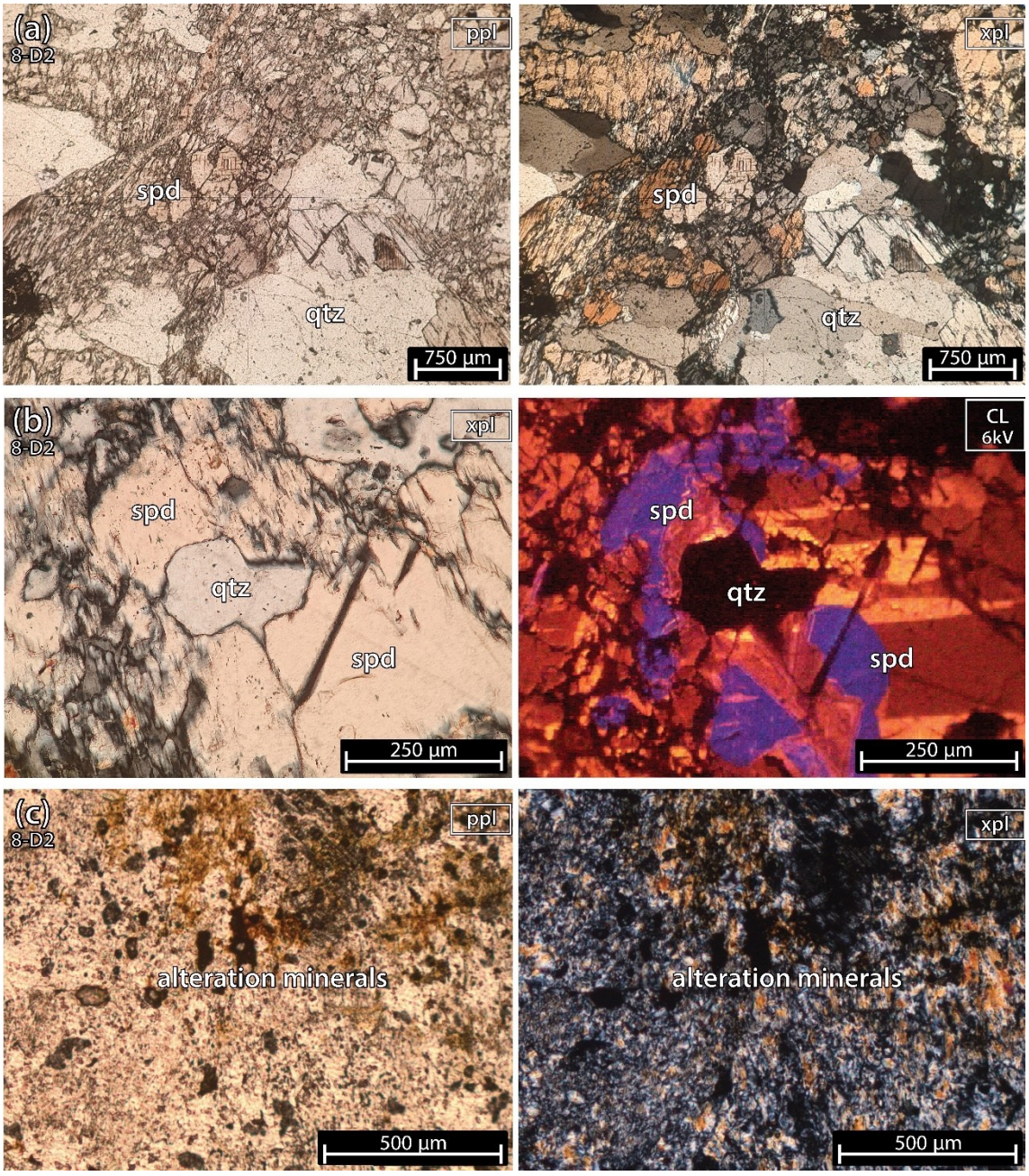

Figure 21. Microphotographs from a fragment of a mixture of spodumene (spd) and quartz (qtz) sample 2 of the aplite-pegmatite 8 (8-D2), also known as 59-AL-52. (a) parallel polarized light (ppl) and crossed polarized light (xpl). (b) xpl and cold cathodoluminescence (CL) microscopy (CL). This sample is almost all pure spodumene and quartz, except for a small portion of alteration minerals composed of clays and micas (c). In cold-CL microscopy, at 6 kV, spodumene has three main colors: yellow, orange and purple. All three colors have a similar strong luminescence. The quartz looks black next to the strong luminescence of spodumene.

1.5.1.6. Mixture of Spodumene and Quartz 2 of the Aplite-Pegmatite 4 (Also Known as 59-AL-22)

Sample 4-D2 (Figure 22), besides containing a part with fine spodumene + quartz (grain size < 500 µm) (Figure 22a,b), also comprises a part of the aplite-pegmatite rock with abundant feldspar, quartz, micas and minor apatite (with grains measuring up to 2 cm in size-Figure 22c).

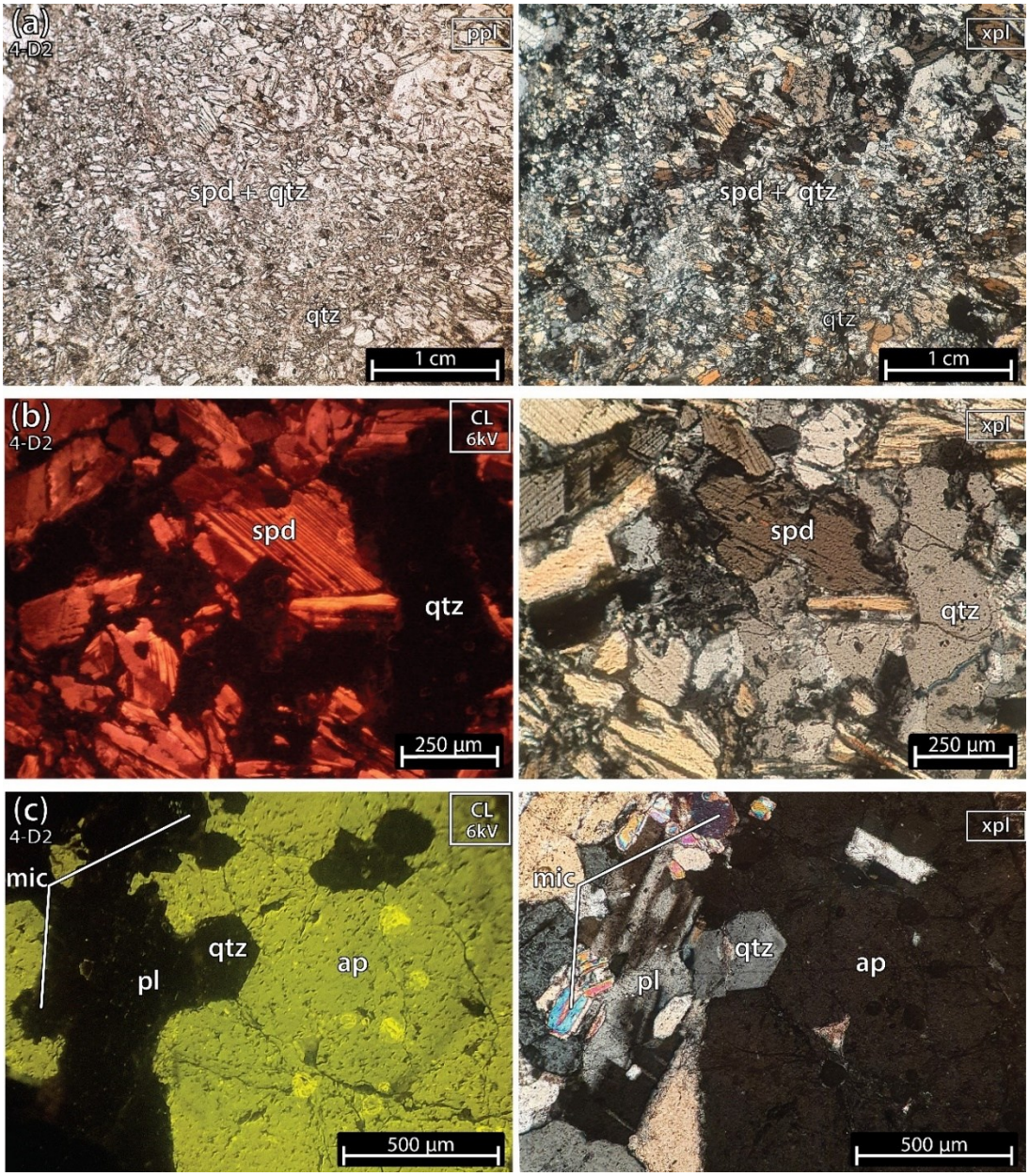

Figure 22. Microphotographs in parallel polarized light (ppl), crossed polarized light (xpl) and cold cathodoluminescence (CL) microscopy from a fragment of a mixture of spodumene (spd) and quartz (qtz) from sample 2 of the aplite-pegmatite 4 (4-D2), also

known as 59-AL-22. (a,b) Mixtures of fine spodumene and quartz. (c) aplite-pegmatite rock constituted by abundant plagioclase (pl), quartz, white mica (mic), and several crystals of apatite (ap) with sizes between 100 µm and 2 cm.

1.5.2. Petalite Pellets Analyzed with Cold-Cathodoluminescence Microscopy

The petrography performed on the petalite thin sections 38-B1 and 5-B2 (Figure 17 and Figure 18) had already alerted us to spodumene and quartz inside the petalite crystals.

CL was chosen to check the purity of the petalite pellets since this method can easily differentiate petalite from spodumene even if the minerals are milled into fine powders (<125 µm of grain size), as their luminescence intensity is very different (Figure 23). Spodumene always has a bright luminescence (with a color between orange and purple) and petalite has a dark luminescence (in shades of blue) (Wise & Brown 2019, Dias & Lima 2021).

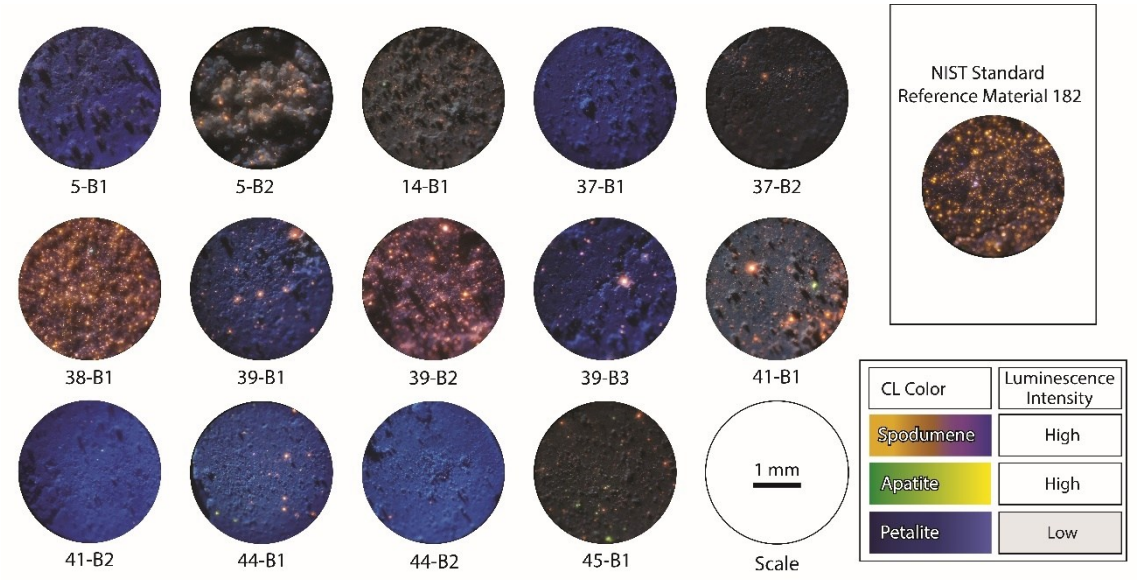

Figure 23. Microphotographs in cold cathodoluminescence (CL) of the petalite pellets made with the different samples of the aplite-pegmatites of the BA field. The CL color of petalite is blue, spodumene has CL colors between orange and purple, and apatite goes from green to yellow. Spodumene and apatite have a very strong luminescence and petalite has a weak luminescence. All pictures were taken with the same acceleration voltage (approximately 6 kV) (Lima 2000, Charoy *et al.* 2001, Dias 2016a, Dias 2016b, Tucker Vasques 2021).

According to the CL observations (Figure 23) and based on the visual percentage estimation, the summarized results are the following (Figure 24):

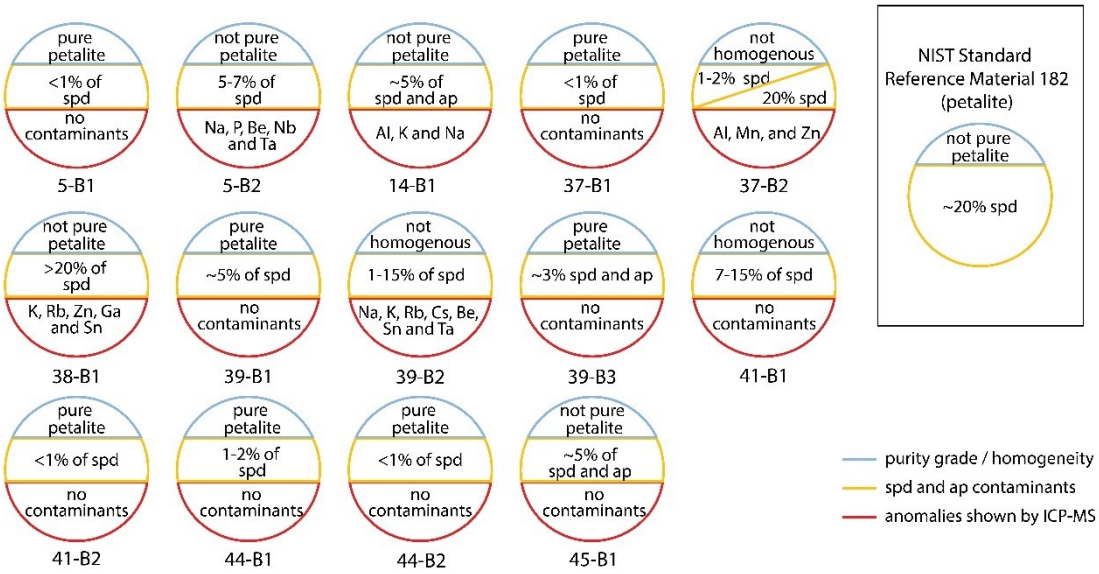

Figure 24. Summarization of the cold cathodoluminescence (CL) observations, based on visual percentage estimation of petalite, spodumene (spd) and apatite (ap). Since the strong luminescence of spd and ap usually creates a halo of light around it (making them seem larger), the results from the visual estimation are probably overestimated.

Detailed CL observations complementing Figure 24:

- sample 5-B1 was essentially pure petalite with less than 1% of possible spodumene and other bright minerals;
- sample 5-B2 had a destroyed surface after the LIBS ablation. However, it was possible to see approximately 5%–7% of bright orange minerals, probably spodumene. The rest of the material was very dark. This could be the result of the pellet being destroyed and the shadows formed by the irregular surface hiding the luminescence of the petalite. Alternatively, the sample could contain several non-luminescent or poorly luminescent minerals. However, since the ICP-MS results for this sample indicated positive anomalies in Na, P, Be, Nb and Ta, the last option is the most likely (Table 2);
- sample 14-B1 had around 5% of bright luminescent minerals, some green and some orange in CL, probably spodumene and apatite. The blue luminescence of the rest of the material was weaker than some of the other petalite pellets, possibly indicating the presence of other non-luminescent or poorly luminescent

minerals. Since the ICP- MS results indicated positive anomalies in Al, K and Na, this could indicate the presence of feldspars and micas mixed with the petalite (Table 2);

- sample 37-B1 was essentially pure petalite with less than 1% of bright orange minerals, probably spodumene;
- sample 37-B2 had zones that were essentially pure petalite (with 1%–2% of spodumene) and zones with aggregates of around 1mm in size of what seems to be spodumene + quartz (Figure 25). In the ICP-MS results, this sample had a positive anomaly in Al, Mn, and Zn (Table 2);

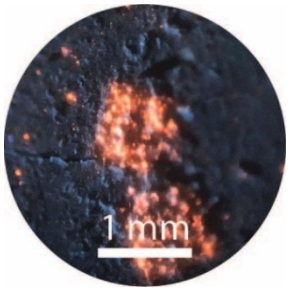

Figure 25. Micro-photograph in cold cathodoluminescence (CL) of spodumene + quartz aggregates in the sample 37-B2.

- sample 38-B1 seemed to have more than 20% of spodumene, since it had a high amount of bright orange minerals. Besides, the ICP-MS results indicated the possible presence of other minerals, such as feldspar and micas, since this sample contained positive anomalies in K, Rb, Zn, Ga and Sn;
- sample 39-B1 was essentially petalite with about 5% of spodumene;
- sample 39-B2 had some zones richer and other zones poorer in strong luminescent minerals, thus varying from 1 to 15% of what seems to be spodumene grains. In the ICP-MS results, this sample also had a positive anomaly in Na, K, Rb, Cs, Be, Sn and Ta (Table 2);
- sample 39-B3 was pure petalite with approximately 3% of other bright minerals, including probable spodumene;
- sample 41-B1 had some zones richer and other zones poorer in strong luminescent minerals, thus varying from 7 to 15% of what seemed spodumene grains;

- sample 41-B2 was essentially pure petalite with less than 1% of bright orange minerals;
- sample 44-B1 was almost pure petalite with 1%–2% of bright orange minerals;
- sample 44-B2 was essentially pure petalite with less than 1% of bright orange minerals;
- sample 45-B1 had around 5% of strong luminescent minerals, some bright orange, others bright green. The CL luminescence of this pellet was darker than the other petalites, but the ICP-MS results from this sample did not have any significant anomalies.

Therefore, according to the CL analysis, the purest petalite pellets should be the 5-B1, 14b-1, 37-b1, 39-B1, 39-B3, 45-B1, and the samples with more than 5% of other minerals are 5-B2; 37-B2; 38-B1, 39-B2; 41-B1 and the NIST SRM 182.

1.5.3. Petalite Pellets Analyzed with Cold-Cathodoluminescence Microscopy NIST SRM 182 (Petalite)

Since the visual estimation from CL seemed to indicate that the NIST SRM 182 (petalite) contained a large amount of spodumene (Figure 23), an analysis of X-ray diffraction (XRD) was performed in this SRM. The XRD results showed that approximately 90% was petalite, 6% was spodumene, 4% was quartz and that there was <1% of phyllosilicates (Figure 26).

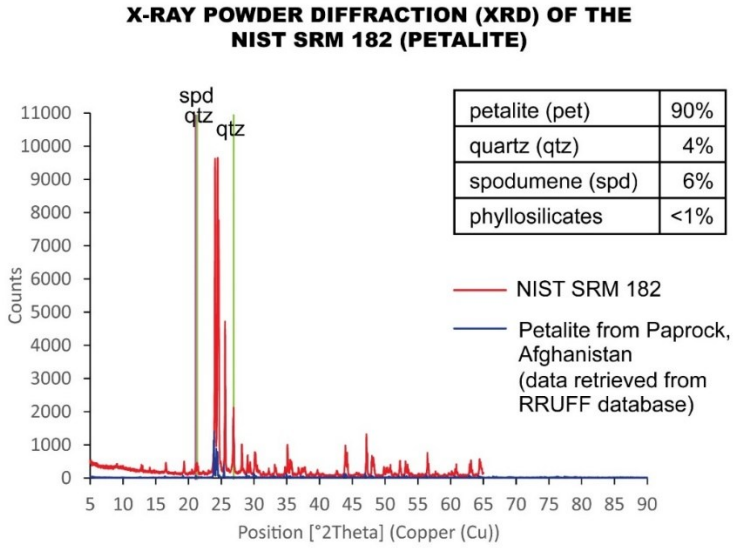

Figure 26. X-ray powder diffraction (XRD) analysis performed on the NIST SRM 182 (petalite) compared to the ICP-MS analysis. ICP-MS errors of the quality control samples sent to Actlabs.

For QC of the ICP-MS analysis, the following samples were sent to the Actlabs laboratories: one duplicate of spodumene (03-C1/03-C2), one duplicate of the mixture of spodumene and quartz (08-D2/08-D3) and one sample with NIST SRM 182 (petalite).

The errors (Table 3) resulting from the comparison between the duplicates and the certified Li content of the NIST SRM 182 (petalite) for the main constituents of the different minerals were:

- spodumene: 16% of error for Si, 0% of error for Al, 1% of error for Li and 11% of error for Fe;
- spodumene and quartz mixture: 18% of error for Si, 1% of error for Al, 3% of error for Li and 0% of error for Fe;
- NIST SRM 182 (petalite): 5% for Li.

Table 3. ICP-MS errors in the samples sent for quality control (QC).

	Spodumene		Spd + Qtz		NIST SRM 182	
	03-C1	03-C2	08-D2	08-D3	NIST*	ICP-MS
Si	error: 16%		error: 18%			
	Si 22.00%	Si 26.30%	Si 33.70%	Si 28.50%		
Al	error: 0%		error: 1%			
	Al 12.70%	Al 12.70% Al	Al 9.97%	Al 10.10%		
Li	error: 1%		error: 3%		error: 5%	
	Li 3.06%	Li 3.08%	Li 2.01%	Li 2.07%	1.92% Li	2.01% Li
K	error: 0%		error: 14%			
	K 0.30%	K 0.30%	K 0.60%	K 0.70%		
Na	error: 9%		error: 0%			
	Na 0.10%	Na 0.11%	Na 0.21%	Na 0.21%		
P	error: 87%		error: 6%			
	P 0.01%	P 0.08%	P 490 ppm	P 520 ppm		
Rb	error: 21%		error: 1%			
	Rb 4.1 ppm	Rb 5.2 ppm	Rb 91.7 ppm	Rb 92.3 ppm		
Ca	error: -		Error: 0%			
	Ca < 0.01%	Ca < 0.01%	Ca 0.02%	Ca 0.02%		
Fe	error: 11%		error: 0%			
	Fe 0.17%	Fe 0.19%	Fe 0.18%	Fe 0.18%		
Mn	error: 5%		error: 2%			
	Mn 237 ppm	Mn 225 ppm	Mn 276 ppm	Mn 271 ppm		
Be	error: 3%		error: 3%			
	Be 105 ppm	Be 108 ppm	Be 9.02 ppm	Be 8.79 ppm		
Cs	error: 3%		error: 2%			
	Cs 2.74 ppm	Cs 2.66 ppm	Cs 2.55 ppm	Cs 2.6 ppm		

Tl	error:33%		error: 0%	
	Tl 0.04 ppm	Tl 0.03 ppm	Tl 0.58 ppm	Tl 0.58 ppm
Sr	error: 3%		error: 3%	
	Sr 3.4 ppm	Sr 3.3 ppm	Sr 21.8 ppm	Sr 21.2 ppm
Ga	error: 5%		error: 2%	
	Ga 10.9 ppm	11.5 ppm Ga	Ga 11.6 ppm	Ga 11.4 ppm
Zn	error: 0%		error: 50%	
	Zn 5 ppm	Zn 5 ppm	Zn 10 ppm	Zn 20 ppm
As	error: 133%		error: 0%	
	As 0.7 ppm	As 0.3 ppm	As 0.9 ppm	As 0.9 ppm
Nb	error: 2%		error: 2%	
	Nb 9.4 ppm	Nb 9.2 ppm	Nb 4.4 ppm	Nb 4.3 ppm
Ni	error: 25%		error: 0%	
	Ni 0.3 ppm	Ni 0.4 ppm	Ni 0.5 ppm	Ni 0.5 ppm
Sn	error: 8%		error: 1%	
	Sn 209 ppm	Sn 194 ppm	Sn 23.2 ppm	Sn 22.9 ppm
Ta	error: 7%		error: 0%	
	Ta 8.64 ppm	Ta 8.09 ppm	Ta 0.96 ppm	Ta 0.96 ppm
U	error: 70%		error: 13%	
	U 0.3 ppm	U 1 ppm	U 0.9 ppm	U 0.8 pp

* According to NIST the reference material can only vary ± 1%. The NIST SRM 182 only has certified values for Li, therefore all the other elements are empty.

The silica (Si) and iron (Fe) errors of the ICP-MS for spodumene were excessively high (16% for Si and 11% for Fe) and negatively affected the calibrations of the portable (p)LIBS.

The Si significant errors of the ICP-MS prevent distinguishing spodumene from petalite based on their Si contents (Figure 27). Other techniques, even qualitative ones such as the energy dispersive X-Ray from scanning electron microscopy (EDS-SEM), can easily distinguish a spodumene from a petalite since their Si and Al contents are very different.

The theoretical values for spodumene are Si 30.18% and Al 14.50%, and for petalite, Si 36.72% and Al 8.75%.

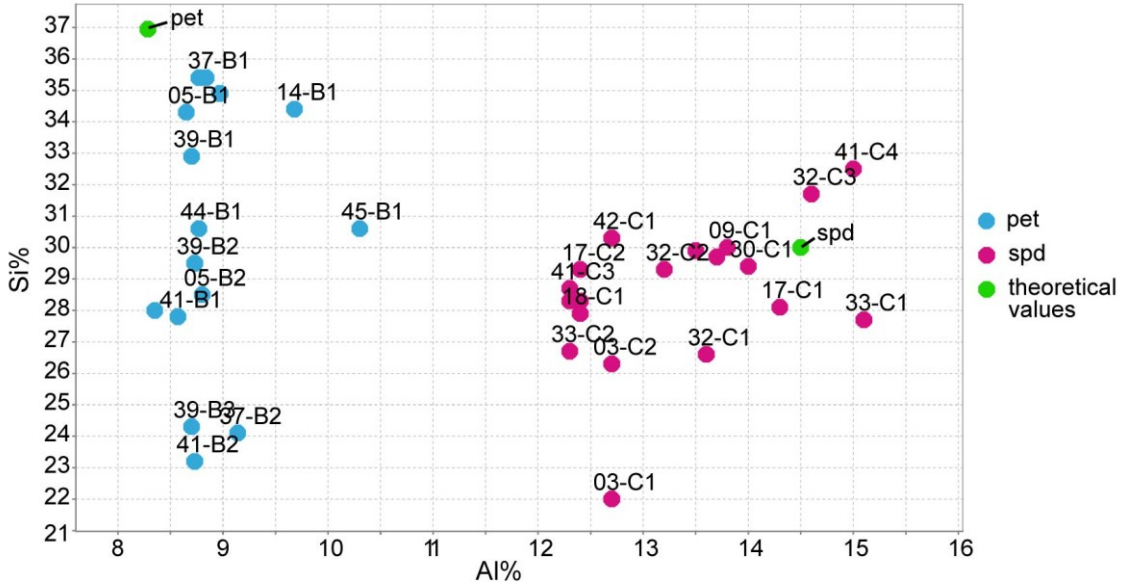

Figure 27. ICP-MS analysis of Si using Al for all the spodumene and petalite samples used on the calibrations of the portable laser-induced breakdown spectroscopy (pLIBS).

1.5.4. ICP-MS Errors from the Duplicates Made by Actlabs

Even the errors from the laboratory itself show that the Si from the ICP-MS cannot be trusted since the Si from the duplicates produced by ActLabs for petalite had an error of 26% (Table 4), and Fe had an error of 10% for spodumene (Table 5)

Table 4. ICP-MS errors from the duplicates made in Actlabs for the major elements of petalite, spodumene and quartz with the method FUS-Na_2O_2

	Det.	Petalite		Spodumene				Spodumene + Quartz			
	Lim.	39-B2	39-B2	09-C1	09-C1	32-C4	32-C4	32-D1	32-D1	41-D3	41-D3
		Orig	Dup	Orig	Dup	Orig	Dup	Orig	Dup	Orig	Dup
Si %	0.01	error: 26%		error: 2%		error: 1%		error: 13%		error: 22%	
		Si 25%	Si 34%	Si 30%	Si 30%	Si 30%	Si 30%	Si 34%	Si 30%	Si 32%	Si 26%
Al %	0.01	error: 1%		error: 0%		error: 1%		error: 0%		error: 2%	
		Al 8.8%	Al 8.7%	Al 14%	Al 14%	Al 13%	Al 14%	Al 9.6%	Al 9.6%	Al 9.4%	Al 9.2%
K %	0.1	error: 0%		error: 0%		error: 0%		error: 0%		error: 0%	
		K 0.3%	K 0.3%	K 0.3%	K 0.3%	K 1.1%	K 1.1%	K 1.6%	K 1.6%	K 0.7%	K 0.7%
Li %	0.01	error: 5%		error: 1%		error: 2%		error: 0%		error: 1%	
		Li 2.1%	Li 2%	Li 3.3%	Li 3.3%	Li 2.7%	Li 2.7%	Li 1.2%	Li 1.2%	Li 1.8%	Li 1.8%

Table 5. ICP-MS errors from the duplicates made in Actlabs for the trace-elements of K-feldspar, petalite, spodumene and quartz with the method 4 Acid “Near Total” digestion.

	NIST Petalite		Spodumene		Spodumene + Quartz			
Det.	SRM 182	SRM 182	32-C1	32-C1	11-1D	11-D1	08-D2	08-D2
Limit	Orig	Dup	Orig	Dup	Orig	Dup	Orig	Dup
			error: 0%		error: 0%		error: 0%	

Na %	0.01			Na 0.04	Na 0.04	Na 0.26	Na 0.26	Na 0.21	Na 0.21
Fe %	0.01			error: 10%		error: 0%			error: 0%
				Fe 0.23	Fe 0.21	Fe 0.13	Fe 0.13	Fe 0.18	Fe 0.18
Ca %	0.01			error: -		error: 0%			error: 0%
				Ca <0.01	Ca <0.01	Ca 0.02	Ca 0.02	Ca 0.02	Ca 0.02
P ppm	10			error: 50%		error: 0%			error: 0%
				P 120	P 80	P 4210	P 4230	P 490	P 490
Rb ppm	0.1	error: 2%		error: 29%		error: 5%			error: 3%
		Rb 258	Rb 262	Rb 2.2	Rb 1.7	Rb 96	Rb 91.7	Rb 90.5	Rb 92.9
Mn ppm	5			error: 1%		error: 0%			error: 1%
				Mn 165	Mn 166	Mn 161	Mn 161	Mn 274	Mn 277
Sr ppm	0.2	error: 6%		error: 0%		error: 2%			error: 0%
		Sr 5.2	Sr 4.9	Sr 0.4	Sr 0.4	Sr 59.5	Sr 60.7	Sr 21.8	Sr 21.8
Cs ppm	0.05	error: 5%		error: 3%		error: 5%			error: 1%
		Cs 24.6	Cs 26	Cs 0.38	Cs 0.37	Cs 4.75	Cs 4.52	Cs 2.56	Cs 2.54
Pb ppm	0.5	error: 50%		error: 14%		error: 12%			error: -
		Pb 2.1	1.4	Pb 0.8	0.7	Pb 2.8	Pb 2.5	Pb <0.5	Pb <0.5
Zn ppm	2			error: 20%		error: 0%			error: 5%
				Zn 8	Zn 10	Zn 41	Zn 41	Zn 23	Zn 22
Ga ppm	0.05	error: 0%		error: 9%		error: 7%			error: 2%
		Ga 17.5	Ga 17.5	Ga 9.48	Ga 8.7	Ga 7.9	Ga 7.41	Ga 11.7	Ga 11.5
Be ppm	0.05	error: 5%		error: 0%		error: 3%			error: 1%
		Be 10.6	Be 11.2	Be 6.58	Be 6.55	Be 3.48	Be 3.38	Be 9.07	Be 8.98
Sn ppm	0.2	error: 8%		error: 8%		error: 3%			error: 4%
		Sn 3.4	3.7	Sn 4.2	3.9	Sn 11.2	Sn 10.9	Sn 22.8	Sn 23.7
Tl ppm	0.02	error: 1%		error: -		error: 2%			error: 2%
		Tl 1.56	Tl 1.58	Tl <0.02	Tl <0.02	Tl 0.44	Tl 0.43	Tl 0.57	Tl 0.58
Cr ppm	1			error: 40%		error: 67%			error: 33%
				Cr 7	Cr 5	Cr 5	Cr 3	Cr 4	Cr 3
Nb ppm	0.1	error: 10%		error: 25%		error: 9%			error: 7%
		Nb 3.5	Nb 3.9	Nb 0.5	Nb 0.4	Nb 3.7	Nb 3.4	Nb 4.3	Nb 4.6
As ppm	0.2	error: 26%		error: 150%		error: 44%			error: 20%
		As 3.1	As 4.2	As 1	As 0.4	As 1.3	As 0.9	As 0.8	As 1
Ta ppm	0.05	error: 13%		error: 28%		error: 15%			error: 4%
		Ta 4.74	Ta 5.47	Ta 0.32	Ta 0.25	Ta 0.68	Ta 0.59	Ta 0.94	Ta 0.98
U ppm	0.1	error: 25%		error: 43%		error: 0%			error: 9%
		U 0.3	U 0.4	U 1	U 0.7	U 2.7	U 2.7	U 1	U 1.1
Ni ppm	0.2	error: 13%		error: 16%		error: 10%			error: 0%
		Ni 0.7	Ni 0.8	Ni 3.6	Ni 3.1	Ni 1.1	Ni 1	Ni 0.5	Ni 0.5
Y ppm	0.1	error: 0%		error: 122%		error: 0%			error: -
		Y 0.2	Y 0.2	Y 4	Y 1.8	Y 0.1	Y 0.1	Y <0.1	Y <0.1

1.6. Discussion

1.6.1. Implications of the Petalite Pellets Analysis with Cathodoluminescence

As feared, the CL demonstrated a high amount of bright orange minerals in some petalite pellets (samples 38-B1, 39-B2 and even the NIST SRM 182, Figure 23). From our petrographic results, these are spodumene minerals (thin sections 38-B1 and 5-B2) (Figure 17 and Figure 18). Since spodumene was intergrown with quartz in the thin sections, the pellets will probably also have quartz (almost non-luminescent in CL and almost black next to spodumene and petalite). However, if spodumene and quartz are the result of the petalite breakdown, then quartz will be in less quantity than

spodumene. This would explain the identical chemical composition to that of petalite if the volumetric proportions are approximately 60% spodumene and 40% quartz (Černý & Ferguson 1972) (Table 6):

Table 6. Breakdown of petalite into spodumene and quartz intergrowth (SQI).

$LiAlSi_4O_{10}$ (Petalite)	→	$LiAlSi_2O_6$ (Spodumene)	+	$2SiO_2$ (Quartz)
2.09% Li		3.73% Li		0% Li
8.75% Al		14.50% Al		0% Al
36.72% Si		30.18% Si		46.74% Si
52.43% O		51.59% O		53.26% O
100 vol%	→	56.3 vol%	+	43.7 vol%

This could also explain why although NIST SRM 182 has the same chemical composition as that of petalite, it has a different mineralogical composition as demonstrated by some strong luminescent minerals in CL together with weak luminescent minerals Figure 23. Therefore, the SRM 182 is not a pure petalite mineral as confirmed using XRD (Figure 26).

The presence of spodumene and quartz in the petalite samples could be a problem for the pLIBS equipment since this equipment can be very sensitive to changes in the matrix that can cause the spectra to change by altering the area of the peaks disproportionately to the element concentration (Lepore et al. 2017). Thus, these samples must be analyzed with extra precautions.

The bright green dots observed in CL in some of the petalite pellets are probably apatite since it is common to find apatite in the aplite-pegmatites of the BA field, as was observed in the thin section of sample 4-D2 (Figure 22c).

1.6.2. Identifying Spodumene, Petalite and Mixtures of Spodumene and Quartz Based on Their Chemical Composition

The Li, Si and Al contents of spodumene and petalite should be sufficient to distinguish both minerals if the analysis method has accurate results (unlike the Si from ICP-MS). However, it may be difficult to distinguish a petalite from fine mixtures of spodumene and quartz (often invisible to the naked eye in the BA field) if they have SQI proportions (Černý & Ferguson 1972). Thankfully, in nature, the minerals will hardly have this theoretical composition since minor substitutions commonly occur in their crystal

structure. For example, spodumene crystals in nature always have some significant amount of Fe and/or Mn substituting some of the Al in their crystal structure. As for petalite, it is usually more difficult for other elements to enter its crystal structure, although it can also happen (Deer *et al.* 1978, Černý & London 1983, Deer *et al.* 2004).

The spodumene from the BA field always has more Fe than Mn (Fe > 1%), which is also evidenced by their color, which is never pink and is always cream-colored or greenish, and the petalite from the BA field always has low Fe contents (Fe < 1%) (ICP-MS analysis from Table 1 and Table 2 (Charoy *et al.* 2001)).

Therefore, with the Fe and Al contents from the ICP-MS chemical analysis, it was possible to distinguish these three types of materials (Figure 28, produced in the IoGas software with the Auto-Domain tool), since the Al contents of spodumene will always be greater than the Al contents of petalite and greater than the Al contents of the mixtures of spodumene and quartz (the presence of quartz dilutes Al), whereas petalite will always have less Fe than spodumene.

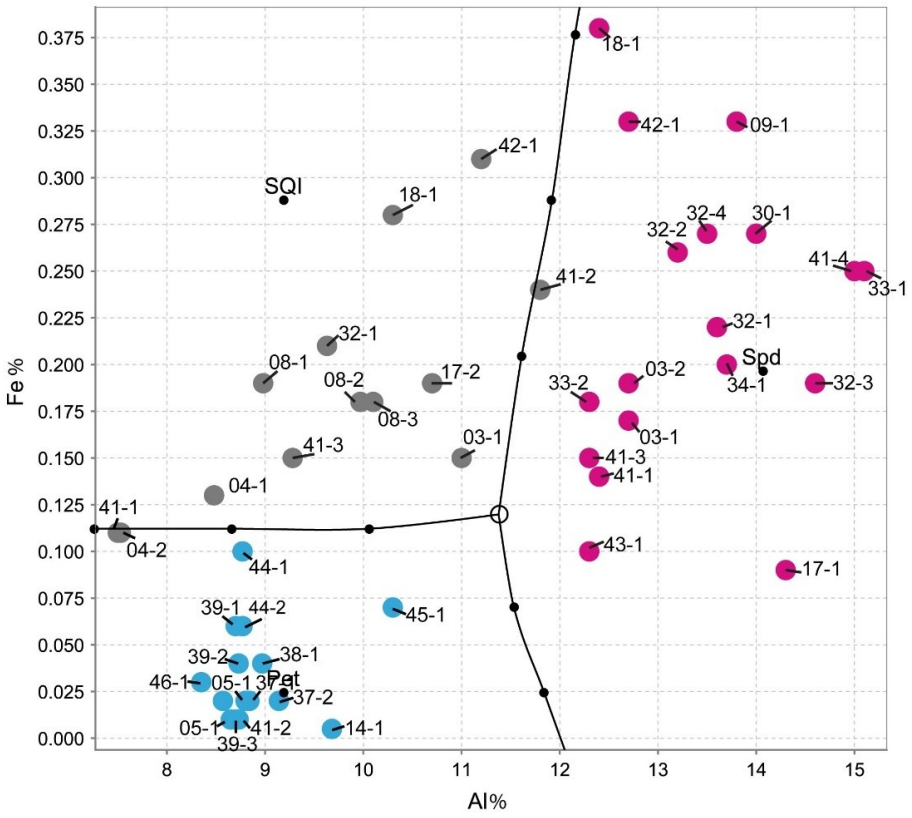

Figure 28. Differentiating spodumene from petalite and from spodumene + quartz mixtures based on the Al and Fe content from the ICP-MS analysis (graph made in the IoGas software with Auto-Domain tool from the analysis tab, with common covariance matrix, coarse accuracy, and no limit in the cutoff M distance). The pink dots are spodumene crystal samples, the grey are mixtures of spodumene and quartz samples and the blue are petalite crystal samples.

Theoretically, with a calibrated handheld LIBS, the same should be possible. However, there was a problem. All the chemical elements with detectable peaks in the spectra (Figure A1) of the pLIBS had overlapping intensity ratios (IR) for spodumene and petalite, except for Fe (Figure 29). Since Al also had overlapping IR, it was impossible to use the pLIBS to separate the fine mixtures of spodumene and quartz from single spodumene crystals (Figure 30). Furthermore, analyzing a spodumene and petalite with a single calibration for both minerals did not work, especially for Li, one of the elements with more overlapping IR (Figure 31). However, Fe solved this problem. Three calibrations were developed for spodumene and petalite: one to analyze spodumene (Figure 32) another to analyze petalite (Figure 33) and another one to distinguish spodumene from petalite by using their different Fe contents (Fe was the only element where one calibration line was possible for both minerals). This worked because the LIBS intensity ratios (IR) for Fe are always higher in spodumene (IR ≥ 0.0038) than in petalite (IR < 0.0038) (Figure 29). This way the Fe_Barroso calibration can guide you to choose the right calibration since an IR of 0.0038 corresponds to 0.128% of Fe by the produced calibration curve: y = −0.0076 + 31.8368x + 1028.9114x2. Thus, every time a petalite is analyzed with the Fe_Barroso calibration, the Fe result will be less than 0.128% indicating that the Pet_Barroso calibration should be used, and the Fe will be greater than 0.128% in a spodumene indicating that the Spd_Barroso calibration should be used.

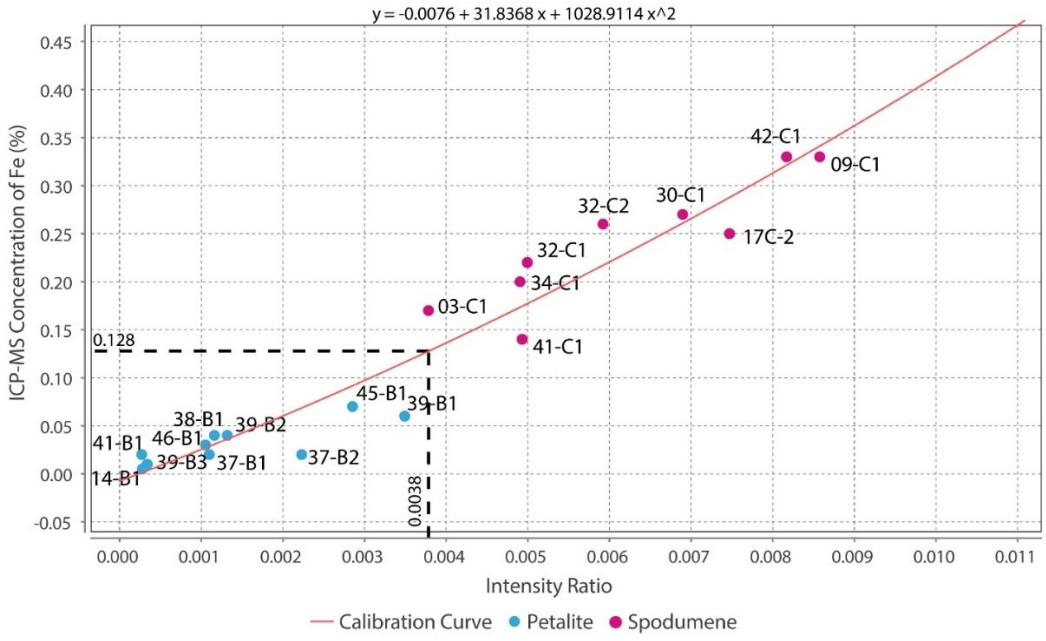

Figure 29. Successful separation of the pLIBS Fe intensity ratios for the spodumene and petalite samples of the Barroso–Alvão aplite-pegmatite field.

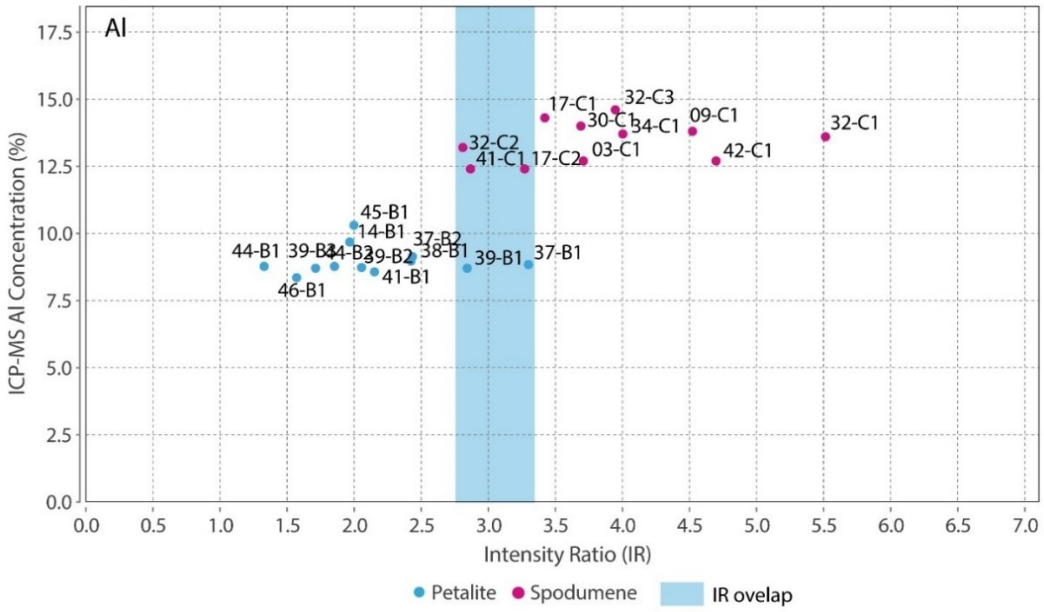

Figure 30. Overlap of the pLIBS Al intensity ratios for the spodumene and petalite samples of the Barroso–Alvão aplite-pegmatite field.

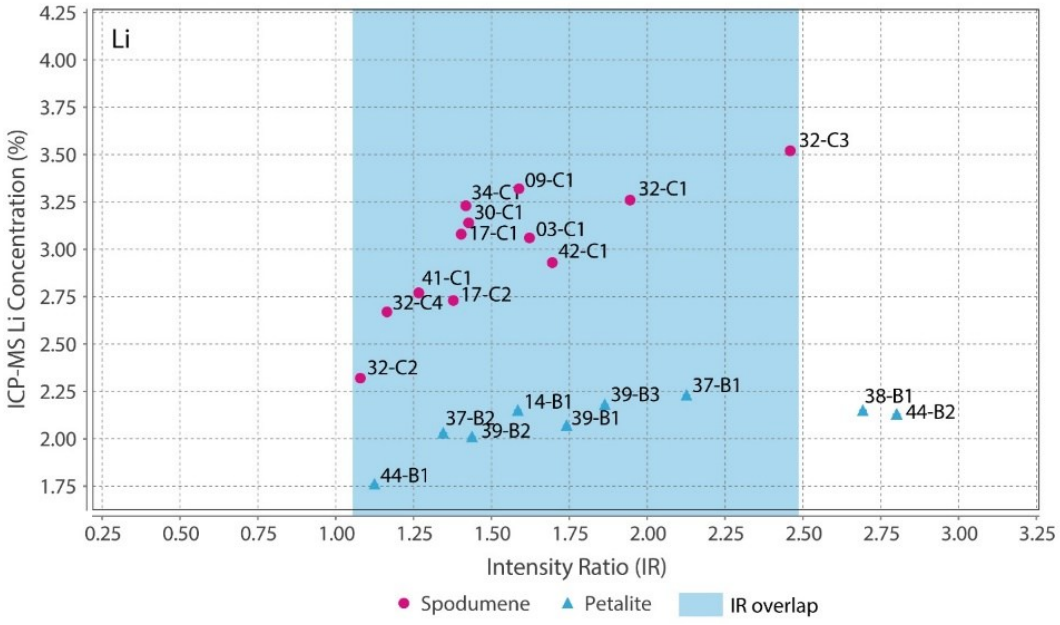

Figure 31. Overlap of the pLIBS Li intensity ratios for the spodumene and petalite samples of the Barroso–Alvão aplite-pegmatite field.

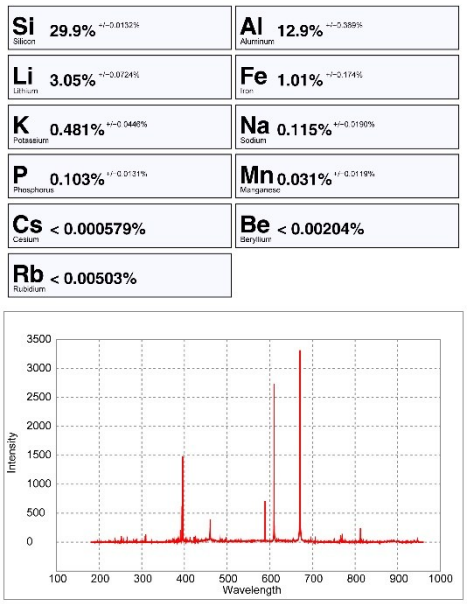

Figure 32. pLIBS analysis of the spodumene sample 32-C1 with the Spd_Barroso calibration.

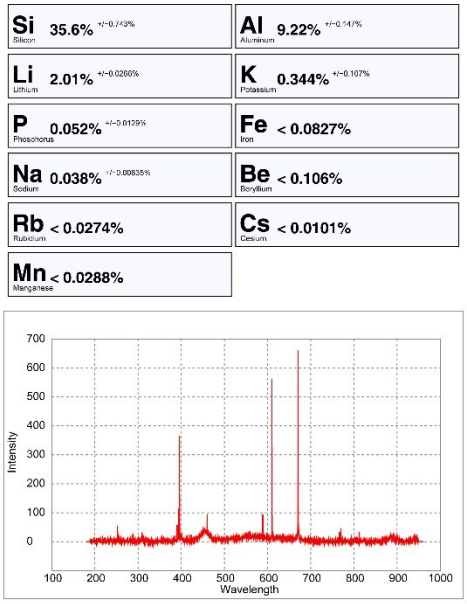

Figure 33. pLIBS analysis of the petalite sample 38-B1 with the Pet_Barroso calibration.

1.6.3. LIBS results

From all the chemical elements analyzed by ICP-MS for the spodumene and petalite samples from the BA field, only the following elements have detectable peaks in the pLIBS spectra: Li, Al, Si, Li, Fe, K, P, Na, Rb, Mn, Cs and Be. The peaks for Be, Rb, Cs and Be are very small and easily get lost in the background signal of the spectra (Figure 33, Figure 32, and Figure 41).

Only the major elements of spodumene and petalite (Al, Si and Li) have accuracy greater than 0.8 (Figure 34) and consistent errors below 20% (Figure 35). All the other analyzed elements have greater errors. As for Fe, despite having large errors, the contents were always consistently higher in spodumene than in petalite. This is because the Fe contents of the BA petalites are so low that even the LIBS sometimes has difficulty quantifying it, resulting in values below the Limit of Detection (LOD). On the other hand, Fe from the BA spodumenes is always easily detected.

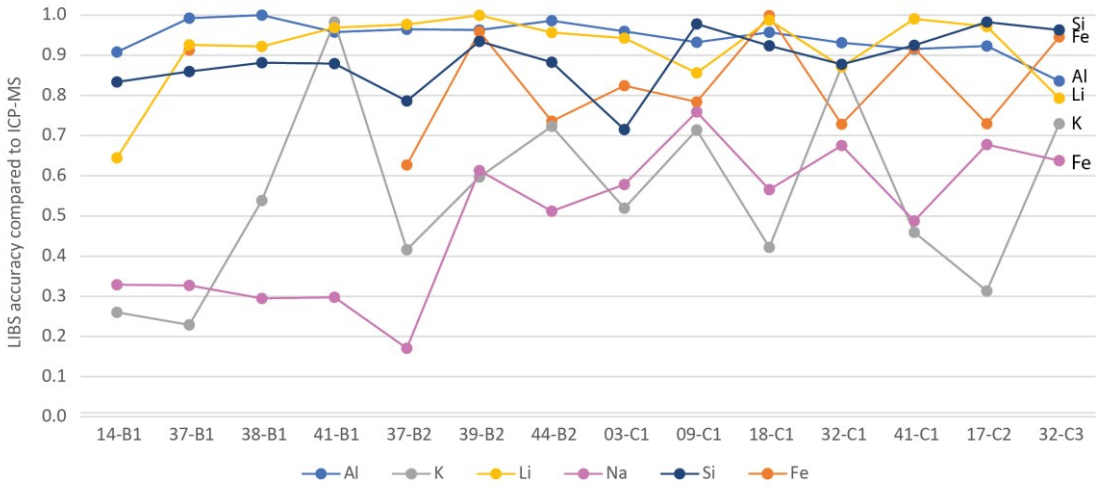

Figure 34. LIBS accuracy compared to the ICP-MS analysis for the spodumene and petalite samples from the Barroso–Alvão aplite-pegmatite field.

The *Spd_Barroso* and the *Pet_Barroso* calibration were also tested in eight different potassium feldspars to evaluate if samples without Li could be giving false positives while using these two calibrations. As it can be seen in Figure 36, Figure 37 and Figure 38 the Li results were always very low (< 0.8% Li). Therefore, even if a K-feldspar is analyzed by mistake with the pLIBS (because sometimes they may have a similar appearance to petalite), the Li results will indicate that the analyzed mineral is not a petalite, nor a spodumene. This was possible because the IRs of Li from the K-feldspars were different from the IRs of Li from the spodumenes and petalites. Thus, it was possible to create one more calibration curve for Li inside the Spd_Barroso and Pet_Barroso. This new curve was made from the IRs and concentrations of K-feldspars. As for the K result for K-feldspars, since K also has overlapping IRs for spodumene, petalite and K-feldspars, the K in the K-feldspars has unreliable results that can change from 10 to 2% of K.

Figure 35. Percentage of the errors of the pLIBS compared to the ICP-MS results for (a) Al, (b) Si, (c) Li and (d) Fe with the Spd_Barroso calibration and Pet_Barroso calibration.

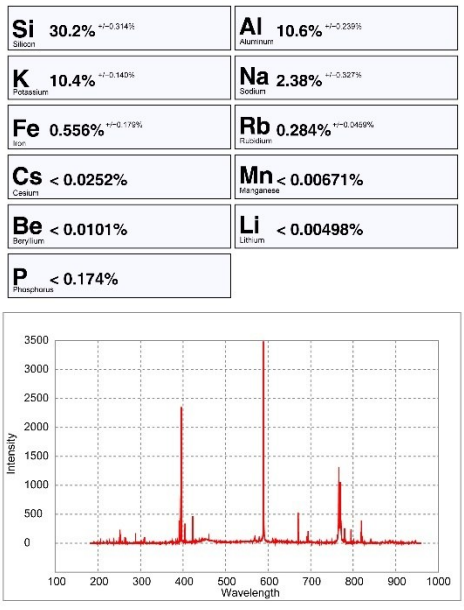

Figure 36. pLIBS analysis of a potassium feldspar with the Spd_Barroso calibration

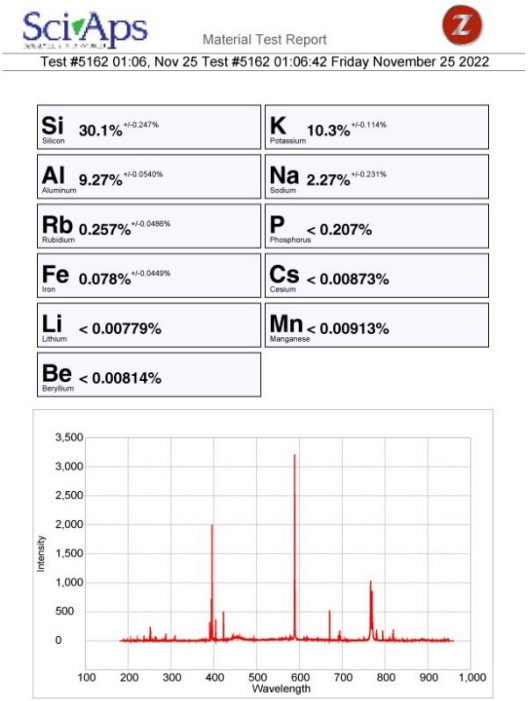

Figure 37. pLIBS analysis of a potassium feldspar with the Pet_Barroso calibration.

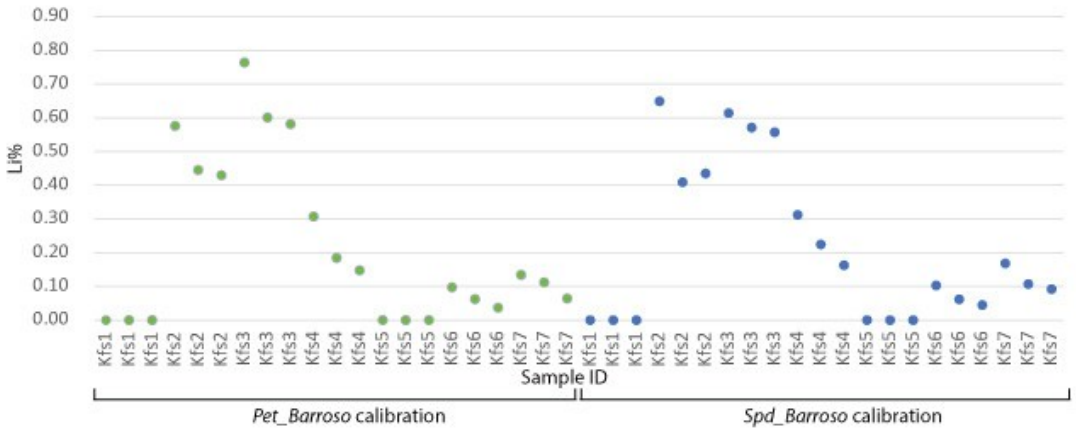

Figure 38. Li results of the analyzed potassium felspars (kfs) with the Pet_Barroso calibration and Spd_Calibration from the pLIBS.

1.6.4. Comparing the handheld LIBS spectra of a crystal versus a pellet of spodumene

Performing an analysis with a handheld LIBS can become a challenge if the crystal has a reflecting surface. This can cause the equipment to stop shooting and give a warning of no sample detected. Milling the sample solves this issue but requires sample preparation. Another way to go past this issue is by painting the surface of the crystal with a graphite pencil, which has a known composition (carbon) and forces the

equipment to start the analysis. However, the resulting spectrum usually has lower intensity stronger background signal and even the main peaks have different proportions from those of the pellets (Figure 39 and Figure 40). Roughening the surface of the crystal helps with the “no sample detection” problem and with the spectra intensity. Thus, shooting the crystal several times in the same place has the advantage of helping to roughen the surface and clean it from superficial contaminations possibly attached to the surface.

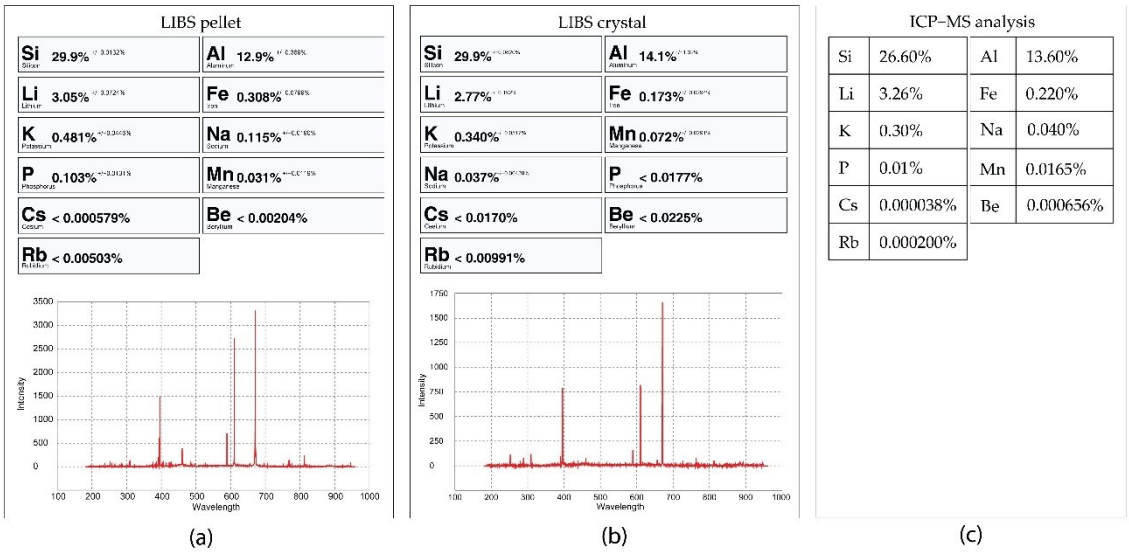

Figure 39. LIBS analysis of the spodumene sample 32-C1 in pellet (a) compared with the crystal sample (b) and the ICP-MS analysis (c). These LIBS analyses were performed with the Spd_Barroso calibration.

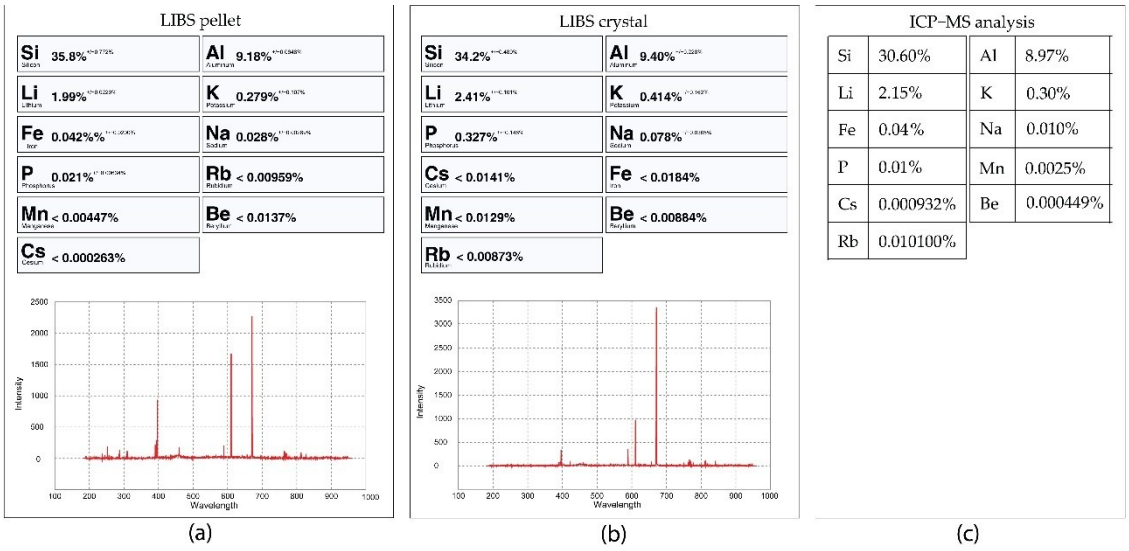

Figure 40. pLIBS analysis of the petalite sample 38-B1 in pellet (a) compared with the crystal sample (b) and the ICP-MS analysis (c). These LIBS analyses were performed with the Pet_Barroso calibration.

Analyzing a crystal versus analyzing a pellet can also provide different results since the analysis of a pellet will be closer to a bulk analysis of the crystal than the crystal analysis made in one place (0.5x0.5 mm) of the crystal surface. Local analyses are more dependent on the trace-element variations along the crystals, such as variations in the Fe and Mn contents. Fe can easily substitute Al in the crystal structure of spodumene (LiAlSi2O6) in different concentrations along the crystal, thus a single crystal can have Fe-richer zones and Fe-poorer zones (Deer *et al.* 1978). Other examples of minor or trace elements that can be found on spodumene are Cr, V, Ga, Mn, Co, Ni, Cu, Sn, Ge, Rb, Be, Ga, Zn, Ta, Nb and Sc (Claffy 1953). Another aspect to be considered is that small contaminations of other minerals can also be attached to the crystal surface, such as a small micas or Fe and Mn oxides (a common phenomenon in the samples from the BA field). Such contaminations, when milled together with the crystal, get scattered and diluted both in the pellet or the ICP-MS analyses. When using the pLIBS the user usually chooses the cleaner spot, which results in different concentrations of the trace elements. Since the results from the ICP-MS and the pLIBS analysis on the pellets are both from milled crystals, they should be closer than the LIBS analysis performed on the crystals. Noticeable differences between the crystal and pellet analysis are for example, the spectrum from the crystal 3-C2 that has more Al than the pellet, 17-C2 has more Fe on the pellet than in the crystal, 18-C2 seems to have more Na in the pellet than in the crystal and 32-C2 has more Na, Al and Fe in the pellet than in the crystal.

1.7. Conclusions

This work successfully developed a new set of calibrations for a handheld LIBS to analyze and identify spodumene and petalite from the BA field.

In fieldwork, it is possible to check if there are Li-minerals in an outcrop with these three calibrations by directly analyzing the crystal. This could be done either by choosing the Spd_Barroso or Pet_Barroso calibration and if the mineral has the Li content of a spodumene or a petalite (~2-3% of Li), then the Fe_Barroso calibration should follow to check what mineral it is and if the right calibration was chosen.

Since petalite has less Li than spodumene, a body with only petalite will have a lower Li content than a deposit with only spodumene. Each aplite-pegmatite should be carefully analyzed since it is possible to have only one of these minerals in one zone, another in depth, or on the other side of the outcrop. Using a pLIBS in outcrops should

only be for the first stages of exploration to identify aplite-pegmatites with Li-mineralization. However, the pLIBS can also be used in drilling cores to learn the Li-mineralization and distribution of the full body.

For precise analysis of the mineral contents, it is recommended to collect samples, mill, press and re-analyze them again in a controlled environment.

This study allowed us to conclude the following:

1. From all the elements detected in ICP-MS (Table 1 and Table 2), only the Li, Al, Si, Fe, K, P, Na, Rb, Mn, Cs and Be had detectable peaks in the pLIBS spectra;

2. The Intensity Ratios (IR) determined by dividing the total area of the peaks for one element by the total area of all the peaks in the spectra resulted in identical IRs for spodumene and petalite. This forced the creation of two calibration lines for each mineral for all the chemical elements, except for Fe, which was the only element with distinct IRs for both minerals. Thus, it was only possible to successfully distinguish and analyze spodumene and petalite because petalite had always more Fe than spodumene and IRs greater than 0.0038 (Figure 29);

3. To distinguish between spodumene and petalite, the calibration Fe_Barroso must be used. For a more complete chemical analysis the Spd_Barroso calibration must be used if Fe > 0.1% and the Pet_Barroso calibration if Fe < 0.1%;

4. The Fe calibration cannot be used carelessly in other pegmatite fields, without first learning the chemical signature of the trace elements of spodumene and petalite for that field because there are petalites that can have higher Fe content than 0.1% (e.g., 0.99% of Fe in a Fe-bearing petalite from a pegmatite with spodumene and quartz from the eastern Transbaikal region, Russia (Deer *et al.* 2004)).

5. The distinction of fine mixtures of spodumene and quartz from single crystals of spodumene and petalite was possible with the Fe and Al results from ICP-MS. However, the pLIBS could not distinguish the spd + qtz mixtures from spodumene due to the IR overlapped for Al (Figure 30);

6. About the LIBS analysis errors, only the major elements of spodumene and petalite (Al, Si and Li) have consistent errors below 20% (Figure 35) and accuracy above 0.8 (Figure 34). All the other elements have errors greater than 20%.

7. Although LIBS is easily affected by changes in the crystal structure, the presence of spodumene in the petalite pellets did not seem to affect the results, as shown by samples 38-B1 and 39-B2, where Li and Al had errors of less than 30% when compared to ICP-MS (Figure 35);

8. If the mineral that is being analyzed is not spodumene or petalite, the Spd_Barroso and the Pet_Barroso will deny the sample as being one of these two minerals. For example, a K-feldspar, will result in a very low analysis for Li, and will have higher K content (Figure 36, Figure 37 and Figure 38);

9. Analyzing pellets and crystals with a pLIBS has different results (Figure 39 and Figure 40). In the pellets, the trace elements are averaged because of the homogenized material, while the trace elements may vary along a crystal. The ICP-MS results will be more similar to a pellet than to a spot analysis in a crystal. Therefore, when calibrating a LIBS with ICP-MS analysis is better to use pellets instead of crystals;

10. The crystal surface reflectiveness (flat or transparent) can be a problem for the pLIBS, since the equipment may not detect the sample or produce low intensity spectra with strong background signal, masking the smaller peaks and producing inaccurate results for the trace elements. Milling the samples and pressing them into pellets helps with this issue;

11. The presence of quartz also seems to affect the spectra intensity even if the minerals are milled, as was observed with the spectra of the pellets of the mixtures of spodumene and quartz (Figure A1);

Author Contributions: Conceptualization, F.D., R.R., F.G. and A.L.; methodology, F.D., R.R., F.G. and A.L.; formal analysis, F.D., R.R., F.G. and A.L.; investigation, F.D., R.R., F.G. and A.L.; resources, A.L.; data curation, F.D., R.R., F.G. and A.L.; validation, F.D., R.R., F.G. and A.L., writing—original draft preparation, F.D.; writing—review and editing,

all remaining authors; visualization, F.D., R.R., F.G. and A.L.; supervision, T.M., E.R.-R. and A.L.; project administration, A.L.; funding acquisition, A.L. All authors have read and agreed to the published version of the manuscript.

Acknowledgments: The authors gratefully acknowledge the comments from three anonymous reviewers and the academic editor. We would also like to thank the people from INESC TEC and Maria Irene Costa for allowing us to use their laboratory and respective tools. We are also grateful for the support of Ariane Mendes Pinto, who helped us produce the pellets used in this study.

Funding: This work was funded by the European Commission's Horizon 2020 innovation programme under grant agreement no. 869274 by the project GREENPEG New Exploration Tools for European Pegmatite Green-Tech Resources. This work was co-funded through the project CAVALI—Cadeia de Valor do Lítio, reference POCI-01-0247-FEDER-047728, cofinanced by FEDER—Fundo Europeu de Desenvolvimento Regional, in the scope of the Programa Portugal 2020, through COMPETE 2020—Programa Operacional. This work was co-funded through the project INOVMINERAL 4.0— Tecnologias Avançadas e Software para os recursos Minerais, reference POCI-01-0247-FEDER-046083, cofinanced by FEDER—Fundo Europeu de Desenvolvimento Regional, in the scope of the Programa Portugal 2020, through COMPETE 2020—Programa Operacional. The work is co-funded by national funds through FCT—Fundação para a Ciência e Tecnologia, I.P., in the framework of the ICT project with the references UIDB/04683/2020 and UIDP/04683/2020. Filipa Dias and Ricardo Ribeiro are financially supported within the compass of their respective Ph.D. theses, ref. 2020.05534.BD and ref. SFRH/BD/140266/2018, by national funds from MCTES through FCT, and co-financed by the European Social Fund (ESF) through POCH—Programa Operacional Capital Humano—and the NORTE 2020 regional program.

1.8. Appendix A

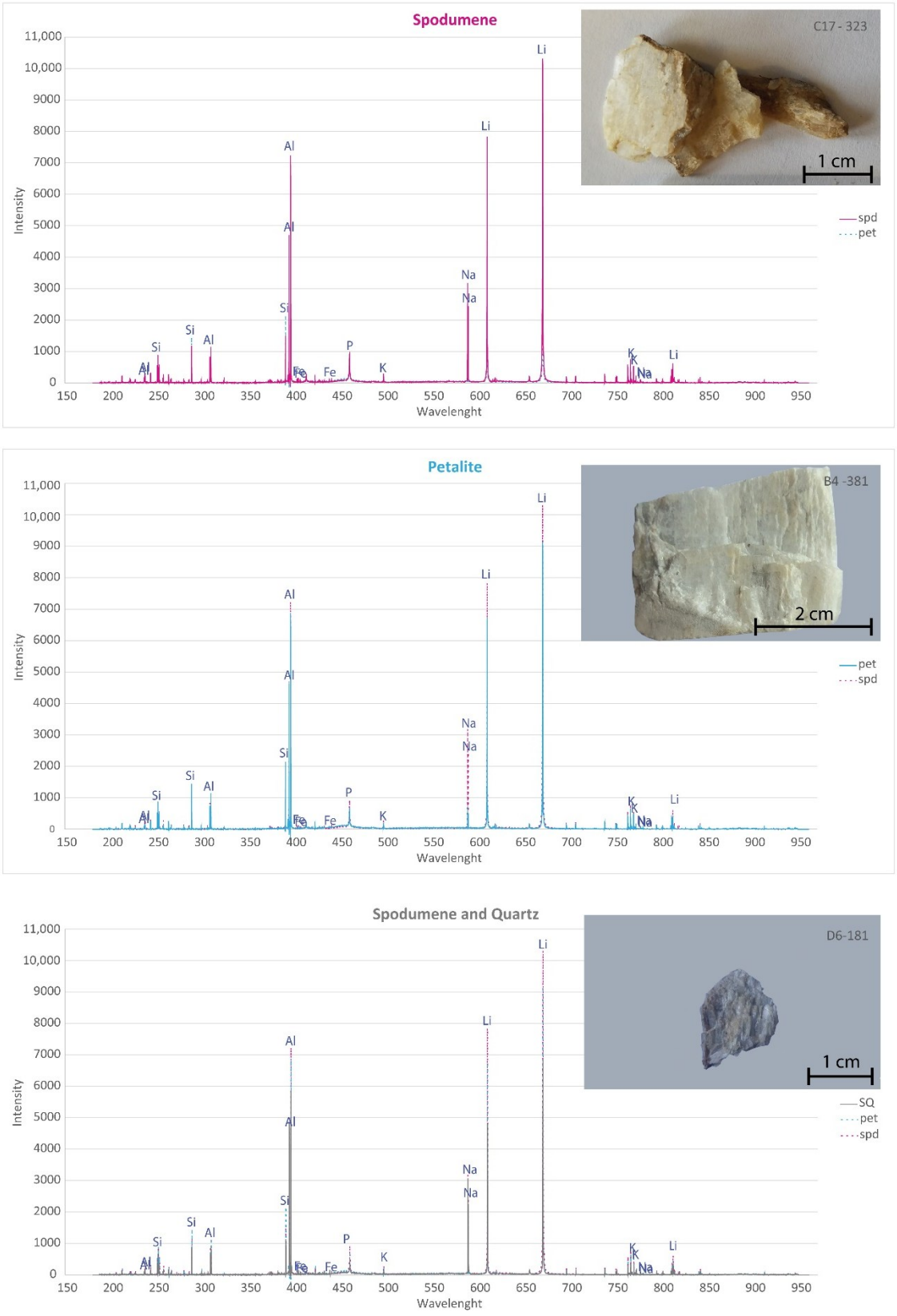

Figure 41. pLIBS spectra for the pellets of the spodumene (spd) sample 32-C3 (pink spectra) compared to the petalite (pet) sample 38-B1 (blue spectra) and to the spodumene and quartz (SQ) sample 18-D1 (black spectra).

2. K-Feldspar Geochemistry as an Indicator of Lithium Mineralization in the Barroso-Alvão Aplite-Pegmatite Field, Northern Portugal

Adapted from: Filipa Dias, Ricardo Ribeiro, Filipe Gonçalves, Alexandre Lima, Encarnación Roda-Robles, Tânia Martins and Diana Guimarães

The Canadian Journal of Mineralogy and Petrology (2025) Early Publication

https://doi.org/10.3749/2500006

Published: 31 October 2025

Abstract

ICP-MS analysis was conducted to examine the geochemical composition of K-feldspars from various aplite-pegmatites in the Barroso-Alvão field, focusing on the differences between Li-rich and Li-barren aplite-pegmatites. The study revealed significant variations in the concentrations of minor and trace elements (Rb, Tl, Li, Ga, Pb, Cs, Ba, Be, Ta, and Sn) present in the K-feldspars of Li-barren, spodumene-rich, and petalite-rich aplite-pegmatites. The data also indicate a geographical trend in both mineralogy and geochemistry across the aplite-pegmatites of the Barroso-Alvão field. Li-barren aplite-pegmatites are more concentrated in the SE, spodumene-rich ones dominate the center, and petalite-rich varieties are more common in the NW. Additionally, portable XRF analysis was performed on the crystals of the same samples to evaluate the feasibility of in situ geochemical analysis of K-feldspars, aiming to determine whether an aplite-pegmatite can be quickly identified as Li-rich. This approach seeks to provide a rapid field assessment of whether an aplite-pegmatite justifies further exploration for Li mining. Notably, the trace amounts of Li, Sn, P, and Ta found in K-feldspars are likely due to mineral inclusions of spodumene, cassiterite, apatite, and columbite-tantalite minerals, as observed petrographically in one of these Li-rich aplite-pegmatites.

Keywords: lithium, rubidium, X-Ray Fluorescence, ore identification, Barroso-Alvão, Portugal, pegmatites, Europe; economic geology, potassium feldspar, trace-elements, ICP-MS, exploration.

2.1. Introduction

In the Barroso-Alvão (BA) aplite-pegmatite field, lithium (Li) primarily occurs in spodumene and petalite. However, not all aplite-pegmatites in this field contain Li-minerals; some are Li-barren, while others are spodumene-rich and/or petalite-rich, and rarely are lepidolite-rich. Adding to the complexity of this field is the fact that the various aplite-pegmatites do not appear to be spatially distributed based on mineralization type, and there seems to be no regional zonation related to nearby granites (Lima *et al.* 1999b, Martins & Lima 2011). Moreover, the internal heterogeneity is common; while one part of the body may be Li-barren, another may be Li-rich, further complicating exploration efforts (Dias *et al.* 2023a) For these reasons, developing an early-stage exploration tool to distinguish between different aplite-pegmatites types without requiring prior identification of Li-minerals would be highly beneficial.

This study focused on using potassium-feldspars (K-feldspars), specifically, orthoclase and microcline ($KAlSi_3O_8$), as exploration guides for identifying Li-rich aplite-pegmatites in the BA field because: 1) K-feldspars are easily recognizable minerals due to their distinct appearance, high abundance and large size (usually centimetric); and 2) variations in their chemical composition (namely in their minor and trace elements) may assist in distinguishing between different types of aplite-pegmatites. Previous studies, including those by Heier (1962), Gordiyenko (1971), Shmakin (1979), Smeds (1992), Černý (1994), Breiter et al. (2002), Larsen (2002), Alfonso et al. (2003), Sánchez-Muñoz et al. (2017) and Garate-Olave et al. (2018) have explored how minor changes in the chemical composition of K-feldspars relate to the type of pegmatite and the degree of fractionation. However, since every pegmatite field is unique due to its formation under various environments and conditions, these results should only be used as general trends. The geochemical signature of each field should be recognized before starting any exploration campaigns. This study aimed to analyze the general trends of K-feldspars in the BA field and utilize this knowledge to optimize time and resources in Li-exploration. This can be achieved using a handheld chemical analyzer, such as a portable XRF, to analyze K-feldspars in outcrops or drill cores and determine whether the aplite-pegmatite is Li-barren, spodumene-rich, or petalite-rich.

Identifying the dominant Li-mineral in the aplite-pegmatites from the BA field is valuable for the battery and ceramics industries. Spodumene is preferred for battery production due to its well-established metallurgical process. Meanwhile, petalite aplite-pegmatites are favored in the ceramics industry because of their lower iron (Fe) content

compared to the spodumene-rich aplite-pegmatites of the BA field (Martins *et al.* 2005, 2007a).

2.1.1. Fractionation Trends in K-Feldspars: A Literature Overview

The most fractionated pegmatites are often of significant economic interest, due to their high concentrations of elements such as Li, Rb, Cs, Be, Ta, Nb, Sn, P, F, and B, making them highly desirable for mining. According to the classical model of pegmatite formation, these bodies form through extensive fractionation of a granitic melt, where a granite must crystallize first. The remaining melt, enriched in incompatible elements, continues to evolve, through further fractionation eventually forming pegmatites enriched in in these economically important elements (Cameron *et al.* 1945, Jahns & Burnham 1969, Černý 1991).

Alternatively, another model suggests that some pegmatites achieve similar enrichment without a preceding granite, instead forming through multiple low-degree partial melting events of metasedimentary rocks. This process also involves fractionation but follows a different path rather than evolving directly from a single large-volume melt (Simmons & Webber 2008, Müller *et al.* 2017, Knoll *et al.* 2023, Koopmans *et al.* 2024).

K-feldspars can serve as key indicators of pegmatite fractionation by incorporating various chemical elements during crystallization, either within their structure or as solid mineral phases. According to Černý (1994), they can contain minor and trace elements of Li, Rb, Cs, Tl, Pb, NH_4^+, Ba, Sr, Fe^{3+}, P, Ga, B, and Be.

Among these elements, Li, Rb, Cs, and Tl are incompatible elements that tend to concentrate more in the K-feldspars of the more fractionated Li-rich pegmatites. According to the literature, the concentration of these elements can reach: Li 500 ppm (Černý *et al.* 1985a), Rb 4.98 wt.%, Cs 4240 ppm (Černý *et al.* 1985b), and T1 650 ppm (Borovik-Romanova & Sosedko 1960). As stated by Černý (1994), a highly fractionated pegmatite often contains Rb in the range of 1000-2500 ppm and Cs in the range of 2000-3000 ppm. Additionally, Gordiyenko (1971) indicates that K-feldspars from spodumene-bearing pegmatites typically contain Li > 80 ppm and K/Rb < 20 ppm. Likewise, Smeds (1992) mentioned Li-bearing pegmatites with spodumene from Sweden, usually with Li > 80 ppm.

Regarding Ga and P, both elements are considered incompatible. In Tres Arroyos (Badajoz, Spain), K-feldspars from aplite-pegmatites with Li–Al phosphates exhibit high P concentrations, around 3000 ppm (Garate-Olave *et al.* 2018). However, Černý *et al.* (1984) and London *et al.* (1990) observed that, although P generally increases in fractionated pegmatites, its concentration can vary significantly. For instance, the co-precipitation of apatite can lead to severe depletion of P in K-feldspars (London *et al.* 1990). Brown *et al.* (2017) reported that in the Tanco spodumene-rich pegmatite (Canada), P content varies with K-feldspar generation: early generations have higher concentrations (960-2000 ppm), while later generations contain almost no P. Similarly, Černý (1994) found significant variability in Ga concentrations in Li-rich pegmatites. For example, Ga content in K-feldspars from the Bikita petalite-rich pegmatite (Zimbabwe) was much lower than in Tanco. Despite this variability in P, Sánchez-Muñoz *et al.* (2017) successfully used P content in K-feldspars to distinguish Li-rich pegmatites from Li-barren ones in various locations worldwide. Li-rich pegmatites generally show high P content (835-5965 ppm) and low Fe content (2-151 ppm), whereas Li-barren pegmatites display the opposite trend.

Regarding Pb, Černý (1994) states that Pb behaves as an incompatible element, and its concentration tends to be higher in pegmatites rich in Niobium, Yttrium, and Fluorine (NYF) compared to Li-rich pegmatites. Consequently, K-feldspar crystals (amazonite) from NYF pegmatites can contain high Pb concentrations, sometimes reaching 1-3% Pb. However, Alfonso et al. (2003) reported that in the Cap de Creus pegmatite field in Spain, a region with Li-rich pegmatites, the concentration of Pb in K-feldspars decreases as the pegmatites become more fractionated, thus behaving as a compatible element.

Barium, Sr, and Fe^{3+} are compatible elements that tipically enter the crystal structure during the initial stages of crystallization. Consequently, high concentrations of these elements generally indicate Li-barren pegmatites (e.g. Věžná, Czech Republic: Ba 13100 ppm / Sr 400 ppm (Černý 1994)). In contrast, Li-rich pegmatites are expected to contain low concentrations of these elements (e.g., Pinilla de Fermoselle, Zamora, Spain: Ba 0.8 ppm / Sr 0.4 ppm (Roda Robles *et al.* 2012); Kings Mountain, USA: Ba 48 ppm / Sr 45 ppm (Shmakin 1979, Černý 1994); and Fe 3-44 ppm Sánchez-Muñoz *et al.* (2017)).

2.2. Geological setting of the Barroso-Alvão (BA) aplite-pegmatite field

The BA aplite-pegmatite field is located in Western Europe, specifically within the Iberian Peninsula, in northern Portugal, between the Vila Real and Braga districts. It extends into parts of the municipalities of Montalegre, Boticas, Vila Pouca de Aguiar, Ribeira de Pena, and Cabeceiras de Basto (Figure 42). This field covers an area of approximately 400 km2 and contains numerous Li-rich aplite-pegmatites that formed during the Variscan Orogeny and were emplaced into Silurian metasediments. These metasediments mainly consist of schists, metagreywackes, quartz-phyllite, and quartzites, part of the Galiza Trás-os-Montes Zone (GTMZ) parautochthonous terrains. Surrounding this field are syn-tectonic and post-tectonic granites, which have intruded these terrains (Noronha & Lima 1992, Noronha et al. 1998).

In this region of the Iberian Peninsula, the Variscan Orogeny (Early Devonian to Late Carboniferous) is defined by three main deformation phases: D1 (Devonian), D2 (Late Devonian–Early Carboniferous), and D3 (mid- to late Carboniferous); with peak metamorphic conditions of the andalusite zone occurring during syn- to late-D3. Although D3 structures control the emplacement of most aplite-pegmatites, they also exhibit D3-related deformation (Charoy et al. 1992, Dias & Ribeiro 1995, Ribeiro 1998, Charoy & Noronha 1999a).

This study area contains both Li-rich and Li-barren aplite-pegmatites with no significant regional zonation relative to the surrounding granites. The Li-barren aplite-pegmatites can be found within the metasediments (along with the Li-rich aplite-pegmatites) or within the syn-tectonic granites. However, the Li-rich aplite-pegmatites occur exclusively within the metasediments (Martins & Lima 2011). The red circles in Figure 42 indicate the aplite-pegmatites sampled for this study. Only aplite-pegmatites emplaced within the metasediments were sampled.

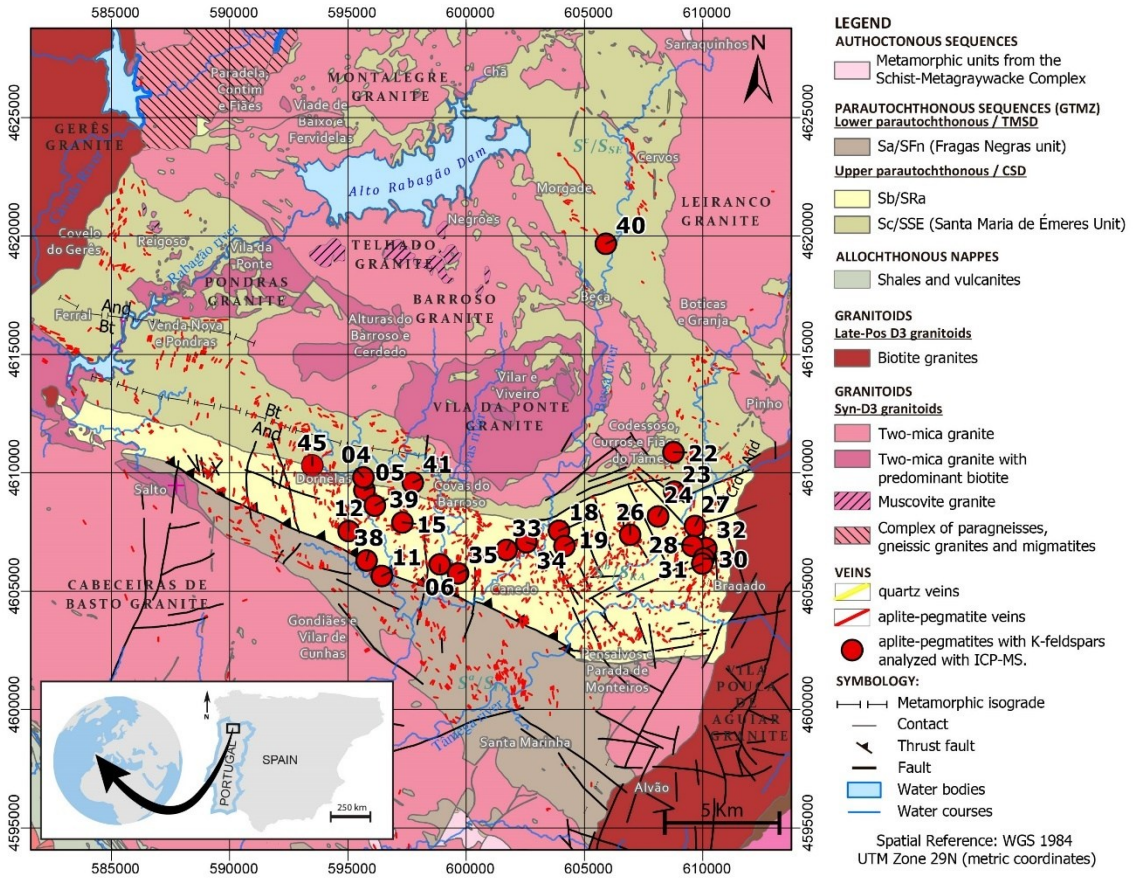

Figure 42. Geologic map of the Barroso-Alvão aplite-pegmatite field with the location of the aplite-pegmatites (red circles) from where the K-feldspars for this study were collected. Adapted from 1:50 000 geological mapping (Teixeira & Cândido de Medeiros 1969, Ávila Martins & Noronha 1982, Noronha & Lima 1992, Noronha et al. 1998). Colored based on Rodríguez Fernández *et al.* (2015). Civil parishes and waterlines: © 2023 DADOS.GOV.PT and © Agência Portuguesa do Ambiente (APA). Available online: https://sniamb.apambiente.pt/content/geo-visualizador (accessed on 19 July 2022) and https://dados.gov.pt/pt/datasets/freguesias-de-portugal/#resources (accessed on 4 March 2023). The Inset shows the location of Barroso-Alvão in Portugal and globally.

2.3. Materials and Methods

This study analyzed 35 K-feldspar crystals from 30 aplite-pegmatites in the BA field. These K-feldspars were extracted from aplite-pegmatite samples (Lima 2000) collected during a field campaign and preserved as archival specimens. Of the 30 sampled aplite-pegmatites, six had unknown mineralogy, three were Li-barren, ten were petalite-rich, ten were spodumene-rich, and one contained equal amounts of spodumene and petalite. The K-feldspar crystals were cut and cleaned of impurities using a diamond saw blade. Each crystal was divided into two portions: one was milled and sifted to a grain size of <125 µm, utilizing a Retsch Mortar Grinder RM 200 (Retsch GmbH, Haan,

Germany) and a Retsch Test Sieve (Retsch GmbH, Haan, Germany); the other portion was kept in its crystal form.

The milled crystals were sent to Activation Laboratories Ltd. (Actlabs) in Ancaster, ON, Canada, for certified Inductively Coupled Plasma Mass Spectrometry (ICP-MS) analysis. The package “Ore-Assays - 8-Peroxide ICP-OES + ICP-MS” analyzed Al, K, and Si through Peroxide “Total” Fusion digestion. The package “UT-6M” was utilized to analyze Ba, Be, Ca, Cr, Cs, Fe, Ga, Li, Mn, Na, Nb, P, Pb, S, Si, Sr, Ta, Tl, and Zn via 4-Acid “Near-Total” Digestion.

The samples, kept in crystal form (up to 2x3 cm), were analyzed using portable X-Ray Fluorescence Equipment (pXRF), specifically the Bruker S1 TITAN 600. This device contains an X-ray tube with a Rh anode operating at 2 W of power and a current of 5-100 µA. The GeoMining calibration (P/N: 730.0203) was utilized to analyze all samples through three analysis phases (15, 30, and 50 keV), each lasting 30 s (90 s total). All samples were analyzed three times at the same location, and the average result was taken as the final measurement.

To ensure the quality of the pXRF analysis, the reference values for the Quality Control (QC) Geo/Soil Sample CS-M2 (provided by Bruker) were compared with the QC results obtained before and after each run of the K-feldspar measurements. This comparison confirmed the proper functioning of the equipment, as all results fell within the expected QC range: Al2O3 (10.89-12.74%); SiO2 (63.82-73.77%); K2O (4.36-5.19%); Mn (950-1260 ppm); Fe (1.70-1.80%); Ni (< LOD); Cu (189- 247 ppm); Rb (122-162 ppm); and Pb (758-1013 ppm). However, after the QC analysis, a blank of boric acid (H3BO3) (Sigma product # B6768) was also analyzed with the pXRF to determine if the instrument had any contamination. The analysis revealed some contamination peaks in SiO_2, S, Ca, Cr, Mn, Fe, and Sn, thus excluding these elements from this XRF study analysis.

Table 7 presents the LODs for the elements detected by ICP-MS and pXRF (from pure SiO2). Since ICP-MS can detect a wider range of elements in K-feldspars compared to pXRF, only those detectable by both techniques are included in the table.

The ICP-MS and pXRF results were plotted in binary graphs using ioGAS™ software from IMDEX Limited Company. This software, designed primarily for the mining industry, retains all measurements without omitting any data. It also plots samples with values below the Limit of Detection (LOD) by utilizing half of the LOD value, which allows

for the visualization of low-concentration samples and the differentiation from higher-concentration ones.

All maps in this study were generated using ArcGIS Pro software from Esri, Inc.

To learn more about the geochemistry of K-feldspars in the BA field, a petrographic analysis was conducted on aplite-pegmatite #41-NOA/AL56, a spodumene-rich aplite-pegmatite containing minor petalite. The study included cathodoluminescence (CL) imaging performed with a Citl Mk 4 system, equipped with a cold cathode electron gun and coupled to a Nikon OPTIPHOT-POL polarizing microscope. Additionally, Backscattered Electron (BSE) imaging was conducted using a Hitachi FlexSEM1000 Scanning Electron Microscope (SEM), equipped with a Bruker QUANTAX 80 Energy Dispersive X-ray Spectroscopy (EDS) system and a silicon drift detector (XFlash 630H) at the Department of Geosciences, Environment, and Spatial Planning, University of Porto, Faculty of Sciences, Portugal.

Table 7. Limit Of Detection (LOD) of the X-Ray Fluorescence (XRF) and Induced Coupled Plasma Mass Spectroscopy (ICP-MS).

ppm	pXRF	ICP-MS
Al_2O_3; Al	1250; 758	189; 100
Ba	62	10
Ca	35	100
Fe	20	100
Ga	1	0.05
K_2O; K	44; 37	1205; 1000
Mn	13	5
P	39	10
Pb	6	0.5
Rb	1	0.1
Ta	43	0.05
Tl	15	0.02
SiO_2; Si	N/A	217; 100
Sn	69	0.2
Sr	2	0.2
Zn	2	2

2.4. K-Feldspar Chemistry in the Barroso-Alvão Aplite-Pegmatite Field

This section presents the ICP-MS results for K-feldspars sampled across the BA field, including Li-rich (spodumene- and petalite-rich), Li-barren, and aplite-pegmatites with unknown Li-mineralization. Table 8 and Table 9 summarize the analytical results. Although the samples are not grouped by mineralogical type, the dataset provides a comprehensive overview of compositional variability across the field.

Table 8. ICP-MS Results of K-Feldspars from Different Aplite-Pegmatites of The Barroso-Alvão Field Sampled in this Study (in some cases, multiple crystals were extracted from the same aplite-pegmatite, labeled as Kfs1, Kfs2, and so forth).

	1 Kfs 1	2 Kfs 1	2 Kfs 2	4 Kfs 1	6 Kfs 1	10 Kfs 1	11 Kfs 1	11 Kfs 2	15 Kfs 1*	16 Kfs 1	18 Kfs 1	19 Kfs 1	22 Kfs 1	23 Kfs 1	24 Kfs 2	26 Kfs 1	27 Kfs 1	Error* %
Si %	30.30	30.40	29.50	30.50	30.10	30.90	30.70	31.50	31.60	31.00	30.90	31.00	30.30	29.90	31.10	30.90	30.00	0-1%
K %	8.70	10.20	10.00	11.80	11.30	11.50	10.90	10.40	7.30	9.60	10.80	10.60	10.50	10.80	10.20	10.70	10.40	1-2%
Al %	9.65	9.78	9.66	9.56	9.95	10.10	9.63	9.94	9.52	9.71	9.76	9.78	9.54	9.72	9.30	9.98	9.86	1-2%
Na %	2.67	1.97	1.96	0.57	0.83	1.16	0.99	1.70	1.55	0.97	0.78	1.09	1.33	1.44	1.15	1.58	1.79	0-1%
P %	0.28	0.29	0.29	0.09	0.34	0.31	0.18	0.16	0.37	0.24	0.07	0.27	0.18	0.27	0.31	0.27	0.36	0-1%
Rb ppm	1090	793	876	2400	1650	1820	1630	1840	2220	2810	1310	1820	291	1380	404	1210	849	1-16%
Fe ppm	600	300	300	400	200	600	300	900	1600	500	700	400	300	200	600	400	400	0-25%
Ca ppm	500	100	100	900	100	< 100	600	1300	< 100	100	300	300	400	100	< 100	100	200	0%
Li ppm	14	18	9	40	185	82	365	201	596	579	785	429	8	35	10	33	12	0-1%
Cs ppm	75	63	51	121	187	119	101	89	125	204	243	174	16	104	24	44	83	1-2%
Mn ppm	30	42	25	26	66	65	67	142	88	21	70	494	19	26	30	52	45	0-2%
Ba ppm	20	40	50	10	< 10	< 10	< 10	< 10	< 10	< 10	10	< 10	210	160	40	20	20	0%
Pb ppm	36	68	65	5	48	21	28	25	14	16	69	37	96	64	48	45	36	0-1%
Sr ppm	23	26	31	56	28	19	35	55	14	75	22	11	63	34	16	59	15	1-3%
Tl ppm	10	9	9	27	27	23	19	18	21	36	13	23	3	14	3	11	7	1-7%
Ga ppm	12	11	13	12	13	17	17	16	24	22	14	15	9	11	13	10	10	0-1%
Sn ppm	9	5	6	2	11	9	8	9	12	17	12	13	5	11	11	7	9	0-5%
Zn ppm	2	5	3	7	8	10	7	12	36	12	12	37	4	4	4	11	4	0-16%
Be ppm	12	4	5	3	4	5	3	2	34	50	8	17	1	4	3	4	5	2-7%
Nb ppm	0	0	0	1	3	1	1	1	5	9	4	1	0	0	2	< 0.1	< 0.1	26-33%
Ta ppm	0.24	0.12	0.06	0.41	0.73	0.35	0.14	0.21	1.36	2.38	2.4	0.18	< 0.05	0.15	0.67	< 0.05	< 0.05	0%

*15-1: negative K anomaly and positive Fe anomaly compared to the other samples.

* Error percentage calculated using duplicate samples from Actlabs

Table 9. ICP-MS Results of K-Feldspars from Different Aplite-Pegmatites of the Barroso-Alvão Field Sampled in this Study (in some cases, multiple crystals were extracted from the same aplite-pegmatite, labeled as Kfs1, Kfs2, and so forth).

	28 Kfs 1	30 Kfs 1	31 Kfs 1	32 Kfs 1	33 Kfs 1	33 Kfs 2	33 Kfs 3	34 Kfs 1	34 Kfs 2	35 Kfs 1	35 Kfs 2*	38 Kfs 1*	38 Kfs 5*	39 Kfs 1	39 Kfs 2*	40 Kfs 1	41 Kfs 3*	45 Kfs 1	Error* %
Si %	29.70	29.80	30.60	30.20	30.70	30.80	30.90	30.70	31.00	30.40	27.60	30.10	30.50	31.00	31.70	30.60	32.30	30.80	0-1%
K %	10.20	9.70	9.70	10.90	11.90	11.60	11.90	10.60	12.20	10.50	9.50	10.80	10.90	11.30	10.50	10.50	10.20	11.50	1-2%
Al %	9.65	9.43	9.50	9.76	9.76	9.56	9.86	9.86	9.51	9.53	8.42	9.97	9.90	9.78	9.39	9.97	9.30	9.95	1-2%
Na %	1.74	1.80	1.84	1.22	0.50	0.69	0.68	1.53	0.64	1.10	1.10	1.13	1.10	0.88	0.58	1.15	1.74	0.83	0-1%
P %	0.26	0.15	0.14	0.21	0.07	0.09	0.18	0.15	0.10	0.21	0.21	0.40	0.40	0.17	0.12	0.09	0.21	0.25	0-1%
Rb ppm	1080	781	812	1240	1710	1860	2380	1380	1260	1830	1820	2730	2810	2430	2500	2430	1260	3030	1-16%
Fe ppm	300	300	200	200	200	300	300	300	300	200	200	200	100	300	300	600	500	200	0-25%
Ca ppm	200	600	600	200	200	1100	1600	1900	1300	200	200	100	100	2600	500	900	1900	200	0%
Li ppm	23	38	37	174	61	149	321	202	119	457	449	863	925	258	2160	133	120	150	0-1%
Cs ppm	45	46	46	54	128	125	129	236	111	105	103	*8202	*8302	108	119	59	42	121	1-2%
Mn ppm	44	46	27	42	28	94	221	35	314	43	46	93	75	154	342	27	430	25	0-2%
Ba ppm	30	200	220	20	50	< 10	20	10	10	< 10	< 10	< 10	< 10	< 10	< 10	30	20	< 10	0%
Pb ppm	46	106	106	74	8	17	25	19	17	14	14	44	43	12	12	10	39	24	0-1%
Sr ppm	52	50	50	30	50	83	211	241	40	11	11	10	11	40	21	100	72	63	1-3%
Tl ppm	9	9	9	13	21	19	23	17	15	21	20	38	39	28	26	23	13	31	1-7%
Ga ppm	10	11	11	15	18	14	14	17	8	16	15	33	32	20	15	17	14	17	0-1%
Sn ppm	8	6	4	5	11	9	12	7	2	7	7	9	9	17	15	15	4	9	0-5%
Zn ppm	12	4	3	7	5	13	31	4	7	21	21	17	15	30	31	15	17	6	0-16%
Be ppm	4	3	5	6	9	19	11	2	17	5	5	63	83	6	12	43	13	4	2-7%
Nb ppm	0	1	1	0	4	2	2	0	0	0	0	12	6	3	2	10	1	1	22%
Ta ppm	0.06	0.44	0.43	0.09	2.02	0.93	0.57	0.33	0.08	0.05	< 0.05	5.24	2.35	0.69	0.75	3.7	0.1	0.12	26-33%

* 35-2: duplicate sample of the 35-1. 35-2 has a negative Si and Al anomaly compared to the other samples.

* 38-5: duplicate sample of the 38-1

* 39-2: positive Li anomaly compared to the other samples.

* 41-3: positive Si anomaly compared to the other samples

* Cs results from Peroxide “Total” Fusion since the maximum limit of detection for the 4-Acid “Near-Total” Digestion method was 500 ppm of Cs.

* Error percentage calculated using duplicate samples from Actlabs

2.4.1. Chemical Variability of K-Feldspar in Relation to Li-Mineralization Type

Several aplite-pegmatites in this study are already known from previous research and are identified by specific names, such as #32-Adagói, #33-Aldeia, #34-Alijó, #35-CHN3, #38-Gondiães, #39-Lousas, #41-NOA /AL56, and #45-Vila Grande. These aplite-pegmatites have the best-documented mineralogy, supported by numerous studies (e.g. Charoy *et al.* 1992, Farinha Ramos & Lima 2000, Lima 2000, Charoy *et al.* 2001, Martins 2009, Dias 2016b, Tucker Vasques 2021). However, this work also includes some aplite-pegmatites with partially or entirely unknown Li-mineralization. The results were categorized into the following classes based on the main Li-mineralogy of the known aplite-pegmatites: 1) petalite-rich; 2) petalite-rich with some spodumene; 3) spodumene-rich; 4) spodumene-rich with some petalite; 5) rich in both spodumene and petalite; and 6) Li-barren. In the case of the partially unknown aplite-pegmatites, the K-feldspars are currently known to belong to an aplite-pegmatite containing spodumene plus quartz. However, because they have not yet been thoroughly studied, it remains unclear whether their main Li-mineralization is spodumene or petalite, as spodumene could be of either primary or secondary origin (Lima & Dias 2019).

Instead of using the K/Rb ratio, Rb was utilized to analyze the chemical variability of K-feldspars in the BA field. This choice is based on significant measurement error in K concentrations, as indicated by the duplicates (Table 8 and Table 9). Potassium content ranges from 7.3% to 12.2% (mean 10.57%) across 35 samples, with 1–2% error in duplicate K measurements—corresponding to an uncertainty of approximately 1000–2000 ppm. In contrast, Rb concentrations vary from 291 to 3030 ppm. As a result, variations in K content are entirely overshadowed by its analytical error, making it impossible to detect any meaningful trend relative to Rb. This is demonstrated in Figure 43, which shows no correlation between K and Rb, despite the expectation that Rb should replace K in the feldspar crystal structure, increasing Rb as K decreases. Therefore, the K/Rb ratio was not used, as it would have introduced unnecessary noise into the fractionation analysis. Instead, to better assess chemical variability, Rb was plotted directly against minor elements (Ba, Be, Cs, Ga, Li, P, Pb, Sn, Sr, Ta, Tl) in binary diagrams (Figure 44 and Figure 46).

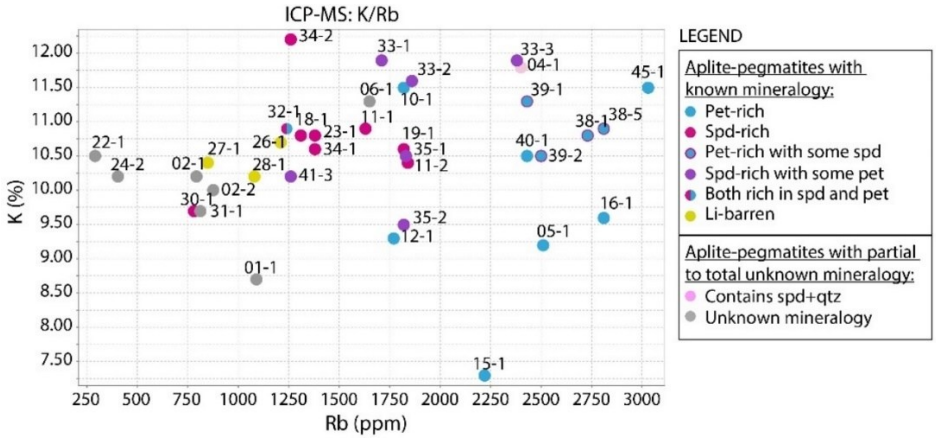

Figure 43. Plot of K by Rb from ICP-MS illustrating the inaccuracy of the K analysis in comparison to the Rb analysis. Since Rb enters the K-feldspar structure by replacing K, an increase in Rb should cause a decrease in K. However, this cannot be observed in this plot due to the significant error of the K analysis, making the K/Rb ratio useless in this study (Pet: petalite; Spd: spodumene; Qtz: quartz).

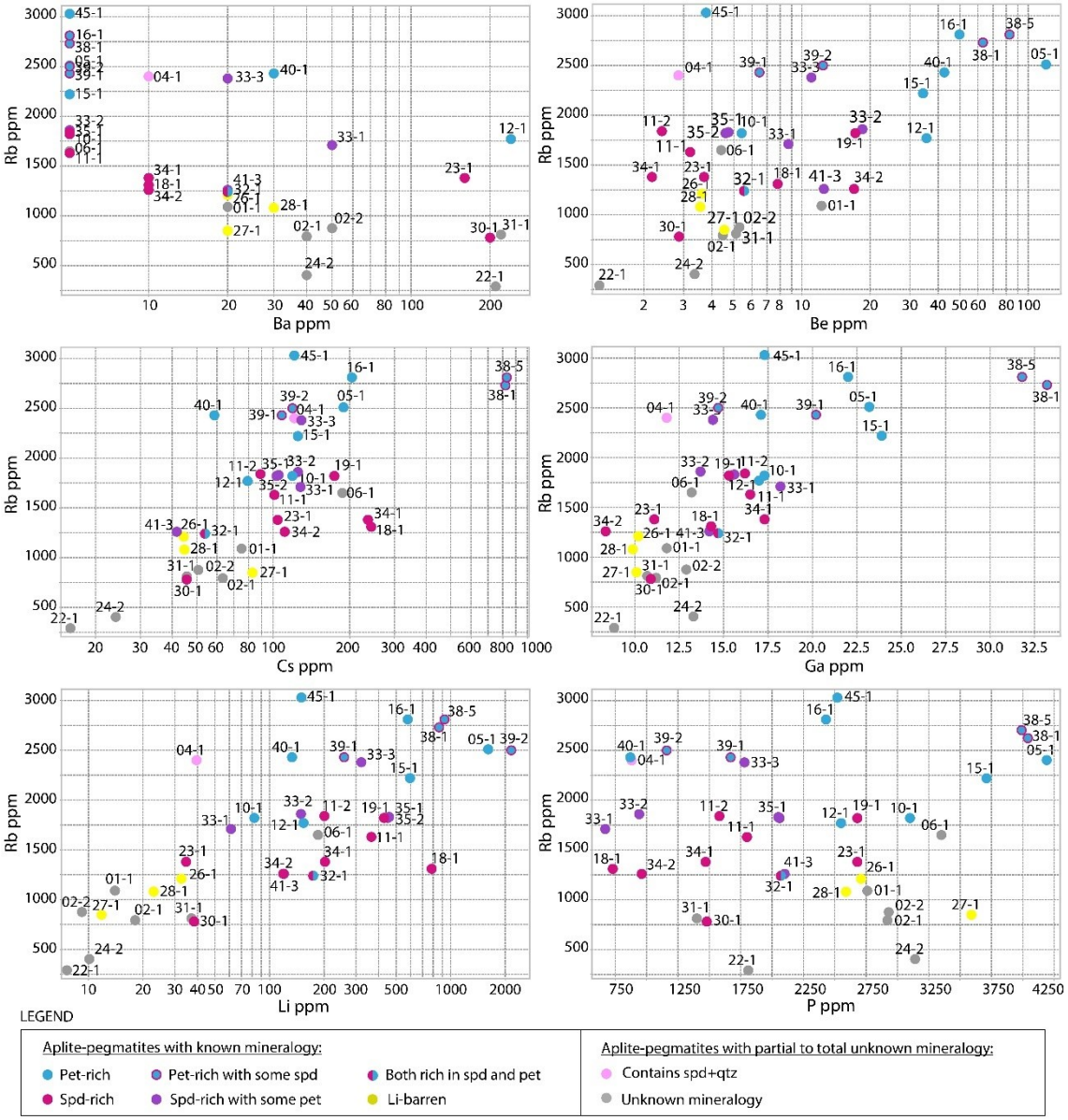

Figure 44. ICP-MS results illustrating the K-feldspar minor and trace element contents and variation of Rb against Ba, Be, Cs, Ga, Li, and P45 for the studied aplite-pegmatites with varying mineralogy from the Barroso-Alvão field (Pet: petalite; Spd: spodumene; Qtz: quartz).

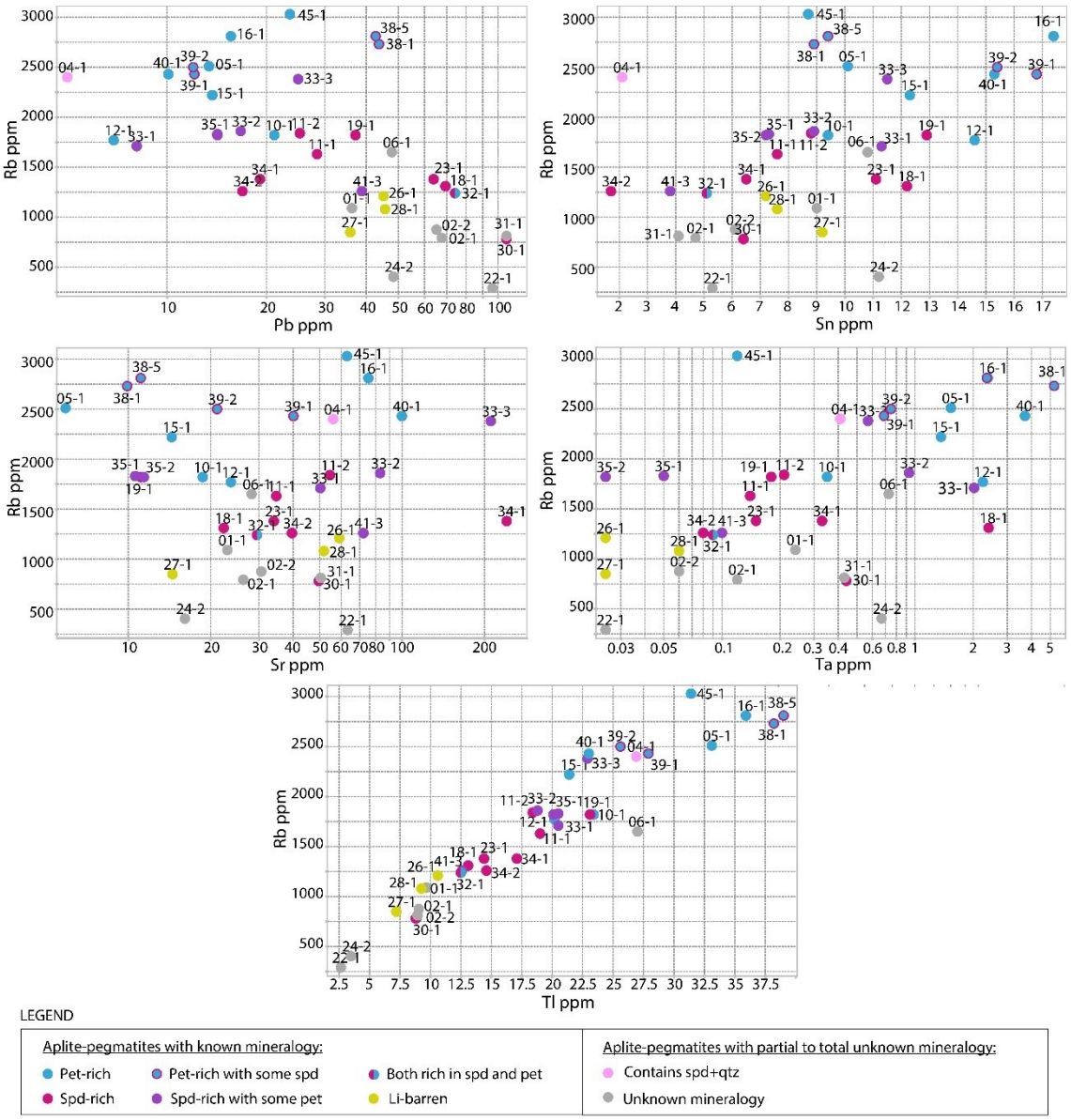

Figure 46. ICP-MS results illustrating the K-feldspar minor and trace element contents and variation of Rb against Pb, Sn, Sr, Ta, and Tl for the studied aplite-pegmatites with varying mineralogy from the Barroso-Alvão field (Pet: petalite; Spd: spodumene; Qtz: quartz).

Barium (Ba) tends to be higher in the K-feldspars of Li-barren aplite-pegmatites (≥ 10 ppm). However, some petalite-rich and spodumene-rich aplite-pegmatites also exhibit high Ba content. Still, when Ba ≤ 10 ppm, the aplite-pegmatites always seem to be Li-rich.

Beryllium (Be) content may be applied to distinguish petalite-rich from the spodumene-rich and Li-barren since only the petalite-rich have Be ≥ 30 ppm. However, just because an aplite-pegmatite has Be < 30 ppm, it does not guarantee that it will not

be petalite-rich, as there are also petalite-rich aplite-pegmatites with very low Be content, such as aplite-pegmatite #10 (Be 5 ppm), #39-Lousas (Be 7-12 ppm) and #45-Vila Grande (Be 4 ppm).

Cesium (Cs) tends to be higher in Li-rich aplite-pegmatites (Cs ≥ 90 ppm) and lower in the Li-barren. However, some Li-rich aplite-pegmatites share the same low Cs content as the Li-barren, such as the aplite-pegmatites #30, #32-Adagói, and #41-NOA/AL56. According to its Cs content, the unidentified aplite-pegmatite #6 seems to be Li-rich (Cs 187 ppm). All the other unidentified aplite-pegmatites have Cs ≤ 90 ppm. However, since some of the Li-rich also contain the same low Cs content, it is impossible to determine if they are really Li-barren only by Cs.

Gallium (Ga) tends to be higher in the petalite-rich aplite-pegmatites and lower in the Li-barren (Ga ≤ 15 ppm). When Ga ≥ 20 ppm, the aplite-pegmatites are always petalite-rich. However, some of the petalite-rich also have Ga 15-20 ppm. As for the spodumene-rich aplite-pegmatites, they can also contain the same low Ga content as the Li-barren, such as the aplite-pegmatites #30 (Ga 11 ppm) and #34-Alijó (Ga 8 ppm). According to their Ga content, all unidentified aplite-pegmatites could be Li-barren or spodumene-rich.

Lithium (Li) tends to separate well the Li-rich (Li ≥ 40 ppm) from the Li-barren aplite-pegmatites (Li ≤ 40 ppm). The exception is the aplite-pegmatite #23 (Li 35 ppm), located on the eastern side of the BA field (Figure 42), which is spodumene-rich. However, it fails to properly distinguish between the spodumene-rich and the petalite-rich (although some of the petalite-rich show the highest Li values). As for classifying the unknown aplite-pegmatites, aplite-pegmatite #6 would be Li-rich (Li 200 ppm), and the other unknown aplite-pegmatites would be Li-barren (Li ≤ 40 ppm).

Phosphorus (P) does not show a readily visible trend with the aplite-pegmatites of the BA field since both Li-rich and Li-barren aplite-pegmatites can contain the same amount of P.

Lead (Pb) tends to gradually increase from petalite-rich aplite-pegmatites (usually Pb ≤ 25 ppm), to spodumene-rich (Pb 15-80 ppm), to Li-barren (Pb ≥ 35). Although the Li-barren tend to have higher Pb content than the spodumene-rich, aplite-pegmatites, such as #34-Alijó (Pb 17 ppm), can also have low Pb content comparable to that of the petalite-rich. On the other hand, some Li-rich aplite-pegmatites located on the

E side of the BA field, such as #30 (Pb 106 ppm) and #32-Adagói (Pb 74 ppm), have Pb content identical to that of the Li-barren.

Rubidium (Rb) concentrations are generally highest in petalite-rich aplite-pegmatites, followed by spodumene-rich, and lowest in Li-barren types, with all Li-barren aplite-pegmatites showing Rb ≤ 1250 ppm. Interestingly, some Li-rich aplite-pegmatites also fall below this threshold, such as #30 (Rb 788 ppm) and #32-Adagói (Rb 1240 ppm), both located on the eastern side of the BA field. Notably, #32-Adagói contains both spodumene and an equivalent amount of petalite. In contrast, all other petalite-rich aplite-pegmatites exhibit Rb ≥ 1800 ppm, although some spodumene-rich types also show similar contents. However, when Rb ≥ 2400 ppm, only petalite-rich aplite-pegmatites reach such concentrations; neither spodumene-rich nor Li-barren types attain these values. Based on its Rb content (1650 ppm), the unknown #6 could be spodumene- or petalite-rich. All other unknown aplite-pegmatites, with Rb ≤ 1250 ppm, are most likely Li-barren, though, like #30, they could still be Li-rich.

Tin (Sn) seems to be always present in the petalite-rich aplite-pegmatites (Sn ≥ 8 ppm), but Li-barren and spodumene-rich can also have similar Sn content. However, Sn ≥ 10 ppm tends to be associated with Li-rich aplite-pegmatites.

Strontium (Sr) does not show a trend with the aplite-pegmatites of the BA field.

Tantalum (Ta) tends to be lower on the Li-barren (Ta ≤ 0.7 ppm) and higher on the petalite-rich. As for the spodumene-rich, most of them contain the same low Ta content as the Li-barren, except for a few aplite-pegmatites that contain the same high Ta content of the petalite-rich, such as #18 (Ta 2.4 ppm) and #33-Aldeia (Ta 2 ppm and Ta 0.93 ppm).

Thallium (Tl) content is very specific for each aplite-pegmatite type. When Tl ≤ 13 ppm, the aplite-pegmatites always seem to be Li-barren, except for aplite-pegmatite #30 (Tl 9 ppm, located on the E side of the BA field). When Tl is between 12-21 ppm, the aplite-pegmatites are spodumene-rich. When Tl ≥ 20 ppm, the K-feldspars tend to be only from petalite-rich aplite-pegmatites. The unidentified aplite-pegmatites #22 and #24 would be Li-barren based on their Tl content. The aplite-pegmatite #6 (Tl 27 ppm) would undoubtedly be Li-rich but with an unknown Li-mineralization since petalite-rich aplite-pegmatites start scarcely appearing when Tl ≥ 20 ppm.

2.5. Discussion

Pearson Product-Moment Correlation analysis of the ICP-MS results from the K-feldspars of the BA field revealed that the elements correlating with Rb include Tl (0.95), Ga (0.70), Pb (-0.65), Be (0.57), Li (0.52), Cs (0.51), Sn (0.49), Ta (0.49), and Ba (-0.45). In contrast, P and Sr show weak correlations of 0.09 and 0.02, respectively. (Note: Correlation values range from 0 to 1, where 1 represents a perfect positive correlation, 0 indicates no correlation, and -1 signifies a perfect inverse correlation, where one variable increases as the other decreases.)

The trends of Rb, Tl, Ga, and Pb exhibit the most variation across aplite-pegmatite types in the BA field, revealing a compositional progression from Li-barren to spodumene-rich and ultimately to petalite-rich aplite-pegmatites (Figure 44 and Figure 46). This pattern suggests that petalite-rich aplite-pegmatites are the most fractionated, followed by spodumene-rich ones, with Li-barren aplite-pegmatites being the least fractionated. This trend, particularly evident in Rb and Tl, reflects a distinct characteristic of this pegmatite field. Generally, spodumene-rich and petalite-rich pegmatites show similar levels of fractionation, while lepidolite-rich pegmatites tend to be more fractionated (Černý 1991a, London 2008, Roda-Robles et al. 2023). However, petalite-rich aplite-pegmatites seem more evolved than their spodumene-rich counterparts in this context. As discussed below, this observation aligns with the findings of Noronha *et al.* (2013), Martins et al. (2011), and Martins et al. (2012), who proposed that spodumene-rich aplite-pegmatites were emplaced before the petalite-rich ones in the BA field.

Lithium, Cs, and Ba only distinguish between Li-rich and Li-barren aplite-pegmatites. In Li-rich aplite-pegmatites, the concentrations of Li and Cs increase while Ba decreases. Although it does not effectively distinguish between spodumene-rich and Li-barren aplite-pegmatites, Be tends to be more concentrated in petalite-rich pegmatites. Lead and Ba negatively correlate with Rb, decreasing with increased fractionation. Lead behaves as a compatible element, which contrasts with Černý (1994) but aligns with Alfonso et al. (2003) for the aplite-pegmatites of Cap de Creus, Spain. Tantalum and Sn are more concentrated in petalite-rich aplite-pegmatites. Although Ta and Sn do not enter the K-feldspar crystal structure, they can be found as inclusions of cassiterite and columbite-tantalite, as observed in the petrographic section below. This observation also aligns with the findings of Martins *et al.* (2007a), who reported that petalite-rich aplite-pegmatites contain higher amounts of cassiterite and columbite-tantalite compared to spodumene-rich aplite-pegmatites. Phosphorous and Sr did not

correlate with Rb or the aplite-pegmatite types. However, theoretically, P should increase with the degree of fractionation of these aplite-pegmatites (Sánchez-Muñoz et al. 2017), while Sr should decrease (Černý 1994).

Table 10 summarizes the key geochemical trends observed in the sampled K-feldspars from the different aplite-pegmatite types, highlighting the behavior of their minor and trace elements.

Table 10. Summary Of ICP-MS Trends Observed for the K-Feldpars of Li-Barren, Li-Rich, Spodumene-Rich, And Petalite-Rich Aplite-Pegmatites of the Barroso-Alvão Field.

ppm	Li-barren	Li-rich	Spodumene-rich	Petalite-rich
Ba	≥ 10	≤ 10	-	-
Be	-	-	≤ 20	≥ 30
Cs	≤ 90	≥ 90	-	-
Ga	≤ 15	≥ 15	≤ 17	≥ 17
Li	≤ 40	≥ 40	-	-
Pb	≥ 35	≤ 35	-	-
Rb	≤ 1250	≥ 1250	1250-1900	≥ 1800
Ta	-	-	≤ 0.7	≥ 0.7
Tl	≤ 13	≥ 13	12-21	≥ 20

These trends were further evaluated by calculating the success rates for each aplite-pegmatite type, as shown in (Table 11) These rates were calculated using the following equation:

$$Success\ Rate = \frac{n}{t} \times 100 \qquad (1)$$

The variable 'n' represents the number of aplite-pegmatite types that match the trends associated with a particular aplite-pegmatite type, while 't' refers to the total number of samples belonging to that same aplite-pegmatite type. The success rate, therefore, indicates what proportion of the total samples for a given type aligns with the identified trends.

Table 11. Success Rates of the Defined Trends for ICP-MS Samples by Mineralization Type (Spd-Spodumene; Pet-Petalite)

	Success Rates				Counts of Correctly Classified Samples			
	Li-barren	Li-rich	Spd-rich	Pet-rich	Li-barren	Li-rich	Spd-rich	Pet-rich
Ba	100%	71%	-	-	3	17	-	-
Cs	100%	79%	-	-	3	19	-	-
Ga	100%	62%	87%	89%	3	15	13	8
Li	100%	92%	-	-	3	22	-	-
Pb	100%	67%	-	-	3	16	-	-
Rb	100%	92%	80%	100%	3	22	12	9
Ta	-	-	80%	67%		10	12	6
Tl	100%	96%	80%	100%	3	23	12	9
			Samples Total		3	24	15	9

Although the Li-barren success rate was 100% (as all Li-barren samples have Rb concentrations below 1250 ppm), not all Li-rich samples (spodumene-rich and petalite-rich) exhibit Rb values above this threshold. Some Li-rich samples have Rb < 1250 ppm, overlapping with the range of Li-barren compositions. This overlap prompted a more detailed regional analysis, which is discussed in the following section.

2.5.1. Regional distribution of the K-feldspar chemistry

While the trends in the chemical elements are evident, certain K-feldspars from Li-rich aplite-pegmatites, particularly those from #23, #30, and #32-Adagói, have similar chemical signatures as those of Li-barren aplite-pegmatites. These exceptions led to the observation that these aplite-pegmatites are all located in the SE of the BA aplite-pegmatite field (Figure 42).

To explore this further, an analysis of the geographic distribution of the sampled aplite-pegmatites was conducted using their ICP-MS results (Figure 47). This analysis revealed a distinct trend: the concentrations of Be, Ga, Li, Pb, Rb, and Ta exhibit a progressive increase (or decrease, in the case of Pb) from the SE to NW. This behavior suggests an evolutionary trend within the BA field from SE to NW. However, this seems to indicate that the Li-rich aplite-pegmatites #23, #30, and #32-Adagói are less fractionated than the other Li-rich aplite-pegmatites in the N and W, which could lead to their misidentification as Li-barren.

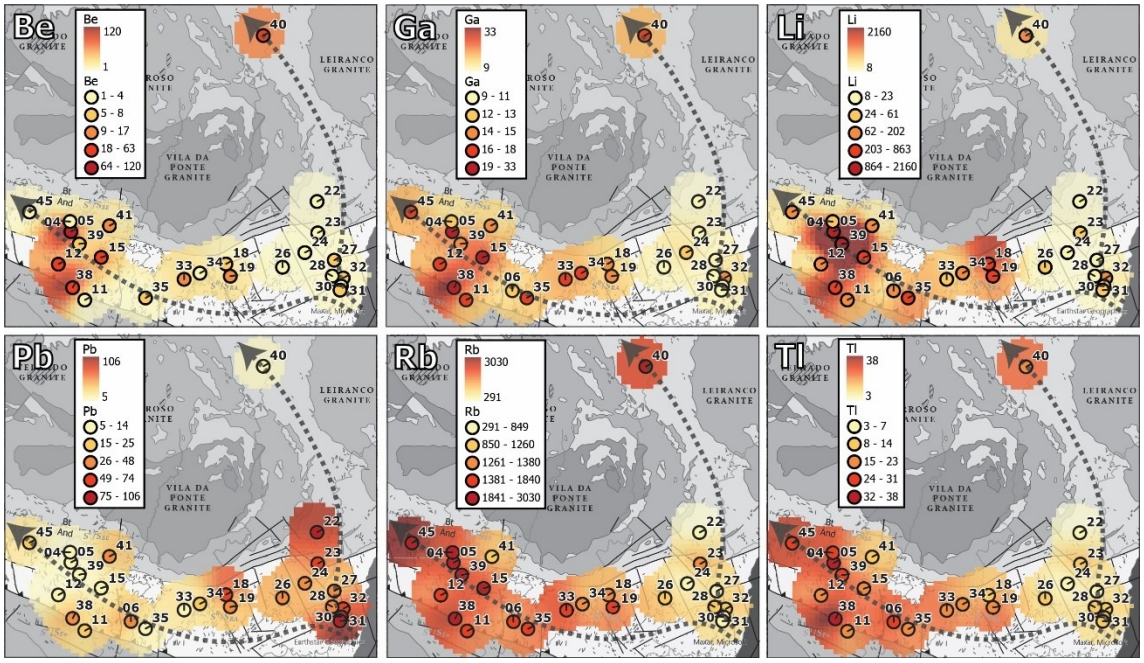

Figure 47. Regional map with the location of the sampled aplite-pegmatites and their K-feldspar contents from ICP-MS showing a regional trend along the Barroso-Alvão field for Be, Ga, Li, Pb, Rb, and Tl.

To clarify these observations, additional aplite-pegmatites with known mineralogy were included in the regional map and color-coded according to their dominant Li-mineralization (lepidolite, petalite, spodumene, or Li-barren) (Figure 48). This included two highly kaolinized lepidolite-bearing bodies (CHN 26 and CHN 27) (Charoy et al. 1992, Martins 2009)), which help contextualize the observed geochemical trends in relation to the mineralogical zonation across the field. This analysis revealed that the aplite-pegmatites are distinctly distributed according to their dominant Li-mineralization, with petalite-rich aplite-pegmatites predominantly located in the northern and western parts of the field, and lepidolite-rich ones further west. Based on this pattern, it is likely that additional lepidolite-rich aplite-pegmatites exist in the north part of the field, to the east of the Alto-Rabagão Dam. However, these potential pegmatites are probably kaolinized, similar to the known lepidolite-rich aplite-pegmatites in the area.

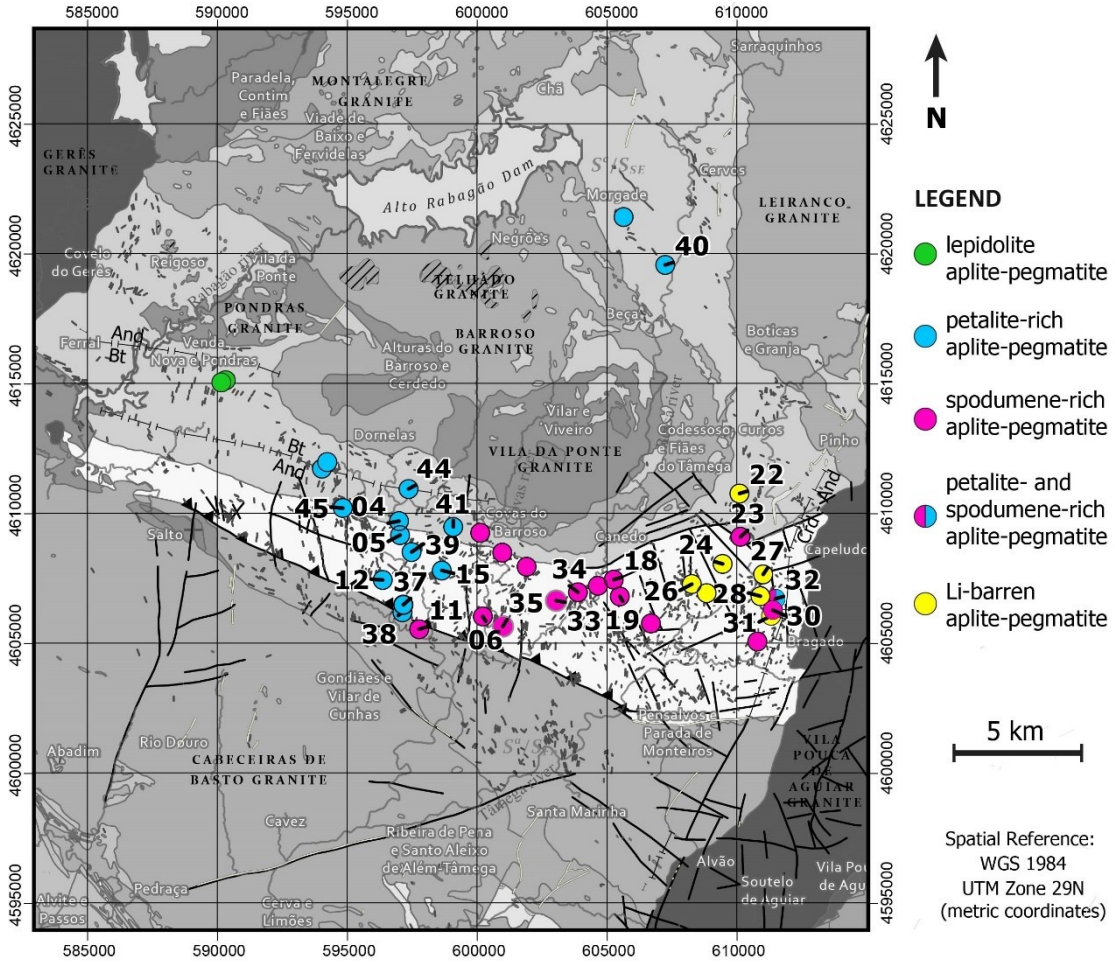

Figure 48. Geographical Distribution of the Aplite-Pegmatites in the Barroso-Alvão Field by Dominant Li-Mineralization. Additional aplite-pegmatites from the literature were included for a comprehensive view of the regional distribution (Charoy et al. 1992, Lima 2000, Martins 2009).

The spodumene-rich aplite-pegmatites are mainly located to the E and S relative to the petalite and lepidolite-rich aplite-pegmatites. In contrast, the Li-barren aplite-pegmatites are further E and S, somewhat intermixed with the spodumene-rich ones. This trend in the geochemistry of the K-feldspars aligns with the findings of Lima (2000), where the study of 17 K-feldspars identified a pattern in Rb indicating a geochemical fractionation of the aplite-pegmatites from the E to the W sides of the BA field. However, an alternative interpretation is that the aplite-pegmatites from the SE underwent late-stage metasomatic and/or hydrothermal activity rather than fractionation. This process could have significantly reduced the concentrations of previously enriched elements, such as Cs and Rb, while increasing the concentrations of elements like Ba, typical of less fractionated pegmatites. According to Černý *et al.* (1985a), Ba tends to become somewhat enriched in the late stages of hydrothermal alteration of pegmatites.

One of these aplite-pegmatites in the SE, namely #32-Adagói, has been the focus of several studies over the years (Farinha Ramos & Lima 2000, Lima 2000, Lima & Martins 2011). A notable characteristic of this aplite-pegmatite is the presence of subsolidus alteration with petalite after spodumene (Charoy et al. 2001). Typically, petalite forms under higher temperatures and lower pressures than spodumene (London 1984), suggesting that a sudden rise in temperature or drop in pressure occurred in the system during spodumene crystallization.

Previous hypotheses explained this as a regional phenomenon: an uplift process (Noronha *et al.* 2013) and a temperature rise caused by the reactivation of the Régua-Verín fault (Lima 2000, Sant'Ovaia 2000, Charoy et al. 2001). This fault is located SE of the aplite-pegmatite field, where the post-tectonic Vila Pouca de Aguiar granite was emplaced.

However, the differences in K-feldspar geochemistry in the aplite-pegmatites of the SE sector may be linked to the same factors responsible for the previously observed changes in mineralogy. One hypothesis is that during the crystallization of the Li-rich bodies, a rupture caused by the exsolution of water could constitute the "hydrothermal activity" responsible for leaching the previously crystallized K-feldspars of their fractionated elements. This escape of water could also have caused the system to open, leading to a rapid decrease in pressure, thereby altering the crystallization dynamics and favoring the crystallization of petalite instead of spodumene (Webber & Simmons 2007, Roda-Robles *et al.* 2018).

On the other hand, the occurrence of lepidolite aplite-pegmatites on the NW side of the field supports the concept of progressive geochemical fractionation progressing from SE to NW, as evidenced by the following mineralogical sequence: Li-barren, spodumene-rich, petalite-rich, and finally, lepidolite-rich. This may indicate the presence of a still unidentified parental granite situated to the SE of the Barroso-Alvão (BA) field.

Previous research also proposed a successive geochemical evolution for the aplite-pegmatites of the BA-field, from Li-barren to spodumene-rich, petalite-rich, and finally lepidolite-rich, evidenced by the mineral chemistry of columbite-tantalite and white micas (Martins 2009, Martins et al. 2011, Martins et al. 2012).

Noronha *et al.* (2013) further supported that spodumene-rich aplite-pegmatites are older than petalite-rich ones due to the emplacement of different generations of

pegmatitic melt at varying structural levels. This study proposed that petalite-rich melts intruded at a shallower crustal level, whereas spodumene-rich melts had previously intruded at a deeper level (uplift process).

2.5.2. Petrographic Insights into K-Feldspar Chemistry

Despite the petrographic analysis being limited to a single aplite-pegmatite sample (#41-NOA/AL56), it appears to offer valuable insights into the ICP-MS results for the entire population of Barroso-Alvão aplite-pegmatites. The ICP-MS data shows higher concentrations of Ta and Sn in K-feldspars from petalite-rich pegmatites, even though these elements do not incorporate into the K-feldspar crystal structure. This finding aligns with the observations of Martins et al. (2007b) and Martins et al. (2011), who reported elevated amounts of columbite-tantalite and cassiterite in petalite-rich aplite-pegmatites. Petrographic analysis, including Scanning Electron Microscopy (SEM) and Energy Dispersive X-Ray Spectroscopy (EDS) analysis, revealed the presence of columbite-tantalite inclusions within K-feldspars (Figure 49). This suggests that the elevated Ta and Sn content in the K-feldspars of petalite-rich aplite-pegmatites may be due to inclusions of cassiterite and columbite-tantalite.

Furthermore, P from ICP-MS does not show any fractionation trend, unlike the other elements or as previously reported in the literature. Petrographic observations identified apatite inclusions within K-feldspars, suggesting that the P content in Barroso-Alvão K-feldspars cannot solely be explained by the crystal structure (Figure 49). This finding supports the conclusions of Martins & Lima (2011), who noted that apatite can also be found in Li-barren aplite-pegmatites. Thus, the possible presence of apatite inclusions in both Li-rich and Li-barren pegmatites helps explain the lack of a distinct P fractionation trend in the ICP-MS data, as well as the comparable P content observed in K-feldspars from both pegmatite types.

The variation in Li content identified by ICP-MS, which clearly distinguishes Li-rich from Li-barren aplite-pegmatites, may be further explained by petrographic observations. The Li content in K-feldspars from Li-rich aplite-pegmatites is likely attributable to inclusions of spodumene, as noted during the petrographic analysis. This provides a plausible explanation for the presence of Li in K-feldspars, as Li is not easily incorporated into their crystal structure (Figure 50) (Černý 1994). Thus, these

spodumene inclusions may be responsible for the clear distinction between K-feldspars from Li-barren and Li-rich aplite-pegmatites.

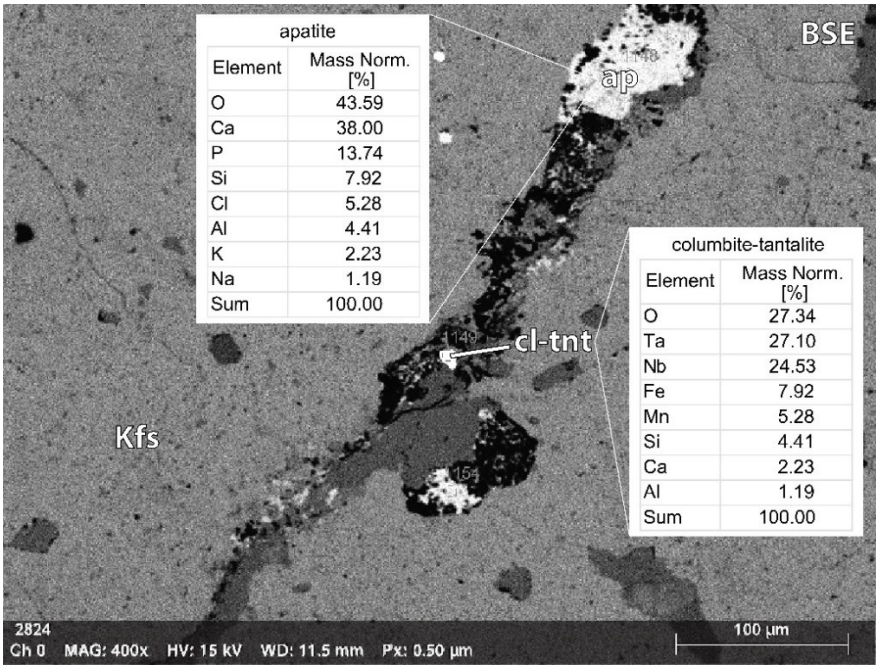

Figure 49. Backscattered Electron Image revealing a fracture within a K-feldspar from the #41- NOA/AL56 aplite-pegmatite, containing apatite (ap) and columbite-tantalite (cl-tnt). These minerals were analyzed with Energy Dispersive X-Ray (EDS).

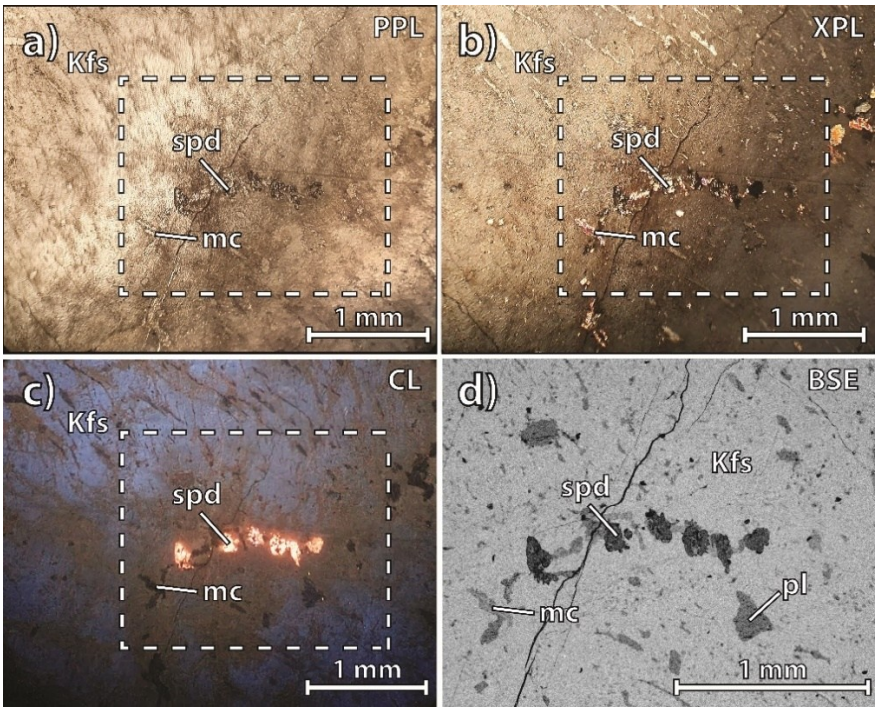

Figure 50. Microphotographs of the interior of a K-feldspar (Kfs) crystal from the Li-rich aplitepegmatite #41-NOA/AL56 revealing inclusions of spodumene (spd), mica (mc), and plagioclase (pl). (a) Parallel Polarized Light (PPL). (b) Crossed Polarized Light (XPL). (c) Cathodoluminescence (CL). (d) Backscattered Electron Imaging (BSE).

2.6. pXRF as a Field Tool for Differentiating Aplite-Pegmatite Types

The pXRF results were compared with the ICP-MS results to test the effectiveness of pXRF in differentiating aplite-pegmatite types. Rubidium (Rb) in pXRF worked very well; it was the only element consistently detected with reliable accuracy and showed a strong correlation with ICP-MS data (0.78 according to Pearson's coefficient), proving that pXRF, through Rb, can be a valuable tool for identifying Li-barren, spodumene-rich, and petalite-rich aplite-pegmatites (Figure 51).

While pXRF tended to overestimate Rb concentrations, often nearly doubling the ICP-MS values, it can be refined by applying custom slope and offset values (0.2879 and 643.1195, respectively), as calculated in this study using Excel's SLOPE and INTERCEPT functions after plotting the XRF and ICP-MS data on a scatter plot. This adjustment, described in the Bruker manual as Adjusting Calibration Using Type Standardization (Coefficients), is performed in Admin mode and requires reference analysis of the material being analyzed with XRF.

Rubidium uncertainty (uc) in XRF was extremely low, usually 1% and maximum 5%. The uncertainties were calculated by combining the standard deviation (SD) of the three XRF measurements with the uncertainty reported by the equipment for each analysis (uE), following the method described by Guimarães et al. (2016) using the formula:

$$uc = \sqrt{SD^2 + uE^2} \qquad (2)$$

Other elements, such as Ga and Tl, were detected less consistently by pXRF compared to ICP-MS, with Ga appearing in 89% of samples and Tl in only 24%. However, the concentrations of Ga and Tl were typically low, with Ga usually less than 30 ppm and Tl less than 40 ppm, and their uncertainties were significantly larger than those for Rb. These aspects make them not useful for analysis with pXRF. However, it is still interesting to note that the pXRF system demonstrates sufficient sensitivity to partially detect these elements and show trends similar to those observed with ICP-MS.

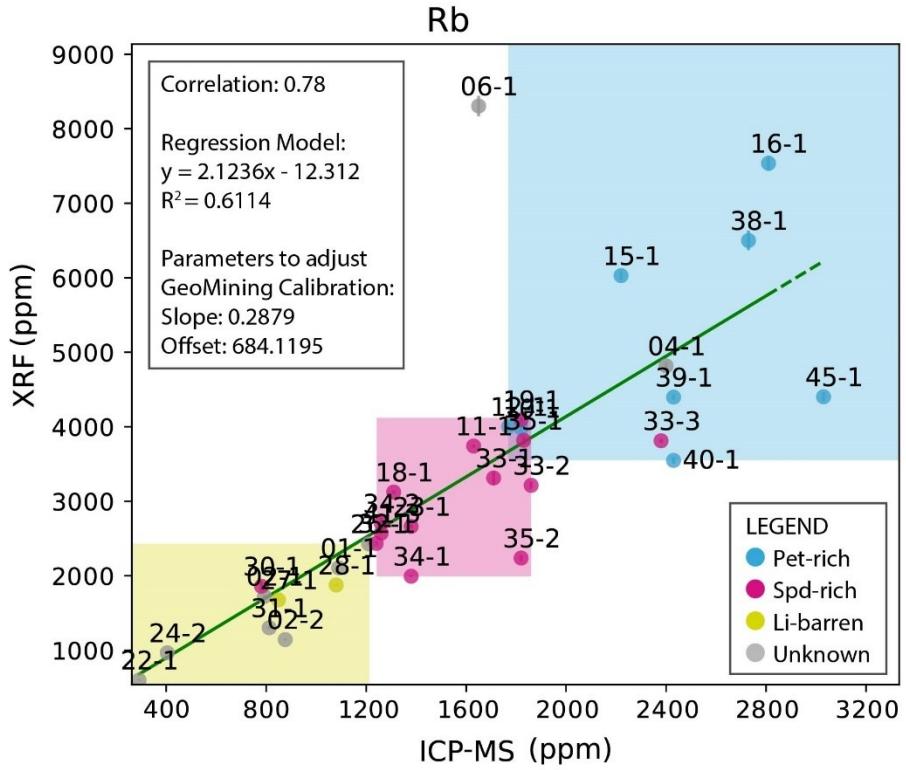

Figure 51. Plot of XRF results versus ICP-MS results used to calculate the slope and offset for XRF calibration adjustment.

2.7. Conclusions

This study brought forth the following insights regarding the geochemistry of K-feldspars from the aplite-pegmatites of the BA field, which can be valuable for Li exploration:

1. *Identification of key minor and trace elements:* The ICP-MS analysis revealed a correlation between the concentrations of Rb, Tl, Li, Ga, Pb, Cs, Ba, Be, Ta, and Sn and the different types of aplite-pegmatites: Li-barren, spodumene-rich, and petalite-rich.

2. *Distinction between Li-rich and Li-barren Aplite-Pegmatites (except SE sector):* Usually the Li-rich aplite-pegmatites tend to differ in their ICP-MS results from the Li-barren by containing lower Ba (≤ 10 ppm), higher Cs (≥ 90 ppm), higher Ga (≥ 15 ppm), higher Li (≥ 40 ppm), lower Pb (≤ 35 ppm), higher Rb (≥ 1250 ppm), and higher Tl (≥ 13 ppm).

3. *Distinction between Spodumene-Rich and Petalite-Rich Aplite-Pegmatites (except SE sector):* Although it can be difficult to distinguish these two types of aplite-pegmatites, the K-feldspar geochemistry (ICP-MS) reveals a tendency for the petalite-rich type to contain a more evolved geochemistry than the spodumene-rich:

    3.1. Spodumene-rich: lower Be (≤ 20 ppm), lower Ga (≤ 17 ppm), lower Rb (1250-1900 ppm), lower Ta (≤ 0.7 ppm), and lower Tl (12-21 ppm);

    3.2. Petalite-rich: higher Be (≥ 30 ppm), higher Ga (≥ 17 ppm), higher Rb (≥ 1800 ppm), higher Ta (≥ 0.7 ppm), and higher Tl (≥ 20 ppm).

4. *Regional Fractionation Trend:* The geographic distribution of the sampled aplite-pegmatites revealed a geochemical trend within the BA field extending from SE to NW. Elements such as Be, Ga, Li, Rb, and Ta increase in concentration, while Pb and Ba decrease. This trend is also reflected in the Li-mineralogy, with a change in the dominant Li-mineralization from Li-barren to spodumene-rich, petalite-rich, and lepidolite-rich progressing from SE to NW.

5. *Challenging K-Feldspar Geochemistry in the SE Sector:* In the SE sector, the K-feldspars of aplite-pegmatites containing Li-rich minerals exhibit geochemical signatures similar to those of Li-barren aplite-pegmatites. Thus, distinguishing between Li-rich and Li-barren types in this sector based solely on K-feldspar geochemistry is not possible.

6. *Petrographic Insights:* The trace amounts of Li, Sn, P, and Ta detected in the K-feldspars from Li-rich aplite-pegmatites are likely attributable to mineral inclusions of spodumene, cassiterite, apatite, and columbite-tantalite minerals.

7. *pXRF for Li Prospection in the Barroso-Alvão Field (excluding the SE sector):* Using a Bruker S1 Titan pXRF proved to be effective in distinguishing between Li-barren (Rb ≤ 1250 ppm), spodumene-rich (Rb 1250–1900 ppm), and petalite-rich aplite-pegmatites. Petalite-rich types begin to appear at Rb concentrations ≥ 1800 ppm; therefore, in the intermediate range of 1800–2400 ppm, both spodumene-rich and petalite-rich aplite-pegmatites may occur, leading to some overlap. However, when Rb values are ≥ 2400 ppm, only petalite-rich aplite-pegmatites were observed in this study.

Acknowledgments

The authors gratefully acknowledge the comments from the reviewers. We would also like to thank INESC TEC (Instituto de Engenharia de Sistemas e Computadores, Tecnologia e Ciência) and Maria Irene Costa (petrographic thin section technician) for their support and access to their laboratories and equipment. We further thank Dr. Cândida Garcia Neto (Scanning Electron Microscope technician) from our department for her technical assistance. We are grateful to Savannah Resources Plc. for providing samples from the #41-NOA/AL56 aplite-pegmatite, which were used for the petrographic study of its K-feldspars. This work was funded by the European Commission's Horizon 2020 innovation programme under grant agreement no. 869274, through the project GREENPEG – New Exploration Tools for European Pegmatite Green-Tech Resource. Additional funding was provided by national funds through FCT—Fundação para a Ciência e Tecnologia, I.P., under the Instituto de Ciências da Terra (ICT) project references UIDB/04683/2020 (https://doi.org/10.54499/UIDP/04683/2020) and UIDP/04683/2020 (https://doi.org/10.54499/UIDB/04683/2020). Filipa Dias and Ricardo Ribeiro were financially supported within the scope of their respective Ph.D. fellowships, ref. 2020.05534.BD (https://doi.org/10.54499/2020.05534.BD) and ref. SFRH/BD/140266/2018, funded by national funds from MCTES through FCT, and co-financed by the European Social Fund (ESF) through POCH—Programa Operacional Capital Humano—and the NORTE 2020 regional program.

Chapter II: Conference Proceedings and Presentations

1. Spodumene and Quartz Intergrowth – Textural and Genesis Point of View

Adapted from: Filipa Dias and Alexandre Lima

EGU General Assembly (2019)

Published Abstract

Abstract

The observation of spodumene quartz intergrowth both in the field and in microscopy is a common texture found in Lithium-rich pegmatites from different parts around the world. However, this texture may result from different environments of formation, it may be a primary texture or a secondary texture resultant from secondary reactions or posterior deformation. This study will approach the meaning of these terminologies and how different types of spodumene and quartz intergrowth can have similar textures but completely different conditions of formation.

The amazing variety of textures and crystal morphologies in pegmatites are related to the crystal growth rate and to the degree of undercooling of the pegmatitic melt (the difference between the liquidus temperature and the actual temperature of the magma) resultant from non-equilibrium kinetic factors (Vernon 2004, Webber & Simmons 2007, London 2008). The fact that pegmatites with symplectites of SQI originated from petalite seems to indicate that the rock after being solid still had some time at an elevated temperature to try to re-equilibrate its mineral phases while cooling down, indicating a low-to-moderate degree of undercooling. Another indication for its relatively low degree of undercooling is the scarcity of unidirectional solidification textures, which reflect a high degree of undercooling, such as skeletal, and radial crystals morphologies.

Several aplite-pegmatite veins of the Barroso-Alvão pegmatitic field are deformed by D3 and can be found in linear or echelon regional structures which seems to indicate that they were emplaced during a ductile to brittle late-D3 phase, still affected by the reminiscences of the heat resultant from the emplacement of the surrounding peraluminous syn-tectonic granites (Noronha *et al.* 2006). Fine-grained needles of spodumene and quartz intergrowth are observed in some aplite-pegmatites veins in Barroso-Alvão filling intergranular spaces and fractures between feldspars, quartz and petalite. This type of spodumene seems to be formed due to a pressure increase, maybe caused by shearzones, related to the D3 phase (Charoy *et al.* 1992, Martins 2009). The dissolution of petalite would have occurred at its contact points with other minerals and then precipitated in intergranular spaces as spodumene + quartz intergrowth. These spaces would be filled with a metamorphic intergranular fluid (maybe groundwater since this would already be a shallow system), resulting in a more compressed rock. For example, at a depth of 10 km and T around 300°C, it is normal for the minerals to start to dissolve and the motion of these fluids could transport several chemical species, and since Li and H_2O are, for example, fluxing elements, they would help keep the fluid from being reabsorbed rapidly.

1.1. Crystallization and Post-Crystallization Textures

The texture of an igneous rock reflects its crystallization and post-crystallization evolution. The challenge lies in deciphering this history despite the many processes that contribute to the final texture of the rock.

Igneous rock textures are typically categorized as either primary or secondary. A primary texture refers to those formed during melt crystallization, resulting from interactions between the melt and minerals. In contrast, a secondary texture forms after the rock has completely solidified, without the involvement of melt. Minerals that grow after full solidification are considered metasomatic in nature, although their formation does not necessarily require a separate, subsequent metamorphic event.

In igneous rocks such as granites, crystallization may continue even after the melt has solidified. If the temperature remains sufficiently high, recrystallization and re-equilibration of both chemistry and texture can still occur. This process is known as autometamorphism (Winter 2014).

1.2. Primary Spodumene and Quartz Intergrowth

Spodumene and quartz intergrowth can occur as a primary texture, known as a skeletal texture. This is a typical pegmatitic texture that forms at the edges and corners of crystals growing from a highly undercooled and viscous melt (Figure 52). Skeletal texture is defined as an imperfect or incomplete crystal, often containing cavities filled with another mineral. It has been interpreted as the result of compositional supersaturation in a boundary layer formed at the interface between a rapidly growing crystal and the surrounding melt, where excluded components accumulate (Vernon 2004, London 2008).

In spodumene crystals from Gelfa, Portugal, where petalite is absent and the spodumene is clearly of primary origin, thin section observations suggest that the spodumene and quartz intergrowth is also primary.

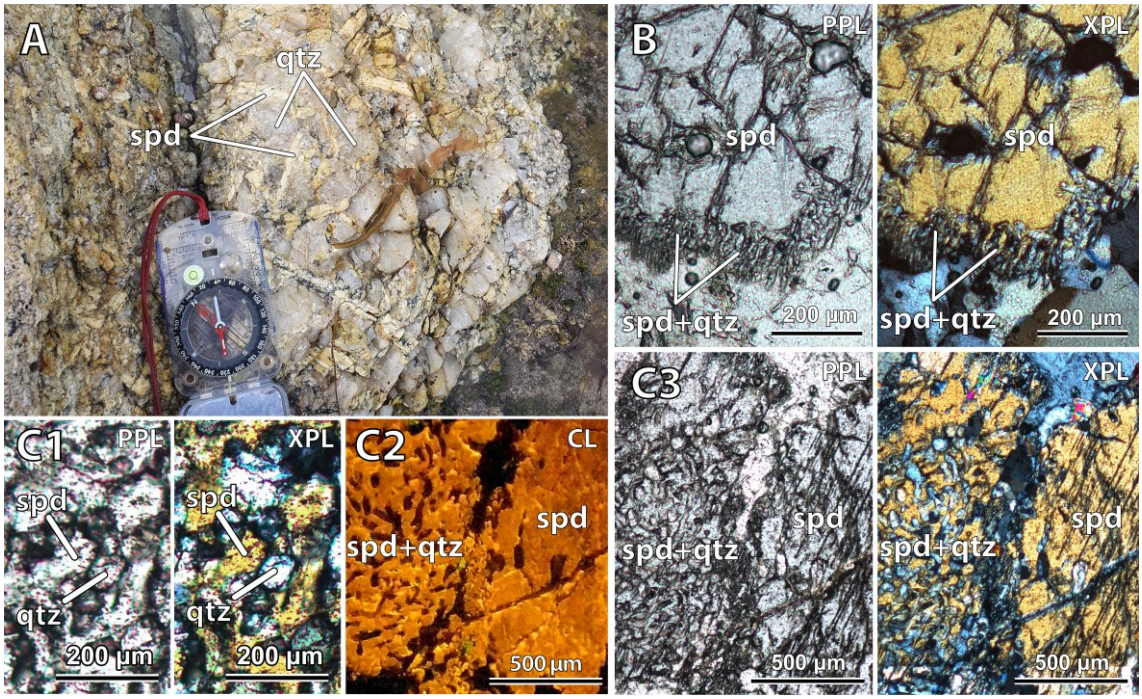

Figure 52. Primary spodumene and quartz intergrowth from Gelfa, Âncora. A) Outcrop rich in primary spodumene; B) Microphotographs of spodumene (spd) and quartz (qtz) intergrowth at the edge of a spodumene crystal (XPL: crossed polarized light; PPL: plane polarized light); C1) Zoom of spodumene and quartz intergrowth; C2) Cathodoluminescence (CL) image of spodumene and quartz intergrowth; C3) PPL and XPL views of spodumene and quartz intergrowth.

When an igneous rock cools, certain mineral phases may fall outside their pressure-temperature (P–T) stability fields and consequently undergo transformations into more stable phases under the new conditions.

The term pseudomorph refers to a mineral that retains the shape of a previous mineral phase, even though its internal structure has been replaced. This allows the original mineral to be identified despite the transformation. However, if the external shape is not preserved, it may be difficult to recognize the replacement as a polymorph, since the initial phase may be entirely lost (Winter 2014)..

According to London (2008, 2017)), spodumene and quartz intergrowth (SQI) in some localities is simply a pseudomorphic replacement of petalite. When the original shape of the replaced mineral can still be observed, a pseudomorphic replacement is identified. SQI is often reported as a replacement of petalite, especially when the outer shape of the original petalite crystal is still visible (Černý & Ferguson 1972, Černý 2005).These textures can also be observed in the Barroso-Alvão field (Figure 53), which shows pseudomorphs of secondary spodumene (spd) and quartz (qtz) intergrowths after petalite from drill core samples.

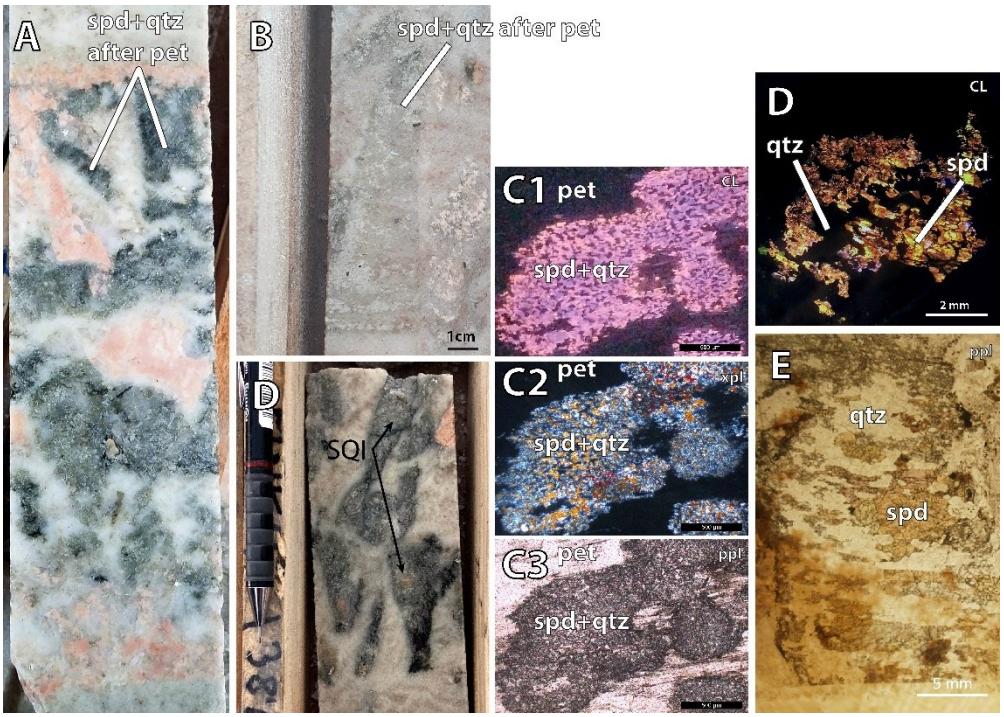

Figure 53. Secondary spodumene (spd) and quartz (qtz) intergrowths from drill core samples from the Barroso-Alvão field. A–D: Complete pseudomorphs of spodumene and quartz intergrowth after petalite (pet) in drill cores. C1–C3: Spodumene and quartz intergrowths within partially replaced petalite. D–E: Complete alteration of petalite to spodumene and quartz intergrowth. PPL: plane-polarized light; XPL: crossed-polarized light; CL: cathodoluminescence.

Recently, Breasley *et al.* (2025) also reported that the Tanco pegmatite hosts a variety of spodumene–quartz intergrowth types, further supporting the idea of multiple

origins or formation mechanisms for these textures—similar to those described in this study for the Barroso–Alvão aplite–pegmatite field.

1.3. What is a Symplectitic Texture?

It is not uncommon to see the term *symplectite* associated with spodumene in Li-rich pegmatites. *Symplectite* refers to a texture formed entirely in the solid state, with no involvement of melt. It describes fine-grained intergrowths produced by the combined growth of two or more minerals as they replace another mineral (Vernon 2004, Winter 2014). This is precisely the case with SQI (Spodumene and Quartz Intergrowth), which results from the breakdown of petalite in Li pegmatites.

To explain this more intuitively, the formation of spodumene and quartz intergrowths replacing petalite can be conceptually compared to the development of myrmekites after K-feldspars in granites. Here, myrmekites are symplectitic intergrowths of quartz and plagioclase (e.g., anorthite, which contains less silica than K-feldspar) (Winter 2014). In these cases, the newly formed plagioclase precipitates together with quartz due to the excess silica. This solid-state process serves as a useful analogue to the transformation of petalite, which has a higher silica content than spodumene. As petalite re-equilibrates under lower-temperature conditions, it breaks down into spodumene and quartz intergowths, with the quartz representing the excess silica no longer accommodated by the spodumene structure.

Interestingly, the quartz in myrmekites should all go extinct simultaneously under crossed polarizers in thin section, indicating that they are parts of a single continuous crystal (Winter 2014). However, this is not the case in the Barroso–Alvão field, where the pegmatites are strongly deformed, and it is common to find quartz that has undergone recrystallization. Therefore, this criterion may not always be reliable for differentiating SQI from zones where spodumene and quartz simply occur together.

1.4. Spodumene-Quartz Intergrowth Related to Regional Deformation: Case Study of the Barroso-Alvão Pegmatite Field

The aplite-pegmatites from the Barroso-Alvão region formed during the Variscan Orogeny, which involved several deformation phases (D1, D2, D3). During D3, anatectic melt began to ascend while retrograde metamorphism occurred under low-

pressure conditions, followed by ductile-brittle to brittle deformation. This deformation created linear and echelon faults that served as conduits to the surface. Several aplite-pegmatites in the Barroso-Alvão pegmatitic field are deformed by D3 and occur along these stuctures, suggesting their emplacement during the ductile-to-brittle late-D3 phase (Noronha *et al.* 2006). Additionally, the metasediments in the West block of the Régua-Verín fault do not show evidence of retrograde metamorphism as observed regionally. Instead, they display prograde metamorphism, indicating stronger local metamorphic conditions caused by the emplacement of syn-tectonic granites in the area. This led to a local pre- to syn-D3 thermal peak, expressed by premature staurolite relative to andalusite, and late- to post-tectonic poikilitic andalusite and cordierite. The final emplacement of anatectic melts occurred post-D3 (Ribeiro 1998). These observations suggest that the pegmatites in this area, besides being affected by tectonic deformation, may also have been influenced by residual heat from the emplacement of the surrounding granites.

The deformation effects seem to be reflected in fine-grained needles of spodumene, surrounded by quartz, are observed in some of these Li-rich aplite-pegmatites (Figure 54A and B). These needles can be found filling intergranular spaces and fractures between feldspars, quartz, and petalite, or cross-cutting the aplite-pegmatites in the form of well-delimited shear zones. This type of texture, along with a more amorphous form of spodumene and quartz intergrowth (Figure 56), seems to be a product of increased pressure, potentially caused by regional shearing during the D3 phase (Charoy *et al.* 1992, Martins 2009).

In the pegmatites where petalite is present, the dissolution of this mineral at the crystal contacts with other minerals seems to explain the formation of fine-grained needles of spodumene. These needles would have precipitated in fluid circulation areas, such as intergranular spaces or shear zones (Figure 54). These spaces could be filled with a metamorphic intergranular fluid, which may have been groundwater, since at a depth of around 10 km and temperatures around 300°C, it is normal for minerals to begin dissolving, and the motion of these fluids could transport various chemical species. Since Li and H_2O are fluxing elements, they would help maintain fluid mobility, preventing rapid reabsorption. Such significant changes accompanying this metamorphism would already be considered metasomatism (Winter 2014).

Additionally, the textures observed in the AL56/NOA aplite-pegmatite, Barroso–Alvão field, provide valuable insight into the mineralogical processes at play. Samples

from this pegmatite show needle-like formations of spodumene and quartz, suggesting a crystallization process driven by fluid movement rather than the typical cooling-induced recrystallization (Figure 54A). This fluid-driven formation is further highlighted by the way the spodumene-quartz intergrowths crosscut petalite crystals and extend between the contacts of other minerals such as quartz and feldspars. Furthermore, fluid circulation appears to promote the in situ breakdown of petalite, leading to the formation of spodumene and quartz intergrowths after petalite, as illustrated in detail in Figure 54B. In this case, however, the process would not be related to phase re-equilibration following petalite crystallization but to metasomatism derived from deformation events.

Building on these observations, the Grandão aplite-pegmatite (Figure 55), located in the Barroso–Alvão field, likewise exhibits remarkable textures of spodumene and quartz intergrowths, with features that clearly indicate deformation played a key role in their formation. These textures appear to have been strongly influenced by shear-related dynamics. In particular, the “snowball”-like texture of spodumene and quartz in one image suggests syn-kinematic growth, with the spiral pattern indicating rotation during crystallization within an active shear zone. In another image, the alignment of fine spodumene and quartz grains along a shear band further supports the role of deformation in guiding fluid circulation and mineral growth.

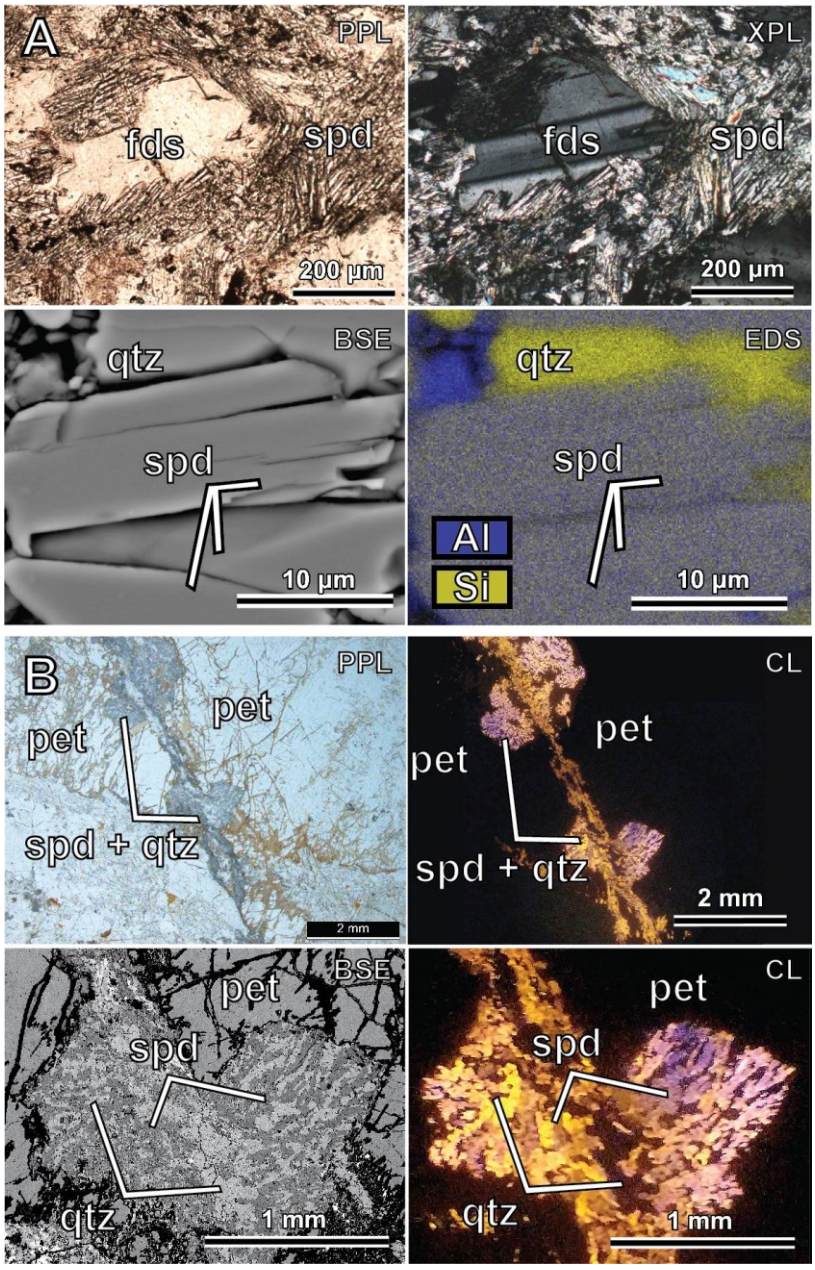

Figure 54. Microphotographs from the AL56/NOA aplite-pegmatite, Barroso–Alvão field, Portugal, showing spodumene and quartz intergrowths, which were not formed by the regular breakdown of petalite due to cooling, but by fluid circulation processes. This texture can crosscut petalite, leaving it behind and following fluid circulation along weak zones and contacts. **A)** Fine-grained spodumene (spd) and quartz form needle-like textures and enclose other minerals such as feldspars (fds). **B)** Fine spodumene and quartz cross-cutting a petalite (pet) crystal. Abbrevations: **PPL:** Plane-Polarized Light; **XPL:** Crossed Polarized Light; **BSE:** Backscattered Electron Image; **EDS:** Energy Dispersive X-ray Spectroscopy Map; **CL:** Cold-Cathodoluminescence Optical Microscopy.

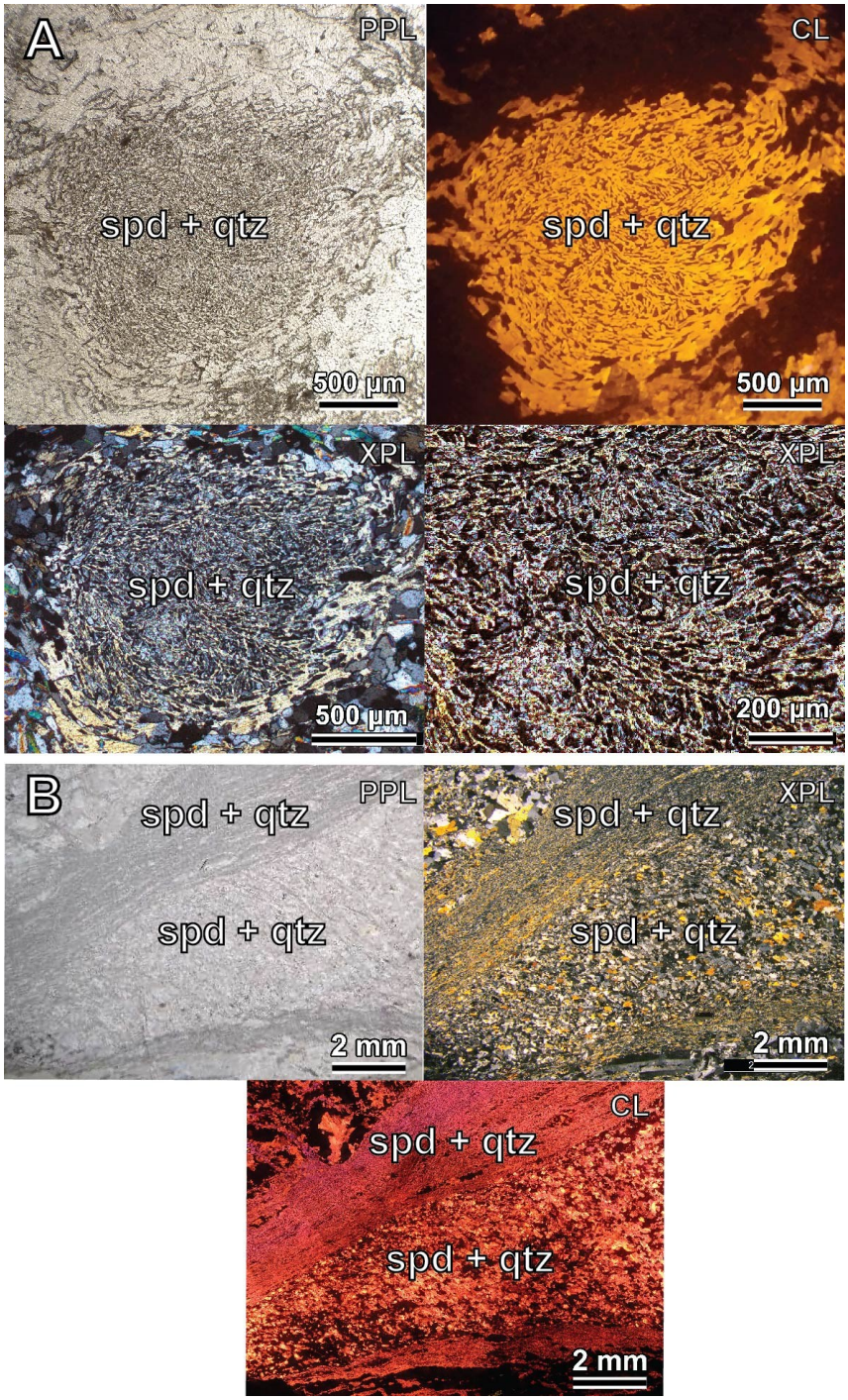

Figure 55. Microphotographs from the Grandão aplite-pegmatite, Barroso–Alvão field, Portugal, showing spodumene and quartz intergrowths that were not formed by the regular breakdown of petalite due to cooling, but rather as a result of deformation along shear zones. A) Spodumene and quartz form a "snowball"-like texture, suggesting syn-kinematic growth of spodumene within the shear zone, characterized by a spiral pattern that indicates rotation during crystal growth. B) Fine-grained spodumene and quartz aligned along a shear zone. Abbreviations: PPL: Plane-Polarized Light; XPL: Crossed Polarized Light; CL: Cathodoluminescence.

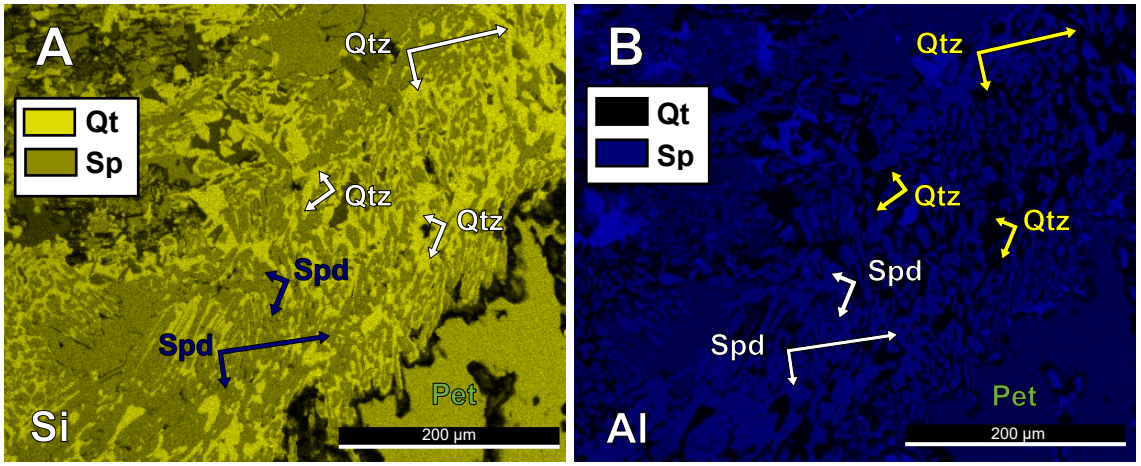

Figure 56. Elemental maps obtained by SEM-EDS (Scanning Electron Microscopy with Energy Dispersive X-ray Spectroscopy) showing the distribution of silica (Si) (Fig. 4A) and aluminum (Al) (Fig. 4B), where intergrowths of spodumene and quartz can be observed filling zones of former fluid circulation. Thin section from the AL51/NOA aplite-pegmatite, Barroso–Alvão field, Portugal.

1.5. Conclusions

Spodumene and quartz intergrowths (SQI) in Li-rich pegmatites can reflect a complex interplay of magmatic, metasomatic, and tectonic processes. These intergrowths may form as: (1) primary skeletal textures from rapid crystallization under highly undercooled conditions, (2) secondary pseudomorphs replacing petalite during post-crystallization re-equilibration (autometasomatism), or (3) through mineral replacement (metasomatism) driven by deformation-related fluid circulation, through mechanisms such as coupled dissolution–reprecipitation (Putnis 2002).

In the specific case of the Barroso–Alvão pegmatite field, the presence of fine spodumene and quartz textures, particularly those associated with deformation structures linked to the D3 phase of the Variscan Orogeny, suggests tectonic activity played a significant role. The occurrence of symplectites here suggests that the rock remained at elevated temperatures long enough for mineral phases to re-equilibrate during cooling, and that deformation occurred while this process was still ongoing.

Distinguishing between these origins of spodumene and quartz intergrowths is therefore essential for accurately reconstructing the thermal and structural evolution of different Li-rich pegmatites.

Acknowledgments

This study has been elaborated in the scope of FLAPSYS project FLaPsys - Fiber Laser Plasma spectroscopy system for real time element analysis, with reference POCI-01-0145-FEDER-031165

2. Cathodoluminescence characteristics of spodumene and petalite from the Iberian massif pegmatites

Adapted from: Filipa Dias and Alexandre Lima

Jornadas do ICT (2021)

Published Abstract

Abstract

Spodumene ($LiAlSi_2O_6$) is the most mined mineral in the world for lithium (Li) (European Commission 2020a). However, it is often found together with another Li mineral, petalite ($LiAlSi_4O_{10}$), that is not so attractive for the Li industry but often looks remarkably alike and sometimes it is harder to tell them apart. A method that could easily distinguish them without requiring knowledge about mineral properties, and would be based only on the color, would be Cold Cathode Optical Microscopy. One interesting use of this type of cathodoluminescence (CL) would be to rapidly check if the Li content from mixtures of crushed rock powder and chips from reverse circulation (RC) drilling has its origin on spodumene or not. Spodumene luminescence has a bright orange color while petalite is a weak dark blue (Wise & Brown 2019). Therefore, theoretically it should be easy to differentiate them.

According to Pagel *et al.* (2000) cathodoluminescence may vary due to several factors, such as activator elements (e.g. Mn^{2+}), quencher elements (e.g. Fe^{3+}, Fe^{2+}, Ni^{2+} and Co^{2+}) or defects on the crystal structure, such as impurities and vacancies.

This study intends to understand the meaning of the color differences observed on the spodumenes and petalites from the Iberian Massif by comparing a large set of samples from Viseu, Guarda, Vila Real and Viana do Castelo (in Portugal) and Galicia and Salamaca (in Spain). Another aspect that has been standing out is that the spodumenes known to be formed by the breakdown of petalite (e.g. Lousas, Vila Real) commonly show areas with purple highly mixed with orange, while spodumenes that are primary usually are formed by large areas where the color and intensity of the luminescence little changes (e.g. Gelfa, Viana do Castelo). In SEM-CL (cathodoluminescence from the Scanning Electron Microscope), these areas are also

very different. The dark orange is a dark grey, the bright orange is a light grey, and the bright purple is even whiter than the bright orange.

Key words: lithium; microscopy; Portugal; CL colors; minerals

2.1. Introduction

Spodumene ($LiAlSi_2O_6$) and petalite ($LiAlSi_4O_{10}$) are both Li-minerals that have been found together in several pegmatites of the Iberian Massif (e.g. Dias (2016b)). According to Wise & Brown (2019), spodumene exhibits a bright orange luminescence under cathodoluminescence (CL), while petalite displays a weaker, dark blue luminescence. As described by Pagel *et al.* (2000), CL can vary due to several factors, including the presence of activator elements (e.g., Mn^{2+}), quencher elements (e.g., Fe^{3+}, Fe^{2+}, Ni^{2+}, Co^{2+}), and defects in the crystal structure, such as impurities and vacancies.

Although spodumene and petalite often occur together, petalite is less attractive to the mining industry (European Commission 2020a). Moreover, due to their similar appearance, distinguishing between them can be challenging without detailed knowledge of their mineralogical properties. Cold Cathode Optical Microscopy-based cathodoluminescence offers a straightforward method to differentiate the two, relying on their distinct luminescence colors.

A practical application of this technique could be the quick identification of spodumene in mixed samples, such as crushed rock powder or chips from reverse circulation (RC) drilling. Since spodumene exhibits a distinctive, strong luminescence compared to other Li-bearing minerals, cathodoluminescence (CL) could help determine whether the Li content is primarily from spodumene or another mineral, such as petalite or amblygonite (which have weaker luminescence), or cookeite, which has no luminescence at all.

Another potential application, though its practicality is uncertain, could involve analyzing RC samples under cathodoluminescence (CL) before sending them for chemical analysis. By quickly identifying the presence of spodumene, distinguished by its strong luminescence, this technique could provide an early indication of Li content, helping to prioritize samples that are more likely to contain the Li-rich mineral.

2.2. Methodology

The analyzed samples consisted of mixtures of crushed rock powder and chips from reverse circulation (RC), as well as thin sections from Li-bearing locations in Portugal (Queiriga, Gonçalo-Seixo Amarelo, Barroso-Alvão, and Serra de Arga), Spain (Catelino, Galicia), and the Portugal-Spain border (Almendra-Barca d'Alva).

The cathodoluminescence (CL) analysis was done with a cold-cathodoluminescence (CL) microscopy with a cold cathode electron gun Citl Mk 4 coupled to a Nikon OPTIPHOT- POL polarizing microscope and Scanning Electron Microscopy (SEM) (Hitachi FlexSEM 1000).

2.3. Results

2.3.1. Cold-Cathodoluminescence of Crushed RC Samples

Crushed samples from different petalite-rich pegmatites were analyzed using cold-cathodoluminescence optical microscopy (Figure 57 and Figure 58). These pegmatites came from Serra de Arga, Almendra–Barca d'Alva, Barroso–Alvão, Gonçalo–Seixo Amarelo, and Queiriga (Figure 3).

The samples from Serra de Arga and Almendra–Barca d'Alva revealed the presence of minor amounts of minerals displaying strong orange luminescence, most likely spodumene, within predominantly petalite-bearing assemblages. In contrast, samples from Barroso–Alvão, Gonçalo-Seixo Amarelo, and Queiriga showed no detectable spodumene under cold-cathodoluminescence. However, small minerals exhibiting intense green luminescence were observed in these samples, which are most likely apatite. Notably, the Queiriga sample exhibited the most intense blue luminescence, potentially indicating a higher petalite content.

Furthermore, two RC samples from the spodumene-rich pegmatite at Reservatório (Barroso–Alvão field) were compared using cold-cathodoluminescence. The sample corresponding to a meter with higher Li content showed a greater abundance of bright orange spodumene grains, while the sample from a meter with lower Li content exhibited fewer spodumene grains and consequently fewer zones of bright orange luminescence (Figure 59).

This correlation suggests that cold-cathodoluminescence imaging may provide a useful qualitative indicator of Li variability in RC drill samples.

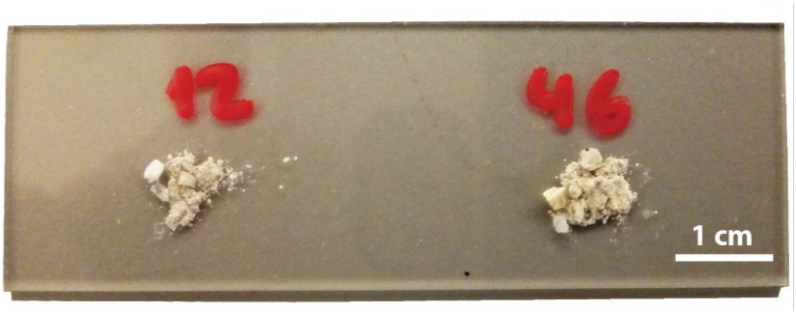

Figure 57. Crushed samples from petalite-rich pegmatites placed over a thin section for cold-cathodoluminescence (CL) imaging.

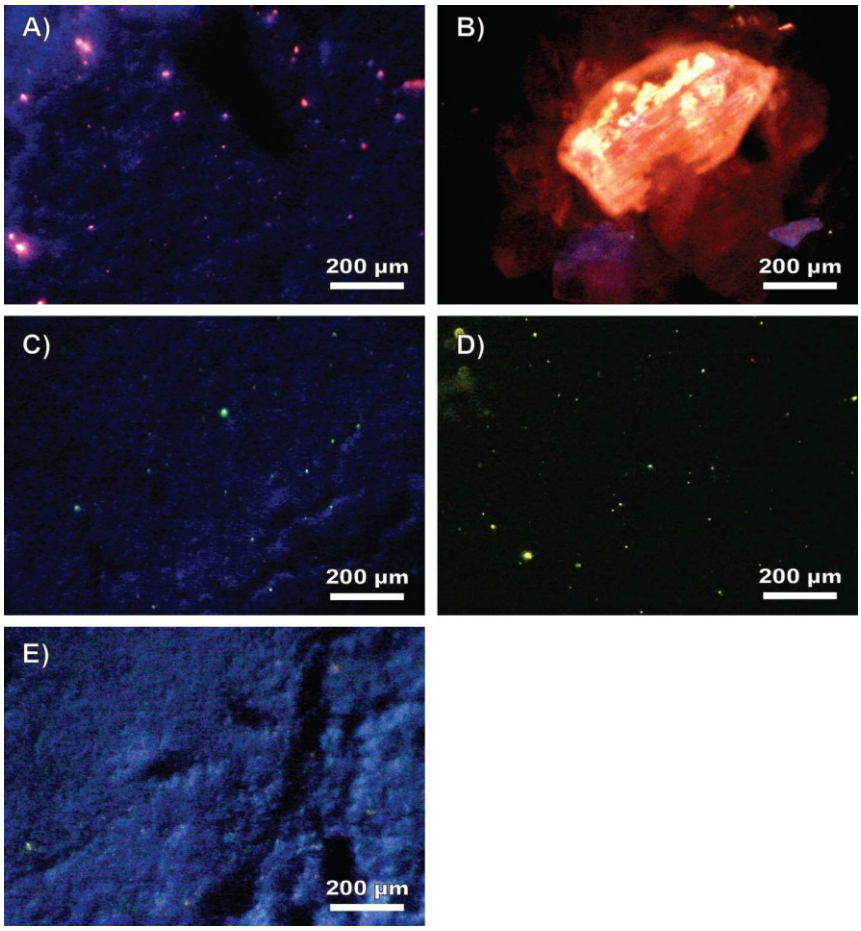

Figure 58. Cold-cathodoluminescence microphotographs of reverse circulation (RC) drill material from petalite-rich pegmatites. A) Serra de Arga; B) Almendra–Barca d'Alva; C) Barroso–Alvão; D) Gonçalo–Seixo Amarelo; E) Queiriga.

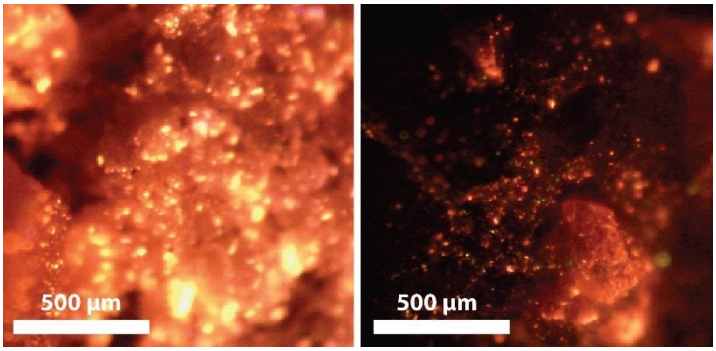

Figure 59. Cold-cathodoluminescence images of two RC (Reverse Circulation) samples from a spodumene-rich pegmatite (Reservatório, Barroso–Alvão field). The left image, from a meter with higher Li content, shows more bright orange luminescence, most likely from spodumene, than the right image, which corresponds to a meter with lower Li content.

2.3.2. Cold-Cathodoluminescence of Individual Grains

In addition to the RC samples, three individual crystal grains were analyzed using cold-cathodoluminescence (Figure 60). These included one grain from Queiriga, one from Gondiães (Barroso–Alvão), and another from Gonçalo (Gonçalo–Seixo Amarelo) (Figure 3). The grains from Queiriga and Gonçalo appeared to be pure petalite, exhibiting uniform dark blue luminescence. However, the crystal from Gondiães seems to display small inclusions of spodumene, identified by their bright orange luminescence contrasting with the dark blue background of the host petalite crystal (Figure 61B).

Figure 60. Individual petalite grains mounted on a thin section for cold-cathodoluminescence (CL) observation. 1) petalite from Queiriga, 2) petalite from Gondiães and 3) petalite from Gonçalo.

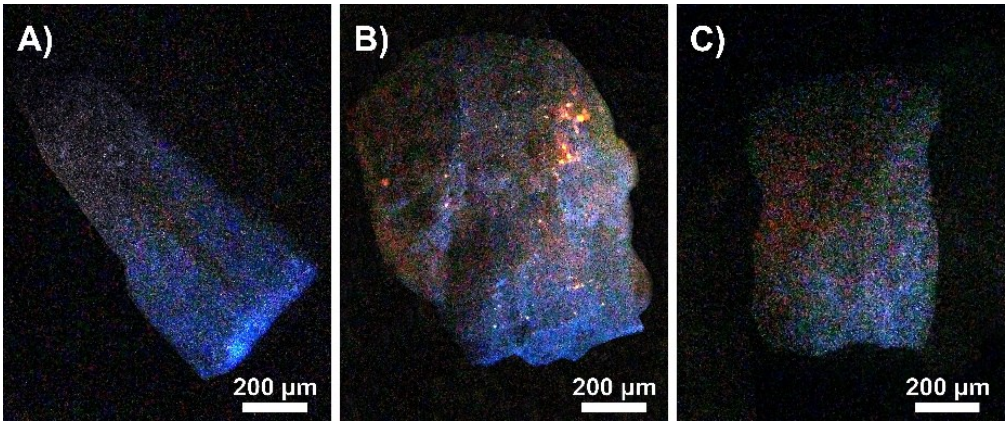

Figure 61. Individual petalite grains imaged under cold-cathodoluminescence (CL). A) Queiriga; B) Gondiães; C) Gonçalo.

2.3.3. Thin Section Analysis of Petalite-Rich Pegmatites

Thin sections from petalite-rich pegmatites, specifically from Lousas and Gondiães (Barroso–Alvão), and Almendra–Barca d'Alva, were examined using cold-cathodoluminescence.

The thin sections of Lousas are predominantly composed of petalite. The petalite exhibits undulose extinction, and in certain areas, symplectitic textures are present, where the petalite has broken down into intergrowths of spodumene and quartz. In these regions, the spodumene shows both orange and purplish luminescence, with the purplish hues being more pronounced. These intergrowths generally form along the cleavage planes and at the edges of the petalite crystals (Figure 62).

The Gondiães thin sections, although sourced from a petalite-rich pegmatite, were from a zone containing only spodumene. The observed spodumene grains predominantly exhibited bright orange luminescence under cold-CL. Some crystals featured small purple zones, while many showed internal zoning with alternating bands of darker and lighter orange. In several grains, dark orange cores aligned along the c-axis were encircled by successive bands of varying luminescence intensity, indicating complex growth patterns (Figure 63).

In contrast, the Almendra–Barca d'Alva thin sections reveal several spodumene crystals with purple luminescent cores aligned along the c-axis of the crystals, bordered by thinner orange luminescent zones on the inner sides of the crystals, parallel to the cleavage planes. These thin sections contain both petalite and spodumene. Although the spodumene with purple cores is located in areas without petalite, there are zones

where petalite is present, with some parts having broken down into spodumene and quartz. These breakdown areas are primarily orange, with only small patches of purple luminescence observed in cathodoluminescence (CL) (Figure 64).

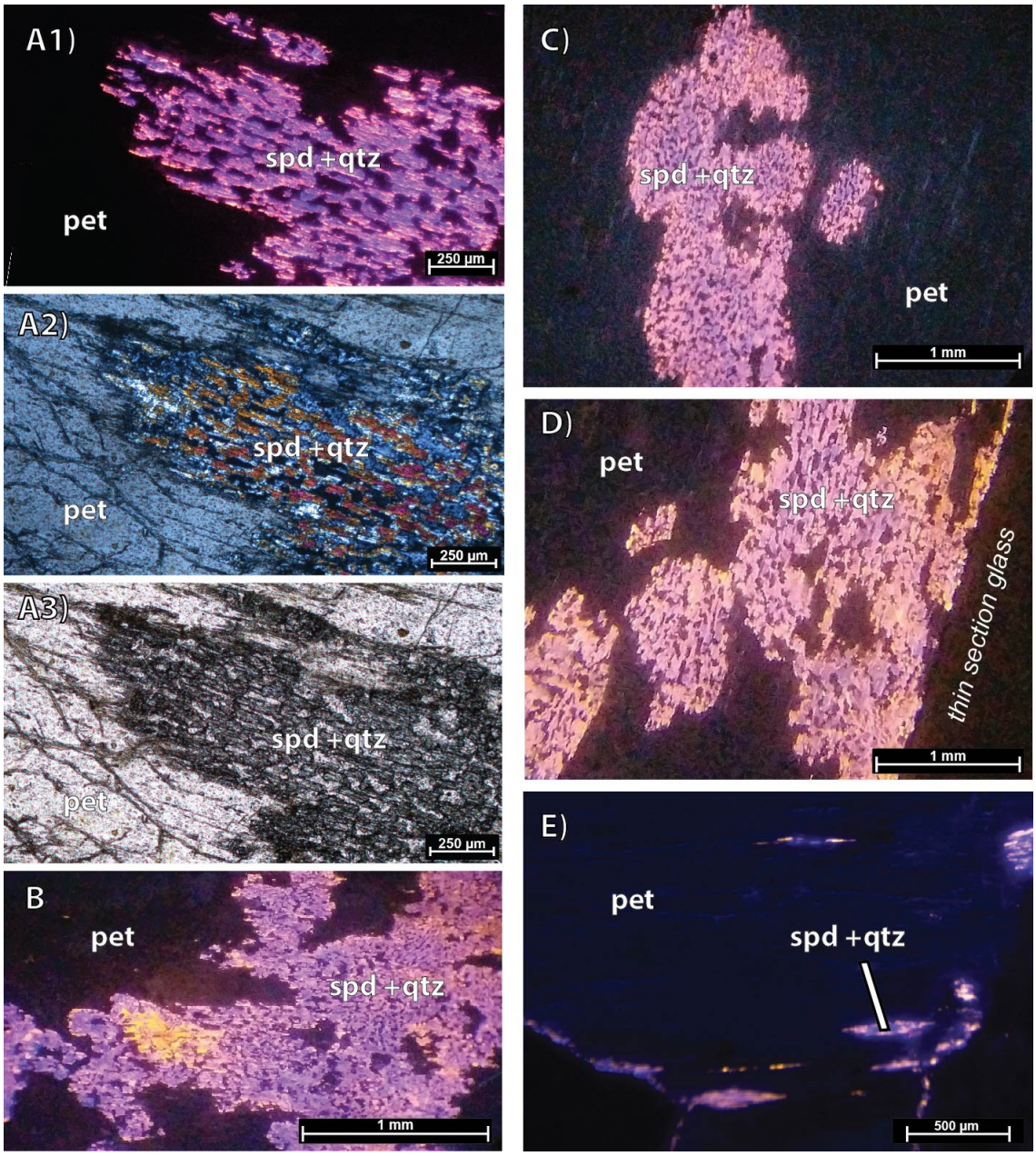

Figure 62. Microphotographs of a petalite-rich pegmatite from the Barroso–Alvão field (Lousas), showing purple and orange spodumene within spodumene–quartz intergrowths formed by the breakdown of petalite. These intergrowths are observed inside petalite crystals. A1) Cold-cathodoluminescence (CL) image; A2) Cross-polarized light (XPL); A3) Plane-polarized light (PPL); B–E) Additional CL images highlighting spodumene and quartz textures.

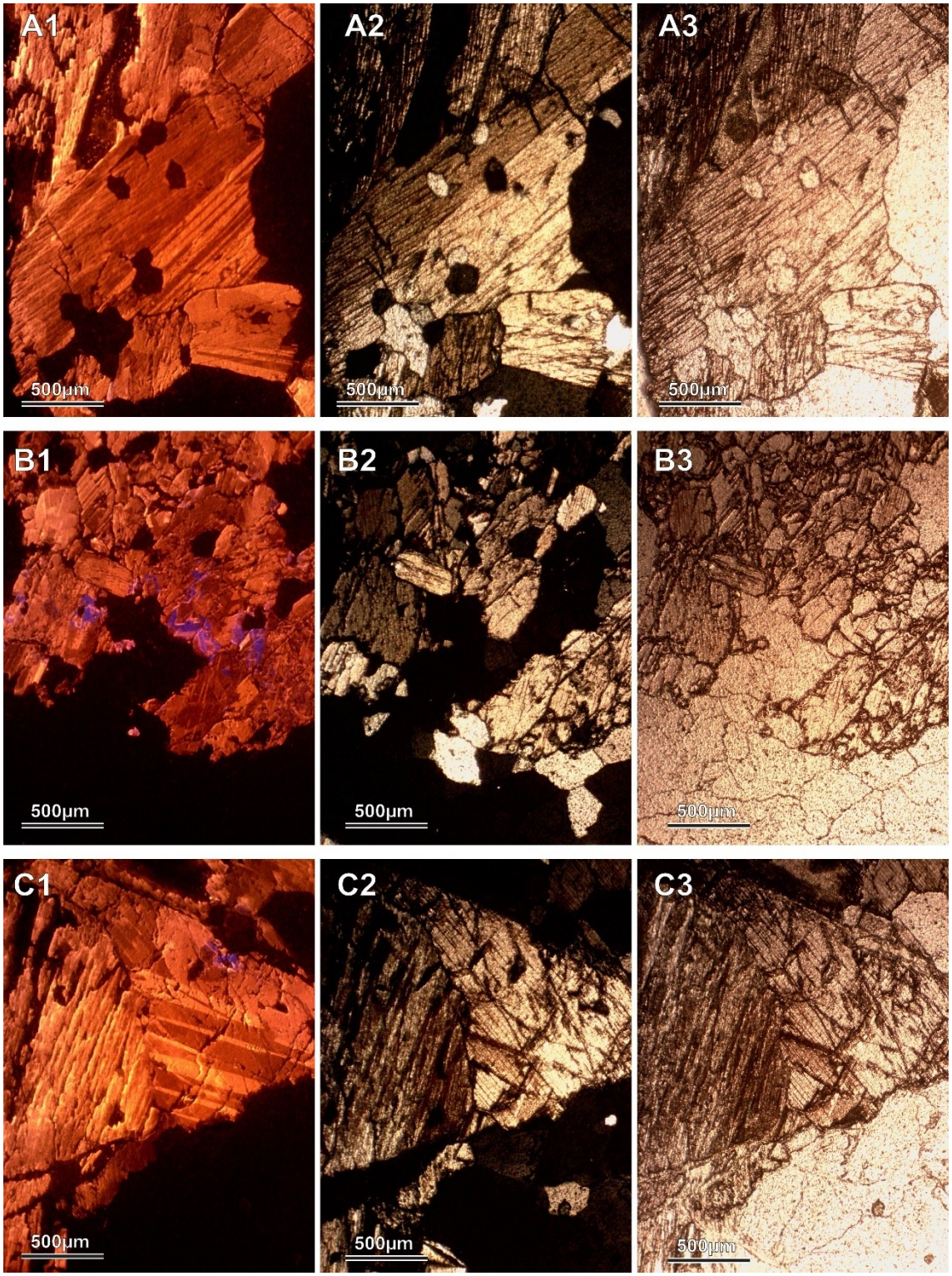

Figure 63. Microphotographs of a petalite-rich pegmatite from the Barroso–Alvão field (Gondiães), showing abundant spodumene with alternating zones of darker and lighter orange luminescence under cold-cathodoluminescence (CL). A1–C1: CL images. A2–C2: Cross-polarized light (XPL) images. A3–C3: Plane-polarized light (PPL) images.

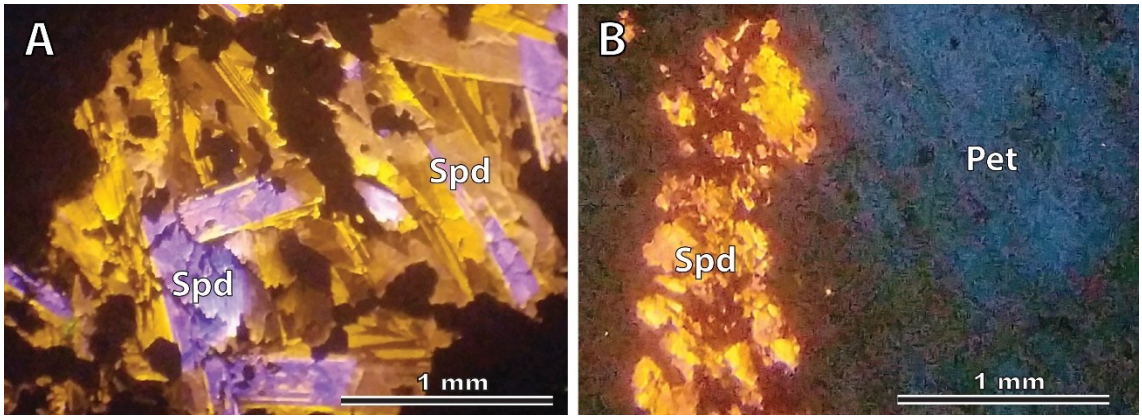

Figure 64. Microphotographs in cold-CL of a petalite-rich pegmatite from Almendra-Barca d'Alva, showing: A) spodumene with purple cores in CL, and B) petalite with intergrowths of spodumene and quartz.

2.3.4. Thin Section Analysis of Spodumene-Rich Pegmatites

Thin sections from spodumene-rich pegmatites—Gelfa, Castelino, Galiza, and Grandão (Barroso–Alvão)—were also analyzed using cold-cathodoluminescence. The Gelfa sample showed clear growth zoning, with alternating bands of dark and light orange luminescence in spodumene crystals (Figure 65), with no purple luminescence observed.

The sample from Castelino, Galiza similarly showed variations in orange intensity but lacked any purple zones. The Grandão pegmatite, however, revealed striking textures in sheared zones. Fine-grained, aligned spodumene in these areas displayed linear purple luminescence features running parallel to shear bands, embedded within broader zones of orange luminescence.

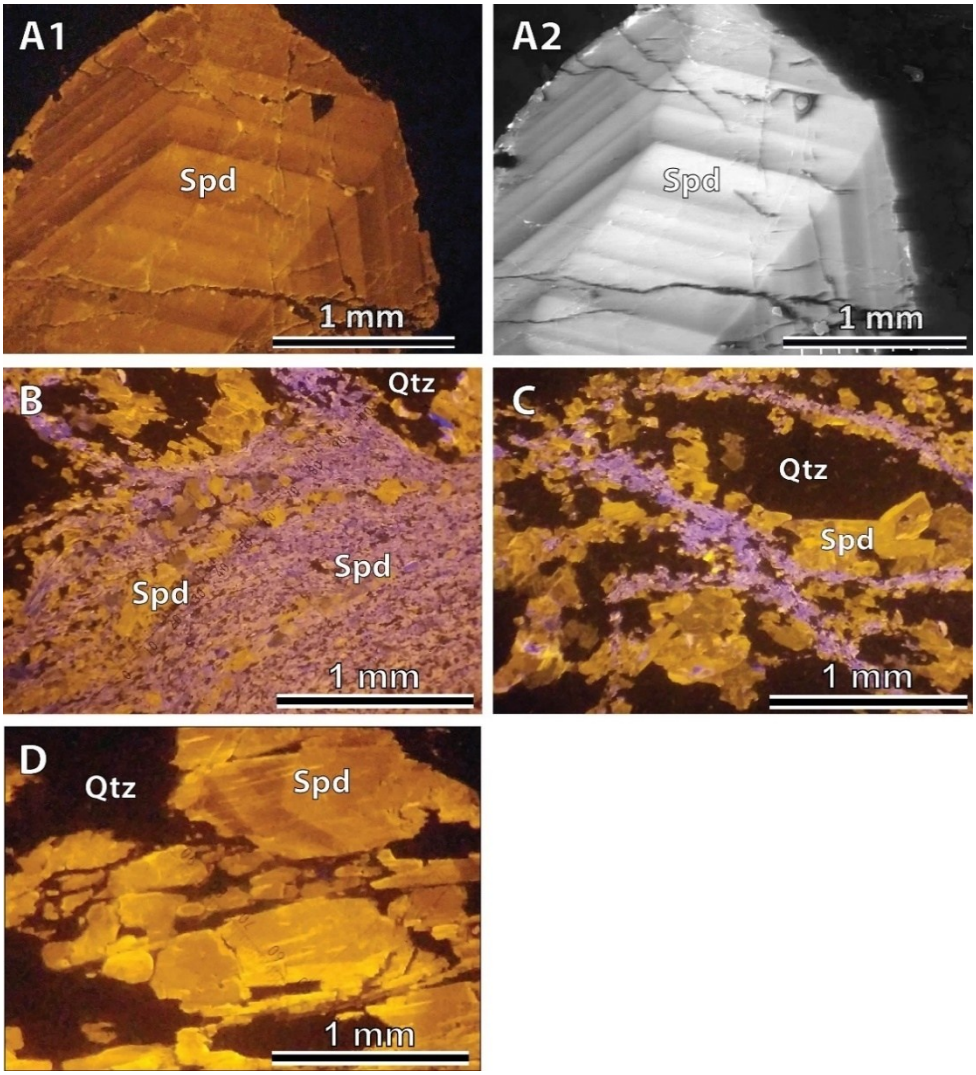

Figure 65. Microphotographs of spodumene-rich pegmatites under cathodoluminescence (CL). A1) Gelfa cold-CL; B) Gelfa SEM-CL; B-C) Grandão (Barroso–Alvão) cold-CL; D) Castelino (Galiza) cold-CL.

2.3.5. SEM-Cathodoluminescence vs Cold-Cathodoluminescence

A comparative analysis of cold-cathodoluminescence (CL) and SEM-based CL was conducted on thin sections containing spodumene from two localities: Almendra–Barca d'Alva and the AL37 pegmatite (Barroso–Alvão). In both cases, a clear correlation was observed between luminescence intensity and color across the two techniques. Darker orange zones in cold-CL corresponded to darker regions in SEM-CL, while lighter orange areas aligned with brighter zones (Figure 66).

An unexpected result emerged with the purple zones seen under cold-CL. These areas appeared almost white in SEM-CL, making them indistinguishable from the

surrounding lighter orange zones. This effect is visible in several spodumene crystals throughout the thin sections. In Figure 66, one of these areas has been circled to aid visualization.

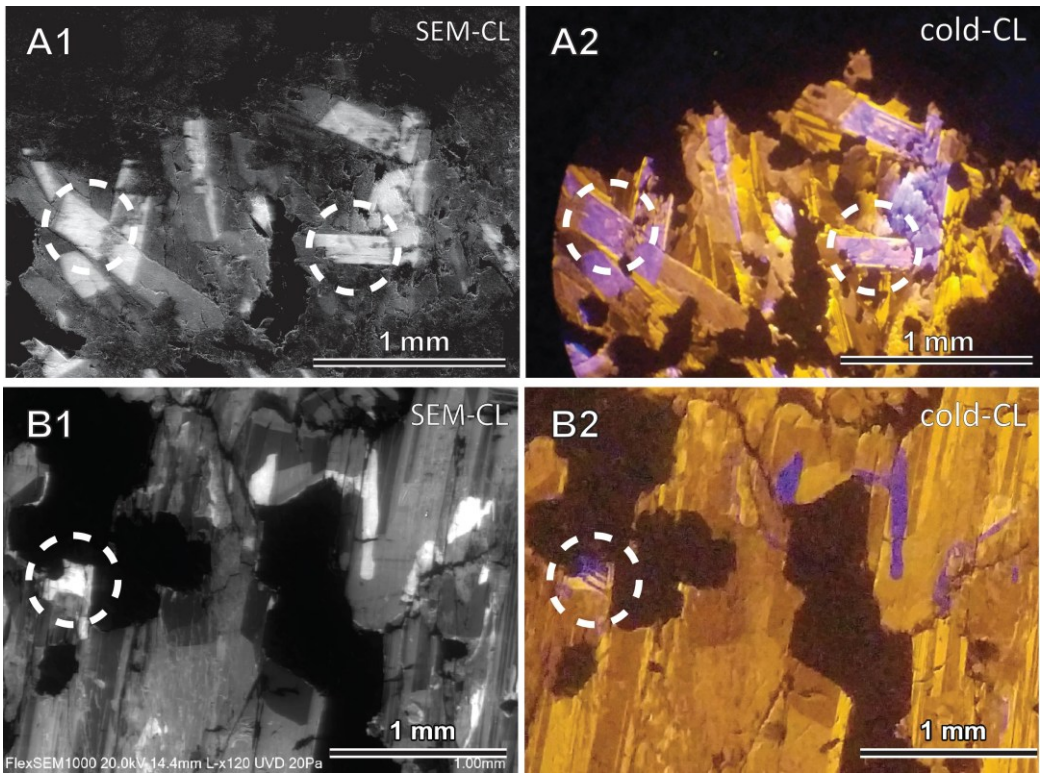

Figure 66. Comparison between scanning electron microscope cathodoluminescence (SEM-CL) and cold-cathodoluminescence (cold-CL) optical microscopy. A1–A2) Almendra–Barca d'Alva; B1–B2) Barroso–Alvão (AL37). A1 and B1 show SEM-CL images, while A2 and B2 show the corresponding cold-CL optical microscopy images.

2.4. Discussion and Conclusions

The cathodoluminescence (CL) behavior of petalite and spodumene observed in this study reveals important mineralogical contrasts with potential applications in both research and exploration. Petalite consistently displayed a blue luminescence color, with variations in shade (i.e., intensity) ranging from darker to brighter blue. This consistent chromatic response suggests a relatively uniform luminescence mechanism across petalite samples, likely linked to limited variation in activator or quencher elements (Černý & London 1983).

In contrast, spodumene exhibited both variations in intensity and color under cold-CL, ranging from bright orange to purple. These differences in luminescence behavior indicate a more complex set of influencing factors. Previous studies (e.g. Pagel

et al. (2000)) have attributed intensity changes to variations in the Fe/Mn ratio within the crystals. SEM-cathodoluminescence (SEM-CL) data from this study partially support that interpretation, as zones with varying luminescence intensity in cold-CL correspond to variations in shades of orange. However, an interesting observation emerged when comparing cold-CL and SEM-CL: areas that appeared purple in cold-CL were consistently observed as very light—often white—regions in SEM-CL, making them indistinguishable from the light orange zones observed in cold-CL. This suggests that color variations observed in cold-CL, particularly the purple luminescence, may not be directly related to Fe/Mn ratios (Dias *et al.* 2018) and that other mechanisms or elements could be involved.

This leads to several open questions. For instance, is there a link between the purple luminescence in spodumene and its formation through the breakdown of petalite, as observed in the symplectitic textures from Lousas and Almendra–Barca d'Alva? Alternatively, could the purple color be related to secondary processes such as fluid circulation or deformation? The alignment of purple luminescence features with shear-related textures in the Grandão pegmatite supports the latter possibility. These hypotheses warrant further investigation through detailed geochemical analyses and microstructural studies.

On a practical level, cold-CL proved to be an effective and rapid tool for spodumene detection in exploration samples. In the case of the Reservatório pegmatite (a spodumene-rich system), cold-CL analysis of two RC samples from different depths, each with differing Li content, quickly revealed a correlation between Li grade and spodumene abundance. This analysis took less than ten minutes and successfully identified spodumene in the higher-Li sample through the presence of bright orange luminescence. This rapid identification method could be particularly useful in exploration workflows.

In conclusion, cold-cathodoluminescence is a valuable tool for both distinguishing Li minerals and gaining insight into their textural and compositional variations.

Acknowledgments

The authors would like to thank the National Funds through FCT within ICT. This study has been financed by FCT through the PhD Scholarship with reference 2020.05534.BD.

3. Quantification of spodumene in thin-sections by crossing cathodoluminescence microscopy with a software of image analysis

Adapted from: Filipa Dias and Alexandre Lima

XI Congresso Jovens Investigadores em Geociências, LEG 2021

Published Abstract

Abstract

Mining spodumene in lithium-rich pegmatites is currently a key objective for many mining companies. Therefore, it is essential to develop reliable methods for quantifying this mineral and determining how much lithium (Li) in the total rock originates from spodumene, rather than from other Li minerals. This study proposes quantifying this mineral using cathodoluminescence (CL) microscopy and image analysis software. CL images significantly enhance the capacity of the image analysis software for accurate detection. Spodumene exhibits extremely high luminescence, making it easily distinguishable from other commonly associated mineral phases, such as quartz, feldspar, petalite, and amblygonite, which have much lower luminescence.

Key words: Leica Phase Expert, pegmatite, cold cathodoluminescence, microscopy, luminescence

3.1. Introduction

Spodumene is currently the primary source of lithium (Li) in the world because Australia began investing in the exploration and mining of spodumene-rich pegmatites, becoming the largest Li producer in the world and surpassing Chile in 2013, which was extracting Li from brine deposits (Jaskula 2015, Jaskula 2021).

Finding and quantifying spodumene in a pegmatite becomes crucial when assessing the potential of a pegmatite for mining, as well as knowing which Li minerals

are present (e.g. petalite, amblygonite, lepidolite, triphylite, etc.), and their relative abundance to correctly assess how much Li from the bulk rock is actually incorporated in spodumene. The traditional method for identifying the minerals present in a rock involves using optical microscopy and thin sections made from samples representative of the rock under study. The advantage of using a tool such as cathodoluminescence (CL) microscopy is the ease of detecting spodumene without requiring a background in petrography, as spodumene has such a strong luminescence that distinguishes it from all other minerals. (Figure 67) (Wise & Brown 2019). The idea is to map thin sections using microphotographs from CL and then add them to an image analysis software to calculate how much spodumene is present in each thin section.

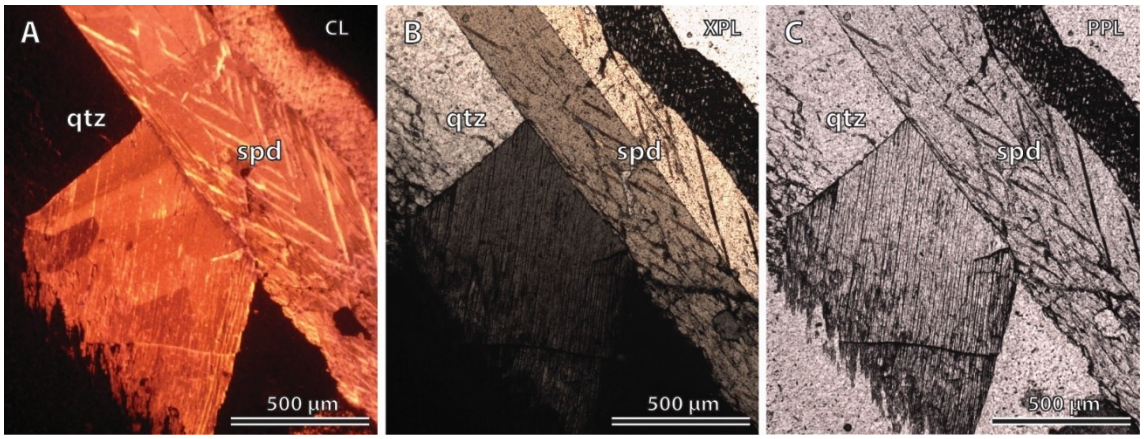

Figure 67. Microphotograph of spodumene (spd) and quartz (qtz) in A) cold-cathode microscopy (CL), B) crossed polarized light (xpl) and C) parallel polarized light

3.2. Methodology

Two thin sections (26 × 45 mm) were selected for this study from rock fragments collected during reverse circulation (RC) drilling conducted by Savannah Resources, PLC, while exploring a spodumene-rich pegmatite in the Barroso–Alvão aplite-pegmatite zone. The fragments represent specific meters along the drill core, with bulk-rock geochemical analysis performed for each meter using Laser Ablation Inductively Coupled Plasma Mass Spectrometry (LA-ICP-MS). Figure 68 shows the drilling log with corresponding Li content, where the locations for thin-section sampling are marked. Thin-sections A to L were collected, but only thin-sections E and I were used for this analysis.

Thin-section E (meters 22-23) has a Li content of 0.47% Li, and thin-section I (meters 41-42) has a Li content of 1.41% Li.

Figure 69 shows the grains from these two meters, providing context for the samples used in the test.

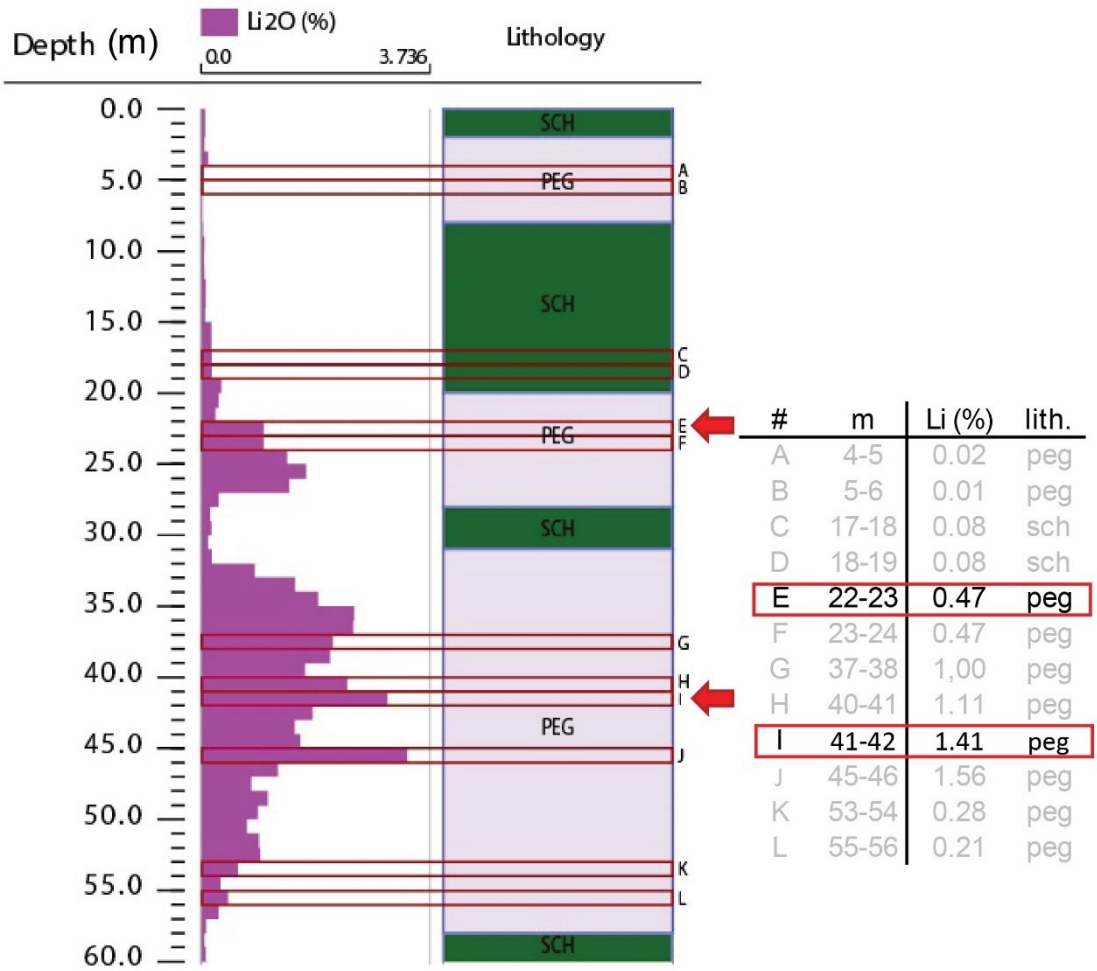

Figure 68. Drilling log showing lithium (Li) content along a borehole from a spodumene-rich aplite-pegmatite in the Barroso–Alvão field. Locations of collected thin-sections are marked in red; thin-sections E (meters 22–23) and I (meters 41–42) were selected for this study. Abbreviations: PEG: pegmatite, SCH: schist.

Figure 69. Representative Reverse Circulation (RC) drill fragments collected from different meters along the borehole. Thin sections were prepared from fragments selected from these meters. Thin sections E (meters 22–23) and I (meters 41–42) were analyzed in this study.

The software utilized in this experiment included DinoCapture 2.0 for capturing the CL images, Agisoft Metashape Professional 1.7.5 for processing the images and creating a comprehensive map of the thin-section, and Leica Phase Expert from the Leica Application Suite (LAS X 5.0.2) for analyzing the images and quantifying the mineral phases.

One thin section at a time was placed on the stage of a CITL CCL 8200 MK4 optical cathodoluminescence (CL) microscope, coupled with a Nikon OPTIPHOT-POL polarizing microscope. A total of 1137 images were captured sequentially using a 4x objective, with approximately 80% overlap, to fully cover the 1st thin section (thin-section I). For the 2nd thin section (thin-section E), 502 images were taken, covering only the luminescent area.

Afterwards, the pictures were added to the *Agisoft Metashape Professional 1.7.5* software, which proceeded to align the pictures, build a dense cloud based on common points, build a mesh, and create a final image from merging all the pictures (a CL map for each thin section). The final image was then added to Leica Phase Expert (Smart Software for Analysis of Multi-Phase Microstructures), where three different phases were included for analysis: 1- spodumene; 2- other minerals; and 3- glass. A color range was chosen for each mineral phase; for spodumene, a range from light yellow-orange to purple was set, while shades of black and red were selected for the glass and other minerals due to the glow of spodumene affecting its surroundings (Figure 70) (Wise & Brown 2019, Dias & Lima 2021).

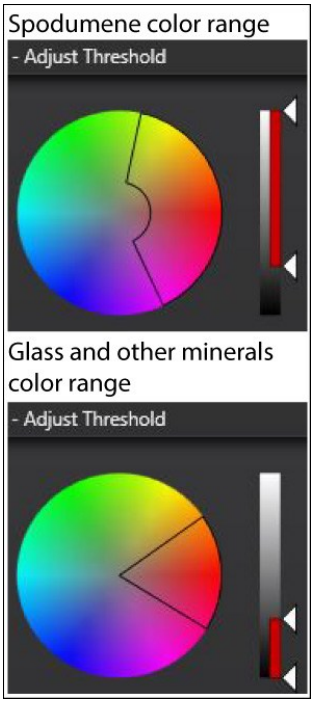

Figure 70. The color ranges set for spodumene, glass and other minerals.

The contact with the glass had to be manually drawn so that it would not be included in the calculations.

Finally, the percentage results for the three mineral phases were recalculated to exclude the area occupied by the glass.

Figure 71 illustrates the workflow followed in this study, outlining the key steps: RC drilling, preparation of thin sections from RC fragments, capturing CL images, merging the images into a single CL image, and using image analysis software to calculate the relative percentages of spodumene and other minerals.

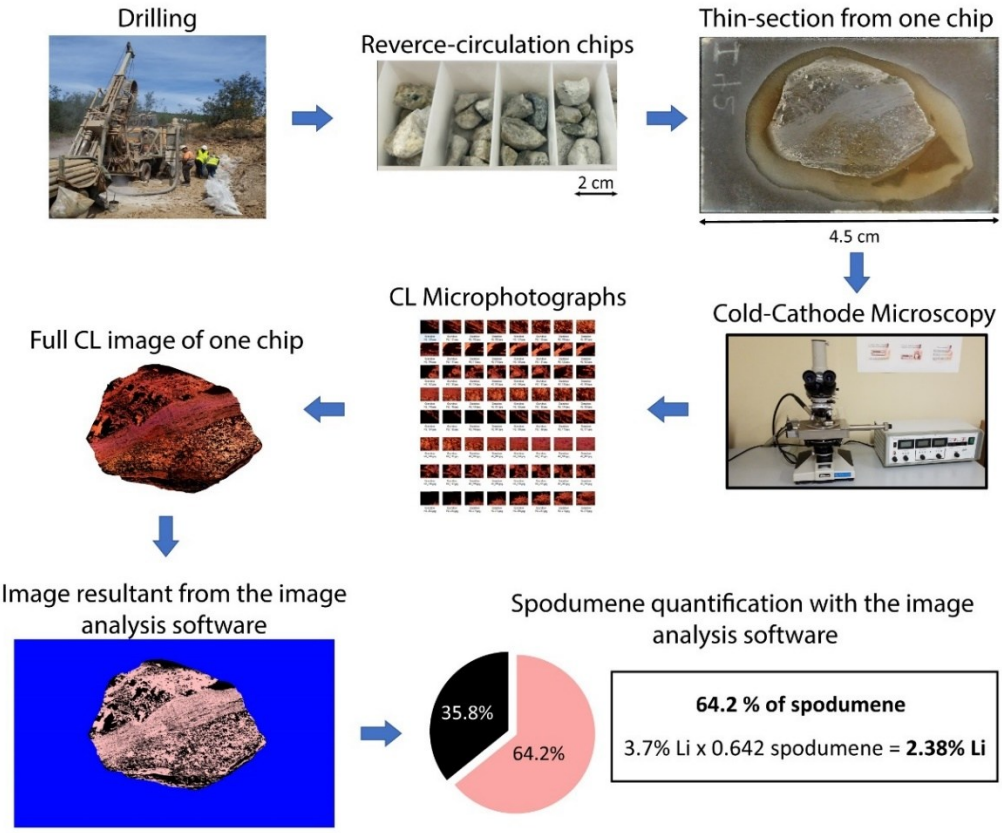

Figure 71. Workflow illustrating the methodology followed in this study.

3.3. Results

The Leica Phase Expert software successfully detected and quantified spodumene in both thin sections. In the first thin section (thin-section I), spodumene accounted for 64.2%, while 35.8% consisted of other minerals (Figure 72). In the second thin section (thin section E), spodumene made up only 8.6%, with 91.4% attributed to other minerals (Figure 73).

In the first thin section, a small shear zone, approximately 0.5 cm in width, was observed cross-cutting the section. This shear zone is composed of abundant, fine-grained spodumene, with the smallest grains measuring as little as 40 μm. In contrast, the second thin section exhibited an average spodumene grain size of approximately 5 mm, with no evidence of a shear zone.

Assuming a theoretical Li content of 3.7% (Kogel *et al.* 2006) in spodumene, multiplying this by the spodumene concentrations in each thin section yields a Li content

of 2.38% for the first thin section and 0.32% for the second. However, spot analysis of individual spodumene crystals using LA-ICP-MS from samples of the Barroso-Alvão field (specifically the NOA aplite-pegmatite) revealed an average Li content of 3.1% in spodumene, corresponding to 1.99% Li in the first thin section and 0.27% Li in the second thin section (see Table A. 1 from Appendix).

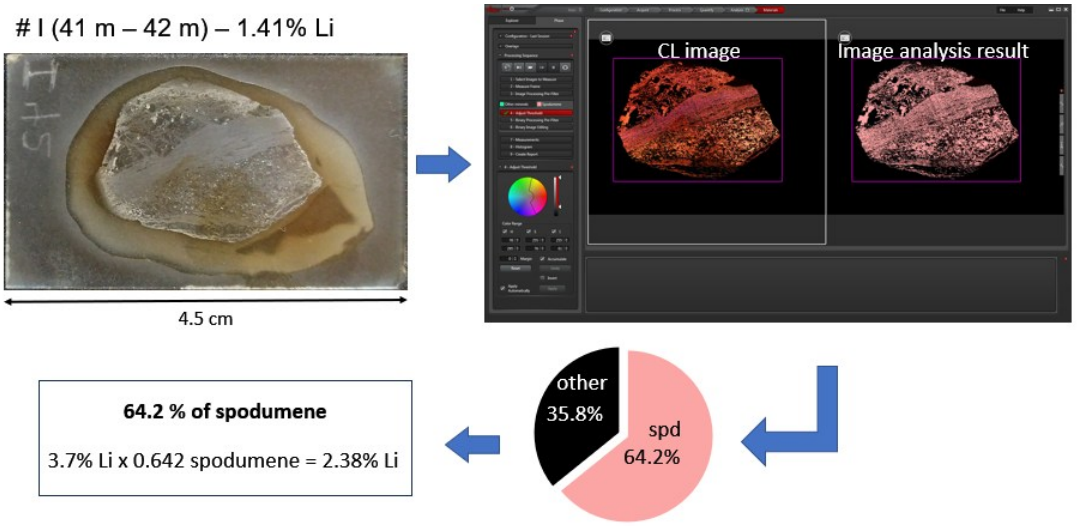

Figure 72. Results of image analysis software applied to the first thin section (Thin-section I), showing the distribution and quantification of spodumene and other mineral phases.

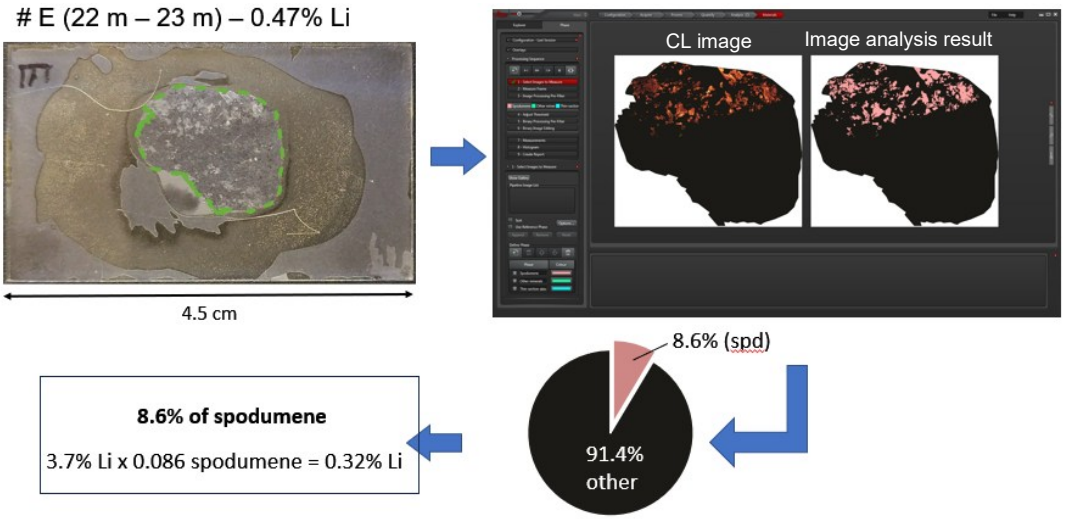

Figure 73. Results of image analysis software applied to the second thin section (Thin-section E), showing the distribution and quantification of spodumene and other mineral phases.

3.4. Discussion and Conclusions

Using image analysis software on cathodoluminescence (CL) images to map and quantify spodumene in thin sections proved effective and can also provide an estimate of grain size, which is relevant for subsequent mineral processing stages. Assuming that the thin sections, each derived from a single reverse circulation (RC) chip, are representative of the corresponding drilled meters, they can be used to estimate the spodumene-derived Li content in the pegmatite.

However, the Li results obtained from image analysis did not fully align with those from the bulk-rock ICP-MS analysis. In the case of the first thin section (I), the image analysis software indicated a higher Li content than that measured in the corresponding meter of the bulk-rock sample. This discrepancy may be attributed to the presence of a small shear zone (approximately 0.5 cm wide) captured within the analyzed grain. It is plausible that another grain from the same meter, which did not intersect the shear zone, would show a lower spodumene abundance and, consequently, a reduced Li concentration. To more reliably evaluate the representativeness of cathodoluminescence (CL) imaging for Li quantification, a broader dataset including multiple thin sections per meter is required.

Additionally, LA-ICP-MS analysis of spodumene crystals from another Barroso–Alvão pegmatite (NOA) revealed an average Li concentration of 3.1% (see Table A. 1 in the Appendices). When this empirical value is applied, the calculated Li content for the thin section drops to 1.99%, which aligns more closely with the 1.41% Li obtained from bulk-rock analysis for the same meter.

For the second thin section (E), the image analysis software showed a lower Li value than the bulk analysis for the corresponding meter. This could be attributed to the lack of representativeness from using only one grain, which contained spodumene in a small portion. Other grains from the same meter may have larger spodumene-rich zones, leading to a higher Li concentration.

Additionally, the actual Li content in spodumene can be different from the theoretical one, as evidenced by spot analyses of spodumene crystals from thin-sections of the AL56/NOA aplite-pegmatite, using LA-ICP-MS (Table A. 1). The Li content of spodumene is known to vary across pegmatite fields, and it is normal to observe that spodumene from different fields tends to exhibit distinct geochemical signatures, forming different compositional “families”. Also, spodumene formed in miarolitic cavities

(crystallizing from late-stage magmatic fluids), tend to show fewer impurities compared to those crystallizing directly from the melt (Deer *et al.* 1978, Dias *et al.* 2018). Therefore, spodumene from pegmatites within the same field should generally have similar Li content, unless altered by processes such as meteoric alteration, which can substitute Li with Na, reducing the Li content in spodumene. However, this typically occurs only at the surface, with deeper pegmatites usually remaining unaltered.

Acknowledgments

The author appreciates the collaboration and support of Savannah Resource, Plc. This work is supported by national funding awarded by FCT - Foundation for Science and Technology, I.P., projects UIDB/04683/2020 and UIDP/04683/2020. Filipa Dias is financially supported within the compass of her respective PhD theses (ref. 2020.05534.BD).

4. Li-Exploration and Processing: The Case Study of Spodumene from the Barroso-Alvão Field, Northern Portugal

Adapted from: Filipa Dias, Alexandre Lima, Encarnación Roda-Robles, Tânia Martins

GAC-MAC-SGA 2023 Sudbury Meeting: Abstracts, Volume 46. https://doi.org/10.12789/geocanj.2023.50.200.

Published Abstract

Abstract

This study investigates the mineralogical and textural characteristics of spodumene-rich aplite–pegmatites from the Barroso–Alvão (BA) field to support efficient lithium extraction and processing. The work focuses on three main aspects: spodumene texture, paragenesis, and geochemistry. Two distinct types of aplite–pegmatites were identified. Type A is dominated by spodumene, while Type B contains both spodumene and petalite. Both types display significant internal heterogeneity in terms of texture and composition. The occurrence of additional lithium-bearing minerals, such as cookeite and montebrasite, adds further complexity to mineral processing. Preliminary geochemical analysis using portable Laser-Induced Breakdown Spectroscopy (LIBS) suggests this method has potential for distinguishing between different lithium minerals (Dias et al., 2023). These findings emphasize the need for detailed mineralogical characterization to improve spodumene recovery and milling efficiency.

4.1. Introduction

To optimize the extraction and processing of spodumene from the Barroso-Alvão Aplite-Pegmatite Field, a comprehensive understanding of its characteristics is required. This preliminary study focuses on three essential aspects: (1) spodumene texture, (2) spodumene paragenesis, and (3) spodumene geochemistry.

By examining the texture of spodumene, including grain size, this study aims to determine milling requirements and processing efficiency. Understanding the

paragenesis, or the mineral associations within the pegmatite bodies, is key to identifying co-occurring minerals that may influence processing strategies. Finally, analyzing the geochemical composition of spodumene will help distinguish it from other Li-bearing minerals, optimizing exploration tools and refining extraction methods. This research aims to provide valuable insights for developing more efficient, targeted Li extraction strategies in the Barroso-Alvão field.

4.2. Results and Discussion

In the Barroso–Alvão (BA) field, spodumene occurs in Li-rich aplite-pegmatites, single intrusive bodies that exhibit alternating fine-grained (aplitic) and coarse-grained (pegmatitic) textures. For instance, a typical body may contain a 10 cm thick aplite zone followed by a 20 cm pegmatite zone, then another 10 cm aplite, and a 5 cm pegmatite zone. These alternating textures appear continuous, and in the pegmatitic zones, it is often possible to observe feldspar crystals and former petalite crystals, now fully replaced by spodumene and quartz, growing from the contact with the adjacent aplitic zones toward the interior of the pegmatitic zones. This seems to suggest that both textures are magmatic in origin and that crystallization alternated between aplite and pegmatite as the melt evolved (Figure 74).

In addition to textural variation, compositional variation is also common, with alternating Li-rich and Li-barren zones. This pattern seems to support the boundary layer effects, where the overall composition of the melt did not have time to fully equilibrate during crystallization. As a result, the composition of the crystallizing phases fluctuated back and forth depending on what had just formed, since only the crystallization front experienced temporary depletion on the elements that had just crystallized (London 2014).

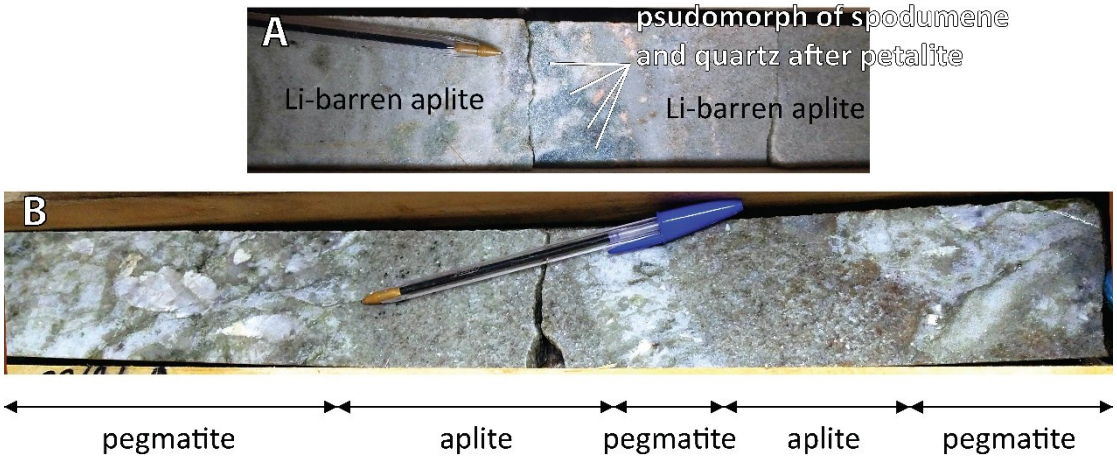

Figure 74. Alternating aplitic and pegmatitic textures in an aplite-pegmatite from the Barroso–Alvão field.

In these aplite-pegmatites, spodumene occurs in a wide range of grain sizes, from micrometric to millimetric crystals to centimetric crystals (Figure 75). This grain size variability likely reflects multiple generations of spodumene crystallization. Additionally, spodumene is found across different pegmatite bodies in the Barroso–Alvão (BA) field, which include at least two types of spodumene-bearing aplite-pegmatites. Type A contains spodumene as the dominant Li-bearing mineral, while Type B hosts both spodumene and petalite in varying proportions. These two types also exhibit distinct bulk-rock geochemical signatures: Type A typically shows higher Fe content, whereas Type B has lower Fe and elevated Sn concentrations (Martins *et al.* 2005).

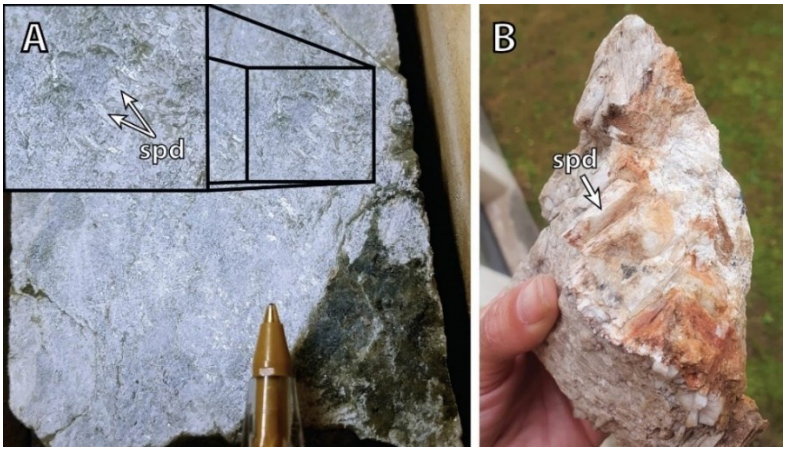

Figure 75. Variation in spodumene grain size from the Barroso-Alvão field. A) Fine millimetric spodumene crystals; B) Coarse centimetric spodumene crystals.

Secondly, the aplite-pegmatites have undergone deformation, and fine-grained spodumene can be observed surrounding coarse spodumene and/or petalite within the pegmatitic zones of both Type A and Type B bodies.

In Type A aplite-pegmatites, zones with higher Li concentrations are typically associated with one of the following contexts: (1) isolated centimetric spodumene crystals, which are relatively rare; (2) fine centimetric spodumene intergrown with similarly sized quartz; (3) fine-grained mixtures of micrometric to millimetric spodumene and quartz, often surrounding earlier-formed feldspar and quartz crystals; and (4) the frequent presence of cookeite next to spodumene, which is commonly observed in these pegmatites (Figure 76).

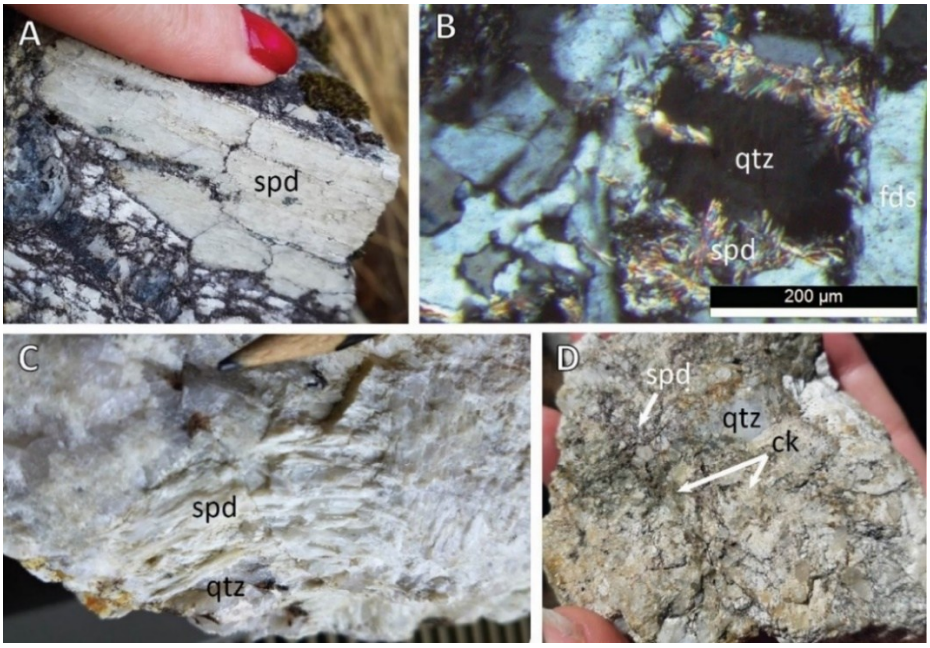

Figure 76. Type A pegmatites, where spodumene is the dominant Li-bearing mineral and petalite is absent. A) Isolated centimetric spodumene crystals; B) Microphotograph of fine-grained mixtures of micrometric to millimetric spodumene and quartz surrounding earlier-formed feldspar and quartz; C) Fine centimetric spodumene intergrown with similarly sized quartz; D) Cookeite adjacent to spodumene, a texture commonly observed in these pegmatites.

In Type B aplite-pegmatites, zones with higher Li concentrations can be associated with a range of contexts: (1) fine centimetric spodumene crystals intercalated with centimetric quartz, sometimes occurring alongside centimetric petalite; (2) fine centimetric bands composed of micrometric to millimetric spodumene intergrown with quartz of similar grain size; (3) micrometric to millimetric spodumene–quartz mixtures occurring inside, crosscutting, or surrounding centimetric petalite crystals; these fine-

grained assemblages may also envelop other minerals such as feldspar and quartz; (4) isolated petalite crystals; (5) centimetric to millimetric spodumene grains surrounded by micrometric petalite, which can also go around quartz and feldspar (Lima & Martins 2011, Dias *et al.* 2023b); (6) next to abundant centimetric to millimetric cookeite (Li-rich chlorite), which is a common texture; and (7) found near micrometric to millimetric montebrasite–amblygonite or (8) adjacent to centimetric triphylite, although these occurrences are rare (Figure 77 and Figure 78).

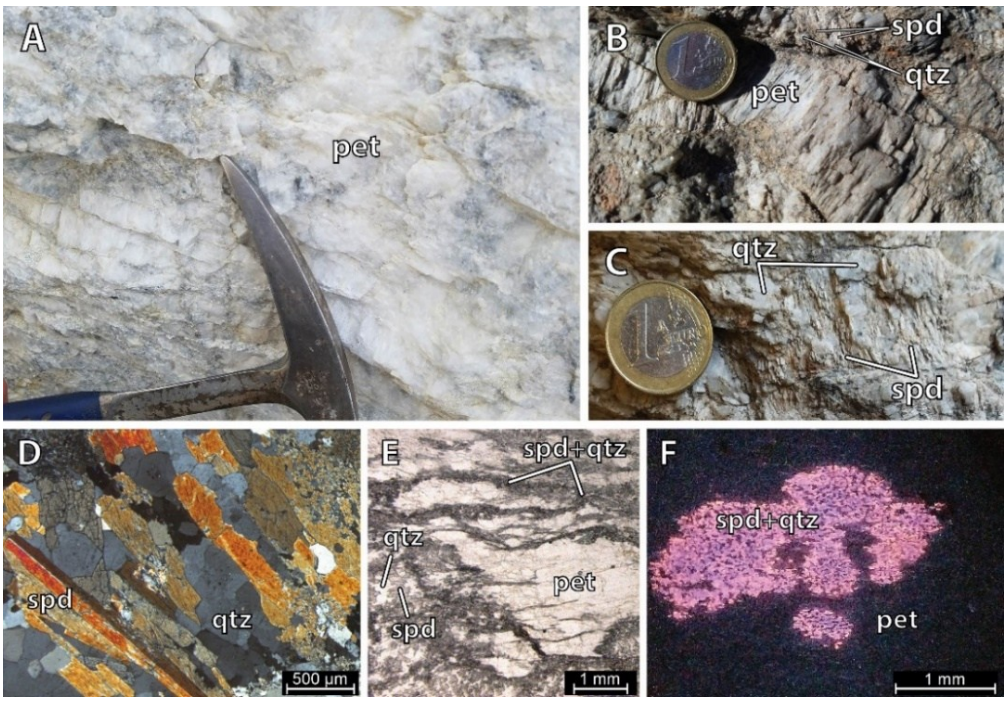

Figure 77. Type B pegmatites where spodumene (Spd) and petalite (Pet) occur in varying proportions. A) Centimetric single crystals of petalite; B) Centimetric petalite adjacent to fine centimetric spodumene and quartz (Qtz); C) Fine centimetric spodumene intergrown with quartz; D) Microphotograph of fine centimetric spodumene and quartz under crossed polarized light; E) Microphotograph showing petalite surrounded and crosscut by micrometric spodumene–quartz mixtures, under parallel polarized light; F) Cathodoluminescence image of micrometric spodumene–quartz mixtures within petalite crystals.

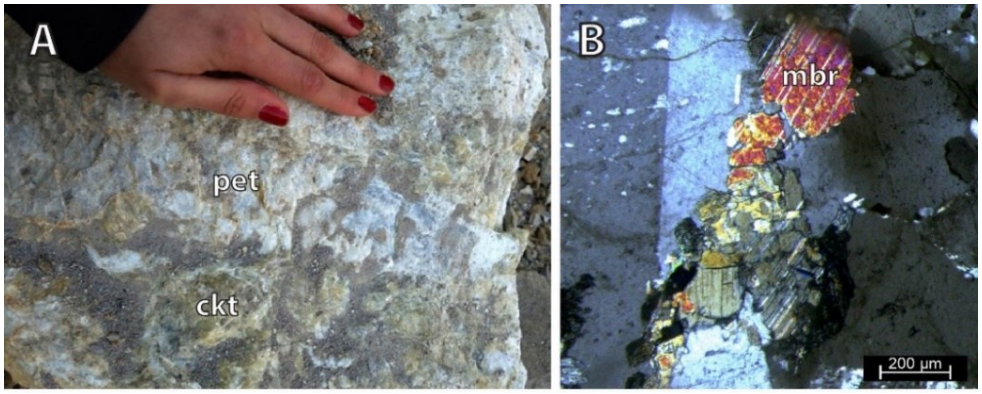

Figure 78. Other Li-rich minerals found in Type B aplite-pegmatites, including: A) cookeite (ckt); and B) montebrasite (mbr).

In summary, the Barroso–Alvão (BA) field features:

(I) both Li-barren and Li-rich aplite–pegmatites;

(II) internal heterogeneity in Li-rich pegmatites, where Li-rich and Li-barren zones occur alternately;

(III) visually similar Li minerals (spodumene and petalite), which can sometimes be difficult to distinguish.

(IV) large variation in grain size including micrometric spodumene–quartz intergrowths invisible to the naked eye.

(V) other Li-minerals besides spodumene occur in these aplite-pegmatites, such as petalite, cookeite, montebrasite and tryphilite.

Regarding the geochemistry of spodumene for Li exploration, portable Laser Induced Breakdown Spectroscopy (pLIBS) equipment may offer a practical solution for distinguishing between different Li-bearing minerals. Recently, Dias *et al.* (2023b) calibrated one of these devices using selected samples from the Barroso-Alvão field, including (a) spodumene, (b) petalite, and (c) mixtures of spodumene and quartz, to improve mineral identification. The study highlights that when collecting Li-rich material from these pegmatites, special attention should be given to the composition of the extracted material. Other Li-bearing minerals, such as petalite or montebrasite, may be together with spodumene, and if not properly identified, their presence could lead to lower-than-expected Li results. This is because standard metallurgical processes tailored for spodumene are not suitable for other Li-bearing phases.

4.3. Conclusions

Regarding the geochemistry of spodumene for Li exploration, portable Laser Induced Breakdown Spectroscopy (pLIBS) equipment may offer a practical solution for distinguishing between different Li-bearing minerals. However, the spodumene composition of each field should be known in time since spodumene composition can vary from field to field (Dias et al, 2018, Deer et al., 1978).

The study highlights that when collecting Li-rich material from these pegmatites, special attention should be given to the composition and texture of the extracted material (learn how much to mill). Other Li-bearing minerals, such as petalite or cookeite, may be together with spodumene, and if not properly identified, their presence could lead to lower-than-expected Li results. This is because standard metallurgical processes tailored for spodumene are not suitable for other Li-bearing phases.

Acknowledgements

The authors gratefully acknowledge the CAVALI project – Cadeia de Valor do Lítio (POCI-01-0247-FEDER-047728) for supporting their participation in this conference. The project aims to develop the full value chain of Li-based battery production for electric vehicles in Portugal, maximizing the added value of the significant Li resources of Portugal. Its activities span from exploration and ore processing to Li refining, battery research, and cell prototype development. As part of this initiative, particular attention is given to the recovery and processing of spodumene from the Alijó and Adagói aplite-pegmatites in the Barroso-Alvão field.

5. Textural and mineralogical characterization of one lithium deposit, from the Barroso-Alvão aplite-pegmatite field: preliminary study

Adapted from: Filipa Dias, Alexandre Lima, Encarnación Roda-Robles, Tânia Martins

SEG 2023 Conference: Resourcing the Green Transition

Published Abstract

Abstract

The AL56 deposit is located in the Barroso-Alvão aplite-pegmatite field in the north of Portugal and has outcrops along an area of approximately 500 × 300 meters. The western side of the area has several small bodies (4–5 meters wide) of aplite-pegmatites where lithium (Li) is majorly in the form of spodumene and/or petalite. The bodies tend to be N130° dipping 30° to 50° to the NE. They also have a preferred type of zonation from top to bottom: 1) up to 0.5 cm of border zone; 2) up to 10 cm of a pegmatitic zone constituted by quartz and feldspar (crystals up to 2 cm) and occasionally white mica; 3) aplite-pegmatite alternations with thickness typically varying from 4 to 10 cm each; 4) Li-mineralization in the shape of fine spodumene and/or petalite in the center of the body; 5) last meter without Li-mineralization that can either be a layered aplite or pegmatite with megacrystals of feldspar (up to 10 cm).

In the area of the AL56 deposit, Li-mineralization occurrence and distribution seem to be related to deformation, which was still active during the crystallization of these bodies. Zones with spodumene petalite seem to be aligned with zones of greater stress. It is possible that while the aplite-pegmatites were cooling and entering the zone of stability of spodumene, zones with greater stress led to the dissolution of petalite and precipitation of fine spodumene and quartz around other minerals in zones of lesser stress. The zones of lower stress can correspond to the zones where petalite can still be observed or to the zones where the breakdown to spodumene and quartz occurred, preserving in a great extent the outer shape of the petalite crystals.

5.1. Results and Discussion

Field observations and petrographic analysis revealed a typical internal zonation in the aplite-pegmatite bodies of the AL56 deposit, as well as two main foliation directions crosscutting the pegmatite (N104° and N136°) (Figure 79):

1. UST Zone (up to 0.5 cm): located adjacent to the contact with the country rock, consisting of coarse albite, quartz, and mica. Plagioclase may exhibit unidirectional solidification textures, growing inward from the contact with the country rock.

2. Li-barren aplite or pegmatite zone (up to 10 cm): Composed of quartz, feldspar, and white mica.

3. Central layered zone: Composed of alternating aplite and pegmatite layers, each typically 4 to 10 cm thick. Li mineralization occurs primarily in the pegmatitic layers as fine-grained spodumene.

4. Li-barren zone (up to 10 cm): Composed of layered aplite or pegmatite with feldspar megacrysts.

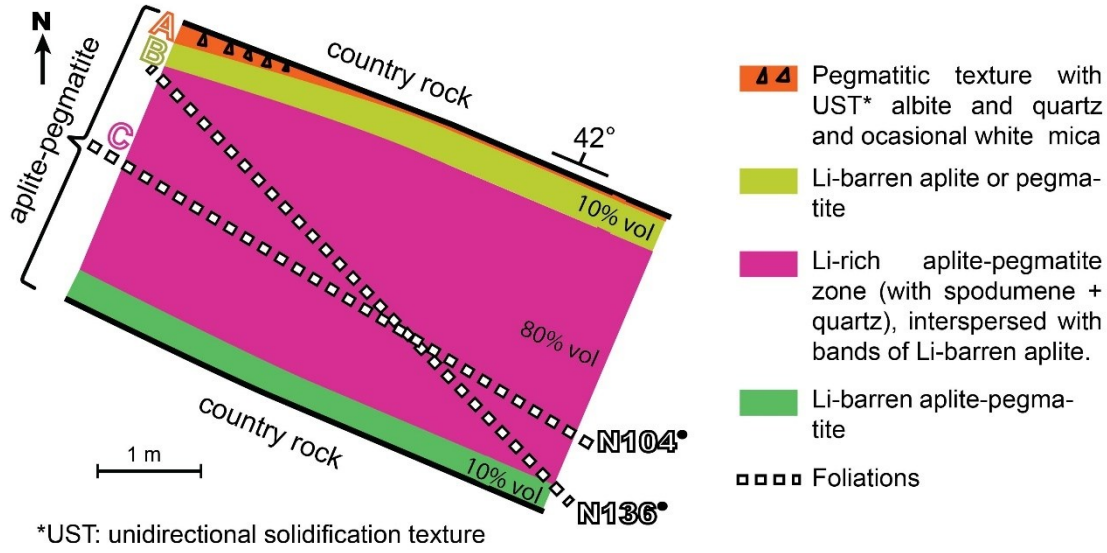

Figure 79. Preliminary model illustrating the typical internal zoning observed across various outcrops of the AL56 lithium deposit.

Sample analysis (Figure 80 and Figure 81) from three of the main internal zones within the aplite-pegmatite bodies, from the contact with the country rock toward the center: (A) Li-barren pegmatite with Unidirectional Solidification Textures (UST) in plagioclase; (B) Fine-grained, Li-barren aplite composed of plagioclase, quartz, white mica, and K-feldspar; and (C) Li-rich pegmatite, consisting of fine-grained spodumene and quartz, corresponding to the central layered zone.

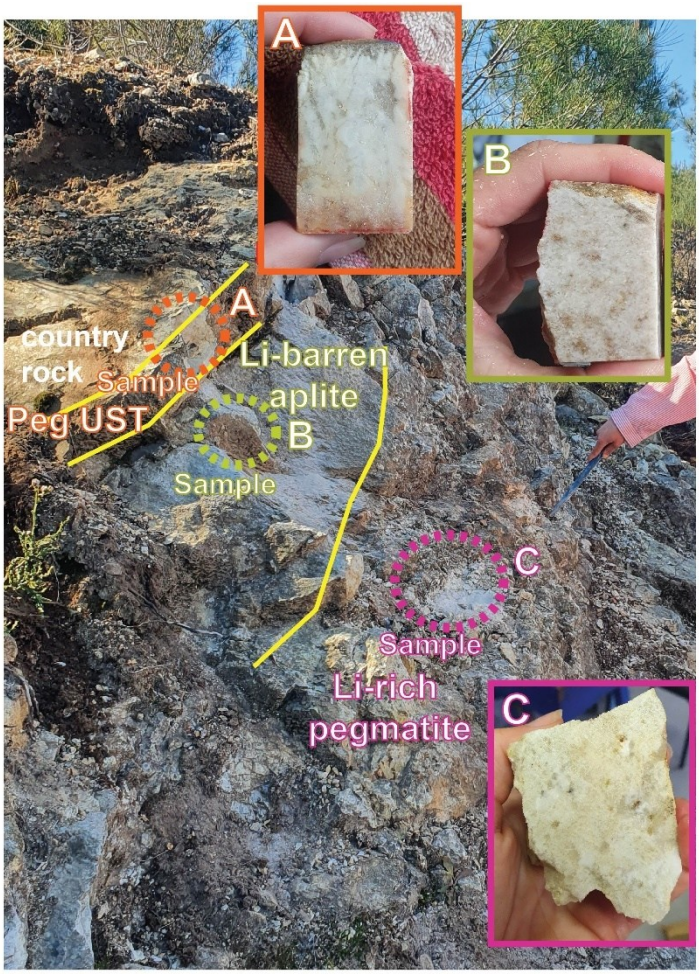

Figure 80. Location of samples A, B, and C collected from an outcrop on the western side of the AL56 deposit, showing three distinct zones: A) Lithium-barren pegmatitic texture with Unidirectional Solidification Textures (UST); B) Lithium-barren aplite; and C) Lithium-rich pegmatite.

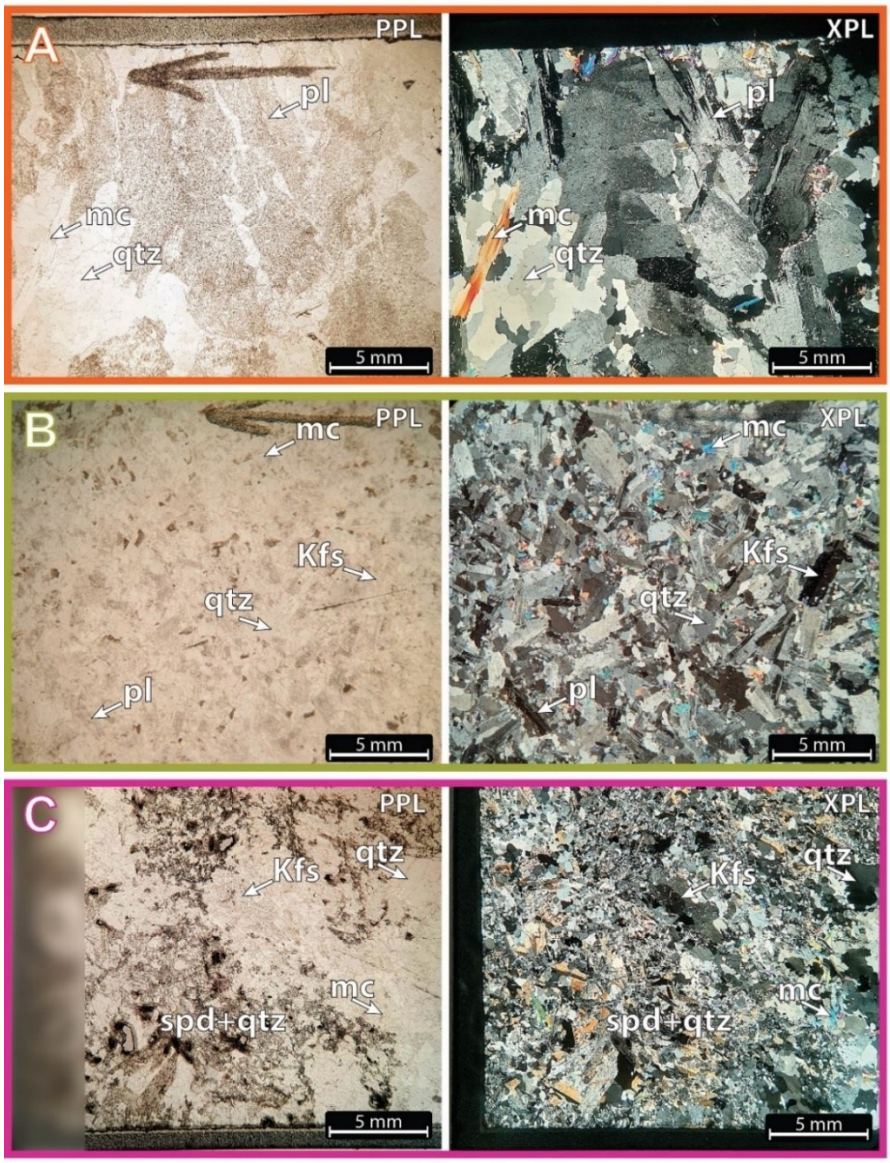

Figure 81. Microphotographs showing the mineralogy and texture of the different zones observed in the samples collected from the outcrop from the western side of the AL56/NOA pegmatite. A) Li-barren pegmatitic texture with Unidirectional Solidification Textures in plagioclases (pl); B) Li-barren aplite constituted by plagioclase, quartz (qtz), white mica (mc) and K-feldspar (Kfs); and C) Li-rich pegmatite constituted by fine grained spodumene (spd) and quartz.

Outcrop observations across the AL56 deposit revealed significant internal variability in texture and mineralogy within the aplite–pegmatite bodies, along with widespread evidence of deformation. To capture this variability, 15 representative samples were collected from various outcrops for thin-section analysis. These analyses confirmed that spodumene is the dominant Li-bearing mineral in the deposit. It typically

occurs as fine-grained aggregates intergrown with quartz within the pegmatitic portions of the alternating aplite–pegmatite layers that define the central zones of the bodies.

In the outcrop shown in Figure 82D, which is visibly affected by deformation, spodumene exhibits a preferred orientation parallel to foliation planes, suggesting that its growth or reorganization was influenced by syn- to post-magmatic deformation. Notably, finer spodumene grains are concentrated along these structural alignments, while coarser crystals occur adjacent to them—implying that foliation may have disrupted earlier-formed spodumene, promoting grain-size reduction and reorientation along deformation corridors.

In contrast, another outcrop from the same deposit (Figure 82C) also displays strong deformation but does not contain spodumene. In this case, the foliation is marked by the preferred alignment of white mica. This contrast indicates that, although deformation is widespread, its role in spodumene formation and redistribution is spatially variable and likely dependent on the presence or absence of pre-existing Li mineral phases.

Deformation features are prominent across both outcrops and thin sections. Two dominant structural orientations—N104° and N136°—were identified, both of which control mineral alignment and fabric development. White mica is commonly aligned along these foliations, reinforcing their role as planes of weakness and pathways for fluid flow. Importantly, spodumene and associated quartz also exhibit alignment along these directions, further supporting the hypothesis that deformation actively controlled the redistribution and recrystallization of Li-bearing phases.

Secondary Li-bearing minerals were also identified (Figure 83). Cookeite, a Li-rich chlorite-group mineral, typically occurs adjacent to spodumene, suggesting formation during low-temperature hydrothermal alteration. Montebrasite, a lithium-aluminum phosphate, was also observed, although it is less abundant than cookeite.

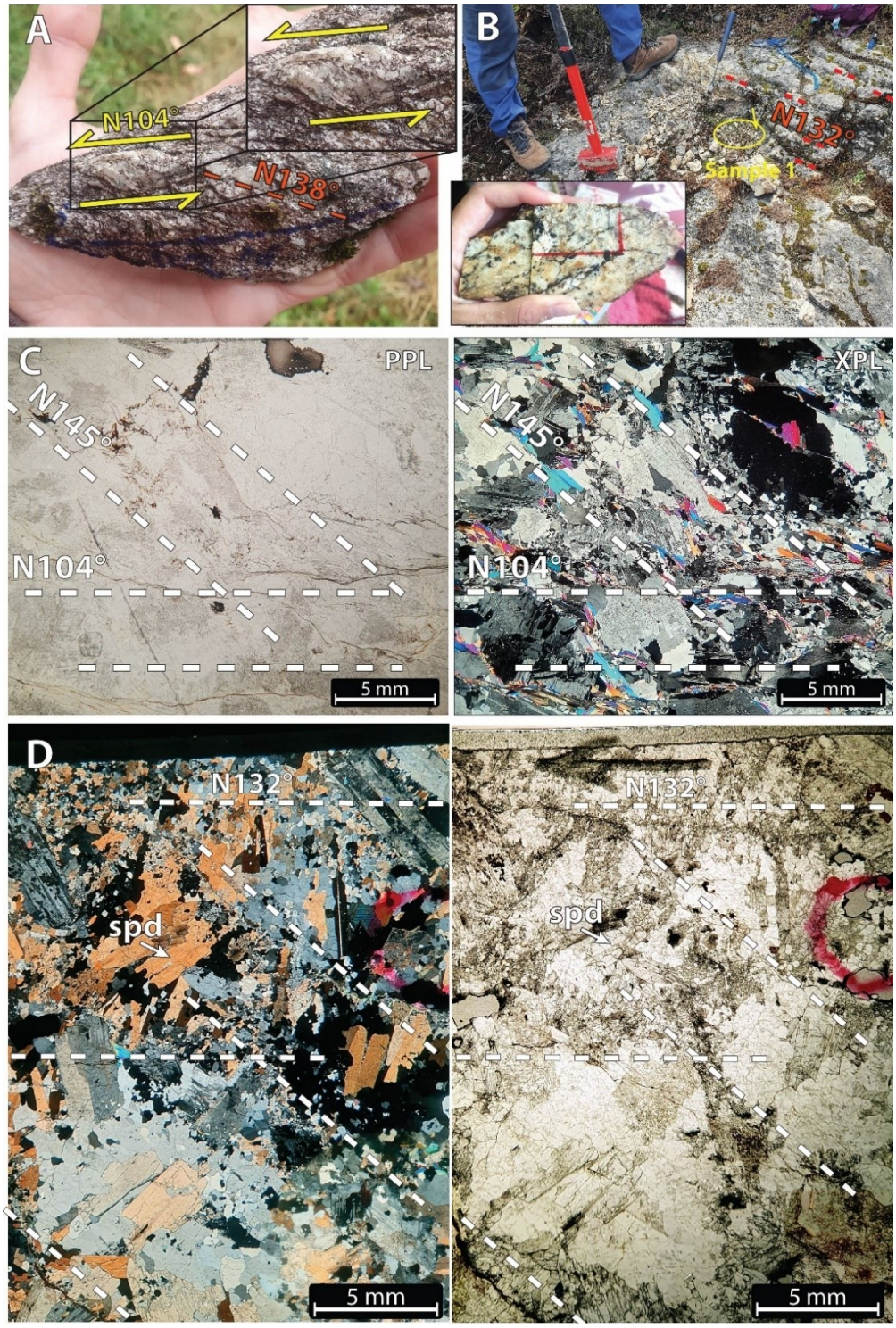

Figure 82. Deformation features of the AL56/NOA aplite-pegmatite showing the two main orientations observed in the western outcrops: N104° and N136°. A-B) deformed pegmatite dyke as observed in the outcrops and hand samples; C) thin sections from the deformed outcrops showing foliation in white mica; D) thin-sections of the deformed outcrops where it is possible to see alignements of fine spodumene and quartz following the foliation observed in the outcrop.

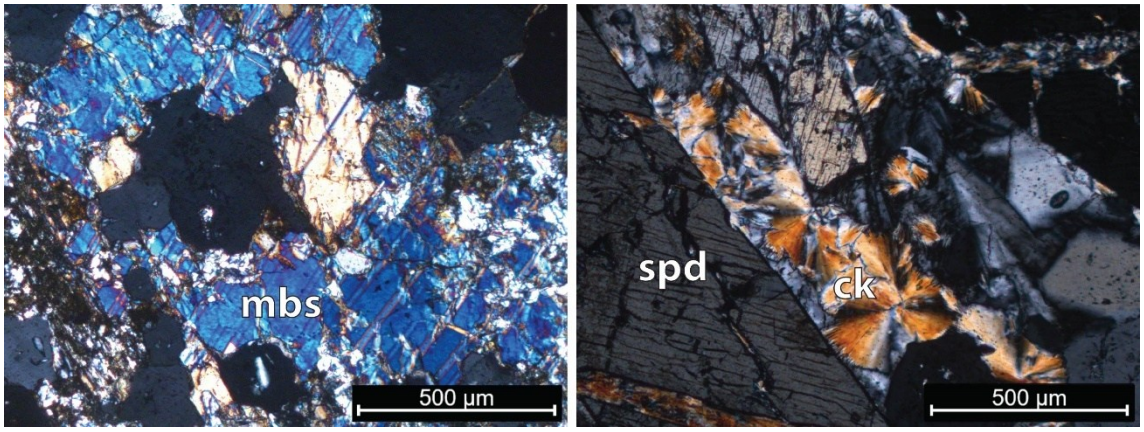

Figure 83. Other Li-minerals (montebrasite (mbs) and cookeite (ck) observed in the thin-section together with spodumene (spd).

5.2. Conclusions

The AL56 deposit, located within the Barroso-Alvão aplite–pegmatite field, presents a clear internal zonation and complex textural evolution influenced by deformation. Field observations and petrographic analysis identified a consistent internal structure, including a Li-rich central zone composed of alternating aplite and pegmatite layers. Spodumene is the dominant Li-bearing mineral, occurring primarily in the pegmatitic portions of these central alternations, intergrown with quartz.

Deformation played a critical role in the redistribution and recrystallization of Li-bearing phases. Spodumene frequently aligns with foliation planes, and finer-grained spodumene is concentrated along these structural orientations, suggesting that syn- to post-magmatic deformation significantly influenced its texture and distribution. In more deformed zones lacking spodumene, foliation is defined by white mica, indicating that deformation alone does not guarantee Li mineralization—its effects are dependent on pre-existing mineral assemblages and structural context.

The identification of two dominant deformation orientations (N104° and N136°) highlights the structural control over mineral alignment and fluid pathways. In addition to spodumene, other Li-bearing minerals such as cookeite and montebrasite were also observed in the deposit. These minerals should be considered in future Li exploration efforts, as they contribute to the overall Li content of the system.

Overall, these findings suggest that deformation not only altered the primary textures but also played a key role in controlling the distribution of Li within the bodies.

Future studies, including drill core analysis, will further enhance our understanding of the factors influencing Li distribution in this and similar pegmatite bodies.

Acknowledgements

This work has national funding awarded by FCT, I.P., in the framework of the ICT project with the references UIDB/04683/2020 and UIDP/04683/2020. Filipa Dias is financially supported by her PhD thesis (ref. 2020.05534.BD) and by national funds from MCTES (Ministério da Ciência, Tecnologia e Ensino Superior) through FCT, co-financed by the European Social Fund (ESF) through POCH-Programa Operacional Capital Humano-and the NORTE 2020 regional program.

6. Evaluating the purity of the NIST Standard Reference Material 182 (petalite) when compared with the petalite from the Barroso-Alvão field, Portugal

Adapted from: Filipa Dias, Ricardo Ribeiro, Filipe Gonçalves, Alexandre Lima, Encarnación Roda-Robles and Tânia Martins

Mineral Deposits Studies Group 2023

Published Abstract

Abstract

The Standard Reference Material (SRM) from NIST (National Institute of Standards and Technology) are known to be certified materials with well-characterized composition and/or properties intended to be used when performing instrument calibrations, verifying the accuracy of specific measurements and to support the development of new measurement methods.

Some new calibrations for a portable equipment of Laser Induced Breakdown Spectroscopy (LIBS) were developed with the goal of analyzing the composition of the Li-minerals, spodumene and petalite, from the Barroso-Alvão aplite-pegmatite field (Portugal). During this process the SRM 182 (petalite) used as a QC (Quality Control) for the petalite samples showed other minerals in cathodoluminescence (CL).

In the Barroso-Alvão aplite-pegmatite field is very frequent to find Spodumene Quartz Intergrowth (SQI), a common texture resultant from the breakdown of petalite, which could result from decreasing the temperature (T) of the emplaced rock. Petalite becomes unstable and recrystallizes to spodumene + quartz, a more stable form. Since petalite ($LiAlSi_4O_{10}$) has more Si than spodumene ($LiAlSi_2O_6$), the excess of Si forms quartz that is intergrown with spodumene. The chemical composition of spodumene + quartz after petalite should be similar to the chemical composition of petalite and thus, chemical results from the mixture of spodumene + quartz after petalite should have similar results to the analysis of a petalite (Černý & Ferguson 1972).

However, although for some other quantitative equipment what is important is the certified chemical composition, LIBS equipment is extremely sensitive to changes of the crystal structure. Therefore, when the matrix changes the spectra also changes, altering the peaks area disproportionately to the element concentration. For that reason, CL was being used to evaluate the purity of the petalite samples and check if any spodumene + quartz was mixed with them.

Petalite is a Li-aluminosilicate that emits a weak blue light (luminescence) when bombarded with cathode-rays in vacuum; while spodumene, although having a similar composition, has a strong luminescence (usually orange). The different optical characteristics allow to distinguish pure petalite samples from samples of petalite with spodumene and quartz even if the materials are milled into fine powders (Wise & Brown 2019, Dias & Lima 2021).

X-ray diffraction (XRD) was also used to analyze the NIST SRM 182 standard. Our results indicate the presence of a large amount of petalite but also indicated that quartz, spodumene and traces of phyllosilicates are also present.

6.1. Methods

6.1.1. Sample Preparation

Crystals of spodumene and petalite from the Barroso-Alvão aplite-pegmatite field (Portugal) were milled and pressed into pellets as part of a study focused on calibrating a portable Laser-Induced Breakdown Spectroscopy (LIBS) device (Dias *et al.* 2023b). A pellet of NIST SRM 182 (petalite) was also prepared following the same procedure and used as a Quality Control (QC) material.

6.1.2. Cold Cathodoluminescence (CL) Microscopy

Given that petalite from the Barroso-Alvão field commonly contains spodumene and quartz intergrowths (SQI) resulting from the breakdown of petalite at lower temperatures, all petalite pellets, including SRM 182, were examined using cold cathodoluminescence (CL) microscopy at the Department of Geosciences, Environment, and Spatial Planning, Faculty of Sciences, University of Porto, during the LIBS calibration work (Dias *et al.* 2023b).

While the bulk geochemistry of spodumene and quartz after petalite is similar to that of pure petalite and may be difficult to distinguish using techniques like ICP-MS, they are different minerals, and their crystal structures differ significantly. This distinction could be critical for LIBS, as the technique is highly sensitive to matrix effects, where even small changes in crystal structure could significantly alter spectral responses (Lepore *et al.* 2017). Thus, for LIBS calibration, CL imaging was used to screen all the petalite pellets for the presence of spodumene before they were used in LIBS, with the same acceleration voltage (approximately 6 kV) (Figure 84).

CL was performed using a CITL CCL 8200 MK4 coupled to a Nikon OPTIPHOT-POL polarizing microscope (Figure 85). Under CL, petalite exhibits a weak blue luminescence, whereas spodumene shows a strong orange luminescence, allowing for visual discrimination even in finely powdered and pelletized samples.

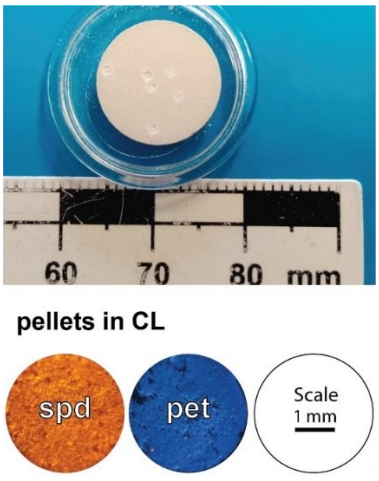

Figure 84. Pellets from Dias *et al.* (2023b) used for LIBS (Laser Induced Breakdown Spectroscopy) calibration, prepared from Barroso-Alvão samples. Under cathodoluminescence (CL), spodumene (spd) pellets exhibit bright luminescence, typically orange but occasionally purple, while petalite (pet) pellets display the characteristic dark blue luminescence of petalite .

Figure 85. Cold cathodoluminescence microscopy equipment used to verify mineralogical purity of petalite pellets.

6.1.3. X-Ray Powder Diffraction (XRD)

To investigate the mineralogical composition of SRM 182 (petalite), a small quantity of the reference material—as received from the supplier—was sent to the National Laboratory of Energy and Geology (LNEG), located in S. Mamede de Infesta, Portugal (Figure 86). X-ray powder diffraction (XRD) was performed using a Panalytical XPERT-PRO diffractometer. The objective was to confirm the presence of additional mineral phases, such as spodumene and quartz, in the SRM 182 material, since the pellet made from this reference material exhibited minerals with strong orange luminescence under cathodoluminescence (CL), indicating that it was not composed of pure petalite.

XRD is a powerful technique for identifying and characterizing crystalline materials based on the diffraction of X-rays by their atomic planes. When a sample is irradiated with X-rays, the atoms in its crystal lattice diffract the X-rays at specific angles, producing a pattern of peaks that is characteristic of the mineral phases present. These diffraction patterns are then compared against reference databases, allowing for the identification of each phase based on its unique set of peaks.

Figure 86. X-Ray Diffraction (XRD) equipment at LNEG (Laboratório Nacional de Energia e Geologia) used for the mineralogical characterization of NIST SRM 182 (petalite).

6.1. Results

6.1.1. Spodumene and Quartz Intergrowths (SQI) in Petalite from the Barroso-Alvão Field

The Barroso-Alvão pegmatite field includes both spodumene-rich and petalite-rich aplite-pegmatites, with petalite-rich ones not being free of spodumene, as observed

in aplite-pegmatites such as Lousas and Gondiães (Dias 2016b). While these intergrowths can be minor in quantity relative to petalite as the dominant Li mineral (as seen in the Lousas aplite-pegmatite), they are a widespread feature within Barroso-Alvão pegmatites and can be easily recognized optically under cathodoluminescence (CL), as observed in a thin section made from petalite crystals of the Lousas aplite-pegmatite (Figure 87 and Figure 88).

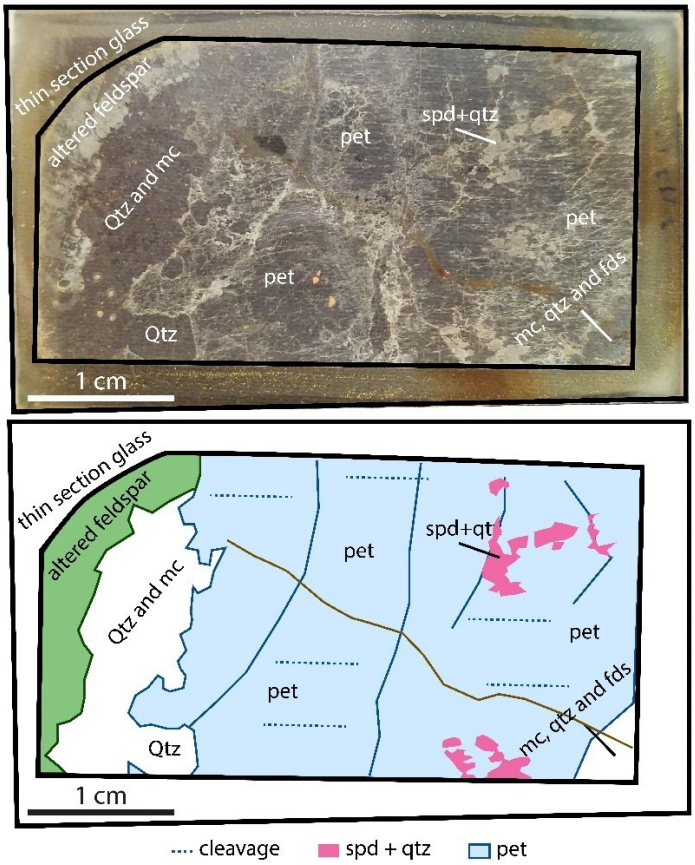

Figure 87. Thin section of petalite from the Lousas aplite-pegmatite showing spodumene + quartz intergrowths (SQI) within the crystal, formed as a result of petalite breakdown.

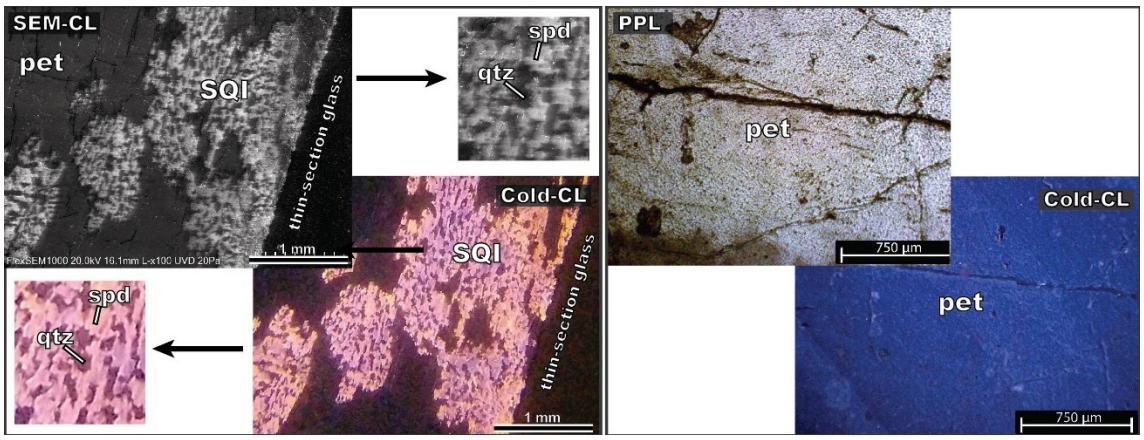

Figure 88. Microphotographs showing spodumene and quartz intergrowths within a petalite crystal from the Lousas aplite-pegmatite, Barroso–Alvão field.

6.1.2. Cold Cathodoluminescence of Petalite Pellets

Under CL, not all petalite pellets from the Barroso-Alvão field exhibited the typical weak blue luminescence of petalite; some revealed bright orange luminescence, indicating the presence of spodumene, as previously suspected. What was surprising, however, was that when NIST SRM 182 (petalite) was observed under the same conditions, it too displayed bright orange luminescence, suggesting the presence of spodumene within the reference material and confirming that the material is not pure petalite (Figure 89).

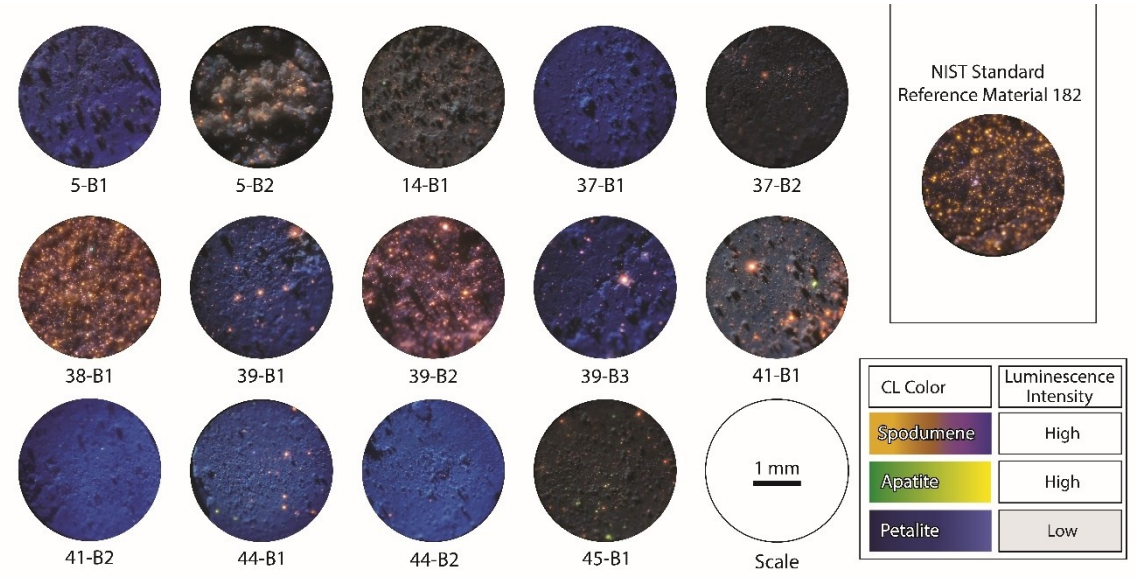

Figure 89. Cathodoluminescence (CL) image of petalite pellets from the Barroso-Alvão field, showing the characteristic weak blue luminescence of petalite. Some pellets exhibit bright orange luminescence, indicating the presence of spodumene. The image also includes the CL of NIST SRM 182 (petalite), which displays numerous bright orange luminescent minerals suggesting the presence of spodumene and indicating that the material is not pure petalite.

6.1.3. XRD Analysis of SRM 182

X-ray diffraction (XRD) analysis of SRM 182 confirmed the presence of multiple mineral phases within the material. While the majority phase was petalite, constituting approximately 90% of the sample, there was also 6% spodumene, 4% quartz, and trace amounts of phyllosilicates (<1%) (Figure 90). These results align well with the cathodoluminescence (CL) observations, where spodumene displayed its characteristic

bright orange luminescence, further confirming the multi-phase composition of the material and indicating the impurity of this standard reference material.

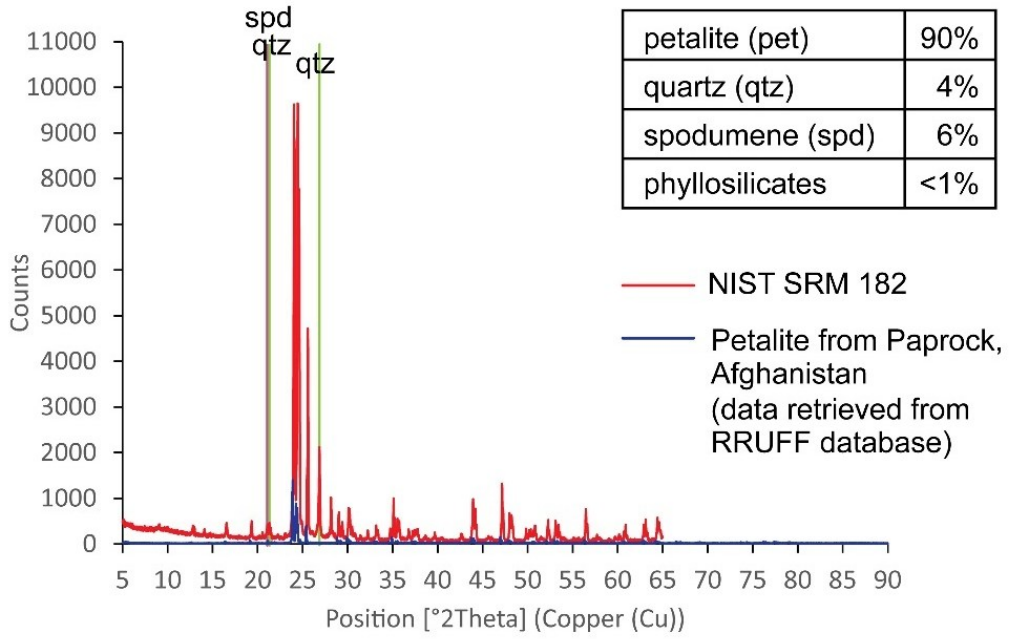

Figure 90. X-ray diffraction (XRD) diffractogram of SRM 182, analyzed by the National Laboratory of Energy and Geology (LNEG), confirming a multi-phase composition with petalite as the dominant phase (~90%), along with minor spodumene (~6%), quartz (~4%), and trace phyllosilicates (<1%).

6.2. Discussion and conclusions

The Standard Reference Material 182 (Petalite) from NIST contains approximately 6% spodumene, 4% quartz, and less than 1% phyllosilicates, as determined by X-Ray Diffraction (XRD) analysis conducted by the National Laboratory of Energy and Geology (LNEG, Portugal). The presence of spodumene is also clearly observable under cold-cathodoluminescence microscopy, as demonstrated in this study. Since SRM 182 consists of only about 90% petalite, it may not be suitable for techniques that are highly sensitive to crystal structure, such as XRD. However, analytical methods focused on elemental concentrations, such as ICP-MS, are unlikely to be affected, as the bulk chemical composition remains consistent with petalite—likely because the spodumene and quartz present result from the breakdown of petalite, preserving the overall stoichiometry:

Theorectically:

$LiAlSi_4O_{10}$ (petalite)	→	$LiAlSi_2O_6$ (spodumene)	+	$2SiO_2$ (quartz)
2.09% Li		3.73% Li		~0% Li
100 vol%	→	56.3 vol%	+	43.7 vol%

Therefore, although the certificate of analysis for Standard Reference Materials 181, 182, and 183 (Lithium Ores) from 1981 does not specify the geological origin of the petalite used, the presence of breakdown products such as spodumene and quartz suggests that it likely came from a pegmatite where petalite underwent a certain degree of phase transformation, similar to what can be observed in the Barroso-Alvão field. Consequently, the petalite used in SRM 182 should have been subjected to additional verification techniques, such as CL or XRD, before being marketed as a pure reference material by NIST, an institution expected to maintain rigorous analytical standards.

7. Lithium Aluminosilicate Textures and Lithium Distribution from the Aplite-Pegmatites of Northern Portugal: Outcrop and Drill Core Comparisons

Adapted from: Filipa Dias, Alexandre Lima, Encarnación Roda-Robles and Tânia Martins

The Canadian Journal of Mineralogy and Petrology (GAC-MAC-PEG 2024). https://doi.org/10.3749/AB00032

Published Abstract

Summary

The Barroso-Alvão field in Northern Portugal has Li-rich pegmatites with complex structures, textures, and mineral distributions. In this study, a Li deposit constituted by multiple aplite-pegmatite bodies was thoroughly examined using outcrops and drill cores to characterize the spatial distribution of Li, which can be quite heterogeneous.

The aplite-pegmatites in this deposit range in width from a few centimeters to approximately 8 meters.

Some parts of the bodies were strongly deformed, resulting in Li remobilization and shear zones that are extremely Li-rich. Other parts retain the primary texture of a layered pegmatite, with the aplitic units often Li-poor or Li-barren. In addition, a late-stage fluid phase rich in Li and Si partially overprinted these primary textures, resulting in Li-enriched zones.

7.1. Introduction

The Barroso-Alvão field hosts numerous Li-enriched aplite-pegmatites. The high Li contents are primarily related to spodumene and petalite mineralization. These minerals are not distributed uniformly along the strike of the bodies (Dias 2016, Martins & Lima 2011).

Recently, Dias *et al.* (2023a) showed that there are outcrops with Li-rich, Li-barren, and strongly deformed zones, where the primary crystallization texture has been overprinted. In this study, outcrop observations are compared with drill core data of this deposit, both macroscopically and microscopically using an optical microscope and electron probe micro analyzer (EPMA). The goal is to understand the behavior and distribution of Li within these pegmatite bodies.

7.2. Results and Discussion

Thin sections of outcrop and drill core samples show that Li is mainly associated with spodumene, but the Li minerals cookeite and montebrasite were also observed. Although petalite has been described previously from this deposit (Dias 2016b), so far only relics of petalite crystals have been observed in the outcrops and drill cores.

The petalite relics that did not break down into spodumene and quartz seem to have almost completely altered to clay minerals such as kaolinite, montmorillonite, and a Li chlorite (cookeite).

Observations made on the drill cores are as follows: (1) the layered aplite parts are usually Li-barren or Li-poor, with only small amounts of spodumene and quartz, which still retain the cone shape of replaced petalite crystals (1 to 2 cm) that formed between the aplitic layers; (2) Li-rich pegmatitic parts, usually in the center of the apophyses (around 80 vol.%), occurring as very rich zones of millimetric spodumene and quartz, typically around megacrystals of light pinkish feldspar; and (3) similarly to the outcrops, shear zones consisting of microcrystalline spodumene and quartz were also found in the drill cores crosscutting the previous textures at about 100 m depth (Figure 91A).

These shear zones have a mylonitic texture and seem to have an important role in concentrating Li inside these bodies (Figure 91A). In addition, the activity of late-stage Li- and Si-rich fluids seems to have produced fronts of spodumene and quartz that replace the primary textures. These fluids are unrelated to deformation but most probably are due to a second boiling process that took place during late stages of crystallization, after formation of magmatic quartz and feldspars in these mica-poor bodies. The brecciation showed by some feldspar crystals (Figure 91B) could attest to this late exsolution process, as those crystals could have broken due to the increase of fluid pressure due to the separation of H_2O from the pegmatitic melt.

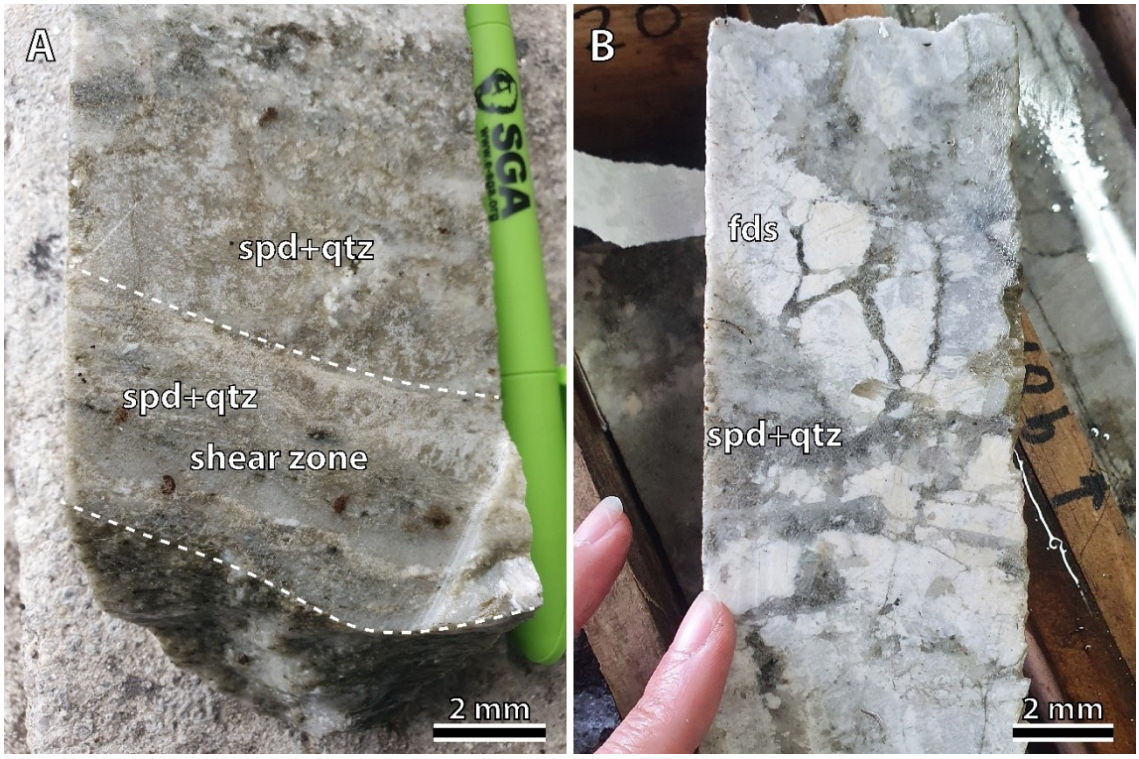

Figure 91. (A) Shear-zone cross-cutting previous texture. (B) Spodumene (spd) and quartz (qtz) replacing previous texture rich in coarse feldspars (fds).

7.2.1. Interpretation and Evolutionary Model for One Li-deposit of the BA field

Although the aplite-pegmatites from the Barroso-Alvão field have been considered internally unzoned (e.g., Noronha & Lima 2006), this study shows a tendency to an internal zonation in these bodies, and for this were specifically observed the drillings and outcrops of AL56, showing the following tendency from the contact with the inwards: 1) border zone (usually with less than 1 cm), fine grained, not visible in all the pegmatite contacts; 2) wall zone, where is common to observe UST textures usually in plagioclase, Li-barren zone (usually less than 1 m), typically coarse grained, but sometimes can be fine grained; 3) intermediate zone: aplite-pegmatite alternating bands with Li-mineralization in the pegmatitic parts; 4) no core zone, although a late fluid that crystallized as spodumene + quartz is observed breaking and replacing the previous textures.

However, besides these replacement fronts that start masking the original textures, the regional deformation that affected these pegmatites even masked more the primary textures.

Therefore, the following evolutionary model is proposed based on the field and drillings observations (Figure 92):

1) Magmatic Stage:

- This pegmatite formed from a flux-rich melt enriched in H_2O, Li, B, and P. Its low viscosity allowed it to intrude along structural weaknesses in the host rock, creating multiple relatively small bodies (typically up to 8 m in size).
- Crystallization occurred under strong disequilibrium conditions, which resulted in internal zonation, including the development of unidirectional solidification textures near the contacts.
- The initial crystallizing zones near the margins, the border zone and wall zone, are Li-barren and typically account for about 20% of the total pegmatite volume.
- As crystallization progressed, the melt became increasingly enriched in Li, leading to the formation of aplite–pegmatite alternations. These may reflect a type of boundary layer effect, where rapid crystallization prevents full chemical equilibrium, producing alternating Li- and K-rich pegmatitic zones and Na-rich, Li-poor aplitic zones throughout the central portion of the body (~80% vol).
- The dominant Li mineral crystallizing from this enriched melt would have been petalite. However, as cooling continued, petalite became unstable and began to break down into spodumene and quartz intergrowths (SQI), forming the first generation of spodumene.

2) Metasomatic Stage:

- Second Boiling and Fluid Exsolution: In the final stages of crystallization, the remaining melt, located at the center, experienced "second boiling," leading to the exsolution of fluids. These fluids, enriched in Li and Si, played a key role in the partial replacement of the primary textures.
- Formation of Late Spodumene-Quartz Assemblages: As fluid exsolution continued, it led to the formation of late-stage spodumene + quartz fronts (2^{nd} generation of spd). These assemblages reflect the final crystallization phases, contributing to the overall Li concentration in the system.

- Formation of Cookeite (Li-Chlorite): Later, fluid interactions led to the formation of cookeite, a Li-bearing chlorite mineral. This occurs as the system cools and undergoes further alteration, capturing residual Li in the alteration zones.

3) Deformation Stage:

- Shear Zone Formation: Tectonic forces induce shear zones that cut through the aplite-pegmatite bodies. These zones are areas of intense deformation.
- Dissolution and Recrystallization: As shear stress affects the rocks, the original minerals, including petalite and spodumene, dissolve due to the intense pressure and movement. The dissolved materials then recrystallize as spodumene and quartz (3rd generation of spodumene) within the shear zones, forming new mineral assemblages.
- Spodumene and Quartz Concentration: The deformation leads to the concentration of spodumene and quartz, which crystallizes along the shear zones, creating distinctive textures and mineral fabrics.

7.3. Conclusions

This study reveals that Li-rich aplite–pegmatites in the Barroso-Alvão field are more complex than previously thought, in terms showing internal zoning and textural variability consistent with strong disequilibrium crystallization.

Outcrop and drill core analyses identified three key processes controlling Li enrichment and redistribution:

1. Magmatic differentiation formed alternating aplite–pegmatite bands, with Li concentrated in pegmatitic zones as petalite, later replaced by spodumene + quartz (1st generation of spodumene).

2. Late-stage autometasomatism from fluid exsolution ("second boiling") produced secondary spodumene–quartz fronts.

3. Tectonic deformation created shear zones where spodumene–quartz intergrowths formed through dissolution–reprecipitation, concentrating Li along structural pathways (3rd generation of spodumene).

These overlapping processes generated significant heterogeneity in Li distribution, underscoring the need to integrate structural, mineralogical, and geochemical data for accurate genetic interpretation and resource evaluation.

Acknowledgments

This work was supported by FCT (UIDB/04683/2020 - https://doi.org/10.54499/UIDB/04683/2020 and UIDP/04683/2020 - https://doi.org/10.54499/UIDP/ 04683/2020) and by the project GREENPEG (no. 869274) from the European Commission Horizon 2020. Filipa Dias was supported by her PhD thesis (2020.05534.BD) and MCTES through FCT, ESF through POCH and NORTE 2020.

Appendix

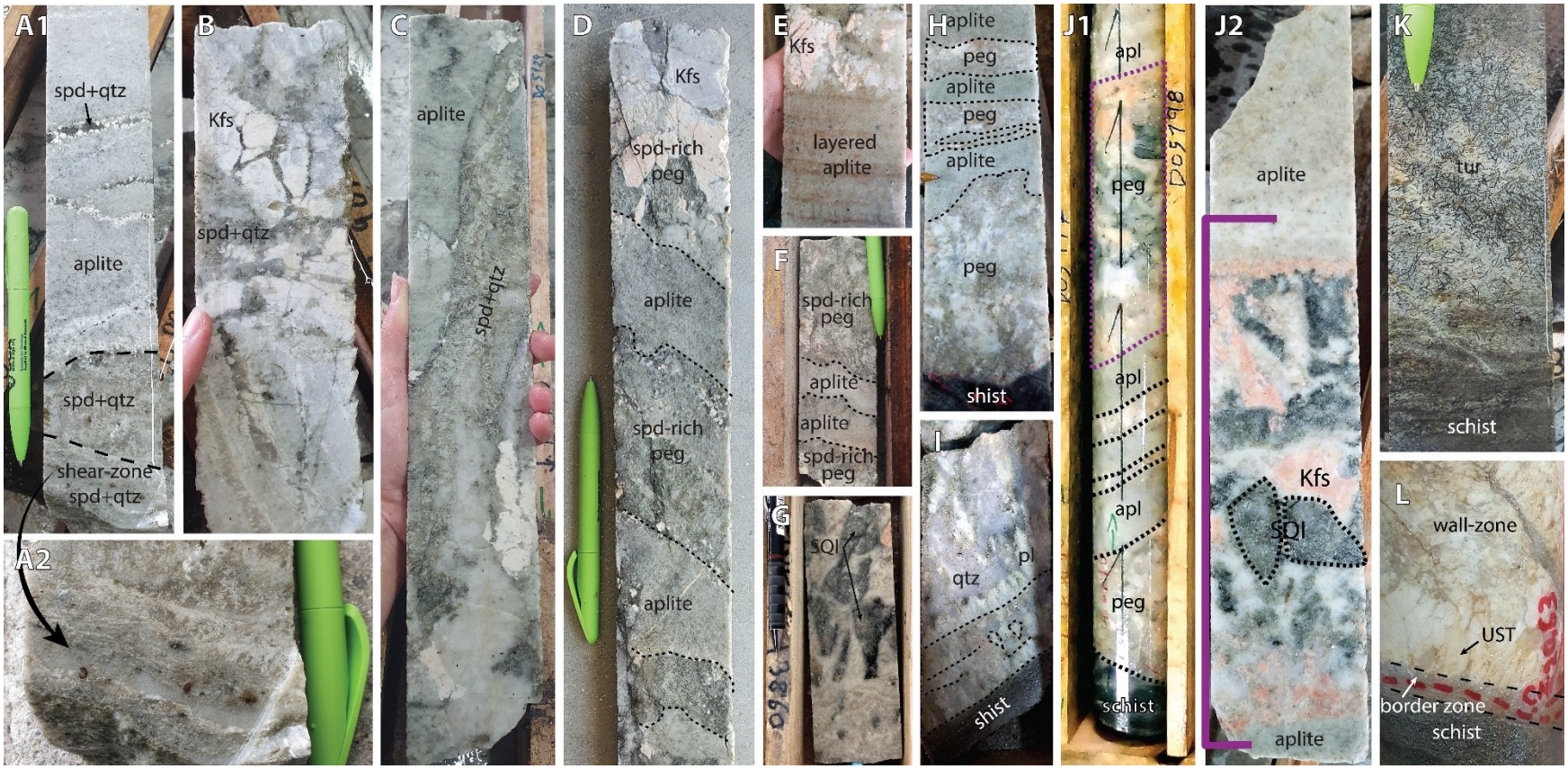

Figure 92. Different textures observed in drill cores from the AL56/NOA deposit: A1–A2) third-generation spodumene and quartz crosscutting second-generation spodumene and quartz, which in turn crosscut the aplite; B) spodumene (Spd) and quartz (Qtz) replacing coarse feldspar (Fds)-rich primary textures; C) second-generation spodumene and quartz crosscutting the aplite; D) alternation of pegmatite and aplite, where Li-mineralization occurs in K-feldspar–rich pegmatite, while the aplite is Li- and K-poor and Na-rich; E) layered aplite adjacent to a pegmatitic zone; F) alternation between Li-rich pegmatite and Li-barren aplite; G) pseudomorphs of spodumene and quartz after petalite (first-generation spodumene) within layered aplite; H) contact with schist followed by Li-barren pegmatite/aplite alternations; I) unidirectional solidification textures (UST) growing inward from the contact with the country rock; J1–J2) alternating Li-barren aplite and pegmatite at the contact, followed by Li-rich pegmatite with pseudomorphs of spodumene and quartz after petalite, where both K-feldspars and the former petalite crystals (now pseudomorphs) appear to grow inward from the Li-barren contact; K) tourmaline crystals in the schist; L) schist, border zone, and wall zone with UST textures.

8. Impact of using a 3.5 µm film to analyze the chemical composition of crystal samples with a handheld X-Ray Fluorescence equipment

Adapted from: Filipa Dias, Ricardo Ribeiro, Alexandre Lima, Filipe Gonçalves, Encarnación Roda-Robles and Tânia Martins

European Geosciences Union (EGU2024). https://doi.org/10.5194/egusphere-egu24-21098

Published Abstract

Abstract

Some K-feldspar crystals from lithium-rich aplite-pegmatites from Northern Portugal have been analyzed with a handheld X-Ray-Fluorescence (XRF) equipment. This study compares the impact of analyzing the samples with an XRF film versus analyzing them without it. The film used was a Hitachi Poly-S High Performance XRF Sample Film of 3.5 µm, commonly used for analyzing samples in cups and powders. Although Hitachi alerts for the unsuitability of the film for analyzing light elements, this study helps understand the extent of error that this film can cause when analyzing this type of sample. Fifteen cleaned potassium feldspar crystals with a size between 1-3 cm have been analyzed with a Bruker S1 TITAN 600 containing an X-ray tube with a 2 W and 5-100 μA Rh anode. The Geomining factory calibration was used for the sample analysis.

The results show that the potassium-feldspars analyzed with the film had their major elements drop by 20-40% for silica (SiO_2), 30-50% for aluminum (Al_2O_3) and 10-20% for potassium (K_2O). As for the trace elements, calcium (Ca) dropped by 20-30%, phosphorous (P) by 20-40% and rubidium (Rb) and iron (Fe) have small errors that can vary from plus 0-10% to minus 0-10%. Knowing the film impact will hopefully be of assistance for the correct interpretation of portable XRF results during field campaigns for mineral exploration.

8.1. Methods

Fifteen potassium-feldspar crystals, each measuring approximately 1–3 cm, were collected from twelve aplite-pegmatites in the Barroso-Alvão Field, in Northern Portugal. The crystals were cut and cleaned using a diamond saw blade to remove surface contamination and ensure consistency across samples. XRF analysis was conducted using a portable Bruker S1 TITAN 600 spectrometer equipped with a Rhodium (Rh) anode X-ray tube, operating at 2 W and a current range of 5–100 μA. The Geomining factory calibration from Bruker was applied throughout the study. Each sample was analyzed under two conditions: first without any film (direct exposure), and then with a 3.5 μm Hitachi Poly-S High Performance XRF Sample Film applied over the sample surface (Figure 93 and Figure 94). Each measurement consisted of three sequential phases using different beam energies: Phase 1 at 30 kV, Phase 2 at 50 kV, and Phase 3 at 15 kV, with each phase lasting 30 seconds, resulting in a total acquisition time of 90 seconds per sample. A photograph of the analyzed crystals is shown in Figure 95. Elemental concentrations obtained under both conditions were compared to evaluate the influence of the film on the detection of major and trace elements in aluminosilicate minerals. This study was conducted as a side investigation to the K-feldspar research by Dias et al. (2025), though it was not included in that paper.

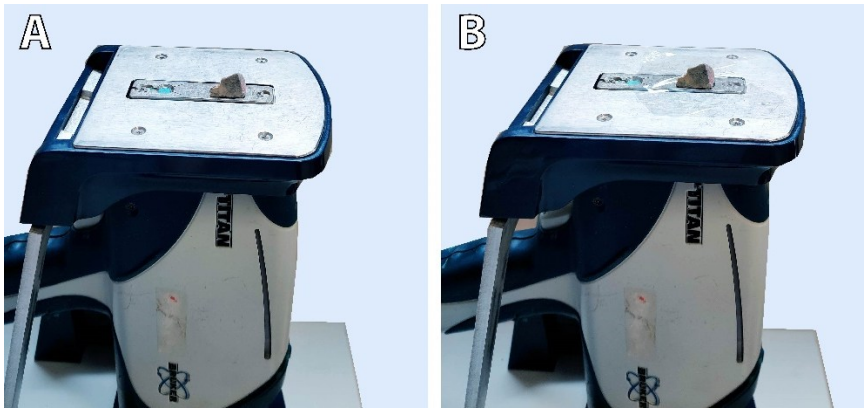

Figure 93. Analysis of a potassium-feldspar crystal without and with a 3.5 μm film using the portable XRF Bruker S1 TITAN 600. A) Without film; B) With film.

Figure 94. Hitachi Poly-S High Performance XRF Sample Film (3.5 µm) tested for the analysis of K-feldspar crystals.

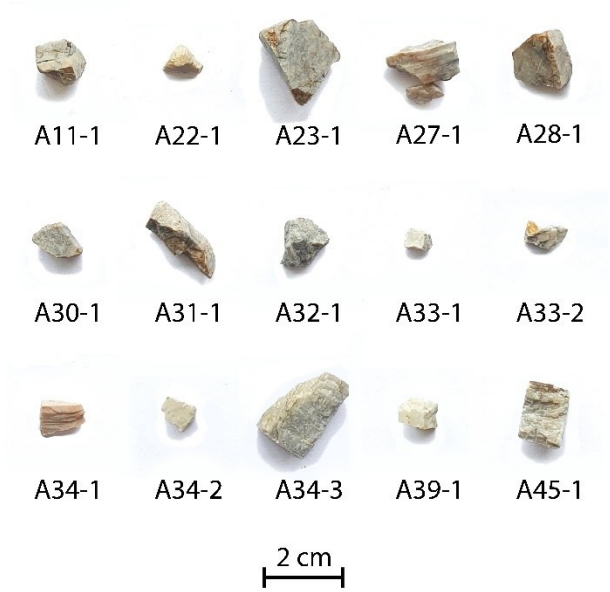

Figure 95. Fifteen K-feldspar crystals from the Barroso-Alvão Field analyzed using portable XRF (pXRF) with and without the 3.5 µm film.

8.2. Results

The use of the 3.5 µm Hitachi Poly-S film resulted in a noticeable decrease in the measured concentrations of major elements across all potassium-feldspar samples. The quantitative results are presented in Table 12.

- Major Element Reductions:
  - SiO_2: 20–40%
  - Al_2O_3: 30–50%
  - K_2O: 10–20%

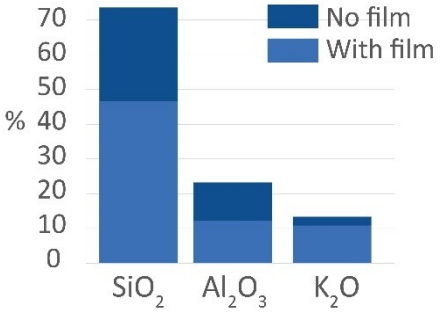

Figure 96. Column chart illustrating the changes in SiO_2, Al_2O_3, and K_2O concentrations in a K-feldspar crystal sample from the Barroso-Alvão Field, analyzed with and without the 3.5 µm film.

- Minor and Trace Element Reductions:
  - Ca: 20–30%
  - P: 20–40%
  - Rb and Fe: 0–10%

These reductions are visualized in Figure 96, where a column chart clearly illustrates the drop in SiO_2, Al_2O_3, and K_2O concentrations when the film is used.

Table 12. Comparison of X-Ray Fluorescence (XRF) results for K-feldspar crystals analyzed without film (original) and with a 3.5 µm Hitachi Poly-S film.

Sample ID	SiO2	Si_dif	Al2O3	Al_dif	K2O	K_dif	Ca	Ca_dif	Rb	Rb_dif	P	P_dif	Fe	Fe_dif
	%	(%)	%	(%)	%	(%)	ppm	(%)	ppm	(%)	ppm	(%)	ppm	(%)
A11-1_film	49.25	-39	12.71	-50	11.92	-24	2939	-26	3106	-7	973	-44	633	4
A11-1_original	80.23		25.47		15.68		3956		3344		1750		608	
A22-1_film	46.53	-37	12.34	-47	10.80	-19	2441	-27	527	-11	979	-42	480	4
A22-1_original	73.53		23.43		13.40		3363		595		1685		463	
A23-1_film	47.50	-34	12.29	-44	11.15	-18	2403	-26	2509	-6	1348	-40	438	1
A23-1_original	72.42		22.05		13.60		3249		2662		2241		433	
A27-1_film	55.44	-34	15.00	-46	13.94	-12	3303	-16	1600	-5	2565	-40	779	11
A27-1_original	84.15		27.81		15.92		3954		1676		4308		699	
A28-1_film	56.47	-22	15.77	-29	12.30	-11	2918	-14	1837	-1	1899	-26	535	1
A28-1_original	72.22		22.17		13.78		3382		1859		2574		530	
A30-1_film	48.00	-31	12.18	-43	11.16	-9	2447	-19	1849	-1	609	-39	424	3
A30-1_original	69.90		21.34		12.32		3006		1859		996		412	
A31-1_film	45.12	-36	10.30	-49	6.68	-19	2080	-29	1277	-2	533	-42	657	12
A31-1_original	70.62		20.21		8.28		2911		1301		921		587	
A32-1_film	50.45	-39	12.67	-43	11.41	-5	2733	-26	2675	10	1073	-24	578	-12
A32-1_original	82.62		22.09		12.02		3692		2434		1417		660	
A33-1_film	38.32	-23	10.08	-34	7.68	-11	2385	16	2989	-10	901	-35	426	7
A33-1_original	49.53		15.18		8.59		2060		3312		1383		398	
A33-2_film	34.85	-43	10.99	-49	6.88	-24	2906	-33	2951	-8	1466	-40	1720	9
A33-2_original	61.58		21.47		9.08		4359		3213		2461		1584	
A34-1_film	51.46	-33	12.31	-46	8.80	-8	2086	-28	1990	0	0	0	433	8
A34-1_original	77.08		22.74		9.61		2915		1993		0		402	
A34-2_film	51.95	-27	13.18	-37	12.50	-6	3624	5	2590	-6	306	20	641	13
A34-2_original	70.81		20.86		13.36		3437		2765		254		569	
A34-3_film	49.67	-26	13.89	-38	12.22	-6	12710	-29	2780	2	12825	-37	2821	0
A34-3_original	67.30		22.27		13.01		18010		2716		20513		2830	
A39-1_film	50.71	-34	13.11	-46	12.57	-12	3349	-27	4200	-4	933	-39	538	10
A39-1_original	76.70		24.23		14.30		4595		4397		1529		488	
A45-1_film	39.98	-30	10.86	-40	9.71	-9	2267	-11	4464	1	1436	-30	592	13
A45-1_original	57.01		17.98		10.67		2551		4402		2057		526	

8.3. Discussion and Conclusions

This study demonstrates that the 3.5 µm Hitachi Poly-S film significantly alters the XRF analysis of potassium-feldspar crystals, primarily by attenuating signals from major elements with low atomic numbers. Notably, concentrations of silicon, aluminum, and potassium decreased by up to 40% for SiO_2, 50% for Al_2O_3, and 20% for K_2O. This observation aligns with the warning provided by the manufacturer regarding the

unsuitability of the film for light-element detection. Therefore, when analyzing aluminosilicates, the use of this film should be carefully considered, especially when its application is necessary.

In contrast, trace elements such as rubidium and iron were largely unaffected, with reductions of no more than 10 percent. This suggests that the film has minimal impact on the detection of elements with higher atomic numbers.

Although the film may be necessary in practical field settings, particularly when analyzing powdered or sediment samples in sample cups, its effect on analytical results must be accounted for. Awareness of this influence is crucial for accurate interpretation of XRF data.

Acknowledgments

This study was financially supported by FCT, I.P., in the framework of the ICT (UIDB/04683/2020 and UIDP/04683/2020), by the PhD project (2020.05534.BD) and by national funds from MCTES, through FCT, co-financed by ESF through POCH and NORTE 2020. This work is also supported by the Greenpeg project, reference 869274, funded by the Horizon 2020 framework program of the European Union.

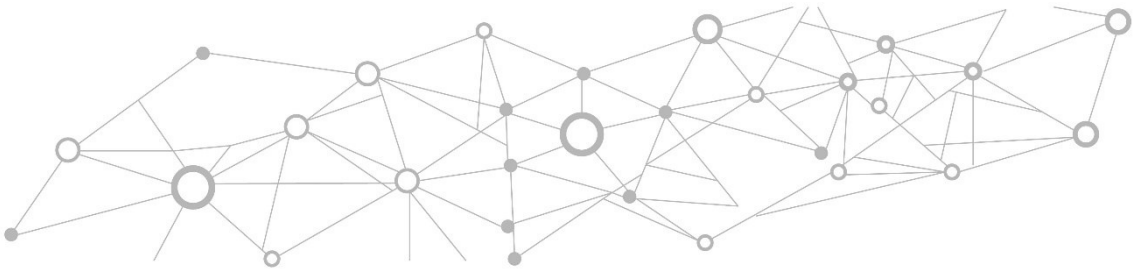

Part IV – Final Conclusions

This thesis investigates lithium (Li) mineralization in the Barroso-Alvão (BA) pegmatite field, Northern Portugal, through a combination of geological, mineralogical, and geochemical techniques aimed at characterizing Li-rich minerals and their distribution. Based on the findings presented throughout this work, the following conclusions are drawn:

1. **Portable LIBS Calibration and Application**: Portable Laser Induced Breakdown Spectroscopy (pLIBS) is still an emerging tool for Li exploration. Factory calibrations were found to be inadequate for analyzing spodumene and petalite, prompting this study to develop a custom calibration specifically for these Li-rich minerals from the BA field. Although challenges related to intensity ratios limited the ability to distinguish spodumene from petalite directly, it was possible to use the iron content in spodumene to establish two distinct calibration curves. This enabled accurate analysis of both minerals, demonstrating that, with appropriate calibration, pLIBS can be a rapid and effective method for field-based Li exploration.

2. **K-Feldspar Geochemistry as an Indicator of Lithium Mineralization:**

   Our results demonstrate that K-feldspar geochemistry is a reliable indicator of Li mineralization in the Barroso-Alvão pegmatite field. Using portable X-Ray Fluorescence (pXRF) on K-feldspars, rubidium (Rb) concentrations effectively distinguish between different types of aplite-pegmatites: Li-barren pegmatites (Rb ≤ 1250 ppm), spodumene-rich aplite-pegmatites (Rb: 1250–1900 ppm), and petalite-rich pegmatites (Rb > 1800 ppm).

   The study also revealed both geochemical and mineralogical trends across the field, with increasing concentrations of Be, Ga, Li, Pb, Rb, and Tl from SE to NW. This spatial variation corresponds to a general transition in Li-mineralization types, from Li-barren aplite-pegmatites in the SE, to spodumene-rich, petalite-rich, and eventually lepidolite-rich aplite-pegmatites towards NW. However, it is important to note that Li-rich pegmatites containing spodumene and petalite also occur in the SE part of the field. These pegmatites exhibit K-feldspar geochemistry similar to that of Li-barren aplite-pegmatites, suggesting that, rather than reflecting a simple magmatic fractionation trend from SE to NW, the original geochemical signatures may have been altered by late-stage metasomatic and/or hydrothermal processes, particularly through the leaching of Rb and other fractionation-sensitive elements from the K-feldspars.This alteration could be related to the proximity of the Vila Pouca de Aguiar

post-tectonic granite and the Régua–Verín fault zone, which could have facilitated fluid circulation and geochemical resetting.

3. **Spodumene and Quartz Intergrowth – Textural and Genetic Point of View:** The occurrence of spodumene and quartz intergrowths in Li-rich pegmatites can reflect a complex interplay of magmatic, metasomatic, and tectonic processes. In the Barroso-Alvão field, spodumene and quartz intergrowth textures are not only associated with the breakdown of petalite, but as well with fluid circulation and with deformation structures. Understanding the origins of spodumene and quartz intergrowth textures is essential for reconstructing the thermal and structural evolution of Li-bearing pegmatites and for guiding exploration in areas with similar tectonic influences.

4. **Cathodoluminescence Characteristics of Spodumene and Petalite:** The cathodoluminescence behavior of petalite and spodumene in this study revealed important contrasts that can be utilized for mineral identification and Li exploration. The consistent dark blue luminescence of petalite versus the strong, although variable, color (between yellow, orange, and purple) luminescence of spodumene demonstrated that cathodoluminescence can be used as a tool for distinguishing between spodumene and some other Li-bearing minerals in Li-exploration.

5. **Spodumene Quantification with Cathodoluminescence**: The study demonstrated that cathodoluminescence (CL) microscopy combined with image analysis software is effective for mapping and quantifying spodumene in thin sections. Reverse Circulation (RC) samples were tested by producing thin sections from chips representative of each meter of drilling. This method allowed for estimating spodumene abundance and, through its Li content, calculating the Li concentration for that sample. Comparing these results with ICP-MS bulk Li analysis for the same meters showed that the sample with higher Li content from CL analysis corresponded with the meter that had higher Li concentrations, and the sample with lower Li content corresponded with the meter that had lower Li content. Although a broader sample set is recommended for more accurate comparisons, this approach effectively linked spodumene abundance to Li content in pegmatite RC samples.

6. **Li-Exploration and Processing Considerations**: The study highlighted that careful attention should be given to the paragenesis of the pegmatites with spodumene, as well as to their texture, since the presence of other Li-bearing phases (such as petalite or cookeite), and the occurrence of spodumene in fine mixtures with quartz, could lead to lower-than-expected Li results in processing. This underscores the need for a

careful evaluation of mineralogical composition in exploration workflows, their variations in crystal size, and the application of methods tailored to the pegmatites from each field. The metallurgical process must be adapted according to the characteristics of the material being collected and processed.

7. Structural and Mineralogical Features of the AL56/NOA Pegmatite:

The Barroso-Alvão pegmatite field, specifically the AL56/NOA deposit, exhibits a complex textural evolution influenced by deformation and metasomatic processes. Spodumene is the dominant Li-bearing mineral in this deposit, and its alignment with some foliation planes indicates that deformation played a significant role in controlling its distribution. In addition to spodumene, the body contains significant cookeite and montebrasite, as well as some petalite, although the latter has not been found *in situ*.

The deposit consists of multiple aplite-pegmatite segments emplaced along various weak zones in the country rock, such as fractures, faults, and foliations. In exploration, schist commonly occurs between these aplite-pegmatite segments, meaning that mining and exploration must navigate through multiple schist zones to follow the pegmatite network. This characteristic (where pegmatites form a spatially linked, branched system rather than a single, continuous body) is also observed in other pegmatites from the Barroso-Alvão field

8. Internal Zonation and Geochemical Variation in the AL56/NOA Pegmatite

Although the AL56/NOA aplite-pegmatite bodies were previously considered internally unzoned, detailed observations from outcrops and drill cores have revealed the presence of distinct internal zones: a border zone, a wall zone, and an intermediate zone. The intermediate zone is characterized by alternating aplite-pegmatite layers, where the pegmatitic portions are Li- and K-rich, while the aplitic parts are Li-barren, K-poor, and Na-rich. Notably, quartz cores were not observed in any of the studied sections.

The absence of quartz cores, combined with evidence of late-stage metasomatism (autometasomatism) by a Si-rich fluid, which brecciated earlier crystals and formed replacement fronts, has significantly overprinted many primary textures. This overprinting likely contributed to earlier interpretations of the pegmatites as unzoned. The lack of quartz cores could also be related to the late-stage Si- and Li-rich zones that crosscut other zones, possibly representing the residual fluid that escaped prior to quartz core formation. These new observations were made possible by improved exposure of outcrops due to ongoing exploration and extraction activities, as well as by drill core data providing access to previously unstudied parts of the pegmatite. While this enhanced

understanding currently applies mainly to the studied pegmatite, it enables more systematic tracking of Li distribution within these bodies and may help inform interpretations of other pegmatites in the Barroso-Alvão field.

9. **Petalite and Spodumene in the NIST SRM 182:** The analysis of the NIST Standard Reference Material 182 (petalite) revealed the presence of spodumene and quartz as breakdown products of petalite. This finding suggests that the petalite used in SRM 182 may have undergone phase transformations similar to those observed in the Barroso-Alvão field, emphasizing the need for additional verification techniques such as cathodoluminescence or XRD when using this material as a reference for analytical purposes.

10. **Impact of XRF Analysis Using a 3.5 µm Film:** The study demonstrated that the use of a 3.5 µm Hitachi Poly-S film in handheld XRF analysis significantly affects the detection of light elements in feldspar crystals. Specifically, signal intensity decreased by up to 40% for SiO_2, 50% for Al_2O_3, and 20% for K_2O. This highlights the film's limitation for aluminosilicate analysis, in line with manufacturer warnings. In contrast, trace elements such as Rb and Fe were minimally affected, with reductions of less than 10%. While the film may be necessary in certain cases (e.g., for powders or sediments), its impact must be considered to ensure accurate data interpretation.

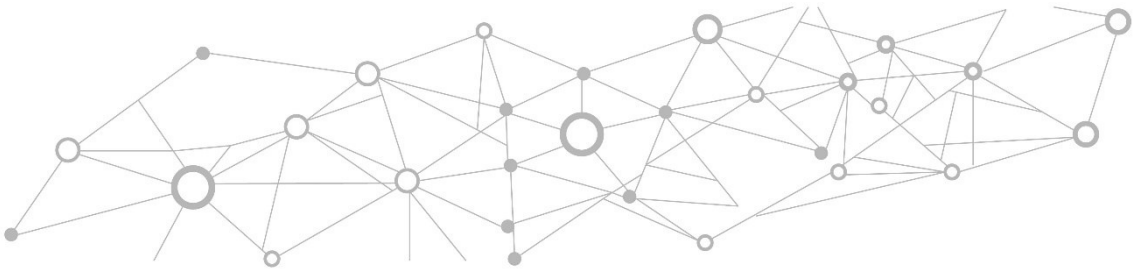

Part V – Future Work and Publication Plan

Stemming from this thesis, three follow-up studies are planned to improve exploration strategies for Li-bearing pegmatites in the Barroso–Alvão field, with a particular focus on the AL56/NOA deposit. These studies aim to combine methodological innovation with applied geological insight and will be developed as standalone scientific papers:

1. Correlation of Cathodoluminescence Imaging and LIBS Lithium Mapping

The first study will investigate the relationship between cathodoluminescence (CL) imaging and Laser-Induced Breakdown Spectroscopy (LIBS) for mapping lithium distribution in thin sections from the AL56/NOA pegmatite. The primary objective is to assess whether CL imaging, in combination with image analysis software (Phase Expert module from Leica Microsystems), can reliably identify spodumene-rich zones and whether these correspond to Li-enriched areas detected by bench-top LIBS.

Selected thin sections will be imaged using CL microscopy, highlighting spodumene based on its strong luminescence properties. These images will be processed using the LAS X Phase Expert module. The same samples will then be analyzed with LIBS to generate detailed lithium distribution maps.

If successful, this approach could provide a rapid and efficient method for mapping spodumene and lithium distribution, particularly useful in early-stage exploration and resource evaluation.

2. 3D Geological Modeling of the AL56/NOA Pegmatite Based on Drill Core Data

The second study will focus on developing a 3D geological model of the AL56/NOA aplite-pegmatite using Leapfrog Geo, based on the detailed drill core logging conducted during this thesis. This model will incorporate the newly proposed internal zonation, comprising border, wall, and intermediate zones, which had not been previously recognized in this pegmatite. Although reliably classifying and correlating all textural features related to deformation and metasomatism presents challenges, these elements will be incorporated where possible. The overarching goal is to enhance the spatial understanding of Li distribution within the pegmatite body. Additionally, this work aims to establish a standardized internal zoning framework for the AL56/NOA pegmatite,

which could serve as a reference for modeling and predicting Li distribution in other pegmatite bodies throughout the Barroso–Alvão field.

3. Integrated Remote Sensing, Geophysics, and Artificial Intelligence for Mineral Exploration in the Barroso–Alvão Field

The third study will apply integrated remote sensing, geophysical techniques, and artificial intelligence to Li exploration in the Barroso–Alvão field, in collaboration with colleagues from the University of Porto within the MineSpot project, a first step toward the creation of the spin-off Spotmine, Lda.

The Barroso–Alvão field provides an ideal test area due to the extensive existing geological knowledge, enabling systematic testing and validation of innovative exploration methodologies. A multi-scale, multi-sensor approach will be employed, combining satellite data (hyperspectral, multispectral, and SAR- Synthetic Aperture Radar), drone-based surveys (radiometry, LiDAR, and TIR), and in situ techniques (LIBS, XRF, and DGPR-Deep Ground Penetrating Radar).

These datasets will be integrated with geological and field data and analyzed using machine learning techniques to generate 2D maps and 3D models of potential mineralized targets, designed to improve target efficiency and accelerate mineral exploration while rapidly reducing exploration uncertainty. The results are expected to contribute to the development of transferable, data-driven exploration workflows applicable to other mineral deposits worldwide.

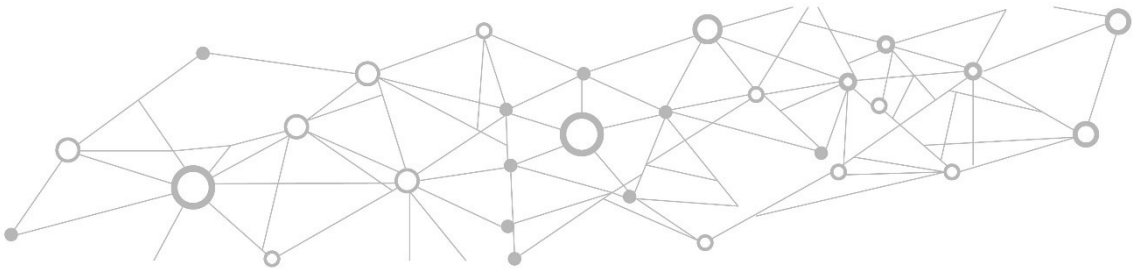

Part VI – References

References

AGÊNCIA PORTUGUESA DO AMBIENTE Massas de água superficiais Rios de Portugal continental: conjunto de dados geográfico SNIAmb. Available from <https://sniamb.apambiente.pt/content/geo-visualizador> [Date accessed: 6th July 2019].

AGÊNCIA PORTUGUESA DO AMBIENTE Massas de água superficiais Rios albufeiras de Portugal continental conjunto de dados geográfico SNIAmb. Available from <https://sniamb.apambiente.pt/content/geo-visualizador> [Date accessed: 19th July 2022].

AGRIPRO AMBIENTE CONSULTORES, S.A. (2021) LusoRecursos. Concessão de Exploração de Depósitos Minerais de Lítio e Minerais Associados – "Romano". Estudo de Impacte Ambiental.

ALFONSO, P., MELGAREYO, J.C., YUSTA, I. & VELASCO, F. (2003) Geochemistry of feldspars and muscovite in granitic pegmatite from the Cap de Creus field, Catalonia, Spain. Canadian Mineralogist 41. 103-116

ALMEIDA, A., MARTINS, H.C. & NORONHA, F. (2002) Hercynian Acid Magmatism and Related Mineralizations in Northern Portugal. Gondwana Research 5(2). 423-434

ALMS, K., HEINELT, M. & GROENEWEG, A. (2025) Lithium prospectivity and capacity assessment in Northern Germany. Geothermics 127. 103207

ALVES, J. (2022) *Sustainable and Responsible Mining Based on Lundin Mining Corporation's Subsidiary, Somincor*. Master Thesis in Mining and Geo-Environmental Engineering, Faculty of Engineering - University of Porto.

ANTUNES, I.M.H.R., NEIVA, A.M.R., SILVA, M.M.V.G. & SILVA, P.B. (2010). Mineralogy of Li-Bearing Granitic Aplite-Pegmatite Veins From Segura, 1. *In* Ciências Geológicas – Ensino e Investigação e sua História. Associação Portuguesa de Geólogos/Sociedade Geológica de Portugal.

ÁVILA MARTINS, J. & NORONHA, F. (1982). Folha 06-A - Montalegre. *In* Carta Geológica de Portugal à escala 1:50 000. Instituto Geológico e Mineiro, Lisboa.

BEAUCHEMIN, D. (2020) *Sample Introduction Systems in ICPMS and ICPOES*. Elsevier B.V. Amsterdam, Netherlands.

BINNEMANS, K., JONES, P.T., BLANPAIN, B., VAN GERVEN, T., YANG, Y., WALTON, A. & BUCHERT, M. (2013) Recycling of rare earths: a critical review. Journal of Cleaner Production 51. 1-22

BOROVIK-ROMANOVA, T. & SOSEDKO, A. (1960) Relation between thallium and rubidium in minerals from pegmatite veins of the Kola Peninsula from the results of spectrographic analysis. Geochemistry International. 34-42

BRAND, N.W. & BRAND, C.J. (2014) Performance comparison of portable XRF instruments. Geochemistry: Exploration, Environment, Analysis 14. 125–138

BRAVO SILVA, P., NEIVA, A.M.R. & FARINHA RAMOS, J. (2007) Geochemistry of granitic aplite-pegmatite veins and sills and their minerals from Pega – Sabugal, Central Portugal. *Granitic Pegmatites: The State of the Art – International Symposium, Porto, Portugal*.

BREASLEY, C.M., MARTINS, T., LINNEN, R.L., DEVEAU, C., GROAT, L.A., KOOPMANS, L., LANDRY, E. & MOSER, D. (2025) The geochemistry, origins and metallurgical implications of different textural types of spodumene-quartz intergrowths (SQUI) from the Tanco pegmatite, Manitoba, Canada. Ore Geology Reviews 180. 106577

BREITER, K., FRÝDA, J. & LEICHMANN, J. (2002) Phosphorus and rubidium in alkali feldspars: case studies and possible genetic interpretation. Bulletin of the Czech Geological survey 77(2). 93-104

BROWN, J.A., MARTINS, T. & ČERNÝ, P. (2017) The Tanco Pegmatite at Bernic Lake, Manitoba. Xvii. Mineralogy and Geochemistry of Alkali Feldspars. Canadian Mineralogist 55(3). 483-500

CAMERON, E.N., JAHNS, R.H., MCNAIR, A.H. & PAGE, L.R. (1945) Internal Structure of Granitic Pegmatites. Geological Society of America Bulletin 56(12). 1151-1151

ČERNÝ, P. & FERGUSON, R.B. (1972) The Tanco pegmatite at Bernic Lake, Manitoba; IV, Petalite and spodumene relations. The Canadian Mineralogist 11(3). 660-678

ČERNÝ, P. & LONDON, D. (1983) *Crystal chemistry and stability of petalite*. **31**, 81-96.

ČERNÝ, P., SMITH, J.V., MASON, R.A. & DELANEY, J.S. (1984) Geochemistry and petrology of feldspar crystallization in the Vezna pegmatite, Czechoslovakia. Canadian Mineralogist 22. 631-651

ČERNÝ, P., MEINTZER, R.E. & ANDERSEN, A.J. (1985a) Extreme fractionation in rare-element granitic pegmatites: selected examples of data and mechanisms. Canadian Mineralogist 23. 381-421

ČERNÝ, P., PENTINGHAUS, H. & MACEK, J.J. (1985b) Rubidian microcline from Red Cross Lake, northeastern Manitoba. *Bull. Geol. Soc, Finland.* **57**, 217-230.

ČERNÝ, P. (1991). Processes controlling evolution of rare-element granitic pegmatites. *In* 25th anniversary meeting of the Society for Geology Applied to Mineral Deposits (M. Pagel & J.L. Leroy eds.). A. A. Balkema, Rotterdam.

ČERNÝ, P. (1994) *Evolution of feldspars in granitic pegmatites*. Feldspars and their reactions. I. Parsons, Kluwer. Dordrecht, The Netherlands.

ČERNÝ, P. (2005) *The Tanco rare-element pegmatite deposit, Manitoba: Regional context, internal anatomy, and global comparisons*. **17**, 127-158.

CHAROY, B., LHOTE, F., DUSAUSOY, Y. & NORONHA, F. (1992) The Crystal Chemistry of Spodumene in Some Granitic Aplite-Pegmatite of Northern Portugal. Canadian Mineralogist 30. 639-651

CHAROY, B. & NORONHA, F. (1996) Multistage growth of a rare-element, volatile-rich microgranite at Argemela (Portugal). Journal of Petrology 37(1). 73-94

CHAROY, B. & NORONHA, F. (1999a) Rare-element (Li-rich) granitic and pegmatitic plutons: A primary or superimposed signature? Revista Brasileira de Geociencias 29. 3-8

CHAROY, B. & NORONHA, F. (1999b) Rare-element (Li-rich) granitic and pegmatitic plutons: a primary or superimposed signature? Revista Brasileira de Geociências, (29). 3-8

CHAROY, B., NORONHA, F. & LIMA, A. (2001) Spodumene-petalite-eucryptite; mutual relationships and pattern of alteration in Li-rich aplite-pegmatite dykes from northern Portugal. The Canadian Mineralogist 39. 729-746

CLAFFY, E.W. (1953) Composition, tenebrescence and luminescence of spodumene minerals. American Mineralogist 38. 11-12

CREMERS, D.A. & RADZIEMSKI, L.J. (2006) *Handbook of Laser-Induced Breakdown Spectroscopy*. John Wiley & Sons, Ltd. England.

CULLITY, B.D. & STOCK, S.R. (2014) *Elements of X-Ray Diffraction*. Pearson Education Limited. Harlow, United Kingdom.

DECLERCQ, Y., DELBECQUE, N., DE GRAVE, J., DE SMEDT, P., FINKE, P., MOUAZEN, A.M., NAWAR, S., VANDENBERGHE, D., VAN MEIRVENNE, M. & VERDOODT, A.A. (2019) A Comprehensive Study of Three Different Portable XRF Scanners to Assess the Soil Geochemistry of An Extensive Sample Dataset. Remote Sensing 11(2490).

DEER, W.A., HOWIE, R.A. & ZUSSMAN, J. (1978) *Rock-forming Minerals: Single-chain silicates. Volume 2A*. Geological Society.

DEER, W.A., HOWIE, R.A. & ZUSSMAN, J. (2004) *Rock-forming Minerals: Silica Minerals, Volume 4B*. Geological Society.

DIAS, C. (2016a) *Abordagem multidisciplinar às mineralizações de lítio no Campo Aplito-Pegmatítico do Barroso-Alvão, Norte de Portugal*. Master in Geology, Faculdade de Ciências da Universidade do Porto, Porto, Portugal.

DIAS, F. (2016b) *Lithium mineralizations of Barroso-Alvão aplite-pegmatite field*. Master in Geology, University of Porto - Faculty of Sciences, Porto.

DIAS, F., SIRBESCU, M.-L., STUDENT, J.J., LIMA, A. & RODA ROBLES, E. (2018) Kinetics controls of spodumene and petalite stability: A preliminary investigation. *Goldschmidt Annual Conference 2018, Boston, MA*.

DIAS, F. & LIMA, A. (2021) Cathodoluminescence characteristics of spodumene and petalite from the Iberian massif pegmatites. *Jornadas do ICT, Faculdade de Ciências da Universidade do Porto - Zoom*.

DIAS, F., LIMA, A., RODA-ROBLES, E. & MARTINS, T. (2023a) Textural and mineralogical characterization of one lithium deposit, from the Barroso-Alvão aplite-pegmatite field: preliminary study. *SEG 2023 - Society of Economic Geologists: Resourcing the Green Transition, London*.

DIAS, F., RIBEIRO, R., GONÇALVES, F., LIMA, A., RODA-ROBLES, E. & MARTINS, T. (2023b) Calibrating a Handheld LIBS for Li Exploration in the Barroso–Alvão Aplite-Pegmatite Field, Northern Portugal: Textural Precautions and Procedures When Analyzing Spodumene and Petalite. Minerals 13(4)(470).

DIAS, R. & RIBEIRO, A. (1995) The Ibero-Armorican Arc: A collision effect against an irregular continent? Tectonophysics 246(1-3). 113-128

EDWARDS, P.R. & LEE, M.R. (2014). Cathodoluminescence hyperspectral imaging in geoscience, Short course series 45. *In* Cathodoluminescence and its Application to Geoscience (I. Coulson ed.). Mineralogical Association of Canada, Canada (29-45).

EUROPEAN COMMISSION (2020a). Lithium. *In* Study on the EU's list of Critical Raw Materials. Critical Raw Materials Factsheets, Luxembourg (287-322).

EUROPEAN COMMISSION (2020b) *Critical materials for strategic technologies and sectors in the EU - a foresight study*. S. Bobba, S. Carrara, J. Huisman, F. Mathieux & C. Pavel, Publications Office of the European Union. Luxembourg, 10.2873/58081.

EUROPEAN COMMISSION (2023) *Study on the critical raw materials for the EU 2023 – Final report*. Directorate-General for Internal Market, Industry, Entrepreneurship

SMEs. M. Grohol, C. Veeh & D. Grow, Publications Office of the European Union. Luxembourg, doi/10.2873/725585.

EUROPEAN COMMISSION, E. (2020c) Countries 2020 — 1:1 million — Geographic Coordinate System — EPSG:4326 (GISCO) [Shapefile]. Available from <https://gisco-services.ec.europa.eu/features/collections/gisco.cntr_rg_01m_2020_4326.html > [Date accessed: June 8, 2021].

EUROPEAN UNION (2024) Regulation (EU) 2024/1252 of the European Parliament and of the Council of 11 April 2024 establishing a framework for ensuring a secure and sustainable supply of critical raw materials and amending Regulations (EU) No 168/2013, (EU) 2018/858, (EU) 2018/1724 and (EU) 2019/1020. Official Journal of the European Union L 1252.

FABRE, C., OURTI, N.E., MERCADIER, J., CARDOSO-FERNANDES, J., DIAS, F., PERROTTA, M., KOERTING, F., LIMA, A., KAESTNER, F., KOELLNER, N., LINNEN, R., BENN, D.,

MARTINS, T. & CAUZID, J. (2021) Analyses of Li-Rich Minerals Using Handheld LIBS Tool. Data 6.

FARINHA RAMOS, J. (1998). Sondagens de reconhecimento em filões aplitopegmatíticos mineralizados em espodumena, Região do Alto Tâmega (Concelhos de Boticas, Vila Pouca de Aguiar e Ribeira de Pena). *In* Relatório Interno #5733 (Instituto Geológico e Mineiro ed.).

FARINHA RAMOS, J. (2000). Mineralizações de metais raros de Seixo Amarelo-Gonçalo (Breve nota), 42. *In* Estudos, Notas e Trabalhos. Instituto Geológico e Mineiro (67-160).

FARINHA RAMOS, J. & LIMA, A. (2000). Estudo dos filões aplitopegmatíticos litiníferos da Região do Barroso Alvão (Norte de Portugal), 42. *In* Estudos, Notas e Trabalhos (A. Casal Moura, J.M. Santos Oliveira & L. Torres eds.). Instituto Geológico e Mineiro, Porto (3-49).

GARATE-OLAVE, I., RODA-ROBLES, E., GIL-CRESPO, P.P. & PESQUERA, A. (2018) Mica and feldspar as indicators of the evolution of a highly evolved granite-pegmatite system in the Tres Arroyos area (Central Iberian Zone, Spain). Journal of Iberian Geology 44.

GAUTNEB, H., GLOAGUEN, E. & TÖRMÄNEN, T. (2021) DELIVERABLE D5.3 Energy critical elements and minerals in Europe; occurrence, types, characteristics, formation, and future potential for European production (Part 1 report). Forecasting and Assessing Europe's Strategic Raw Materials needs (FRAME).

GOLDSTEIN, J.I., NEWBURY, D.E., ECHLIN, P., JOY, D.C., LYMAN, C.E., LIFSHIN, E., SAWYER, L. & MICHAEL, J.R. (2003) *Scanning Electron Microscol and X-Ray Microanalysis*. Kluwer Academic/Plenum Publishers. New York.

GORDIYENKO, V.V. (1971) Concentrations of Li, Rb, and Cs in potash feldspar and muscovite as criteria for assessing the rare-metal mineralization in granite pegmatites. International Geology Review 13(2).

GÖTZE, J. & KEMPE, U. (2008) A comparison of optical microscope- and scanning electron microscope-based cathodoluminescence (CL) imaging and spectroscopy applied to geosciences. Mineralogical Magazine 72(4). 909–924

GOURCEROL, B., GLOAGUEN, E., MELLETON, J., TUDURI, J. & GALIEGUE, X. (2019) Re-assessing the European lithium resource potential – A review of hard-rock resources and metallogeny. Ore Geology Reviews 109. 494-519

GUIMARÃES, D., PRAAMSMA, M.L. & PARSONS, P.J. (2016) Evaluation of a new optic-enabled portable X-ray fluorescence spectrometry instrument for measuring toxic metals/metalloids in consumer goods and cultural products. Spectrochimica Acta 122. 192–202

HEIER, K.S. (1962) Trace elements in feldspars - a review. Norwegian Journal of Geology 198. 415-454

IEA (2021) The Role of Critical Minerals in Clean Energy Transitions. *IEA*.

IEA (2024) Global Critical Minerals Outlook 2024.

IEA (2025) *Energy and AI*. F. Birol, L. Cozzi, T. Spencer & S. Singh, International Energy Agency. Paris.

JAHNS, R.H. & BURNHAM, C.W. (1969) Experimental studies of pegmatite genesis: I. A model for the derivation and crystallization of granitic pegmatites. Economic Geology 64. 843-864

JASKULA, B.W. (2015) Lithium. *U.S. Geological Survey*.

JASKULA, B.W. (2021) Lithium. *U.S. Geological Survey*.

KNOLL, T., HUET, B., SCHUSTER, R., MALI, H., NTAFLOS, T. & HAUZENBERGER, C. (2023) Lithium pegmatite of anatectic origin – A case study from the Austroalpine Unit Pegmatite Province (Eastern European Alps): Geological data and geochemical modeling. Ore Geology Reviews 154. 105298

KOGEL, J., TRIVEDI, N., BARKER, J. & KRUKOWSKI, S. (2006) *Industrial Mineral & Rocks*. Society for Mining, Metallurgy, and Exploration, Inc. Colorado, Estados Unidos da América (USA), 601.

KOOPMANS, L., MARTINS, T., LINNEN, R., GARDINER, N.J., BREASLEY, C.M., PALIN, R.M., GROAT, L.A., SILVA, D. & ROBB, L.J. (2024) The formation of lithium-rich pegmatites through multi-stage melting. Geology 52(1). 7–11

LARSEN, R.B. (2002) The distribution of rare-earth elements in K-feldspar as an indicator of petrogenetic processes in granitic pegmatites; examples from two pegmatite fields in Southern Norway. The Canadian Mineralogist 40. 137-151

LEAL GOMES, C. (1994) *Estudo estrutural e paragenético de um sistema pegmatóide granítico – O campo filoniano de Arga – Minho (Portugal)*. Tese de Doutoramento, Universidade do Minho, Braga.

LEPORE, K.H., FASSETT, C.I., BREVES, E.A., BYRNE, S., GIGUERE, S., BOUCHER, T., RHODES, J.M., VOLLINGER, M., ANDERSON, C.H., MURRAY, R.W. & DYAR, M.D. (2017) Matrix Effects in Quantitative Analysis of Laser-Induced Breakdown Spectroscopy (LIBS) of Rock Powders Doped with Cr, Mn, Ni, Zn, and Co. Applied Spectroscopy 71(4). 1-27

LIMA, A., CHAROY, B., NORONHA, F. & FARINHA RAMOS, J. (1999a) Fases Minerais Fosfatadas Dos Aplitopegmatitos Litiníferos Da Região Barroso-Alvão. *Congresso Ibérico de Geoquímica, Lisboa*.

LIMA, A., NORONHA, F., CHAROY, B. & FARINHA, J. (1999b). Exploration for lithium deposits in the Barroso-A Ivão area, Northern Portugal. *In* Mineral Deposits: Processes to Processing (S.e.a. (eds) ed.). Balkema, Rotterdam (1112-1116).

LIMA, A. (2000) *Estrutura, mineralogia e génese dos filões aplitopegmatíticos com espodumena da região do Barroso-Alvão*. PhD in Sciences (Geology), Faculty of Sciences of the University of Porto, Porto.

LIMA, A., VIEIRA, R., MARTINS, T., NORONHA, F. & CHAROY, B. (2003) A ocorrência de petalite como fase litinífera dominante em numerosos filões do campo aplitopegmatítico do Barroso-Alvão (Norte de Portugal). *VI Congresso Nacional de Geologia, Caparica.* **Volume Especial V**, F52-F55.

LIMA, A., RODRIGUES, R., GUEDES, A. & NOVÁK, M. (2009) The Rare Elements-Rich Granite of Seixoso Area (Outeiro Mine). Preliminary results. Estudos Geologicos 19(2). 182-187

LIMA, A., VIEIRA, R., MARTINS, T. & NORONHA, F. (2010). Minerais e Lítio. Exemplos Dos Campos Aplitopegmatíticos De Barroso-Alvão e Almendrabarca D'alva, 1. *In* Ciências Geológicas-Ensino e Investigação e sua história. Volume I: Geologia Clássica. Associação Portuguesa de Geólogos/Sociedade Geológica de Portugal (89-98).

LIMA, A. & MARTINS, T. (2011) Unusual Textural Relationships Between Spodumene and Petalite at Spodumene Bearing Aplite-Pegmatite of Barroso-Alvao Field (Northern Portugal). *PEG2011- 5th International Symposium on granitic pegmatites, Argentina*, 123-125.

LIMA, A., MARTINS, T., VIEIRA, R. & NORONHA, F. (2011) *Campo aplitopegmatítico litinífero do Barroso-Alvão. Os seus diferentes minerais de lítio e sua melhor aplicação futura*. LNEG-Laboratório Nacional de Energia e Geologia, Lisboa, Portugal.

LIMA, A. & DIAS, F. (2019) Spodumene and Quartz Intergrowth – Textural and Genesis Point of View. *EGU General Assembly 2019, Vienna.* **21**, 13404.

LONDON, D. (1984) Experimental phase equilibria in the system $LiAlSiO_4$-Si_2O-H_2O: a petrogenetic grid for lithium-rich pegmatites. American Mineralogist 69. 995-1004

LONDON, D., ČERNÝ, P., LOOMIS, J.L. & PAN, J.J. (1990) Phosphorus in alkali feldspars of rare-element granitic pegmatites. Canadian Mineralogist 28. 771-786

LONDON, D. (2008) Pegmatites. The Canadian Mineralogist, Special Publication 10. 347

LONDON, D. (2014) A petrologic assessment of internal zonation in granitic pegmatites. Lithos 184. 74-104

LONDON, D. (2017) Reading Pegmatites: Part 3—What Lithium Minerals Say. Rocks & Minerals 92. 144-157

MARTÍNEZ CATALÁN, J.R., ARENAS, R., DÍAZ GARCÍA, F., GONZÁLEZ CUADRA, P., GÓMEZ-BARREIRO, J., ABATI, J., CASTIÑEIRAS, P., FERNÁNDEZ-SUÁREZ, J., SÁNCHEZ MARTÍNEZ, S., ANDONAEGUI, P., GONZÁLEZ CLAVIJO, E., DÍEZ MONTES, A., RUBIO PASCUAL, F.J. & VALLE AGUADO, B. (2007). Space and time in the tectonic evolution of the north-western Iberian Massif: Implications for the Variscan belt, doi: 10.1130/2007. *In* 4-D Framework of Continental Crust: Geological Society of America Memoir (R.D.J. Hatcher, M.P. Carlson, J.H. McBride & J.R. Martínez Catalán eds.). The Geological Society of America, Boulder, CO (403–423).

MARTÍNEZ CATALÁN, J.R., ALLER, J., ALONSO, J.L. & BASTIDA, F. (2008). The Iberian Variscan orogen. *In* Contextos geológicos españoles (A. García Cortés ed.) (14-30).

MARTINS, T., LIMA, A. & VIEIRA, R. (2005) Barroso-Alvão Pegmatite-aplite Field: a case study in Northern Portugal. *ELBA2005 Crystallization Processes in Granitic Pegmatites, Elba Island, Italy*.

MARTINS, T., LIMA, A., GUEDES, A. & NORONHA, F. (2007a) Cassiterite from petalite-bearing veins of the Barroso-Alvão pegmatitic field: preliminary study. *Granitic Pegmatites: the state of the art – International Symposium, Porto, Portugal*.

MARTINS, T., LIMA, A. & NORONHA, F. (2007b) *Locality No. 1 -An overview of the Barroso-Alvão Aplite-Pegmatite Field. Memórias Nº 9 - Granitic Pegmatites: The State of the Art - Field Trip Guidebook*. Alexandre Lima and Encarnación Roda Robles, Porto.

MARTINS, T. (2009) *Multidisciplinary study of pegmatites and associated Li and Sn-Nb-Ta mineralisation from the Barroso-Alvão region*. PhD, Faculty of Sciences of University of Porto, Porto.

MARTINS, T. & LIMA, A. (2011) Pegmatites from Barroso-Alvao, Northern Portugal: anatomy, mineralogy and mineral geochemistry. Cadernos Do Laboratorio Xeoloxico De Laxe 36. 177-205

MARTINS, T., LIMA, A., SIMMONS, W.B., FALSTER, A.U. & NORONHA, F. (2011) Geochemical Fractionation of Nb-Ta Oxides in Li-Bearing Pegmatites from the Barroso-Alvao Pegmatite Field, Northern Portugal. Canadian Mineralogist 49(3). 777-791

MARTINS, T., RODA-ROBLES, E., LIMA, A. & DE PARSEVAL, P. (2012) Geochemistry and Evolution of Micas in the Barroso- Alvao Pegmatite Field, Northern Portugal. Canadian Mineralogist 50(4). 1117-1129

MOREIRA, N., DIAS, R., COKE, C., PEREIRA, E., RODRIGUES, J.F., SOARES, A. & RIBEIRO, A. (2011). O Autóctone da Zona Centro Ibérica na região da Serra do Marão e o Complexo Alóctone de Morais: Livro Guia da Excursão pós-congresso. *In* I Congresso Jovens Investigadores Em Geociências (N. Moreira, R. Dias & A. Soares eds.). Leg 2011, Estremoz (11).

MÜLLER, A., FRIIS, H., JOHANSEN, S., WERNER, R. & THORESEN, Ø. (2017) Sveconorwegian pegmatites of the Evje-Iveland area, South Norway. Geological Guides, Geological Society of Norway (NFG) 6(Norwegian Pegmatites I: Tysfjord-HamarØy, Evje-Iveland, Langesundsfjord). 48-102

NEIVA, A.M.R. & FARINHA RAMOS, J. (2010) Geochemistry of granitic aplite-pegmatite sills and petrogenetic links with granites, Guarda-Belmonte area, central Portugal. European Journal of Mineralogy 22(6). 837-854

NEIVA, A.M.R., BRAVO SILVA, P. & FARINHA RAMOS, J. (2011) Geochemistry of granitic aplite-pegmatite veins and sills and their minerals from the Sabugal area, central Portugal. Neues Jahrbuch für Mineralogie Abhandlungen 189(1). 49-74

NEWLANDER, K., GOODALE, N., JONES, G.T. & BAILEY, D.G. (2015) Empirical study of the effect of count time on the precision and accuracy of pXRF data. Journal of Archaeological Science: Reports 3. 534-548

NORONHA, F. (1987) Nota sobre a ocorrência de filões com espodumena na folha de Dornelas. (Occurrence of pegmatite bodies with spodumene in the Dornelas geological map). Portuguese Geological Survey Internal report.

NORONHA, F. (1988). Mineralizações, 10. *In* Geonovas. Associação Portuguesa de Geológos, Lisboa (37-54).

NORONHA, F. & LIMA, J. (1992). Folha 6C-Cabeceiras de Basto. *In* Carta Geológica de Portugal à escala 1:50 000. Serviços Geológicos de Portugal, Lisboa.

NORONHA, F., RIBEIRO, M.A., MARTINS, H.C. & LIMA, J. (1998). Folha 6D-Vila Pouca de Aguiar. *In* Carta Geológica de Portugal à escala 1:50 000. Instituto Geológico e Mineiro, Lisboa.

NORONHA, F. & LIMA, A. (2006) Da génese à aplicação tecnológica dos aplitopegmatitos litiníferos da Região do Barroso-Alvão e de Almendra. VII Congresso Nacional de Geologia.

NORONHA, F., RIBEIRO, M.A., ALMEIDA, A., DÓRIA, A., GUEDES, A., LIMA, A., MARTINS, H., SANT'OVAIA, H., NOGUEIRA, P., MARTINS, T., RAMOS, R. & VIEIRA, R. (2006). Jazigos filonianos hidrotermais e aplitopegmatíticos espacialmente associados a granitos (Norte de Portugal). *In* Geologia de Portugal no Contexto da Ibéria. Évora University, Évora (123 – 135).

NORONHA, F., RIBEIRO, M.A., ALMEIDA, A., DÓRIA, A., GUEDES, A., LIMA, A., MARTINS, H., SANT'OVAIA, H., NOGUEIRA, P., MARTINS, T., RAMOS, R. & VIEIRA, R. (2013). II.1.8. Jazigos filonianos hidrotermais e aplitopegmatíticos espacialmente associados a granitos (Norte de Portugal), 1 - Geologia Pré-mesozóica de Portugal. *In*

Geologia de Portugal (R. Dias, A. Araújo, P. Terrinha & J.C. Kullberg eds.). Escolar Editora, Évora (404-438).

NORONHA, F. (2017) Fluids and Variscan metallogenesis in granite related systems in Portugal. Procedia Earth and Planetary Science 1 17. 1-4

PAGEL, M., BARBIN, V., BLANC, P. & OHNENSTETTER, D. (2000) *Cathodoluminescence in Geosciences*. Springer-Verlag. Berlin, Heidelberg, New York, 10.1007/978-3-662-04086-7.

PEREIRA, M. & LEAL GOMES, C. (2014) Paragéneses contrastantes no campo pegmatítico de Arga (NW de Portugal), diversidade e equilíbrio. Comunicações Geológicas 101. 181-185

PIRES, M. (1995). Prospeção de Jazigas Litiníferas e de Metais Associados entre as Serras do Barroso e Alvão - Ribeira de Pena. *In* Prospecção Geológica e Geoquímica 1993-1994. DPMM-IGM, Alfragide.

PUGA, M., LEAL GOMES & VIDE, R. (2003) Modo de ocorrência e ensaios de aplicação industrial da petalite do jazigo pegmatítico da Queiriga – Sátão (Viseu). IV Congresso Ibérico de Geoquímica. 196-198

PUTNIS, A. (2002) Mineral replacement reactions: from macroscopic observations to microscopic mechanisms. Mineralogical Magazine 66(5). 689-708

PUTZOLU, F., ARMSTRONG, R.N., BENSON, T.R., BOUTT, D.F., BUTLER, K.L., DOLGOPOLOVA, A., HERRINGTON, R.J., IBARRA, D.E. & MUNK, L.A. (2025) Volcano-Sedimentary Deposits: Overview of an Emerging Type of Lithium Resource. Economic Geology 120(3). 541-573

REED, S.J.B. (2005) *Electron Microprobe Analysis and Scanning Electron Microscopy in Geology*. Cambridge University Press. New York.

RIBEIRO, A., MUNHÁ, J., DIAS, R., MATEUS, A., PEREIRA, E., RIBEIRO, L., FONSECA, P., ARAÚJO, A., OLIVEIRA, T., ROMÃO, J., CHAMINÉ, H., COKE, C. & PEDRO, J. (2007) Geodynamic evolution of the SW Europe Variscides. Tectonics 26(6).

RIBEIRO, M.A. (1998) *Estudo litogeoquímico das formações metassedimentares encaixantes de mineralizações em Trás-os-Montes Ocidental. Implicações metalogénicas*. Faculdade de Ciências da Universidade do Porto, Porto, Portugal.

RIBEIRO, M.A., MARTINS, H.C.B., ALMEIDA, A. & NORONHA, F. (2000) *Notícia explicativa da Folha 6-C- Cabeceiras de Basto. Carta Geológica de Portugal na escala 1/50 000*. D.d. Geologia, Instituto Geológico e Mineiro. Lisboa, 48.

RIBEIRO, R., CAPELA, D., FERREIRA, M., MARTINS, R., JORGE, P., GUIMARÃES, D. & LIMA, A. (2021) *X-ray Fluorescence and Laser-Induced Breakdown Spectroscopy Analysis of Li-Rich Minerals in Veins from Argemela Tin Mine, Central Portugal*.

RODA-ROBLES, E., PESQUERA, A., GIL-CRESPO, P., VIEIRA, R., MARTINS, T. & LIMA, A. (2011). Pegmatites from the Central Iberian and Galizia-Trás-os-Montes zones (Iberian Massif) (Spain and Portugal): Characteristics and exploration significance for Li and other rare-elements. *In* Valorização de pegmatitos litiníferos (L. Martins, D. Oliveira, R. Silva, H. Viegas & R. Villas Bôas eds.). DGEG/LNEG/ADI/CYTED, Lisboa, Portugal (67-68).

RODA-ROBLES, E., PESQUERA, A., GIL-CRESPO, P.P., VIEIRA, R., LIMA, A., GARATE-OLAVE, I., MARTINS, T. & TORRES-RUIZ, J. (2016) Geology and mineralogy of Li mineralization in the Central Iberian Zone (Spain and Portugal). Mineralogical Magazine 80(1). 103-126

RODA-ROBLES, E., VILLASECA, C., PESQUERA, A., GIL-CRESPO, P.P., VIEIRA, R., LIMA, A. & GARATE-OLAVE, I. (2018) Petrogenetic relationships between Variscan granitoids and Li-(F-P)-rich aplite-pegmatites in the Central Iberian Zone: Geological and geochemical constraints and implications for other regions from the European Variscides. Ore Geology Reviews 95. 408-430

RODA-ROBLES, E., GIL-CRESPO, P.P., PESQUERA, A., LIMA, A., GARATE-OLAVE, I., MERINO-MARTÍNEZ, E., CARDOSO-FERNANDES, J. & ERRANDONEA-MARTIN, J. (2022) Compositional Variations in Apatite and Petrogenetic Significance: Examples from Peraluminous Granites and Related Pegmatites and Hydrothermal Veins from the Central Iberian Zone (Spain and Portugal). Minerals 12.

RODA-ROBLES, E., VIEIRA, R., LIMA, A., ERRANDONEA-MARTIN, J., PESQUERA, A., CARDOSO-FERNANDES, J. & GARATE-OLAVE, I. (2023) Li-rich pegmatites and related peraluminous granites of the Fregeneda-Almendra field (Spain-Portugal): A case study of magmatic signature for Li enrichment. Lithos 452-453. 107195

RODA ROBLES, E., PESQUERA PEREZ, A., GIL CRESPO, P.P. & TORRES RUIZ, J. (2012) From granite to highly evolved pegmatite: A case study of the Pinilla de Fermoselle granite–pegmatite system (Zamora, Spain). Lithos 153. 192-207

RODRIGUES, R. (2008) *Contribuição para o conhecimento do Campo Aplitopegmatítico Seixoso-Vieiros (Baixo Tâmega). O caso de estudo do Granito da Mina do Outeiro*. Mestrado em Geomateriais e Recursos Geológicos, Faculdade de Ciências da Universidade do Porto, Porto.

RODRÍGUEZ FERNÁNDEZ, L.R., LÓPEZ OLMEDO, F., OLIVEIRA, J.T., MEDIALDEA, T., TERRINHA, P., MATAS, J., MARTÍN-SERRANO, A., MARTÍN PARRA, L.M., RUBIO, F., MARÍN, C., MONTES, M. & NOZAL, F. (2015) Mapa Geológico de la Península Ibérica, Baleares y Canarias a Escala 1/1.000.000. ©Instituto Geológico y Minero de España (IGME); ©Laboratório Nacional de Energia e Geologia (LNEG).

SÁNCHEZ-MUÑOZ, L., MÜLLER, A., ANDRÉS, S.L., MARTIN, R.F., MODRESKI, P.J. & DE MOURA, O.J.M. (2017) The P–Fe diagram for K-feldspars: A preliminary approach in the discrimination of pegmatites. Lithos 272-273. 116-127

SANT'OVAIA, H. (2000) *O Maciço Granítico Pós-Tectónico De Vila Pouca De Aguiar Estudo Petro-Estrutural E Mecanismo De Instalação*. PhD in Sciences (Geology), Faculty of Sciences of the University of Porto, Porto.

SANT'OVAIA, H., RIBEIRO, M.A., MARTINS, H.C.B. & NORONHA, F. (2011) *Notícia explicativa da Carta geológica de Portugal na escala 1:50000 - Folha 6D – Vila Pouca de Aguiar*. LNEG - National Laboratory of Energy and Geology, Lisboa.

SAVANNAH RESOURCES (2023) JORC Mineral Resource Estimate for Lithium (June 2023, 05% Li2O cut-off). Available from <https://savannahresources-wwwsavannahresourcescom.azurewebsites.net/project/barroso-lithium-project-portugal/> [Date accessed: 20th March 2025].

SHMAKIN, B.M. (1979) Composition and structural state of K-feldspars from some U.S. pegmatites. American Mineralogist 64. 49-56

SILVA, D. (2014) *Spatial analysis applied to the Barroso-Alvão rare-elements pegmatite field (Northern Portugal)*. Master Thesis in Geology, Faculdade de Ciências da Universidade do Porto, Porto.

SIMMONS, W. & WEBBER, K.L. (2008) Pegmatite genesis: state of the art. European Journal of Mineralogy 20(4). 421-438

SMEDS, S.-A. (1992) Trace elements in potassium-feldspar and muscovite as a guide in the prospecting for lithium- and tin-bearing pegmatites in Sweden. Journal of Geochemical Exploration 42(2-3). 351-369

SOUSA, R., RAMOS, V., GUEDES, A., NORONHA, F., BOTELHO DE SOUSA, A., MACHADO LEITE, M., SELTMANN, R. & DOLGOPOLOVA, A. (2018) The Alvarrões-Gonçalo Li project: an example of sustainable lithium mining. Adv. Geosci. 45. 1-5

SWAIN, B. (2017) Recovery and recycling of lithium: A review. Separation and Purification Technology 172. 388-403

TEIXEIRA, C. & CÂNDIDO DE MEDEIROS, A. (1969). Folha 06-B - Chaves. *In* Carta Geológica de Portugal à escala 1:50 000. Instituto Geológico e Mineiro, Lisboa.

THOMAS, R. (2004) *Pratica Guide to ICP-MS*. Marcel Dekker, Inc.,. New York, USA.

TORRE DE ASSUNÇÃO, C.F. (1954). III Ocorrência de espodumena em Gelfa (Âncora), 7a Série 22. *In* Notas de Mineralogia e Petrologia. Bol. Mus. Lab. Minerai. Geol. Fac. Ciênc, Lisboa (29-32).

TUCKER VASQUES, J. (2021) *Lithogeochemistry and Prospection of Lithium-Bearing Pegmatites and Their Host-Rocks.* Master in Geology, Faculty of Sciences of the University of Porto, Porto, Portugal.

U.S. GEOLOGICAL SURVEY (2025) Mineral Commodity Summaries 2025: Lithium. Available from <https://pubs.usgs.gov/periodicals/mcs2025/mcs2025-lithium.pdf.> [Date accessed: 20th March 2025].

VERNON, R.H.P.S.R. (2004) *A practical guide to rock microstructures*. Cambridge University Press. 593.

VIEIRA, R. (2010) *Aplitopegmatitos com Elementos Raros da Região entre Almendra (V. N. de Foz-Côa) e Barca d'Alva (Figueira de Castelo Rodrigo). Campo Aplitopegmatítico da Fregeneda-Almendra*. Faculty of Sciences of the University of Porto, Porto, Portugal.

VILLASECA, C., BARBERO, L. & HERREROS, V. (2011) On the origin of granite types in the Central Iberian Zone: contribution from integrated U-Pb and Hf isotope studies of

zircon. *VIII Congresso Ibérico de Geoquímica, Castelo Branco, Portugal*, 271–276.

WEBBER, K.L. & SIMMONS, W.B. (2007) Crystallization dynamics. *Grantic Pegmatites: the state of the art - International Symposium, Porto, Portugal*.

WINTER, J. (2014) *Principles of Igneous and Metamorphic Petrology*. Pearson Education Limited. USA.

WISE, M.A. & BROWN, C.D. (2019) Cathodoluminescence (CL) Microscopy – A Technique for Understanding The Dynamics of Pegmatite Crystallization. The Canadian Mineralogist 57. 821-823

WISE, M.A., HARMON, R.S., CURRY, A., JENNINGS, M., GRIMAC, Z. & KHASHCHEVSKAYA, D. (2022) Handheld LIBS for Li Exploration: An Example from the Carolina Tin-Spodumene Belt, USA. Minerals 12.

YOUNG, K.E., EVANS, C.A., HODGES, K.V., BLEACHER, J.E. & GRAFF, T.G. (2016) A review of the handheld X-ray fluorescence spectrometer as a tool for field geologic investigations on Earth and in planetary surface exploration. Applied Geochemistry 72. 77-87

ZHOU, S., WANG, J., WANG, W. & LIAO, S. (2022) Evaluation of portable X-ray fluorescence analysis and its applicability as a tool in geochemical exploration. Minerals 12.

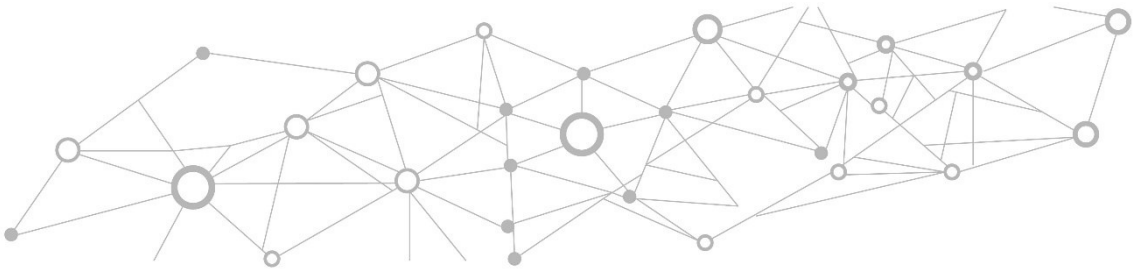

Part VII – Appendices

LA-ICP-MS analysis

Table A. 1. Spodumene crystals analyzed by Laser Ablation Inductively Coupled Plasma Mass Spectrometry (LA-ICP-MS), from thin sections of drill core and outcrop samples from the NOA aplite-pegmatite (Barroso-Alvão Pegmatite Field). Analyses conducted at the Universidad del País Vasco (UPV/EHU), Bilbao.

Sample #	19DD003-1	19DD003-6	19DD003-6	19DD003-6	19DD003-17	19DD003-22	NOA-1-OUT	NOA-1-OUT	NOA-1-OUT	NOA-1-OUT
Circle #	Circle 1	Circle 2	Circle 2	Circle 2	Circle 2	Circle 1	Circle 1	Circle 1	Circle 1	Circle 1
Analysis #	11	7	7.2	7.3	8	3	2	3	4	5
Si from	30.57	30.55	30.55	30.55	31.02	30.65	30.57	30.57	30.57	30.57
Al %	14.69	14.13	14.69	14.59	14.39	15.55	14.58	14.23	14.08	14.56
Li %	3.03	3.36	3.44	2.72	3.04	3.37	3.08	3.05	3.06	3.13
Fe ppm	2450	1662	1729	2301	845	1595	1395	3155	1493	1909
Na ppm	607	491	488	528	479	540	491	663	538	398
Mn ppm	232	133	122	90	216	70	171	134	105	304
Ti ppm	109	138	132	105	107	129	103	100	97	102
Ca ppm	108	< LOD	129	< LOD	< LOD	< LOD	< LOD	< LOD	< LOD	< LOD
P ppm	82	< LOD	< LOD	< LOD	523	< LOD	456	< LOD	251	< LOD
Nb ppm	36	0	0	0	0	0	0	40	0	7
Ga ppm	13	21	21	19	11	18	11	13	11	11
Mg ppm	11	1	23	62	6	7	7	13	4	7
K ppm	9	< LOD	280	10	< LOD	< LOD	< LOD	< LOD	< LOD	8
Sc ppm	6	6	6	6	5	6	6	6	6	6
Zn ppm	5	< LOD	2	< LOD	8	3	2	4	< LOD	6
Sn ppm	3	31	39	25	346	12	2	6	2	2
Be ppm	3	1	< LOD	1	16	< LOD	11	3	5	1
Ta ppm	2	< LOD	0	1	1	0	1	1	0	6
Zr ppm	0	< LOD	< LOD	< LOD	7	< LOD	1	1	0	1
Sr ppm	0	0	0	1	1	0	0	< LOD	< LOD	0
Ba ppm	0	< LOD	1	1	0	< LOD	< LOD	< LOD	0	< LOD
Cs ppm	0	< LOD	0	0	< LOD	< LOD	< LOD	< LOD	< LOD	< LOD
Cu ppm	< LOD	< LOD	1	< LOD	0	< LOD	< LOD	< LOD	< LOD	< LOD
Rb ppm	< LOD	< LOD	1	< LOD	< LOD	< LOD	< LOD	< LOD	< LOD	< LOD
Tl ppm	< LOD	< LOD	< LOD	0	0	< LOD	< LOD	< LOD	< LOD	< LOD
V ppm	< LOD	< LOD	< LOD	< LOD	< LOD	< LOD	< LOD	< LOD	< LOD	< LOD
Cr ppm	< LOD	< LOD	< LOD	< LOD	< LOD	< LOD	< LOD	< LOD	< LOD	< LOD
Ni ppm	< LOD	< LOD	< LOD	< LOD	< LOD	< LOD	< LOD	< LOD	< LOD	< LOD
U ppm	0	< LOD	< LOD	< LOD	< LOD	0	< LOD	< LOD	0	0

Table A. 2. Cookeite crystals analyzed by Laser Ablation Inductively Coupled Plasma Mass Spectrometry (LA-ICP-MS), from thin sections of drill core samples from the NOA aplite-pegmatite (Barroso-Alvão Pegmatite Field). Analyses conducted at the Universidad del País Vasco (UPV/EHU), Bilbao.

Sample #	19DD003-1 Circle 1	19DD003-1 Circle 1	19DD003-1 Circle 1	19DD003-1 Circle 1	19DD003-17 Circle 2	19DD003-17 Circle 5	19DD003-21 Circle 2	19DD003-21 Circle 2	19DD003-22 Circle 1
Analysis #	10	B-6	B-7	B-8	4	9	1	2	1
Si from EPMA (%)	16.10	16.10	16.10	16.10	16.66	16.91	16.12	16.50	16.72
Al %	21.26	24.30	22.25	22.09	23.12	25.41	23.21	22.51	23.58
Fe %	2.87	3.13	3.54	2.73	0.69	1.06	0.52	1.88	1.90
Li %	0.94	1.33	1.21	1.15	1.33	1.56	1.48	1.82	1.73
Mn ppm	602	653	738	569	117	119	804	865	518
K ppm	551	536	738	489	9626	1333	34	28	92
Ca ppm	< LOD	< LOD	< LOD	< LOD	126	2524	213	< LOD	158
Mg ppm	428	361	445	309	375	378	207	288	751
Na ppm	321	251	404	205	131	77	19	10	34
Zn ppm	134	150	142	126	22	44	82	111	71
Be ppm	122	158	140	143	75	84	207	140	183
P ppm	101	< LOD	< LOD	52	< LOD	1209	< LOD	< LOD	< LOD
Sn ppm	79	127	96	116	105	179	35	63	58
Rb ppm	9	10	12	8	178	26	1	1	2
Ti ppm	84	110	101	102	58	58	80	109	104
Sr ppm	1	1	1	1	2	84	2	1	2
Ga ppm	40	51	46	44	34	32	38	49	39
Cs ppm	23	26	27	20	43	32	5	4	9
Ba ppm	9	7	8	5	5	2	2	2	1
Ta ppm	4	5	5	6	1	0	7	5	32
Sc ppm	3	3	4	3	3	3	3	3	3
U ppm	2	0	0	0	0	< LOD	1	3	0
Cu ppm	1	1	1	1	2	2	5	5	3
Nb ppm	< LOD	1	1	1	1	1	2	1	7
Cr ppm	< LOD	< LOD	< LOD	< LOD	< LOD	< LOD	< LOD	5	< LOD
Pb ppm	0	0	0	< LOD	< LOD	< LOD	1	1	1
Zr ppm	0	0	0	0	0	< LOD	1	0	1
Tl ppm	< LOD	0	0	< LOD	1	< LOD	< LOD	< LOD	< LOD
Co ppm	0	0	< LOD	0	< LOD	< LOD	< LOD	< LOD	< LOD
Y ppm	0	0	0	0	0	0	< LOD	0	0

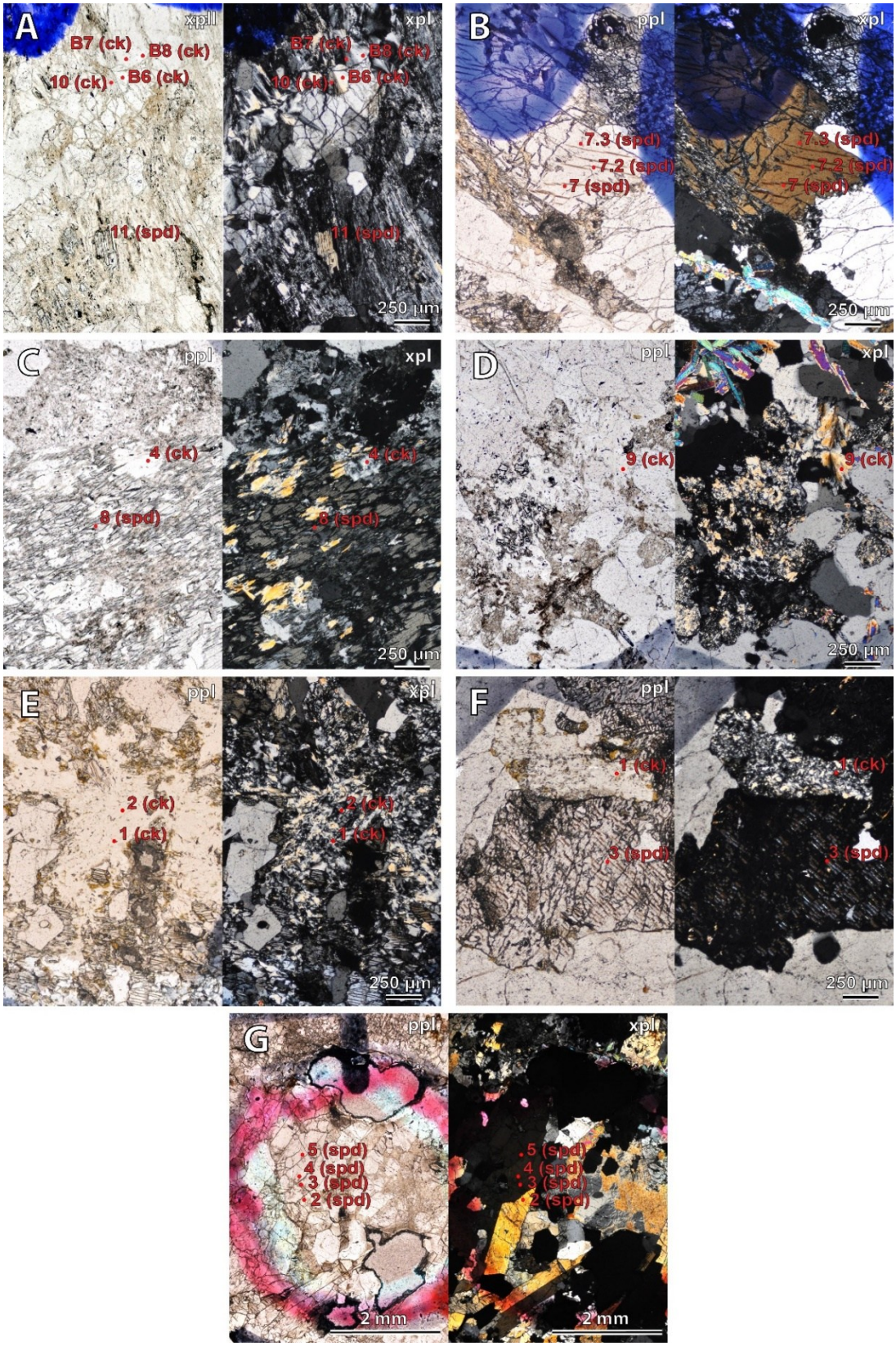

Figure A. 1. Locations of LA-ICP-MS and EPMA analyses performed on spodumene (Spd) and cookeite (Ck) in thin sections from the AL56/NOA aplite-pegmatite, Barroso–Alvão Field. A: 19DD003-1, Circle 1; B: 19DD003-6, Circle 2; C: 19DD003-17, Circle 2; D: 19DD003-17, Circle 5; E: 19DD003-21, Circle 2; F: 19DD003-22, Circle 1; G: NOA-1-OUT, Circle 1.